UNIVERSITÀ DEGLI STUDI DI MILANO
FACOLTÀ DI SCIENZE MATEMATICHE,
FISICHE E NATURALI

Dipartimento di Chimica

Doctorate School of Chemical Sciences and Technologies

Doctorate in Industrial Chemistry
XXV Cycle
CHIM/06

SUPERPARAMAGNETIC IRON OXIDE NANOPARTICLES (SPIONS): DESIGN AND SYNTHESIS OF NEW NANOCONJUGATES

Claudio CARRARA
Matr. R08777

Advisor: Prof. Emanuela LICANDRO

Co-advisor: Prof. Stefano MAIORANA

Coordinator: Prof. Dominique ROBERTO

A.A. 2011-2012

A voi,

che rendete la mia vita speciale...

Una storia come la mia non andrebbe mai raccontata, perché il mio mondo è tanto proibito quanto fragile, senza i suoi misteri non può sopravvivere.

Di certo non ero nata per una vita da geisha, come molte cose nella mia strana vita, ci fui trasportata dalla corrente.

La prima volta che seppi che mia madre stava male, fu quando mio padre ributtò in mare i pesci, quella sera soffrimmo la fame, "per capire il vuoto", lui ci disse.

Mia madre diceva sempre che mia sorella Satsu era come il legno, radicata al terreno come un albero sakura.

Ma a me diceva che ero come l'acqua, l'acqua si scava la strada attraverso la pietra, e quando è intrappolata, l'acqua si crea un nuovo varco.

"Memorie di una Geisha"

Arthur Golden

Table of Contents

Preface

In the last decade, Nanotechnology and its applications have been among the research topics of great interest in the scientific community. In particular, nanomedicine has perhaps been the most popular application due to its potential as a tool directed towards life quality improvement and welfare.

As part of a multidisciplinary approach including different scientific disciplines (chemistry, physics, biology and medicine), this research project is only a "brick" in a much larger building-project which aims to the synthesis of new nanosystems as both novel diagnostic and therapeutic agents. The work of a chemist is therefore fundamental for the construction of these new nanoscopic "objects" that have to be characterized in terms of their chemical and physical properties, as well as for their biological activities. Medical applications are an ambitious, but possible goal for the future.

Being an organic chemist, the approach I used was to consider the nanoparticles used in this project as molecules, and consequently to study their surface reactivity from a chemical perspective.

This made possible to discover (also thanks to the careful observation and explanation of one of the many early failures) a novel synthetic method for the functionalization of Superparamagnetic Iron Oxide Nanoparticles (SPIONs). Such method has been successfully employed for the support of biomolecules onto the magnetic metallic core. The "usual" experimental failures observed early in the project were, in reality, the gateway leading to significant, tangible results obtained in the second half of the three years of doctoral research.

These results are instrumental for the preparation of several scientific papers which we plan to publish as soon as possible. Meanwhile, we got positive feedbacks from the presentation of some of our results at various conferences. We believe there is, thus, the possibility to start new fruitful collaborations with chemical and biomedical research groups working in the field.

To this regard, in the last months, we have begun a collaboration with Prof. Seneci's research group of the University of Milan. Our goal is to study and synthesize novel nanosystems composed by SPIONs "decorated" with bioactive molecules able to modulate the apoptotic process. The first nanoconjugates of this new family of molecules have been synthesized in

the last few weeks. Their characterization will be reported elsewhere, but will be dependent from the efforts described in this thesis.
Our research group is also part of a wider research project that will start in 2013, through the granted funding of a Cariplo grant. The project will be aimed to the study of the interaction of new nanosystems within the central nervous system, and therefore to the possible modulation of neurodegenerative diseases.

Regarding the structure of this thesis, I divided it into two main parts. The first includes a comprehensive introduction to the world of Nanotechnology, then goes more into the specifics of magnetic metal nanoparticles, and finally focuses on the SPIONs. Reading the first 3 chapters can be quite demanding, but it is essential for those who (like me at first), are not aware of the characteristics and properties of these nanomaterials.
The second part of the thesis is its real foundation, as it contains all the novel experimental data obtained in these years.
Chapter 4 is perhaps the true heart of the thesis, in which I discuss the experimental data to demonstrate the discovery of a new method of surface functionalization for SPIONs. Earlier in this chapter some fundamental theoretical concepts are remarked, so to enable the reader to understand all the information given in the following paragraphs, even without having read the first three introductory chapters.
Chapter 5 presents some early results in the SPIONs applications as magnetic supports for biomolecules, in particular for a class of mimics of natural oligonucleotides, the Peptide Nucleic Acids (PNAs). It was therefore necessary to begin the chapter with an exhaustive introduction on PNAs - what they are, their characteristics, synthesis and properties, as well as their possible biomedical applications. Subsequently, I focused the discussion on new magnetic PNAs, and in particular on four new nanoconjugates that have been synthesized and have demonstrated their unique ability to recognize complementary nucleic acids with high affinity binding.

Good reading,

Claudio Carrara

Abstract

Abstract

Superparamagnetic Iron Oxide Nanoparticles (SPIONs) have demonstrated great promise for diagnostic and therapeutic applications. Thanks to their magnetic properties and to their size, comparable to that of biologically objects, they are very useful for biomedical applications, such as, for example, automated DNA extraction, targeted gene delivery, magnetic resonance imaging (MRI), and magnetic field induced hyperthermia for cancer therapy. For these applications, SPIONs must be coupled with targeting agents, therapeutic drugs, and other functional probes. Hence, the need to develop efficient synthetic strategies for the conjugation of molecules to SPIONs is an important and appealing target.

The strategies used can involve passive noncovalent adsorption on the outer particle surface (for instance, by a carboxylate moiety) or the formation of a more stable covalent bond by using appropriate heterobifunctional linkers, in which one functional group specifically binds the nanoparticle, while the other reacts with the biomolecule in order to form the new nanoconjugate (*Figure 1*).

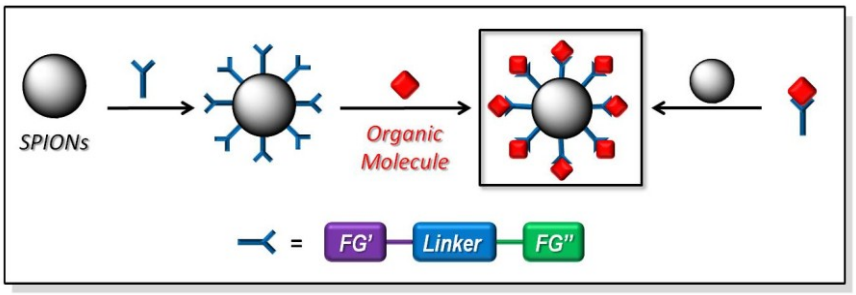

Figure 1 *- The heterobifunctional linker bears two orthogonal functional groups (FG' and FG'') able to selectively react with the SPION surface or with the organic molecule that we want to support on nanoparticle.*

During this Ph.D. research work, both *non-covalent* and *covalent* surface interactions were investigated in order to obtain new bionanoconjugates. Specifically, we were interested in the search for new heterobifunctional linkers able to covalently bind the SPIONs surface, as an alternative to the most used methodology which involves the use of the 3-(aminopropyl)triethoxysilane (APTES) **1**.

In this work, commercially available *γ-Fe_2O_3* maghemite SPIONs (Alfa Aesar) with an average diameter of 10±2 nm were used. Generally, APTES functionalized nanoparticles can be easily synthesized as reported in *Scheme 1*.

APTES **1** is added to a suspension of naked maghemite SPIONs under sonication; after 4 hours at 60 °C it is possible to isolate the corresponding NP-APTES **2**. The free amino-groups can be used to bind proper biomolecules as itself or after a functional group interconversion.

Using the same strategy, we decided to use the 3-(triethoxysylil)propyl isocyanate (TESPI) **3**, instead of APTES **1**, in order to obtain a new nanoconjugates bearing free NCO-groups on the surface (*Scheme 2*).

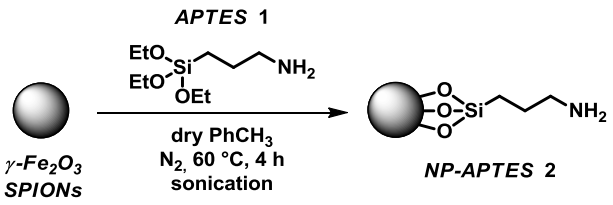

Scheme 1

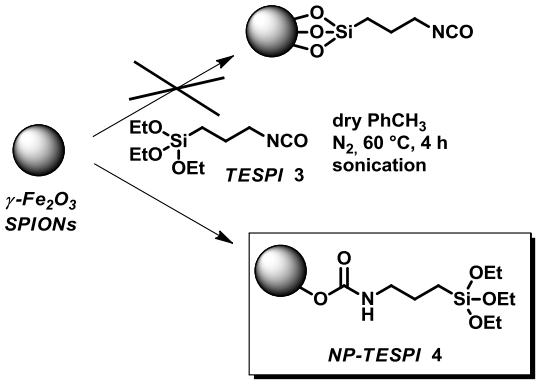

Scheme 2

Unexpectedly, we didn't obtain the desired product in which the alkoxysilane reacted with the SPION surface. From FTIR spectroscopy and elemental analysis (E.A.) we have deduced that the isocyanate group of TESPI **3** had interacted with the SPION surface leading to a new species of nanoconjugate. Our hypothesis was that the NCO moiety reacted with the surface OH-groups of the nanoparticle, forming carbamate-like bond, affording the new nanoconjugate NP-TESPI **4** (*Scheme 2*). This unexpected result led us to further investigate the reactivity of the isocyanate group towards the SPION surface.

To the best of our knowledge, only two examples of the use of an isocyanate moiety as the anchoring group onto nanoparticle materials (silica and titania) are reported in literature. Since in these papers no exhaustive studies are made to demonstrate the formation of a carbamate bond between the isocyanate group and the nanoparticles surface, and nothing is reported in literature about iron oxide nanoparticle grafting with isocyanates, we decided to deep investigate this new anchoring methodology.

In fact, the generality of the grafting of isocyanate molecules onto SPIONs surface, could be exploited as a new anchoring system and a new class of heterobifunctional linkers for SPIONs could be proposed.

The scope of this new possible anchoring strategy was evaluated preparing a small library of new nanoconjugates starting from commercially available (**5**-**9**) or easily synthesizable (**10**) differently substituted isocyanates, reported in *Figure 2*.

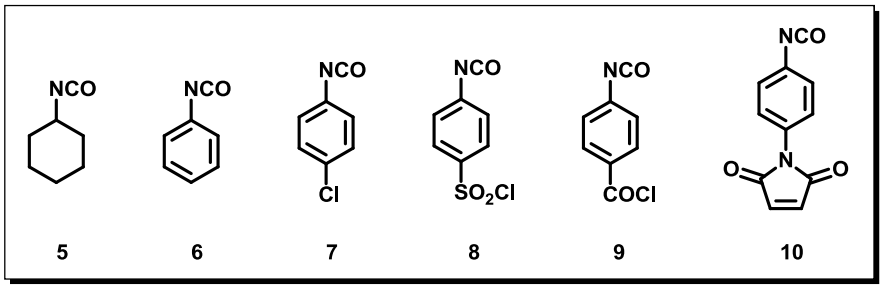

Figure 2

Isocyanates **8**-**10** were endowed with a second functional group which, in principle, could be used to support organic molecules to the SPIONs surface through the linker.
The general procedure used to anchor isocyanates **5**-**10** onto the naked SPIONs is shown in *Scheme 3*.

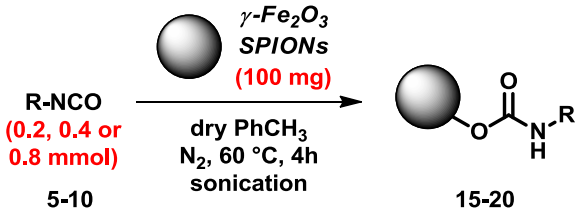

Scheme 3 *- Standard procedure for the synthesis of new carbamate-based nanoconjugates.*

The proper isocyanate (0.2, 0.4 or 0.8 millimoles) was added to a suspension of 100 mg of naked SPIONs in dry toluene, under sonication at 60 °C for 4 hours. The resulting suspension was then centrifugated at 5000 round per minute for 10 minutes; the supernatant was eliminated and the solid residue was washed with fresh toluene (3x5 ml) and diethyl ether (3x5 ml) affording the desired nanoconjugates **15**-**20** (*Figure 3*).

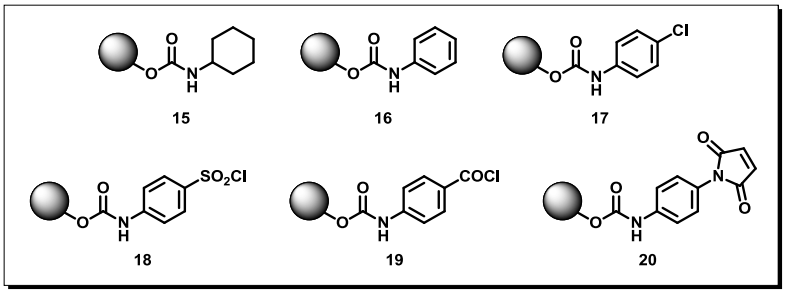

Figure 3

All nanoconjugates were characterized by elemental analysis (E.A.) and infrared spectroscopy (FTIR), while only some of them have been further characterized by High Resolution Magic Angle Spinning NMR technique (HR-MAS NMR). The results obtained confirmed us the formation of a stable carbamate-like bond between the isocyanate group of the organic molecules and the surface hydroxyl groups of the nanoparticles.
The synthetic protocol used to synthesize nanoconjugates **15**-**20**, was set up in order to verify the reproducibility of the methodology and the possibility to tune the quantity of

organic molecule grafted onto the SPIONs surface. For these reasons the final loading of each nanoconjugate was determined by E.A. and the results obtained in the three series of test reactions with 0.2, 0.4 and 0.8 millimoles of isocyanates *per* 100 milligrams of naked nanoparticles have been compared. An average loading was calculated (as the arithmetic mean of those obtained for each nanoconjugates) and as shown in *Figure 4*, the loadings can be easily tuned just increasing the amount of starting isocyanate, confirming the efficacy of this new grafting methodology.

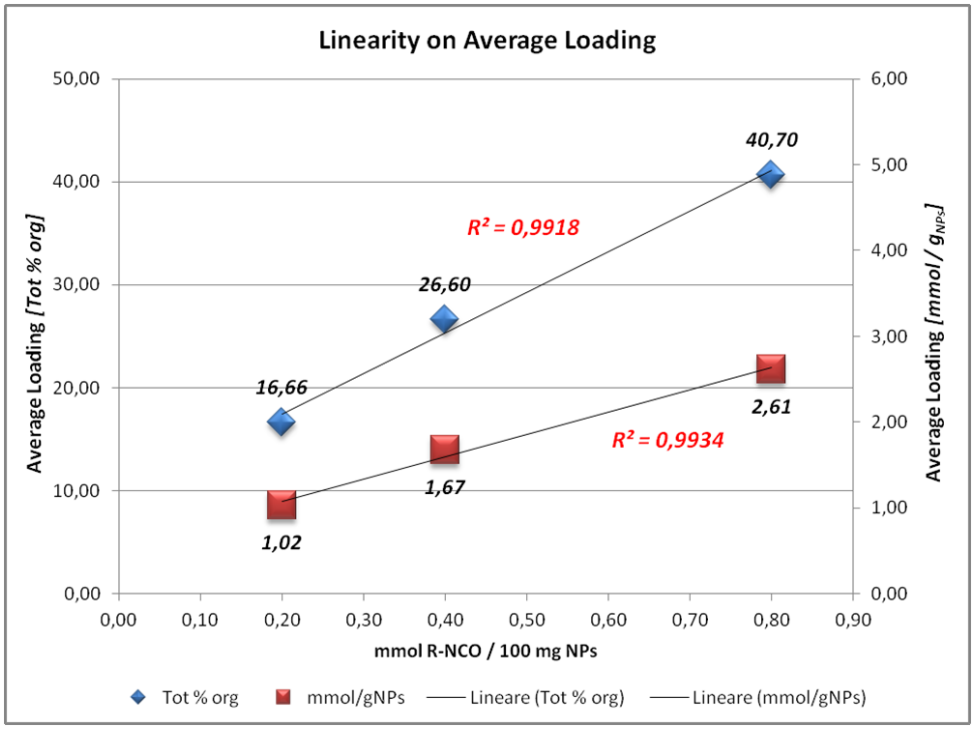

Figure 4 *- Linear regressions on average loading values.*

FTIR spectroscopy helps to point out the interaction between the isocyanate group and the SPIONs surface, confirming the formation of a carbamate bond for all products as reported in *Table 1*, in which the stretching of the obtained carbamate bond are reported. Furthermore, FTIR spectroscopy has proved to be the choice technique for the analysis of these kind of nanoconjugates.

In *Table 2*, the HR-MAS experiments performed on nanoconjugates **15**-**17** and **20** are summarized proving the versatility of this technique, while nanoconjugates **18** and **19** were not characterized with NMR spectroscopy due to the lability of the additional -SO_2Cl and -COCl moieties. Concerning the general use of the HR-MAS technique, we can state that the results obtained demonstrate the grafting of isocyanate molecules onto the SPIONs surface, leading to the formation of a carbamate bond. The MAS tool has proved to be versatile and furthermore, can be used to overcome all the problems related to the presence of a superparamagnetic core. Very nice spectra were obtained and preliminary DOSY experiments were performed.

R-NCO	*Nanoconjugate*	*Stretching [cm^{-1}]*	
		-N=C=O	*C=O carbamate*
5	**15**	2258	1626
6	**16**	2259	1647
7	**17**	2265	1632
8	**18**	2265	1699
9	**19**	2265	1682
10	**20**	2306	1693

Table 1 *- C=O Stretching values of starting isocyanate and corresponding nanoconjugates.*

Nanoconjugate	HR-MAS experiments
15	^{1}H, ^{13}C, COSY, HSQC
16	^{1}H, ^{13}C
17	^{1}H, ^{13}C
20	^{1}H, DOSY

Table 2 *- HR-MAS experiments performed on some nanoconjugates.*

Having established the easy anchoring of isocyanates onto the SPIONs surface by the formation of a carbamate bond, we decided to compare the efficiency of this new grafting methodology with the already known non-covalent adsorption of carboxylic acid and with the most used linker based on siloxane interaction.

For this purpose we started comparing the loadings of nanoconjugates **16** and **20** (obtained by anchoring the phenyl isocyanate **6** and the (*p*-maleimido)phenyl isocyanate **10**, respectively) *versus* the loadings of the nanoconjugates **23** and **24** that have been synthesized starting from the corresponding carboxylic compounds, the benzoic acid **22** and the (*p*-maleimido)benzoic acid **12** (*Figure 5*). Functionalized nanoparticles **23** and **24** bear the same organic residue of the analogous nanoconjugates **16** and **20**, but differ from the anchoring group.

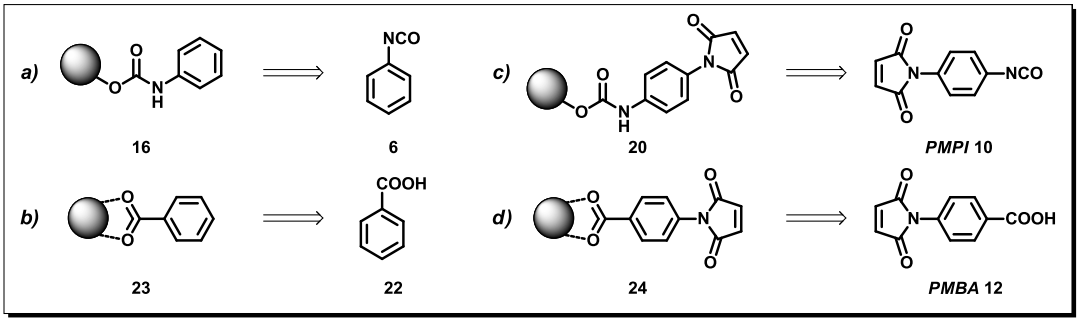

Figure 5 *- Synthesis of comparable nanoconjugates* **16***,* **20***,* **23** *and* **24***. In a) and c)* **16** *and* **20** *are formed by covalent interaction between the starting isocyanates* **6** *and* **10** *with SPIONs, while in b) and d) a non-covalent adsorption were used to obtain nanoconjugate* **23** *and* **24** *from the corresponding carboxylic acids* **22** *and* **12***.*

In order to obtain comparable loading values for the nanoconjugates **23** and **24**, the same synthetic protocol used for the grafting of isocyanates onto SPIONs, previously shown in *Scheme 3*, was applied. Thus, 0.2, 0.4 and 0.8 millimoles of carboxylic acids **22** e **12** were added to a suspension of 100 milligrams of naked SPIONs in toluene. After 4 hours at 60 °C under sonication, the desired functionalized nanoparticles **23** and **24** were isolated. The loadings were determined by E.A. and FTIR spectra were acquired demonstrating the anchoring of the organic carboxylic acid by a non-covalent adsorption with formation of a carboxylate species. From the loading values obtained, we can state that the covalent grafting of isocyanates leads to higher loading compared with the non-covalent interaction of carboxylic acids and in *Figure 6* these values are summarized. Furthermore, only a slight increase in final loading was observed increasing the amount of the starting carboxylic ligand.

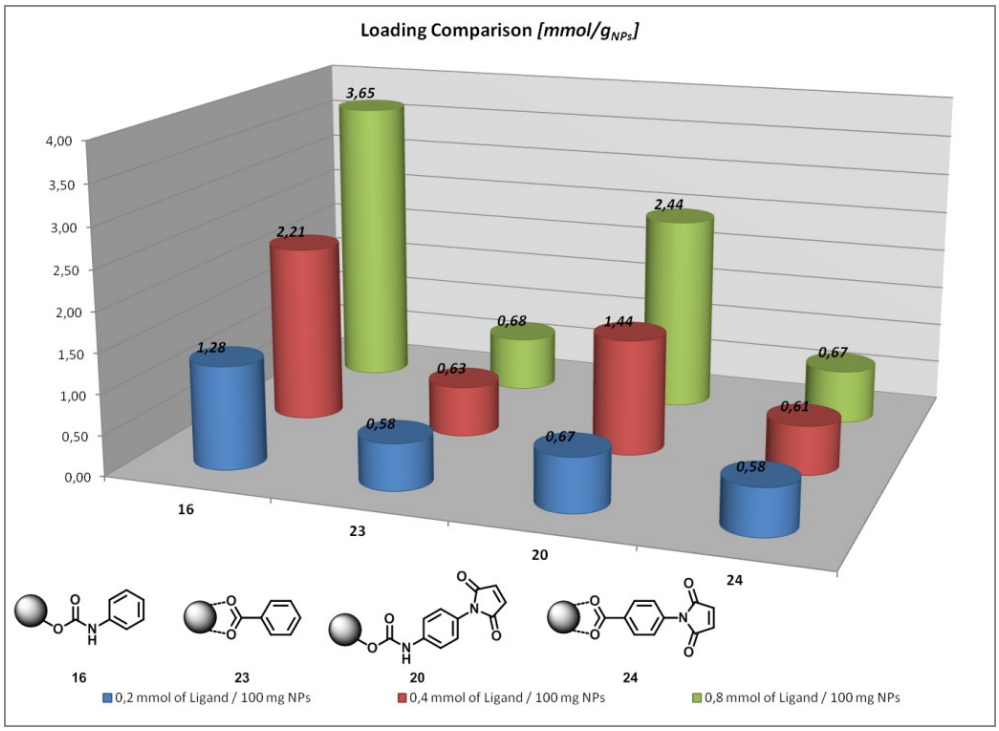

Figure 6 *- Loading comparison of nanoconjugates* **16** *and* **20** *(covalent interaction) versus* **23** *and* **24** *(non-covalent adsorption), express as total percentage in weight of organic part loaded onto SPIONs [mmol/g$_{NPs}$].*

The same approach was used to compare the amount of isocyanate loaded onto SPIONs against the covalent silylation of APTES **1** (*Figure 7*).

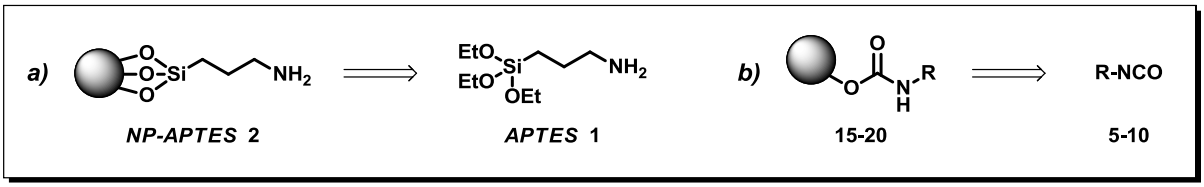

Figure 7 *– Synthetic approach for the synthesis of a) nanoconjugates* **2**, *from the corresponding alkoxysylane APTES* ***1*** *and b) nanoconjugates* **15**-**20**, *from starting isocyanates* **5**-**10**. *The loading values obtained for the silyloxy-derivative will be compared with the average loading calculate for the new grafting methodology.*

Nanoconjugate **2** was therefore synthesized accordingly to *Schemes 1* and *3*, using 0.2, 0.4 and 0.8 millimoles of **1** *per* 100 milligrams of naked nanoparticles. The functionalized SPIONs were analyzed by E.A. and the loadings obtained were compared with the average loading found for the isocyanate covalent interaction. The results are summarized in *Figure 8*.

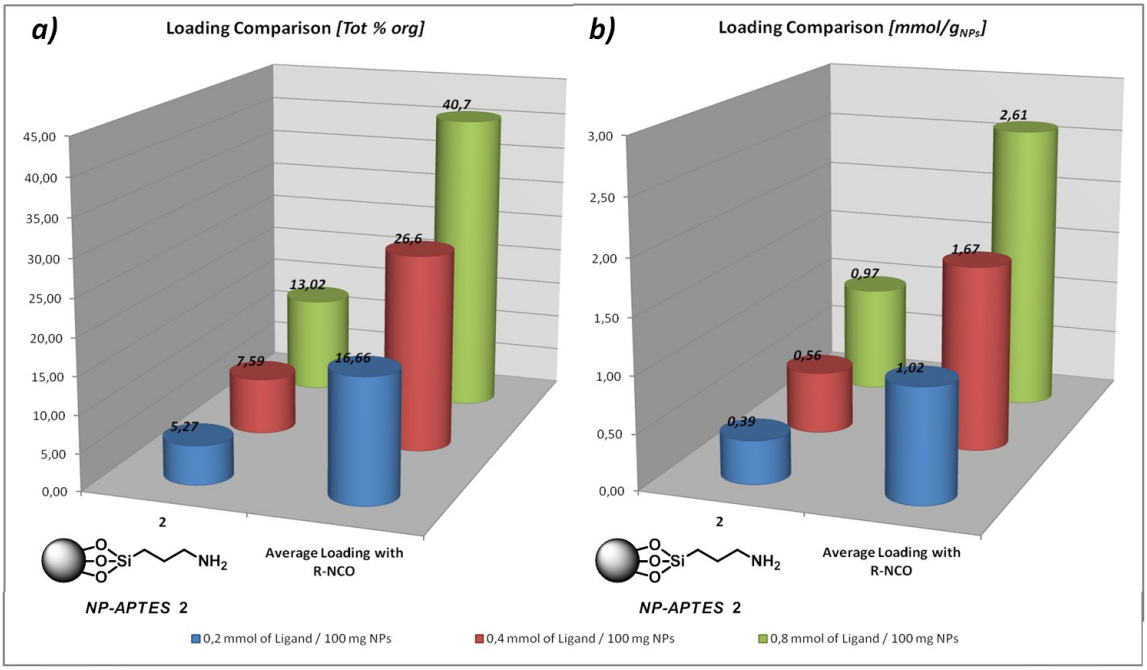

Figure 8 *- Loading comparison of nanoconjugate* **2** *(Si-O covalent interaction) versus the average loading calculated on nanoconjugate* **15-20** *(carbamate covalent interaction).*

We may conclude by stating that the new methodology developed in this research leads to significantly higher loading values if compared to the classical non-covalent adsorption of carboxylic acids and also with respect to the main used covalent silylation of nanoparticles.
The outstanding functionalization of SPIONs with isocyanates, with formation of a covalent carbamate bond, led us to further investigate the possibility of using these organic molecules as heterobifunctional linkers. From the beginning of this research work, we decided to study this new functionalization methodology with the final aim of conjugating bioactive molecules onto the SPIONs surface thanks to the use of specifically designed linkers. For this reason,

isocyanates **8**-**10** were chosen in order to obtain the corresponding nanoconjugates **18**-**20**, that bear an additional reactive functional group.

The chlorosulfonyl and the chloroacyl moieties are highly reactive towards amines and alcohols, affording the corresponding amides and esters, while the maleimido group is a classical Michael acceptor able to react with strong nucleophiles, as thiols and amines.

The first step was to demonstrate that the -SO_2Cl and -COCl groups are not reactive towards the nanoparticles surface. Indeed, the functionalization reaction consists in the direct addition of the isocyanates **8** and **9** in a suspension of naked SPIONs in dry toluene so, in principle, a possible competitive reaction can occur with formation of the corresponding esters with the surface hydroxyl groups.

To verify this possibility, blank reactions were performed with tosyl chloride **25** and benzoyl chloride **26** (*Scheme 4* and *Scheme 5*, respectively).

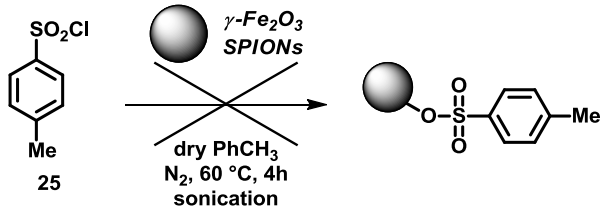

Scheme 4

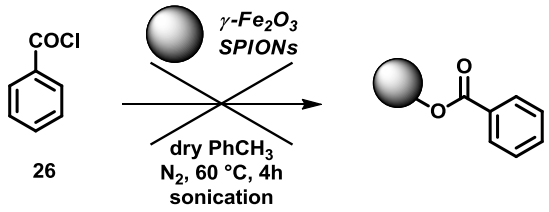

Scheme 5

The recovered nanoparticles were analyzed by E.A. and FTIR spectroscopy, but no significant interaction with the SPIONs surface was detected. Having established that the chlorosulfonyl and the chloroacyl moieties are not able to directly bind the SPIONs surface, we decided to use the (*p*-chlorosulfonyl)phenyl isocyanate **8** and the (*p*-isocyanate)benzoyl chloride **9** as heterobifunctional linkers.

The reactivity of nanoconjugates **18** and **19** was then tested reacting them with *n*-butylamine, in order to form the corresponding sulfonamide and amide derivatives **27** and **28** respectively, as shown in *Scheme 6* and *Scheme 7*.

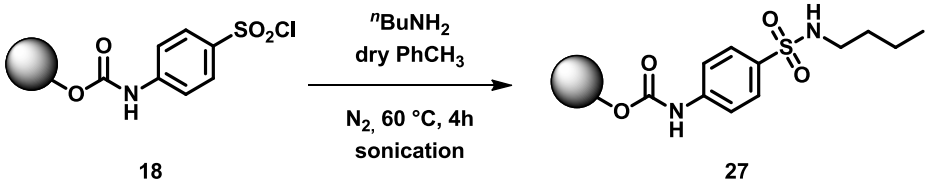

Scheme 6

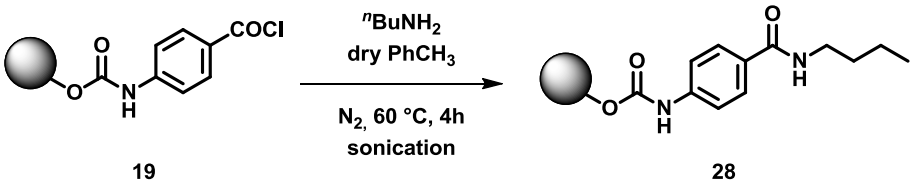

Scheme 7

E.A. and FTIR spectroscopy confirm the formation of the desired product, proving the possibility of use these systems as heterobifunctional linkers for the covalent binding of biomolecules onto SPIONs.

Concerning the nanoconjugate **20**, the maleimido group cannot interact itself with the nanoparticle surface, so it can be present as unreactive functional group during the grafting of the corresponding isocyanate **10**.

To check the reactivity of the maleimido group once anchored onto SPIONs, nanoconjugate **20** was first reacted with the commercially available 1-dodecanthiol (*Scheme 8*) and then with *N*-acetyl-cysteine (*N*-Ac-Cys-OH) as Michael donor (*Scheme 9*).

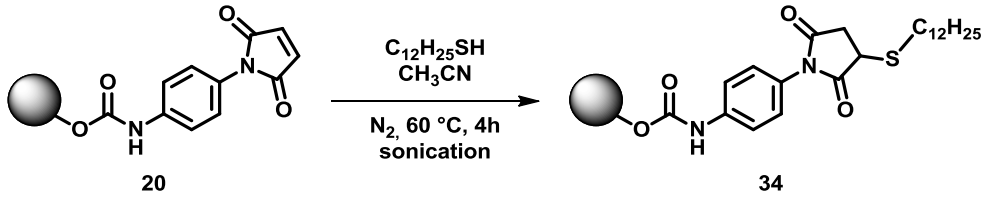

Scheme 8

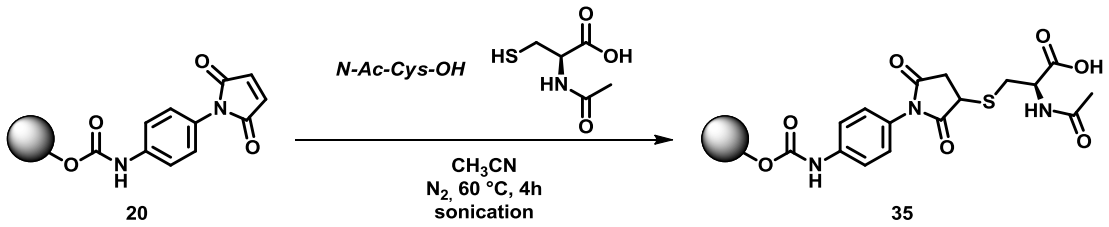

Scheme 9

Functionalized nanoparticles were isolated and characterized, confirming the formation of the desired nanoconjugate **34** and **35**.

Given the results obtained, we can conclude that isocyanate-based heterobifunctional linkers can be easily used for the supporting of organic molecules onto SPIONs. Nanoconjugates **18**-**20** have so proved to be good candidates for this purpose.

In our laboratories, one research field is the synthesis of Peptide Nucleic Acids (PNAs), that are mimics of natural oligonucleotides, in which each ribose phosphate unit is replaced by an aminoethylglycine ones (*aeg*PNA) (*Figure 9*). PNAs bind complementary DNA and RNA strands with excellent affinity. However, the first generation of PNAs suffers from some drawbacks, which hamper their full exploitation in gene therapy, including low cell uptake and some low solubility in physiological media. To overcome these problems, and to improve their physical-chemical properties, many modified PNAs have been synthesized in the last years following different strategies, one of which is to create new bionanoconjugates between SPIONs and PNAs for potential applications in diagnostic and therapy. In our laboratories several PNA-SPION conjugates have already been synthesized, using both passive *noncovalent adsorption* onto the outer particles surface by carboxylate

moiety and *covalent binding* exploiting the reactivity of siloxanes towards the nanoparticles (*Figure 10*).

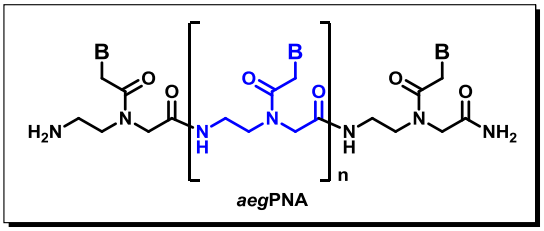

Figure 9 *- PNA oligomer (B: adenine, cytosine, guanine, thymine).*

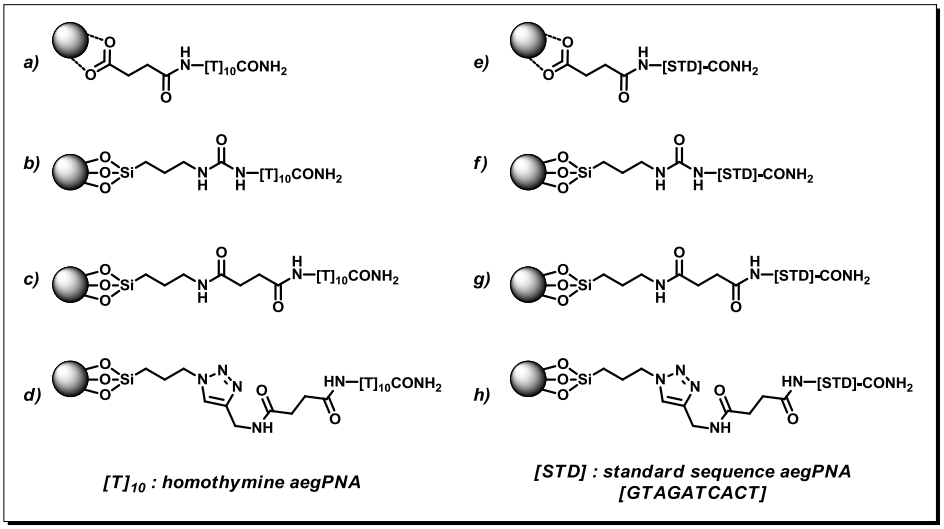

Figure 10 *- Library of SPION-PNA nanoconjugates that have been already synthesized in our laboratories ($[T]_{10}$: homothymine PNA 10-mer, [STD]: standard sequence PNA 10-mer).*

In this Ph.D. Thesis we decided to synthesize new fluorescent PNA nanoconjugates that combine the presence of a magnetic metallic core, PNA strands and a fluorescent probe.
For this purpose we synthesized the two new nanoconjugates **36** and **37**, reported in *Figure 11*, in which a homothymine and a standard sequence decamers were modified with a succinic linker at the *N*-terminus and with a lysine at the *C*-terminus. The free carboxylic moiety can be exploited to bind in a non-covalent interaction the SPION surface, while the *ε*-free amino group of the lysine residue can be used to bind the fluorescent probe, in this case the fluorescein isothiocyanate (FITC), leading to the formation of the corresponding thiourea (FITU).

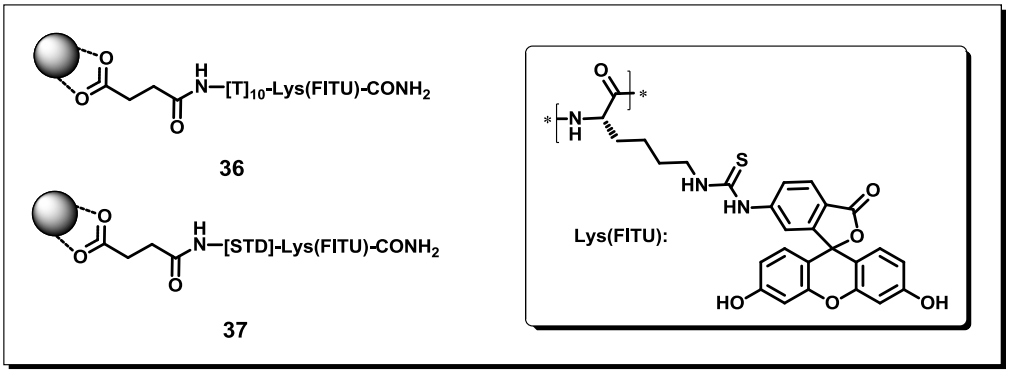

Figure 11 *- New fluorescent PNA nanoconjugates* **36** *and* **37***.*

Nanoconjugates **36** and **37** were isolated and characterized by E.A., FTIR and UV-Vis spectroscopy confirming the grafting of the fluorescent PNAs onto the nanoparticles surface. Furthermore, the ability of **36** and **37** to recognize and bind complementary DNA by the determination of the melting temperature ***Tm*** of the hybrids formed, were tested (*Figure 12* and *13*).

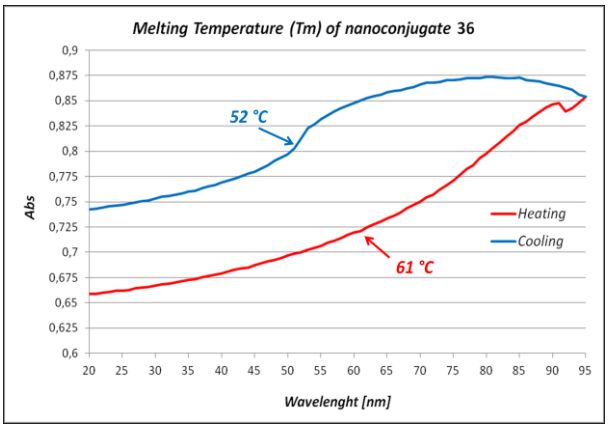

Figure 12

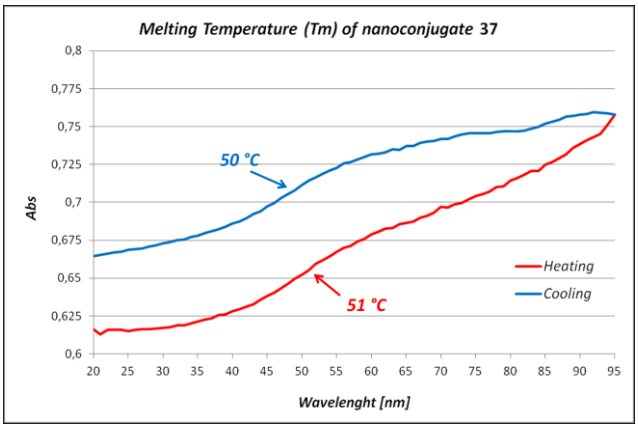

Figure 13

The ***Tm*** values obtained are very encouraging, if we consider that strong binding affinity were obtained regardless of the presence of a strong hydrophobic fluorescent probe and despite the anchoring onto SPIONs. (Reference homothymine PNA_2:DNA hybrid ***Tm***: 72 °C, reference standard sequence PNA:DNA hybrid ***Tm***: 53 °C). Similarly, the *N*-terminus cysteine modified homothymine and standard sequence PNA oligomers were supported onto functionalized nanoparticles **20**, in order to obtained the two new NCO-based SPION-PNA nanoconjugates **45** and **46** (*Figure 14*).

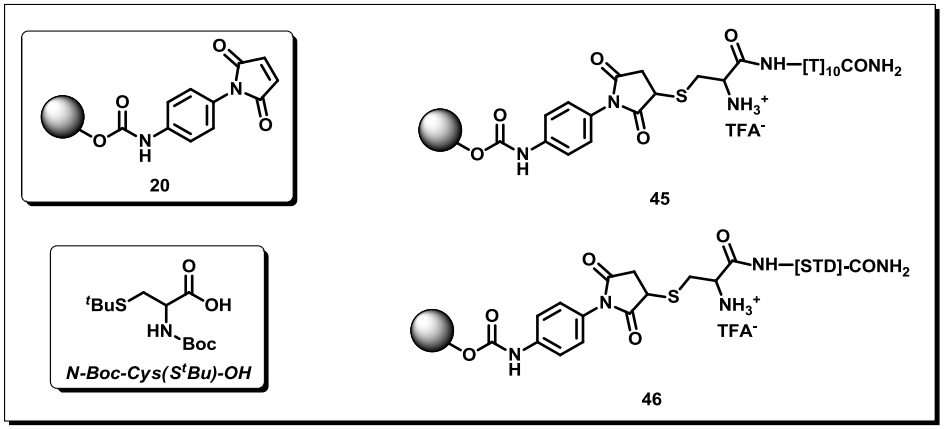

Figure 14 *- New NCO-based SPION-PNA nanoconjugates* **45** *and* **46***. Are also shown the structures of the starting functionalized nanoparticles* **20** *and of the N(α)-Boc-S-^{t}butylmercapto cysteine.*

The two new nanoconjugates **45** and **46** were isolated and characterized by E.A., FTIR and UV-Vis spectroscopy confirming, also in these cases, the grafting of the oligomers onto the nanoparticles surface. Furthermore, to check the ability of **45** and **46** to recognize and bind complementary DNAs, the melting temperature ***Tm*** of the hybrids formed were determined (*Figure 15* and *16*).

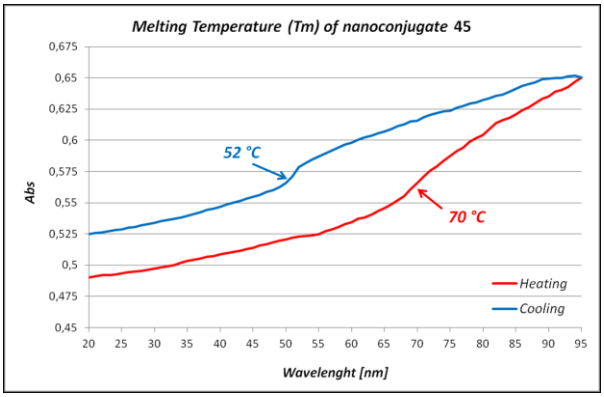

Figure 15

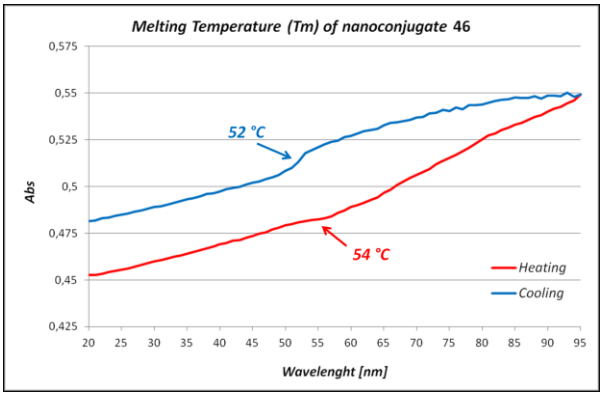

Figure 16

Also for these two new SPION-PNA nanoconjugates the hybridation experiments have confirmed the formation of the corresponding PNA_2:DNA and PNA:DNA hybrids, respectively. The ***Tm*** values obtained confirm the strong affinity binding capacity of these nanoconjugates towards the complementary DNAs, regardless of the presence of nanoparticles.

In conclusion, in this Ph.D. research work a systematic study concerning the surface modification of superparamagnetic iron oxide nanoparticles, is reported.
In particular, the discovery of a new covalent grafting methodology based on the reactivity of isocyanate group towards the surface hydroxyl groups of the nanoparticles, is reported.

In order to demonstrate this innovative anchoring system, a small library of isocyanate-base nanoconjugates has been synthesized (**15**-**20**). Analytical and spectroscopical characterizations helped us to point out the effective formation of a covalent carbamate-like bond between a generic isocyanate molecule and the SPIONs surface.
Some of the nanoconjugates bear different additional functional groups (**18**-**20**), that resulted to be stable in the grafting reaction conditions, while remains still reactive for the binding of other organic molecules (**27**, **28**, **34**, **35**).
Thus, properly functionalized isocyanates could be used as heterobifunctional linkers for the supporting of biomolecules onto SPIONs, opening new strategies for the synthesis of a new class of bionanoconjugates.
Furthermore, in this research work, four new SPION-PNA nanoconjugates have been designed and synthesized (**36**, **37**, **45**, **46**).
36 and **37** are characterized by the presence of a fluorescent probe and have been loaded onto the nanoparticle surface by a carboxylate-base non-covalent interaction, while **45** and **46** were obtained by a covalent C-S bond formation between the properly modified PNAs and the NCO-based functionalize SPIONs **20**. All these SPIONS-PNA nanoconjugates have shown a strong affinity binding towards the complementary DNA strands, regardless of the presence of the magnetic nanoparticles, thus opening the possibility to use these systems in theranostic fields.

We have also recently started a profitable collaboration with Prof. Seneci's research group of the Dept. of Chemistry, University of Milan, with the aim to support apoptosis inhibitors mimics onto SPIONs and to study their bioactivity. Biological studies will be performed in collaboration with the National Institute of Tumors (INT) in Milan. Only preliminary results were obtained and for this reason are not here reported.

INTRODUCTION

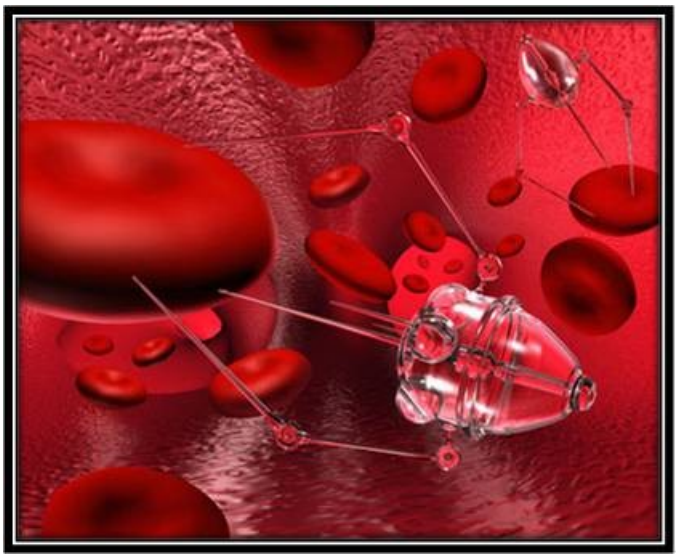

Chapter 1: Something about Nanotechnology

1 Nanotechnology

1.1 Some General Definition

Nanotechnology (sometimes shortened to "**nanotech**") is the manipulation of matter on an atomic and molecular scale. Generally, nanotechnology works with materials, devices, and other structures with at least one dimension sized from 1 to 100 nanometers. Quantum mechanical effects are important at this quantum-realm scale. With a variety of potential applications, nanotechnology is a key technology for the future and governments have invested billions of dollars in its research.

Nanotechnology is very diverse, ranging from extensions of conventional device physics to completely new approaches based upon molecular self-assembly, from developing new materials with dimensions on the nanoscale to direct control of matter on the atomic scale. Nanotechnology entails the application of fields of science as diverse as surface science,

organic chemistry, molecular biology, semiconductor physics, microfabrication, and many others.

Scientists debate the future implications of nanotechnology. Nanotechnology may be able to create many new materials and devices with a vast range of applications, such as in medicine, electronics, biomaterials and energy production. On the other hand, nanotechnology raises many of the same issues as any new technology, including concerns about the toxicity and environmental impact of nanomaterials,1 and their potential effects on global economics, as well as speculation about various doomsday scenarios. These concerns have led to a debate among advocacy groups and governments on whether special regulation of nanotechnology is warranted.

1.1.1 Origins

Although nanotechnology is a relatively recent development in scientific research, the development of its central concepts happened over a longer period of time. The emergence of nanotechnology in the 1980s was caused by the convergence of experimental advances such as the invention of the scanning tunneling microscope in 1981 and the discovery of fullerenes in 1985, with the elucidation and popularization of a conceptual framework for the goals of nanotechnology beginning with the 1986 publication of the book "*Engines of Creation*".

The scanning tunneling microscope, an instrument for imaging surfaces at the atomic level, was developed in 1981 by Gerd Binnig and Heinrich Rohrer at IBM Zurich Research Laboratory, for which they received the Nobel Prize in Physics in 1986.[2,3] Fullerenes were discovered in 1985 by Harry Kroto, Richard Smalley, and Robert Curl, who together won the 1996 Nobel Prize in Chemistry.[4,5]

Around the same time, K. Eric Drexler developed and popularized the concept of nanotechnology and founded the field of molecular nanotechnology. In 1979, Drexler encountered Richard Feynman's 1959 talk *"There's Plenty of Room at the Bottom"*. The term "nanotechnology", originally coined by Norio Taniguchi in 1974, was unknowingly appropriated by Drexler in his 1986 book "*Engines of Creation: The Coming Era of*

Nanotechnology", which proposed the idea of a nanoscale "assembler" which would be able to build a copy of itself and of other items of arbitrary complexity. He also first published the term "grey goo" to describe what might happen if a hypothetical self-replicating molecular nanotechnology went out of control.

In the early 2000s, the field was subject to growing public awareness and controversy, with prominent debates about both its potential implications, exemplified by the Royal Society's report on nanotechnology,[6] as well as the feasibility of the applications envisioned by advocates of molecular nanotechnology, which culminated in the public debate between Eric Drexler and Richard Smalley in 2001 and 2003.[7] Governments moved to promote and fund research into nanotechnology with programs such as the National Nanotechnology Initiative.

The early 2000s also saw the beginnings of commercial applications of nanotechnology, although these were limited to bulk applications of nanomaterials, such as the Silver Nanoplatform for using silver nanoparticles as an antibacterial agent, nanoparticle-based transparent sunscreens, and carbon nanotubes for stain-resistant textiles.[8,9]

1.1.2 Fundamental Concepts

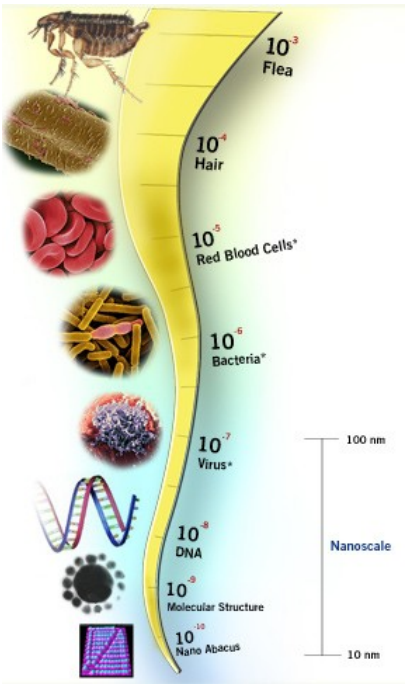

Figure 1

Nanotechnology is the engineering of functional systems at the molecular scale. This covers both current work and concepts that are more advanced. In its original sense, nanotechnology refers to the projected ability to construct items from the bottom up, using techniques and tools being developed today to make complete, high performance products.

One nanometer (nm) is one billionth, or 10^{-9}, of a meter. By comparison, typical carbon-carbon bond lengths, or the spacing between these atoms in a molecule, are in the range 0.12 – 0.15 nm, and a DNA double-helix has a

diameter around 2 nm *(Figure 1)*.

On the other hand, the smallest cellular life-forms, the bacteria of the genus Mycoplasma, are around 200 nm in length. By convention, nanotechnology is taken as the scale range 1 to 100 nm following the definition used by the National Nanotechnology Initiative in the US. The lower limit is set by the size of atoms (hydrogen has the smallest atoms, which are approximately a quarter of a nm diameter) since nanotechnology must build its devices from atoms and molecules. The upper limit is more or less arbitrary but is around the size that phenomena not observed in larger structures start to become apparent and can be made use of in the nano device.[10] These new phenomena make nanotechnology distinct from devices which are merely miniaturised versions of an equivalent macroscopic device; such devices are on a larger scale and come under the description of microtechnology.[11]

To put that scale in another context, the comparative size of a nanometer to a meter is the same as that of a marble to the size of the earth.[12] Or another way of putting it: a nanometer is the amount an average man's beard grows in the time it takes him to raise the razor to his face.[12]

Two main approaches are used in nanotechnology. In the *"bottom-up"* approach, materials and devices are built from molecular components which assemble themselves chemically by principles of molecular recognition. In the *"top-down"* approach, nano-objects are constructed from larger entities without atomic-level control.[13]

Areas of physics such as nanoelectronics, nanomechanics, nanophotonics and nanoionics have evolved during the last few decades to provide a basic scientific foundation of nanotechnology.

1.1.3 From Larger to Smaller: a Materials Perspective

Several phenomena become pronounced as the size of the system decreases. These include statistical mechanical effects, as well as quantum mechanical effects, for example the *"quantum size effect"* where the electronic properties of solids are altered with great reductions in particle size. This effect does not come into play by going from macro to micro

dimensions. However, quantum effects become dominant when the nanometer size range is reached, typically at distances of 100 nanometers or less, the so called quantum realm. Additionally, a number of physical (mechanical, electrical, optical, etc.) properties change when compared to macroscopic systems. One example is the increase in surface area to volume ratio altering mechanical, thermal and catalytic properties of materials. Diffusion and reactions at nanoscale, nanostructures materials and nanodevices with fast ion transport are generally referred to nanoionics. Mechanical properties of nanosystems are of interest in the nanomechanics research. The catalytic activity of nanomaterials also opens potential risks in their interaction with biomaterials.

Materials reduced to the nanoscale can show different properties compared to what they exhibit on a macroscale, enabling unique applications. For instance, opaque substances become transparent (copper); stable materials turn combustible (aluminum); insoluble materials become soluble (gold). A material such as gold, which is chemically inert at normal scales, can serve as a potent chemical catalyst at nanoscales. Much of the fascination with nanotechnology stems from these quantum and surface phenomena that matter exhibits at the nanoscale.[14]

1.1.4 From Simple to Complex: a Molecular Perspective

Modern synthetic chemistry has reached the point where it is possible to prepare small molecules to almost any structure. These methods are used today to manufacture a wide variety of useful chemicals such as pharmaceuticals or commercial polymers. This ability raises the question of extending this kind of control to the next-larger level, seeking methods to assemble these single molecules into supramolecular assemblies consisting of many molecules arranged in a well defined manner.

These approaches utilize the concepts of molecular self-assembly and/or supramolecular chemistry to automatically arrange themselves into some useful conformation through a bottom-up approach. The concept of molecular recognition is especially important: molecules can be designed so that a specific configuration or arrangement is favored due to non-covalent intermolecular forces. The Watson–Crick basepairing rules are a direct result of

this, as is the specificity of an enzyme being targeted to a single substrate, or the specific folding of the protein itself. Thus, two or more components can be designed to be complementary and mutually attractive so that they make a more complex and useful whole.

Such bottom-up approaches should be capable of producing devices in parallel and be much cheaper than top-down methods, but could potentially be overwhelmed as the size and complexity of the desired assembly increases. Most useful structures require complex and thermodynamically unlikely arrangements of atoms. Nevertheless, there are many examples of self-assembly based on molecular recognition in biology, most notably Watson–Crick basepairing and enzyme-substrate interactions. The challenge for nanotechnology is whether these principles can be used to engineer new constructs in addition to natural ones.

1.2 Social Implications

The Center for Responsible Nanotechnology warns of the broad societal implications of untraceable weapons of mass destruction, networked cameras for use by the government, and weapons developments fast enough to destabilize arms races.[15]

Another area of concern is the effect that industrial-scale manufacturing and use of nanomaterials would have on human health and the environment, as suggested by nanotoxicology research. For these reasons, groups such as the Center for Responsible Nanotechnology advocate that nanotechnology be regulated by governments. Others counter that overregulation would stifle scientific research and the development of beneficial innovations. Public health research agencies, such as the National Institute for Occupational Safety and Health are actively conducting research on potential health effects stemming from exposures to nanoparticles.[16]

Some nanoparticle products may have unintended consequences. Researchers have discovered that bacteriostatic silver nanoparticles used in socks to reduce foot odor are being released in the wash.[17] These particles are then flushed into the waste water stream

and may destroy bacteria which are critical components of natural ecosystems, farms, and waste treatment processes.[18]

Public deliberations on risk perception in the US and UK carried out by the Center for Nanotechnology in Society found that participants were more positive about nanotechnologies for energy applications than for health applications, with health applications raising moral and ethical dilemmas such as cost and availability.[19]

Experts, including director of the Woodrow Wilson Center's Project on Emerging Nanotechnologies David Rejeski, have testified[20] that successful commercialization depends on adequate oversight, risk research strategy, and public engagement. Berkeley (California) is currently the only city in the United States to regulate nanotechnology;[21] Cambridge (Massachusetts) in 2008 considered enacting a similar law,[22] but ultimately rejected it.[23] Relevant for both research on and application of nanotechnologies, the insurability of nanotechnology is contested.[24] Without state regulation of nanotechnology, the availability of private insurance for potential damages is seen as necessary to ensure that burdens are not socialized implicitly.

1.2.1 Regulation

Calls for tighter regulation of nanotechnology have occurred alongside a growing debate related to the human health and safety risks of nanotechnology.[25] There is significant debate about who is responsible for the regulation of nanotechnology. Some regulatory agencies currently cover some nanotechnology products and processes (to varying degrees) – by "bolting on" nanotechnology to existing regulations – there are clear gaps in these regimes.[26] Davies (2008) has proposed a regulatory road map describing steps to deal with these shortcomings.[27]

Stakeholders concerned by the lack of a regulatory framework to assess and control risks associated with the release of nanoparticles and nanotubes have drawn parallels with bovine spongiform encephalopathy ("mad cow" disease), thalidomide, genetically modified food,[28] nuclear energy, reproductive technologies, biotechnology, and asbestosis. Dr. Andrew Maynard, chief science advisor to the Woodrow Wilson Center's Project on

Emerging Nanotechnologies, concludes that there is insufficient funding for human health and safety research, and as a result there is currently limited understanding of the human health and safety risks associated with nanotechnology.[29] As a result, some academics have called for stricter application of the precautionary principle, with delayed marketing approval, enhanced labelling and additional safety data development requirements in relation to certain forms of nanotechnology.[30]

The Royal Society report[6] identified a risk of nanoparticles or nanotubes being released during disposal, destruction and recycling, and recommended that "manufacturers of products that fall under extended producer responsibility regimes such as end-of-life regulations publish procedures outlining how these materials will be managed to minimize possible human and environmental exposure". Reflecting the challenges for ensuring responsible life cycle regulation, the Institute for Food and Agricultural Standards has proposed that standards for nanotechnology research and development should be integrated across consumer, worker and environmental standards. They also propose that NGOs and other citizen groups play a meaningful role in the development of these standards.

The Center for Nanotechnology in Society has found that people respond differently to nanotechnologies based upon application – with participants in public deliberations more positive about nanotechnologies for energy than health applications – suggesting that any public calls for nano regulations may differ by technology sector.[19]

1.3 General fields of Nanotechnology Applications

With nanotechnology, a large set of materials and improved products rely on a change in the physical properties when the feature sizes are shrunk. Nanoparticles, for example, take advantage of their dramatically increased surface area to volume ratio. Their optical properties, e.g. fluorescence, become a function of the particle diameter. When brought into a bulk material, nanoparticles can strongly influence the mechanical properties of the material, like stiffness or elasticity. For example, traditional polymers can be reinforced by nanoparticles resulting in novel materials which can be used as lightweight replacements for

metals. Therefore, an increasing societal benefit of such nanoparticles can be expected. Such nanotechnologically enhanced materials will enable a weight reduction accompanied by an increase in stability and improved functionality. Practical nanotechnology is essentially the increasing ability to manipulate (with precision) matter on previously impossible scales, presenting possibilities which many could never have imagined - it therefore seems unsurprising that few areas of human technology are exempt from the benefits which nanotechnology could potentially bring. Some examples are now reported.

1.3.1 Medicine

The biological and medical research communities have exploited the unique properties of nanomaterials for various applications (*e.g.* contrast agents for cell imaging and therapeutics for treating cancer). Terms such as biomedical nanotechnology, nanobiotechnology, and nanomedicine are used to describe this hybrid field. Functionalities can be added to nanomaterials by interfacing them with biological molecules or structures. The size of nanomaterials is similar to that of most biological molecules and structures; therefore, nanomaterials can be useful for both in vivo and in vitro biomedical research and applications. Thus far, the integration of nanomaterials with biology has led to the development of diagnostic devices, contrast agents, analytical tools, physical therapy applications, and drug delivery vehicles.

1.3.1.1 Diagnostics

Nanotechnology-on-a-chip is one more dimension of lab-on-a-chip technology. Magnetic nanoparticles, bound to a suitable antibody, are used to label specific molecules, structures or microorganisms. Gold nanoparticles tagged with short segments of DNA can be used for detection of genetic sequence in a sample. Multicolor optical coding for biological assays has been achieved by embedding different-sized quantum dots into polymeric microbeads. Nanopore technology for analysis of nucleic acids converts strings of nucleotides directly into electronic signatures.

1.3.1.2 Drug Delivery

Nanotechnology has been a boon for the medical field by delivering drugs to specific cells using nanoparticles. The overall drug consumption and side-effects can be lowered significantly by depositing the active agent in the morbid region only and in no higher dose than needed. This highly selective approach reduces costs and human suffering. An example can be found in dendrimers and nanoporous materials. Another example is to use block co-polymers, which form micelles for drug encapsulation.[31] They could hold small drug molecules transporting them to the desired location. Another vision is based on small electromechanical systems; nanoelectromechanical systems are being investigated for the active release of drugs. Some potentially important applications include cancer treatment with iron nanoparticles or gold shells. A targeted or personalized medicine reduces the drug consumption and treatment expenses resulting in an overall societal benefit by reducing the costs to the public health system. Nanotechnology is also opening up new opportunities in implantable delivery systems, which are often preferable to the use of injectable drugs, because the latter frequently display first-order kinetics (the blood concentration goes up rapidly, but drops exponentially over time). This rapid rise may cause difficulties with toxicity, and drug efficacy can diminish as the drug concentration falls below the targeted range.

Buckyballs can "interrupt" the allergy/immune response by preventing mast cells (which cause allergic response) from releasing histamine into the blood and tissues, by binding to free radicals "dramatically better than any anti-oxidant currently available, such as vitamin E".[32]

1.3.1.3 Tissue Engineering

Nanotechnology can help reproduce or repair damaged tissue. “Tissue engineering” makes use of artificially stimulated cell proliferation by using suitable nanomaterial-based scaffolds and growth factors. For example, bones can be regrown on carbon nanotube scaffolds. Tissue engineering might replace today's conventional treatments like organ transplants or artificial implants. Advanced forms of tissue engineering may lead to life extension.

1.3.2 Energy

The most advanced nanotechnology projects related to energy are: storage, conversion, manufacturing improvements by reducing materials and process rates, energy saving (by better thermal insulation for example), and enhanced renewable energy sources.

1.3.2.1 Reduction of Energy Consumption

A reduction of energy consumption can be reached by better insulation systems, by the use of more efficient lighting or combustion systems, and by use of lighter and stronger materials in the transportation sector. Currently used light bulbs only convert approximately 5% of the electrical energy into light. Nanotechnological approaches like light-emitting diodes (LEDs) or quantum caged atoms (QCAs) could lead to a strong reduction of energy consumption for illumination.

1.3.2.2 Increasing of Efficiency of Energy Production

Today's best solar cells have layers of several different semiconductors stacked together to absorb light at different energies but they still only manage to use 40 percent of the Sun's energy. Commercially available solar cells have much lower efficiencies (15-20%). Nanotechnology could help increase the efficiency of light conversion by using nanostructures with a continuum of bandgaps.

The degree of efficiency of the internal combustion engine is about 30-40% at present. Nanotechnology could improve combustion by designing specific catalysts with maximized surface area. In 2005, scientists at the University of Toronto developed a spray-on nanoparticle substance that, when applied to a surface, instantly transforms it into a solar collector.

1.3.2.3 Nuclear Accident Cleanup and Waste Storage

Nanomaterials deployed by swarm robotics may be helpful for decontaminating a site of a nuclear accident which poses hazards to humans because of high levels of radiation and radioactive particles. Hot nuclear compounds such as corium (is a lava-like molten mixture of

portions of nuclear reactor core, formed during a nuclear meltdown, the most severe class of a nuclear reactor accident) or melting fuel rods may be contained in "bubbles" made from nanomaterials that are designed to isolate the harmful effects of nuclear activity occurring inside of them from the outside environment that organisms inhabit.

1.3.3 Information and Communication

Current high-technology production processes are based on traditional top down strategies, where nanotechnology has already been introduced silently. The critical length scale of integrated circuits is already at the nanoscale (50 nm and below) regarding the gate length of transistors in CPUs or DRAM devices.

1.3.3.1 Memory Storage

Electronic memory designs in the past have largely relied on the formation of transistors. However, research into crossbar switch based electronics have offered an alternative using reconfigurable interconnections between vertical and horizontal wiring arrays to create ultra high density memories. Two leaders in this area are Nantero which has developed a carbon nanotube based crossbar memory called Nano-RAM and Hewlett-Packard which has proposed the use of memristor material as a future replacement of Flash memory.

1.3.3.2 Novel Semiconductor Devices

An example of such novel devices is based on spintronics. The dependence of the resistance of a material (due to the spin of the electrons) on an external field is called magnetoresistance. This effect can be significantly amplified (GMR - Giant Magneto-Resistance) for nanosized objects, for example when two ferromagnetic layers are separated by a nonmagnetic layer, which is several nanometers thick (e.g. Co-Cu-Co). The GMR effect has led to a strong increase in the data storage density of hard disks and made the gigabyte range possible. The so called tunneling magnetoresistance (TMR) is very similar to GMR and based on the spin dependent tunneling of electrons through adjacent ferromagnetic layers. Both GMR and TMR effects can be used to create a non-volatile main memory for computers, such as the so called magnetic random access memory or MRAM.

In 1999, the ultimate CMOS transistor developed at the Laboratory for Electronics and Information Technology in Grenoble, France, tested the limits of the principles of the MOSFET transistor with a diameter of 18 nm (approximately 70 atoms placed side by side). This was almost one tenth the size of the smallest industrial transistor in 2003 (130 nm in 2003, 90 nm in 2004, 65 nm in 2005 and 45 nm in 2007). It enabled the theoretical integration of seven billion junctions on a €1 coin. However, the CMOS transistor, which was created in 1999, was not a simple research experiment to study how CMOS technology functions, but rather a demonstration of how this technology functions now that we ourselves are getting ever closer to working on a molecular scale. Today it would be impossible to master the coordinated assembly of a large number of these transistors on a circuit and it would also be impossible to create this on an industrial level.[33]

1.3.3.3 Novel Optoelectronic Devices

In the modern communication technology traditional analog electrical devices are increasingly replaced by optical or optoelectronic devices due to their enormous bandwidth and capacity, respectively. Two promising examples are photonic crystals and quantum dots. Photonic crystals are materials with a periodic variation in the refractive index with a lattice constant that is half the wavelength of the light used. They offer a selectable band gap for the propagation of a certain wavelength, thus they resemble a semiconductor, but for light or photons instead of electrons. Quantum dots are nanoscaled objects, which can be used, among many other things, for the construction of lasers. The advantage of a quantum dot laser over the traditional semiconductor laser is that their emitted wavelength depends on the diameter of the dot. Quantum dot lasers are cheaper and offer a higher beam quality than conventional laser diodes.

1.3.4 Heavy Industry

Nanotechnology has numerous potential applications in heavy industry.

1.3.4.1 Aerospace

Lighter and stronger materials will be of immense use to aircraft manufacturers, leading to increased performance. Spacecraft will also benefit, where weight is a major factor. Nanotechnology would help to reduce the size of equipment and thereby decrease fuel-consumption required to get it airborne.

Hang gliders may be able to halve their weight while increasing their strength and toughness through the use of nanotech materials. Nanotech is lowering the mass of supercapacitors that will increasingly be used to give power to assistive electrical motors for launching hang gliders off flatland to thermal-chasing altitudes.

Space operations can also benefit from the use of nanorobots, presented as single devices or forming swarms of larger sets. For the last option, nano-sized technology may be useful for polishing telescopes with a better accuracy than with existing methods, even in space, or for the exploration of extraterrestrial bodies, such as the Moon or Mars.

Space exploration can take leverage of nanorobotic swarms to study Earth's and outer bodies' atmosphere (when existing) or surface, providing more accurate information about their composition and distribution. For example, it may enhance our knowledge of the water distribution on the Moon's Poles, providing a better accuracy than the obtained with current methods, and thus enabling us a further exploration of the Moon, with the aim to place a future permanent base.

1.3.4.2 Catalysis

Chemical catalysis benefits especially from nanoparticles, due to the extremely large surface to volume ratio. The application potential of nanoparticles in catalysis ranges from fuel cell to catalytic converters and photocatalytic devices. Catalysis is also important for the production of chemicals.

The synthesis provides novel materials with tailored features and chemical properties: for example, nanoparticles with a distinct chemical surrounding (ligands), or specific optical properties. In this sense, chemistry is indeed a basic nanoscience. In a short-term

perspective, chemistry will provide novel "nanomaterials" and in the long run, superior processes such as "self-assembly" will enable energy and time preserving strategies. In a sense, all chemical synthesis can be understood in terms of nanotechnology, because of its ability to manufacture certain molecules. Thus, chemistry forms a base for nanotechnology providing tailor-made molecules, polymers, as well as clusters and nanoparticles.

Platinum nanoparticles are now being considered in the next generation of automotive catalytic converters because the very high surface area of nanoparticles could reduce the amount of platinum required.[34] However, some concerns have been raised due to experiments demonstrating that they will spontaneously combust if methane is mixed with the ambient air.[35] Ongoing research at the Centre National de la Recherche Scientifique (CNRS) in France may resolve their true usefulness for catalytic applications.[36] Nanofiltration may come to be an important application, although future research must be careful to investigate possible toxicity.[37]

References

[1] Cristina Buzea, Ivan Pacheco, and Kevin Robbie. "Nanomaterials and Nanoparticles: Sources and Toxicity". *Biointerphases* **2007**, *2(4)*, MR17–71.

[2] Binnig, G.; Rohrer, H. "Scanning tunneling microscopy". *IBM Journal of Research and Development* **1986**, *30*, *4*.

[3] "Press Release: the 1996 Nobel Prize in Physics". Nobelprize.org. 15 October 1986.

[4] Kroto, H.W.; Heath, J.R.; O'Brien, S.C.; Curl, R.F.; Smalley, R.E. "C60: Buckminsterfullerene". *Nature* **1986**, *318(6042)*, 162–163.

[5] Adams, W.; Baughman, R.H. "Retrospective: Richard E. Smalley (1943–2005)". *Science* **2005**, *310(5756)*, 1916.

[6] "Nanoscience and nanotechnologies: opportunities and uncertainties". Royal Society and Royal Academy of Engineering. **2004**.

[7] "Nanotechnology: Drexler and Smalley make the case for and against 'molecular assemblers'". *Chemical & Engineering News (American Chemical Society)* **2003** *81(48)*, 37–42.

[8] "Nanotechnology Information Center: Properties, Applications, Research, and Safety Guidelines". *American Elements* **2011**.

[9] "Analysis: This is the first publicly available on-line inventory of nanotechnology-based consumer products". *The Project on Emerging Nanotechnologies* **2008**.

[10] Allhoff, F.; Lin, P.; Moore, D. "What is nanotechnology and why does it matter?: from science to ethics". **2010**, John Wiley and Sons. pp. 3–5. ISBN 1-4051-7545-1.

[11] Prasad, S. K. "Modern Concepts in Nanotechnology". **2008**, Discovery Publishing House. pp. 31–32. ISBN 81-8356-296-5.

[12] Kahn, J. "Nanotechnology". *National Geographic* **2006**, 98–119.

[13] Rodgers, P. "Nanoelectronics: Single file". *Nature Nanotechnology* **2006**.

[14] Lubick, N.; Betts, K. "Silver socks have cloudy lining". *Environ Sci Technol* **2008**, *42(11)*, 3910.

[15] "Nanotechnology Basics".

[16] "CDC-Nanotechnology - NIOSH Workplace Safety and Health Topic". National Institute for Occupational Safety and Health, **2012**.

[17] Lubick, N. "Silver socks have cloudy lining", **2008**.

[18] Murray R.G.E., Advances in Bacterial Paracrystalline Surface Layers (Eds.: T. J. Beveridge, S. F. Koval). Plenum.

[19] Barbara Herr Harthorn, "People in the US and the UK show strong similarities in their attitudes toward nanotechnologies", Nanotechnology Today, **2009**.

[20] Testimony of David Rejeski for U.S. Senate Committee on Commerce, Science and Transportation Project on Emerging Nanotechnologies, **2008**.

[21] Berkeley considering need for nano safety (Rick DelVecchio, Chronicle Staff Writer), **2006**.

[22] Cambridge considers nanotech curbs – City may mimic Berkeley bylaws (By Hiawatha Bray, Boston Globe Staff), **2007**.

[23] Recommendations for a Municipal Health & Safety Policy for Nanomaterials: A Report to the Cambridge City Manager, **2008**.

[24] Encyclopedia of Nanoscience and Society, edited by David H. Guston, Sage Publications, **2010**; see Articles on Insurance and Reinsurance (by I. Lippert).

[25] Kevin Rollins (Nems Mems Works, LLC). "Nanobiotechnology Regulation: A Proposal for Self-Regulation with Limited Oversight", **2010**, *Volume 6 – Issue 2*.

[26] Bowman D, and Hodge G. "Nanotechnology: Mapping the Wild Regulatory Frontier". *Futures* **2006**, *38(9)*, 1060–1073.

[27] Davies, J.C. "Nanotechnology Oversight: An Agenda for the Next Administration", **2008**.

[28] Rowe, G.; Horlick-Jones, T.; Walls J.; Pidgeon, N. "Difficulties in evaluating public engagement initiatives: reflections on an evaluation of the UK GM Nation?". *Public Understanding of Science*. *14*, 333.

[29] Maynard, A. *"Testimony by Dr. Andrew Maynard for the U.S. House Committee on Science and Technology"*. **2008**.

[30] a)Faunce T.A. et al. "Sunscreen Safety: The Precautionary Principle, The Australian Therapeutic Goods Administration and Nanoparticles in Sunscreens Nanoethics" **2008,** 2, 231–240. b) Thomas Faunce & Katherine Murray & Hitoshi Nasu & Diana Bowman "Sunscreen Safety: The Precautionary Principle, The Australian Therapeutic Goods Administration and Nanoparticles in Sunscreens". Springer Science **2008**.

[31] University of Waterloo, Nanotechnology in Targeted Cancer Therapy, **2010**.

[32] Abraham, Sathya Achia. *"Researchers Develop Buckyballs to Fight Allergy"*. Virginia Commonwealth University Communications and Public Relations. **2010**.

[33] Waldner, J.B. *"Nanocomputers and Swarm Intelligence."* London: ISTE. **2007**, p. 26.

[34] Press Release: *"American Elements Announces P-Mite Line of Platinum Nanoparticles for Catalyst Applications"*, American Elements, 2007.

[35] "*Platinum nanoparticles bring spontaneous ignition"*, **2005**.

[36] "*Electrocatalytic oxidation of methanol"*, **2005**.

[37] *"Nanotechnology and the challenge of clean water."* Nature.com/naturenanotechonolgy. **2007**, *Volume 2*.

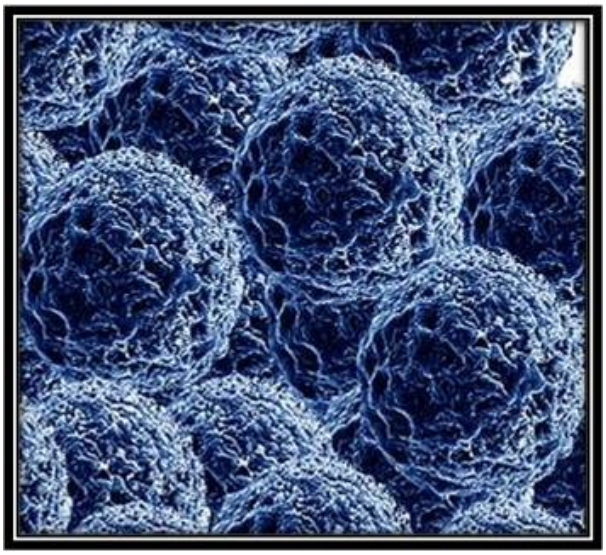

Chapter 2: Magnetic Nanoparticles, an Overview

2 Magnetic Nanoparticles

2.1 Nanoparticles

First of all, it is necessary to consider the general concepts related to the nanosized objects. A nanoobject is a physical object differing appreciably in properties from the corresponding bulk material and having at least 1 nm dimension (not more than 100 nm). When dealing with nanoparticles, magnetic properties (and other physical ones) are size dependent to a large extent. Therefore, particles whose sizes are comparable with (or lesser than) the sizes of magnetic domains in the corresponding bulk materials are the most interesting from a magnetism scientist viewpoint.

As introduced in the *Chapter 1*, nanotechnology is the technology dealing with both single nanoobjects and materials, and devices based on them, and with processes that take place in the nanometer range. Nanomaterials are those materials whose key physical

characteristics are dictated by the nanoobjects they contain. Nanomaterials are classified into compact materials and nanodispersions. The first type includes so-called nanostructured materials,[38] i.e., materials isotropic in the macroscopic composition and consisting of contacting nanometer-sized units as repeating structural elements.[39] Unlike nanostructured materials, nanodispersions include a homogeneous dispersion medium (vacuum, gas, liquid, or solid) and nanosized inclusions dispersed in this medium and isolated from each other. The distance between the nanoobjects in these dispersions can vary over broad limits from tens of nanometers to fractions of a nanometer. In the latter case, we are dealing with nanopowders whose grains are separated by thin (often monoatomic) layers of light atoms, which prevent them from agglomeration. Materials containing magnetic nanoparticles, isolated in nonmagnetic matrices at the distances longer than their diameters, are most interesting for magnetic investigations.

A ***nanoparticle*** (NP) is a quasi-zero-dimensional (OD) nanoobject in which all characteristic linear dimensions are of the same order of magnitude (not more than 100 nm).[40] Nanoparticles can basically differ in their properties from larger particles, for example, from long- and well-known ultradispersed powders with a grain size above 0.5 μm. As a rule, nanoparticles are shaped like spheroids.

Nanoparticles with a clearly ordered arrangement of atoms (or ions) are called nanocrystallites. Nanoparticles with a clear-cut discrete electronic energy levels are often referred to as "quantum dots" or "artificial atoms"; most often, they have compositions of typical semiconductor materials, but not always. Many magnetic nanoparticles have the same set of electronic levels.

Nanoparticles are of great scientific interest because they represent a bridge between bulk materials, molecules and structures at an atomic level. The term "cluster," which has been widely used in the chemical literature in previous years, is currently used to designate small nanoparticles with sizes less than 1 nm. Magnetic polynuclear coordination compounds (magnetic molecular clusters) belong to the special type of magnetic materials often with unique magnetic characteristics. Unlike nanoparticles, which always have the distributions in

sizes, molecular magnetic clusters are the fully identical small magnetic nanoparticles. Their magnetism is usually described in terms of exchange-modified paramagnetism.

Nanorods and nanowires, as shown in *Figure 2*, are quasi-one-dimensional (1D) nanoobjects. In these systems, one dimension exceeds by an order of magnitude the other two dimensions, which are in the nanorange.

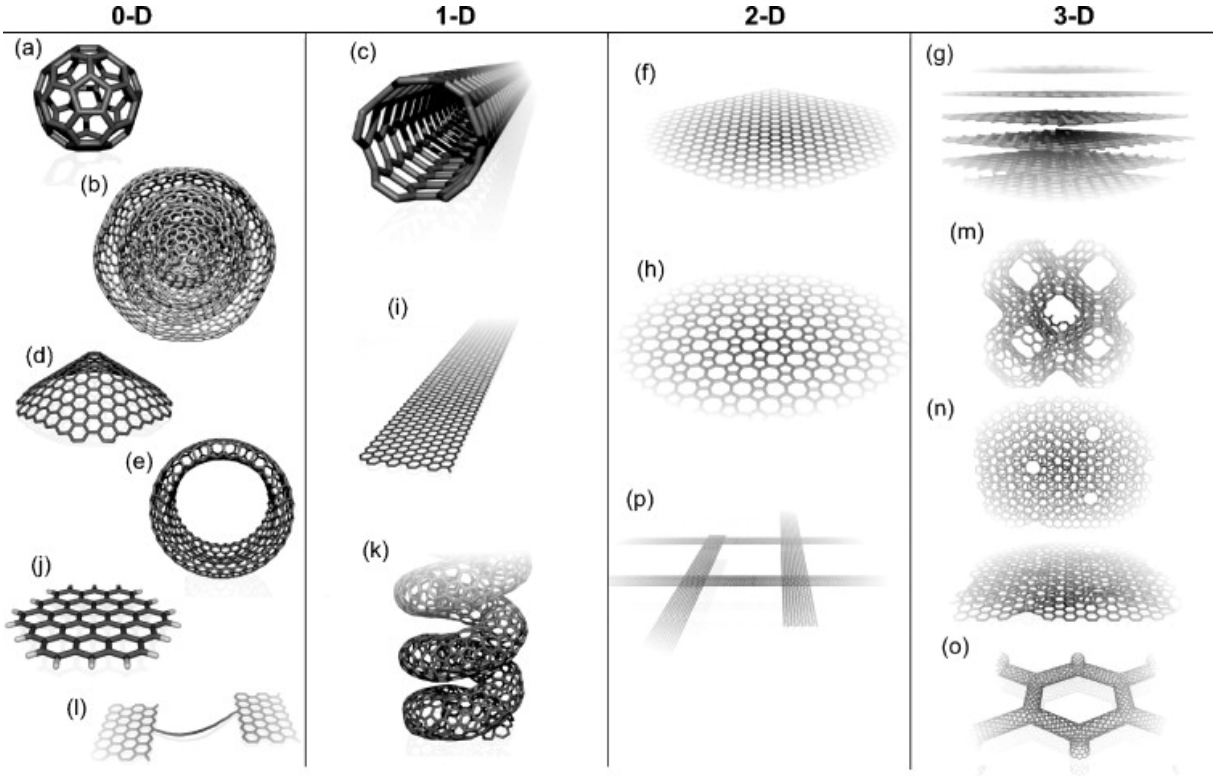

Figure 2 *- Molecular models of different types of sp^2-like hybridized carbon nanostructures exhibiting different dimensionalities, 0D, 1D, 2D and 3D: (a) C_{60}: Buckminsterfullerene; (b) nested giant fullerenes or graphitic onions; (c) carbon nanotube; (d) nanocones or nanohorns; (e) nanotoroids; (f) graphene surface; (g) 3D graphite crystal; (h) Haeckelite surface; (i) graphene nanoribbons; (j) graphene clusters; (k) helicoidal carbon nanotube; (l) short carbon chains; (m) 3D Schwarzite crystals; (n) carbon nanofoams (interconnected graphene surfaces with channels); (o) 3D nanotube networks, and (p) nanoribbons 2D networks.*

The group of two-dimensional objects (2D) includes planar structures nanodisks, thin-film magnetic structures, magnetic nanoparticle layers, etc., in which two dimensions are an order of magnitude greater than the third one, which is in the nanometer range.

The nanoparticles are considered by many authors as giant pseudomolecules having a core and a shell and often also external functional groups. The unique magnetic properties are usually inherent in the particles with a core size of 2-30 nm. For magnetic nanoparticles, this value coincides (or less) with the size of a magnetic domain in most bulk magnetic materials. Methods of synthesis and properties of nanoparticles were considered in this section and reports.[41]

2.2 Scope

Among many of known nanomaterials, the special position belong to those, in which isolated magnetic nanoparticles (magnetic molecular clusters) are divided by dielectric nonmagnetic medium. These nanoparticles present giant magnetic pseudoatoms with the huge overall magnetic moment and "collective spin." In this regard nanoparticles fundamentally differ from the classic magnetic materials with their domain structure. As a result of recent investigations, the new physics of magnetic phenomena - nanomagnetism - was developed. Nanomagnetism advances include superparamagnetism, ultrahigh magnetic anisotropy and coercive force, and giant magnetic resistance. The fundamental achievement of the last time became the development of the solution preparation of the objects with advanced magnetic parameters.

Currently, unique physical properties of nanoparticles are under intensive research.[42] A special place belongs to the magnetic properties in which the difference between a massive (bulk) material and a nanomaterial is especially pronounced. In particular, it was shown that magnetization (per atom) and the magnetic anisotropy of nanoparticles could be much greater than those of a bulk specimen, while differences in the Curie or Néel temperatures between nanoparticle and the corresponding microscopic phases reach hundreds of degrees. The magnetic properties of nanoparticles are determined by many factors, the key of these including the chemical composition, the type and the degree of defectiveness of the crystal lattice, the particle size and shape, the morphology (for structurally inhomogeneous particles), the interaction of the particle with the surrounding matrix and the neighboring particles. By changing the nanoparticle size, shape, composition, and structure, one can

control to an extent the magnetic characteristics of the material based on them. However, these factors cannot always be controlled during the synthesis of nanoparticles nearly equal in size and chemical composition; therefore, the properties of nanomaterials of the same type can be markedly different.

In addition, magnetic nanomaterials were found to possess a number of unusual properties, as giant magnetoresistance, abnormally high magnetocaloric effect, and so on.

Nanomagnetism usually considers so-called single-domain particles; typical values for the single-domain size range from 15 to 150 nm. However, recently the researchers focused their attention on the particles, whose sizes are smaller than the domain size range; a single particle of size comparable to the minimum domain size would not break up into domains; there is a reason to call these particles domain free magnetic nanoparticles (DFMN). Each such particle behaves like a giant paramagnetic atom and shows superparamagnetic behavior when the temperature is above the so-called blocking temperature. The experiment shows that the last one can vary in wide diapasons, from few kelvins till higher than room temperature.

It is important to mention that the intensity of interparticle interactions can dramatically affect the magnetic behavior of their macroscopic ensemble.

Nowadays it became possible to prepare individual nanometer metal or oxide particles not only as ferromagnetic fluids (whose preparation was developed back in the 1960s)[43] but also as single particles covered by ligands or as particles included into "rigid" matrices (polymers, zeolites, etc.).

The purpose of this section is to briefly survey the state-of-the-art views on physics, chemistry and methods of preparation and stabilization of magnetic nanoparticles used in nanotechnology for the design of new instruments and devices.

Some examples of the most important applications of magnetic nanoparticles are: ferrofluids for seals, bearings and dampers in cars and other machines, magnetic recording industry, magnetooptic recording devices and giant magnetoresistive devices. In recent

years, there has been an increasing interest to use magnetic nanoparticles in biomedical applications. Examples of the exciting and broad field of magnetic nanoparticles applications include drug delivery, contrast agents, magnetic hyperthermia, therapeutic *in vivo* applications of magnetic carriers, and *in vitro* magnetic separation and purification, molecular biology investigations, immunomagnetic methods in cell biology and cell separation and in pure medical applications.

2.3 Special Features of Magnetic Nanoparticles

Two key issues dominate the magnetic properties of nanoparticles: finite-size effects and surface effects which give rise to various special features, as summarized in *Figure 3*.[44]

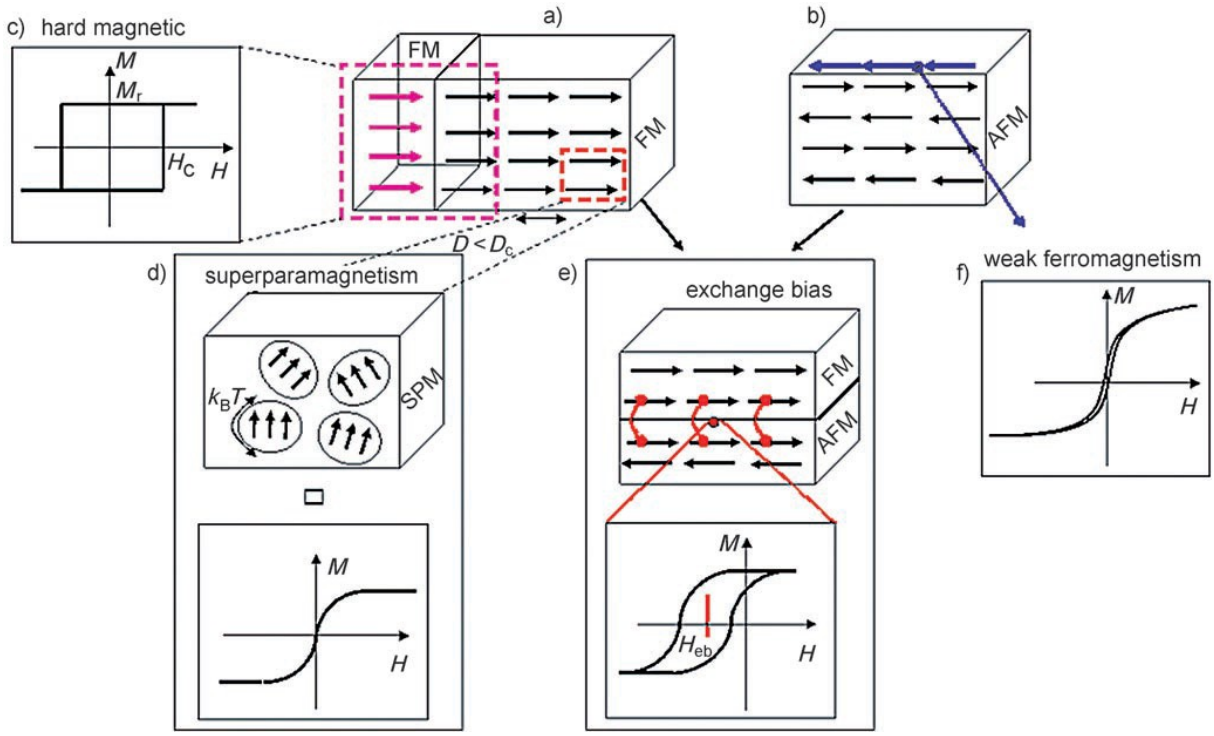

Figure 3 - *The different magnetic effects occurring in magnetic nanoparticles. The spin arrangement in a) a ferromagnet (FM) and b) an antiferromagnet (AFM); D=diameter, Dc=critical diameter. c) A combination of two different ferromagnetic phases (magenta arrows and black arrows in (a)) may be used for the creation of novel functional nanomaterials, for example, permanent magnets, which are materials with high remanence magnetization (M_r) and high coercivity (H_C), as shown schematically in the magnetization curve (c), d) An illustration of the magnetic moments in a superparamagnet (SPM). A superparamagnet is defined as an assembly of giant magnetic moments which are not interacting, and which can fluctuate when the thermal energy, k_BT, is larger than the anisotropy energy. Superparamagnetic particles exhibit no remanence or coercivity, that is, there is no hysteresis in the magnetization curve (d). e) The interaction (exchange coupling; linked red dots) at the interface*

between a ferromagnet and an antiferromagnet produces the exchange bias effect. In an exchange biased system, the hysteresis is shifted along the field axis (exchange bias field (H_{eb}))and the coercivity increases substantially. f) Pure antiferromagnetic nanoparticles could exhibit superparamagnetic relaxation as well as a net magnetization arising from uncompensated surface spins (blue arrows in (b)). This Figure, is a rather simplistic view of some phenomena present in small magnetic particles. In reality, a competition between the various effects will establish the overall magnetic behavior.

Finite-size effects result, for example, from the quantum confinement of the electrons, whereas typical surface effects are related to the symmetry breaking of the crystal structure at the boundary of each particle. Without attempting to be exhaustive, these two issues will be addressed in the next sections. More complete reviews on magnetism in nanoscale systems can be found elsewhere.[45]

2.3.1 Finite-Size Effect

The two most studied finite-size effects in nanoparticles are the singledomain limit and the superparamagnetic limit. In large magnetic particles, it is well known that there is a multidomain structure, where regions of uniform magnetization are separated by domain walls. The formation of the domain walls is a process driven by the balance between the magnetostatic energy (ΔE_{MS}), which increases proportionally to the volume of the materials and the domain-wall energy (E_{dw}), which increases proportionally to the interfacial area between domains. If the sample size is reduced, there is a critical volume below which it costs more energy to create a domain wall than to support the external magnetostatic energy (stray field) of the single-domain state. This critical diameter typically lies in the range of a few tens of nanometers and depends on the material. It is influenced by the contribution from various anisotropy energy terms. The critical diameter of a spherical particle, D_c, below which it exists in a single-domain state is reached when $\Delta E_{MS} = E_{dw}$, which implies that $D_c \approx 18\frac{\sqrt{A\,K_{eff}}}{\mu_0\,M^2}$, where A is the exchange constant, K_{eff} is anisotropy constant, μ_0 is the vacuum permeability, and M is the saturation magnetization.

A single-domain particle is uniformly magnetized with all the spins aligned in the same direction. The magnetization will be reversed by spin rotation since there are no domain walls to move. This is the reason for the very high coercivity observed in small nanoparticles.[46] Another source for the high coercivity in a system of small particles is the

shape anisotropy. The departure from sphericity for single-domain particles is significant and has an influence on the coercivity.[45b]

The second important phenomenon which takes place in nanoscale magnetic particles is the superparamagnetic limit. The superparamagnetism can be understood by considering the behavior of a well-isolated single-domain particle. The magnetic anisotropy energy per particle which is responsible for holding the magnetic moments along a certain direction can be expressed as follows: $E(\theta) = K_{eff}\, V \sin^2\theta$, where V is the particle volume, K_{eff} anisotropy constant and Θ is the angle between the magnetization and the easy axis. The energy barrier $K_{eff}\ V$ separates the two energetically equivalent easy directions of magnetization. With decreasing particle size, the thermal energy, $k_B\ T$, exceeds the energy barrier $K_{eff}\ V$ and the magnetization is easily flipped. For $k_B\ T > K_{eff}\ V$, the system behaves like a paramagnet, instead of atomic magnetic moments, there is now a giant (super)moment inside each particle (*Figure 3d*). This system is named a superparamagnet. Such a system has no hysteresis and the data of different temperatures superimpose onto a universal curve of *M* versus *H/T*. The relaxation time of the moment of a particle, τ, is given by the Néel-Brown expression reported below,[45b] where k^B is the Boltzmann's constant, and $\tau_0 \approx 10^{-9}$ s.

$$\tau = \tau_0 \exp\left(\frac{K_{eff} V}{k_B T}\right)$$

If the particle magnetic moment reverses at times shorter than the experimental time scales, the system is in a superparamagnetic state, if not, it is in the so-called blocked state. The temperature, which separates these two regimes, the so called ***blocking temperature***, $\boldsymbol{T_B}$, can be calculated by considering the time window of the measurement. The blocking temperature depends on the effective anisotropy constant, the size of the particles, the applied magnetic field, and the experimental measuring time. For example, if the blocking temperature is determined using a technique with a shorter time window, such as ferromagnetic resonance which has a $\tau \approx 10^{-9}$ s, a larger value of T_B is obtained than the value obtained from dc magnetization measurements. Moreover, a factor of two in particle diameter can change the reversal time from 100 years to 100 nanoseconds. While in the first

case the magnetism of the particles is stable, in the latter case the assembly of the particles has no remanence and is superparamagnetic.

Many techniques are available to measure the magnetic properties of an assembly of magnetic nanoparticles, as reported in the related references.[47]

2.3.1.1 Determination of the Blocking Temperature, T_B

A simple and rapid way to estimate the blocking temperature is provided by dc magnetometry measurements, in which a zero-field-cooled/field-cooled procedure is employed. Briefly, the sample is cooled from room temperature in zero magnetic field (ZFC) and in a magnetic field (FC). Then a small magnetic field is applied (about 100 Oe) and the magnetization is recorded on warming. As temperature increases, the thermal energy disturbs the system and more moments acquire the energy to be aligned with the external field direction. The number of unblocked, aligned moments reaches a maximum at T_B. Above the blocking temperature the thermal energy is strong enough to randomize the magnetic moments leading to a decrease in magnetization. A distribution of the particle sizes results in a distribution of the blocking temperatures. As pointed out already, the above discussion about the time evolution of the magnetization only holds for particles with one single domain. Taking into account the magnetic interactions between nanoparticles which have a strong influence on the superparamagnetic relaxation, the behavior of the system becomes more complicated. The main types of magnetic interactions which can be present in a system of small particles are: a) dipole– dipole interactions, b) direct exchange interactions for touching particles, c) superexchange interactions for metal particles in an insulating matrix, d) RKKY (Ruderman-Kittel-Kasuya-Yosdida) interactions for metallic particles embedded in a metallic matrix.[45a] Dipolar interactions are almost always present in a magnetic particle system and are typically the most relevant interactions. They are of long-range character and are anisotropic. From an experimental point of view, the problem of interparticle interactions is very complex. First, it is very complicated to separate the effects of interactions from the effects caused by the random distributions of sizes, shapes, and anisotropy axes. Second, several interactions can be present simultaneously in one sample.

This situation makes it even more complicated to assign the observed properties to specific interactions.

2.3.2 Surface Effect

As the particles size decreases, a large percentage of all the atoms in a nanoparticle are surface atoms, which implies that surface and interface effects become more important. For example, for face-centered cubic (fcc) cobalt with a diameter of around 1.6 nm, about 60% of the total number of spins are surface spins.[45a] Owing to this large surface atoms/bulk atoms ratio, the surface spins make an important contribution to the magnetization. This local breaking of the symmetry might lead to changes in the band structure, lattice constant or/and atom coordination. Under these conditions, some surface and/or interface related effects occur, such as surface anisotropy and, under certain conditions, core–surface exchange anisotropy can occur.

2.3.2.1 No or Magnetically Inert Surface Coatings

Surface effects can lead to a decrease of the magnetization of small particles, for instance oxide nanoparticles, with respect to the bulk value. This reduction has been associated with different mechanisms, such as the existence of a magnetically dead layer on the particle's surface, the existence of canted spins, or the existence of a spin-glass-like behavior of the surface spins.[48] On the other hand, for small metallic nanoparticles, for example cobalt, an enhancement of the magnetic moment with decreasing size was reported as well.[49] Respaud *et al.* associated this result with a high surface-to-volume ratio, however, without more detailed explanation. Another surface-driven effect is the enhancement of the magnetic anisotropy, K_{eff} with decreasing particle size.[49,50] This anisotropy value can exceed the value obtained from the crystalline and shape anisotropy and is assumed to originate from the surface anisotropy. In a very simple approximation, the anisotropy energy of a spherical particle with diameter *D*, surface area *S*, and volume *V*, may be described by one contribution from the bulk and another from the surface: $K_{eff} = K_V + \frac{6}{D}K_S$, where K_V e K_S are the bulk and surface anisotropy energy constants, respectively. Bøder *et al.*[50] have shown that K_{eff} changes when the surfaces are modified or adsorb different molecules,

which explains very well the contribution of the surface anisotropy to K_{eff}. For uncoated antiferromagnetic nanoparticles, weak ferromagnetism can occur at low temperatures (*Figure 3f*), which has been attributed to the existence of uncompensated surface spins of the antiferromagnet.[51] Since this situation effectively corresponds to the presence of a ferromagnet in close proximity to an antiferromagnet, additional effects, such as exchange bias, can result. However, only in some cases can a clear correlation between the surface coating and the magnetic properties be established. For example, a silica coating is used to tune the magnetic properties of nanoparticles, since the extent of dipolar coupling is related to the distance between particles and this in turn depends on the thickness of the inert silica shell.[52] A thin silica layer will separate the particles, thereby preventing a cooperative switching which is desirable in magnetic storage data. In other cases, the effect of the coating is less clear. A precious-metal layer around the magnetic nanoparticles will have an influence on the magnetic properties. For example, it was shown that gold-coated cobalt nanoparticles have a lower magnetic anisotropy than uncoated particles, whereas gold coating of iron particles enhances the anisotropy, an effect which was attributed to alloy formation with the gold.[53] Hormes *et al.* also discussed the influence of various coatings (e.g., Cu, Au) on the magnetic properties of cobalt nanoparticles, and came to the conclusion that a complex interplay between particle core and coating determines the properties, and tuning may therefore be difficult.[54]

Organic ligands, used to stabilize the magnetic nanoparticles, also have an influence on their magnetic properties, that is, ligands can modify the anisotropy and magnetic moment of the metal atoms located at the surface of the particles.[53] As Paulus and co-workers reported, cobalt colloidal particles stabilized with organic ligands show a reduction of the magnetic moment and a large anisotropy.[53] Leeuwen *et al.* proposed that surface-bonded ligands lead to the quenching of the surface magnetic moments, resulting in the reduction of magnetization.[55] In the case of nickel nanoparticles, Cordente *et al.* have demonstrated that donor ligands, such as amines, do not alter the surface magnetism but promote the formation of rods, whereas the use of trioctylphosphine oxide leads to a reduction in the magnetization of the particles.[56] Overall, it must be concluded that the magnetic response of

a system to an inert coating is rather complex and system specific, so that no firm correlations can be established at present.

2.3.2.2 Magnetic Coatings for Magnetic Nanoparticles

A magnetic coating on a magnetic nanoparticle usually has a dramatic influence on the magnetic properties. The combination of two different magnetic phases will lead to new magnetic nanocomposites, with many possible applications. The most striking feature which takes place when two magnetic phases are in close contact is the exchange bias effect. A recent review of exchange bias in nanostructured systems is given by Nogués *et al.*[57]

The exchange coupling across the interface between a ferromagnetic core and an antiferromagnetic shell or *vice versa*, causes this effect. Exchange bias is the shift of the hysteresis loop along the field axis in systems with ferromagnetic (FM)–antiferromagnetic (AFM) interfaces (*Figure 3e*). This shift is induced by a unidirectional exchange anisotropy created when the system is cooled below the Néel temperature of the antiferromagnet. This exchange coupling can provide an extra source of anisotropy leading to magnetization stabilization. The exchange bias effect was measured for the first time in cobalt nanoparticles surrounded by an antiferromagnetic CoO layer. There are numerous systems where the exchange bias has been observed, and some of the most investigated systems are: ferromagnetic nanoparticles coated with their antiferromagnetic oxides (e. g., Co/CoO, Ni/NiO), nitrides (Fe–Fe_2N), and sulfides (Fe–FeS), ferrimagnetic–antiferromagnetic (Fe_3O_4–CoO), or ferrimagnetic–ferromagnetic (TbCo–$Fe_{20}Ni_{80}$) nanoparticles.

Recently, single-domain pure antiferromagnetic nanoparticles have shown an exchange-bias effect arising from uncompensated spins on the surface. This reveals a complicated surface spin structure which is responsible for the occurrence of a weak ferromagnetism (*Figure 3f*), the exchange bias effect, and the so-called training effect.[58] The training effect represents a reduction of the exchange bias field upon subsequent field cycling. Metallic particles embedded in a matrix are interesting systems of magnetic-coated particles. Skumryev *et al*. have demonstrated the role of the matrix in establishing the magnetic response of small particles.[59] The magnetic behavior of the isolated 4 nm Co particles with a CoO shell changes

dramatically when, instead of being embedded in a paramagnetic matrix, they are embedded in an antiferromagnetic matrix. The blocking temperature of Co particles embedded in an Al_2O_3 or C matrix was around 10 K, but by putting them in a CoO matrix, they remain ferromagnetic up to 290 K. Thus, the coupling of the ferromagnetic particles with an antiferromagnetic matrix is a source of a large additional anisotropy.

Exchange biased nanostructures have found applications in many fields, such as permanent magnets (*Figure 3c*), recording media, and spintronics. A new approach to produce high-performance permanent magnets is the combination of a soft magnetic phase (easily magnetized), such as Fe_3Pt, and a hard magnetic phase (difficult to magnetize and thus having high coercivity), such as Fe_3O_4 which interact through magnetic exchange coupling.[60]

The right choice of ferromagnetic and antiferromagnetic components can provide a structure suitable for use as a recording medium. The exchange coupling can supply the extra anisotropy which is needed for magnetization stabilization, thus generating magnetically stable particles. Another interesting aspect related to a magnetic coating is given by the bimagnetic core–shell structure, where both the core and the shell, are strongly magnetic (e. g., $FePt/CoFe_2O_4$).[61] These bimagnetic core–shell nanoparticles will allow a precise tailoring of the magnetic properties through tuning the dimensions of the core and shell, which selectively controls the anisotropy and the magnetization.

Some important aspects should be emphasized. The magnetic behavior of an assembly of nanoparticles is a result of both the intrinsic properties of the particles and the interactions among them. The distribution of the sizes, shapes, surface defects, and phase purity are only a few of the parameters influencing the magnetic properties, which makes the investigation of the magnetism in small particles very complicated. One of the great challenges remains the manufacturing of an assembly of monodisperse particles, with well-defined shape, a controlled composition, ideal chemical stability, tunable interparticle separations, and a functionalizable surface. Such particles will tremendously facilitate the discrimination between finite-size effects, interparticle interactions, and surface effects. Thus, the synthesis of magnetic nanoparticles with well-controlled characteristics is a very important task sections.

2.4 The Most Extensively Studied Magnetic Nanoparticles and Their Preparation

A series of general methods for the nanoparticle synthesis have now been developed.[44,62] Most of them can also be used for the preparation of magnetic particles. An essential feature of their synthesis is the preparation of particles of a specified size and shape; at least, the dispersity should be small and controllable, since the blocking temperature (and other magnetic characteristics) depends on the particle size. The shape control and the possibility of synthesis of anisotropic magnetic structures are especially important. In order to eliminate (or substantially decrease) the interparticle interactions, magnetic nanoparticles often need to be isolated from one another by immobilization on a substrate surface or in the bulk of a stabilizing matrix or by surfacing with long chain ligands. It is important that the distance between the particles in the matrix should be controllable. Finally, the synthetic procedure should be relatively simple, inexpensive and reproducible.

The physical characteristics of nanoparticles are known to be substantially dependent on their dimensions. Unfortunately, most of the currently known methods of synthesis afford nanoparticles with rather broad size distributions (dispersion > 10%). The thorough control of reaction parameters (time, temperature, stirring velocity, and concentrations of reactants and stabilizing ligands) does not always allow one to narrow down this distribution to the required range. Therefore, together with the development of methods for synthesis of nanoparticles with a narrow size distribution, the techniques of separation of nanoparticles into rather monodisperse fractions are perfected. This is done using controlled precipitation of particles from surfactant-stabilized solutions followed by centrifugation. The process is repeated until nanoparticle fractions with specified sizes and dispersion degrees are obtained.

The methods of nanoparticle preparation cannot be detached from stabilization methods. For 1-10 nm particles with a high surface energy, it is difficult to select a really inert medium,[63] because the surface of each nanoparticle bears the products of its chemical modification, which affect appreciably the nanomaterial properties. This is especially

important for magnetic nanoparticles in which the modified surface layer may possess magnetic characteristics markedly differing from those of the particle core. Nevertheless, the generaI methods for nanoparticle synthesis are not related directly to the stabilization and the special methods exist where the nanoparticle formation is accompanied by stabilization (in matrices, by encapsulation, etc.).

Among a wide range of the magnetic nanomaterials, nanoparticles of magnetic metals, simple and complex magnetic oxides, and alloys may be separated for detailed analysis.

2.4.1 Metals

The metallic nanoparticles have larger magnetization compared to metal oxides, which is interesting for many applications. But metallic magnetic nanoparticles are not air stable, and are easily oxidized, resulting in the change or loss (fully or partially) of their magnetization.

2.4.1.1 Iron (Fe)

Iron is a ferromagnetic material with high magnetic moment density (about 220 emu/g) and is magnetically soft. Iron nanoparticles in the size range below 20 nm are superparamagnetic.

Procedures leading to monodisperse Fe nanoparticles have been well documented.[64] Nevertheless, the preparation of nanoparticles consisting of pure iron is a complicated task, because they often contain oxides, carbides and other impurities. A sample containing pure iron as nanoparticles (10.5 nm) can be obtained by evaporation of the metal in an argon atmosphere followed by deposition on a substrate.[65] When evaporation took place in a helium atmosphere, the particle size varied in the range of 10-20 nm.[66] Relatively small (100-500 atoms) Fe nanoparticles are formed in the gas phase on laser vaporization of pure iron.[67]

The common chemical methods used for the preparations include thermal decomposition of $Fe(CO)_5$ (the particles so prepared are extremely reactive), reductive decomposition of some iron(II) salts, or reduction of iron(III) acetylacetonate; there is a chemical reduction with TOPO capping (TOPO: trioctylphosphine oxide).[68]

The method of reducing metal salts by $NaBH_4$ has been widely used to synthesize iron-containing nanoparticles in organic solvents.[69] Normally, reductive synthesis of Fe nanoparticles in an aqueous solution with $NaBH_4$ yields a mixture including FeB.[70] Well-dispersed colloidal iron is required for applications in biological systems such as MRI contrast enhancement and biomaterials separation. Nevertheless, the syntheses have as yet a difficulty in producing stable Fe nanoparticle dispersions, especially aqueous dispersions, for potential biomedical applications.

To prevent the iron nanoparticles from agglomerating, dispersing agents were added during synthesis, as a rule poly(vinylpyrolidone) (PVP). The size dispersion of the nanoparticles produced using physical methods is broader than that in nanoparticles synthesized by chemical methods like reverse micelle, coprecipitation, etc. However, chemical methods yield as a rule only limited quantities of materials.

2.4.1.2 Cobalt (Co)

Co nanoparticles depending upon the synthetic route are observed in at least three crystallographic phases: typical for bulk Co hcp, 8-CO cubic,[71] or multiply twinned fcc-based icosahedral.[72] Conditions of synthesis reactions is influence on the final product structure; in rare cases of the determined phase nanoparticles can be obtained. Often a size and phase selection was required to obtain Co nanocrystals with a specific size and even shape. Methods for the synthesis and magnetic properties of cobalt nanoparticles' different structures have been described in detail in a review.[8c]

A popular approach is to synthesize colloidal particles by inversed micelle synthesis; the inverse micelles are defined as a microreactor.[73] In order to obtain stable cobalt nanoparticles with a narrow size distribution, $Co(AOT)_2$ reverse micelles are used (AOT: Aerosol OT, better known as dioctyl sodium sulfosuccinate); their reduction is obtained by using $NaBH_4$ as a reducing agent. Such particles are stabilized by surfactants and are often monodispersed in size, but are also unstable unless kept in a solution. Nevertheless, the chemical surface treatment by lauric acid highly improves the stability and cobalt nanoparticles could be stored without aggregation or oxidation for at least one week.[74] In

many instances it is possible to obtain Co nanoparticles coated by other ligands, which can be either dispersed in a solvent or deposited on a substrate; in the latter case, self-organized monolayers having a hexagonal structure can be obtained.

In some instances of reduction with $NaBH_4$ it is possible to obtain Co- B nanoparticles. The size, composition, and structure of this kind of nanoparticles strongly depend on the concentration of the solution, pH, and the mixing procedure.[75] It is well known that the presence of oxides in magnetic materials, which form spontaneously when the metallic surface is in contact with oxygen, drastically changes the magnetic behavior of the particles. An enhanced magnetoresistance, arising from the uniform Co core size and CoO shell thickness, has been reported.[76] This effect is caused by the strong exchange coupling between the ferromagnetic Co core and the antiferromagnetic CoO layer. However, up to now the understanding of this effect has not been well understood.

2.4.1.3 Nickel (Ni)

In contrast to cobalt and iron, relatively few reports have been dealing with the physical properties and synthesis of nickel particles. However, the nanosized ferromagnetic Ni is also being widely studied as it presents both an interest for fundamental sciences and an interest for applications such as magnetic storage, ferrofluids, medical diagnosis, multilayer capacitors and especially catalysis. Because these properties and applications can be tuned by manipulating the size and structure of the particles, the development of flexible and precise synthetic routes has been an active area of research. A wide variety of techniques have been used to produce nickel nanoparticles: thermal decomposition,[77] sol-gel,[78] spray pyrolysis,[79] sputtering,[80] and high-energy ball milling[81]. The organometallic precursors such as $Ni(CO)_4$, $Ni(COD)_2$, and $Ni(Cp)_2$ have also been used for the synthesis and spectroscopic studies of nickel nanoparticles.[82,83] At present, Ni nanoparticles are generally prepared by microemulsion techniques, using cetyltrimethylammonium bromide (CTAB)[84] or by reduction of Ni ions in the presence of alkyl amines or TOPO.[85] Some authors showed that the surface of Ni-nanoparticles was readily oxidized to NiO. On the basis of this discovery, they envisioned that the synthesis of large-sized Ni nanoparticles and their subsequent oxidation would provide an NiO shell having high affinity for biomolecules.

2.4.2 Nanoparticles of Rare Earth Metals

Six of the nine rare earth elements (REE) are ferromagnetic. The magnetic nanomaterials based on these REE occupy a special place, as they can be used in magnetic cooling systems.[86] However, REE nanoparticles (of both metals and oxides) are still represented by only a few examples, most of all, due to the high chemical activity of highly dispersed REE. A synthesis of coarse (95 x 280 nm) spindle-shaped ferromagnetic EuO nanocrystals suitable for the design of optomagnetic materials has been reported.[87] The EuS nanocrystals were prepared by passing H_2S through a solution of europium in liquid ammonia.[88] The size of the EuS magnetic nanoparticles formed can be controlled (to within 20-36 nm) by varying the amount of pyridine added to the reaction medium.[88]

Gadolinium nanoparticles (12 nm) were prepared by reduction of gadolinium chloride by Na metal in THF. They proved to be extremely reactive and pyrophoric, which, however, did not prevent characterization of these particles and measuring their magnetic parameters.[89] The Gd, Dy, and Tb nanoparticles with an average size of 1.5-2.1 nm and an about 20 degree of dispersion were obtained in a titanium matrix by ion beam sputtering.[90]

2.4.3 Magnetic Alloys

2.4.3.1 Fe-Co Alloy

It is known that Co and Fe form a body-centered-cubic solid solution (CO_xFe_{100-x}) over an extensive range. The ordered Co-Fe alloys are excellent soft magnetic materials with negligible magnetocrystalline anisotropy.[91] The saturation magnetization of Fe-Co alloys reaches a maximum at a Co content of 35 at%; other magnetic characteristics of these metals also increase when they are mixed. Therefore, FeCo nanoparticles attract considerable attention. Thus Fe, Co, and Fe-Co (20 at%, 40 at%, 60 at%, 80 at%) nanoparticles (40-51 nm) with a structure similar to the corresponding bulk phases have been prepared in a stream of hydrogen plasma.[92] The Fe-Co particles reach a maximum saturation magnetization at 40 at% of Co, and a maximum coercive force is attained at 80 at% of Co. Chemical reduction by $NaBH_4$ is also used for the preparation of FeCo

nanoparticles.[93] X-ray data show that the ratio of Co to Fe is around 30: 70 in the prepared nanoparticles.

2.4.3.2 Fe-Ni Alloy

The bulk samples of the iron-nickel alloys are either nonmagnetic or magnetically soft ferromagnets (for example, permalloys containing >30 of Ni and various doping additives). The Fe-Ni nanoparticles have a much lower saturation magnetization than the corresponding bulk samples over the whole concentration range.[94] An alloy containing 37 of Ni has a low Curie point and an fcc structure. It consists of nanoparticles (12-80 nm) superparamagnetic over a broad temperature range.[95] Theoretical calculations predict a complex magnetic structure for these Fe-Ni particles.[96]

2.4.3.3 Fe-Pt Alloy

Nanoparticles of this composition have received much attention in recent years due to the prospects for a substantial increase in the information recording density for materials based on them.[97] The face-centered tetragonal (fct) (also known as L10 phase) Fe-Pt alloy possesses a very high uniaxial magnetocrystalline anisotropy of ca. 6 x 10^6 J/m^3, which is more than 10 times as high as that of the currently utilized CoCr-based alloys and, thus, exhibit large coercivity at room temperature, even when their size is as small as several nanometers.[98] These unique properties make them possible candidates for the next generation of magnetic storage media and high-performance permanent magnets.[99] To realize these potentials it is important to develop synthetic methods that yield magnetic nanoparticles of tunable size, shape, dispersity and composition. For these syntheses the most commonly used is the thermal decomposition of organometallic precursors or reduction of metal salts in the presence of long-chain acid or amine and phosphine or phosphine oxide ligands.[100] The as-synthesized FePt nanoparticles possess an fcc structure and are superparamagnetic at room temperature.

The FePt nanoparticles (6 nm) with a narrow size distribution were prepared by joint thermolysis of $Fe(CO)_5$ and $Pt(acac)_2$ in the presence of oleic acid and oleylamine. Further heating resulted in the formation of a protective film from the products of thermal

decomposition of the surfactant on the nanoparticle surface, which does not change significantly the particle size. These particles can be arranged to form regular films and so-called colloid crystals. For many practical applications, magnetic nanoparticles larger than 6 nm are preferred because coercivity and the saturation magnetization of the nanoparticles are closely related to the size of magnetic nanoparticles.[101] Later it has been however found that most FePt nanoparticles have the broad composition distribution: approximately 40 and 30 of the nanoparticles were Pt-rich and Fe-rich, respectively.

2.4.4 Magnetic Oxides

2.4.4.1 Iron Oxides

Iron oxides have received increasing attention due to their extensive applications, such as magnetic recording media, catalysts, pigments, gas sensors, optical devices, and electromagnetic devices.[102] They exist in a rich variety of structures (polymorphs) and hydration states; therefore until recently, knowledge of the structural details, thermodynamics and reactivity of iron oxides has been lacking. Furthermore, physical (magnetic) and chemical properties commonly change with particle size and degree of hydration. By definition, superparamagnetic iron oxide particles are generally classified with regard to their size into superparamagnetic iron oxide particles (SPIO), displaying hydrodynamic diameters larger than 30 nm, and ultrasmall superparamagnetic iron oxide particles (USPIO), with hydrodynamic diameters smaller than 30 nm. USPIO particles are now efficient contrast agents used to enhance relaxation differences between healthy and pathological tissues, due to their high saturation magnetization, high magnetic susceptibility, and low toxicity. More in general SPIO and USPIO are commonly named SPIONs (Superparamagnetic Iron Oxide Nanoparticles).

The biodistribution and resulting contrast of these particles are highly dependent on their synthetic route, shape, and size.[103] There has been much interest in the development of synthetic methods to produce high-quality iron oxide systems. The synthesis of controlled size magnetic nanoparticles is described in multiple publications. High-quality iron oxide nanomaterials have been generated using high-temperature solution phase methods similar

to those used for semiconductor quantum dots. Other synthesis methods such as polyol-mediated, sol-gel[104] and sonochemical[105] were also proposed.

For the variety of magnetic nanomaterials properties the different morphologies including spheres, rods, tubes, wires, belts, cubes, starlike, flowerlike, and other hierarchical architectures were fabricated by various approaches. Finally, some bacteria couple the reduction of Fe(III) with the metabolism of organic materials, which can include anthropogenic contaminants, or simply use iron oxides as electron sinks during respiration.[106]

2.4.4.1.1 Fe_2O_3

Among several crystalline modifications of anhydrous ferric oxides there are two magnetic phases, namely, rhombohedral hematite *(α-Fe_2O_3)* and cubic maghemite *(γ-Fe_2O_3),* and the less common *ε-Fe_2O_3* phases. In the α-structure, all Fe^{3+} ions have an octahedral coordination, whereas in *γ-Fe_2O_3* having the structure of a cation-deficient AB_2O_4 spinel, the metal atoms A and B occur in tetrahedral and octahedral environments, respectively. The oxide *α-Fe_2O_3* is antiferromagnetic at temperatures below 950 K, while above the Morin point (260 K) it exhibits so-called weak ferromagnetism. Hematite, the thermodynamically stable crystallographic phase of iron oxide with a band gap of 2.2 eV, is a very attractive material because of its wide applications, except magnetic recording materials, also in catalysis, as a gas sensors, pigments, and paints. Its nontoxicity is, attractive features for these applications.

The *α-Fe_2O_3* and FeOOH (goethite) nanoparticles are obtained by controlled hydrolysis of Fe^{3+} salts.[107] In order to avoid the formation of other phases, a solution of ammonia is added to a boiling aqueous solution of $Fe(NO_3)_3$ with intensive stirring. After boiling for 2.5 h and treating with ammonium oxalate (to remove the impurities of other oxides), the precipitate forms a red powder containing *α-Fe_2O_3* nanoparticles (20 nm).[108] These nanoparticles are also formed on treatment of solutions of iron salts (Fe^{2+} : Fe^{3+} = 1 : 2) with an aqueous solution of ammonium hydroxide in air.[109] The synthesis of regularly arranged *α-Fe_2O_3* nanowires with a diameter of 2-5 nm and a length of 20-40 nm has been described.[110]

A bulk *γ-Fe_2O_3* sample is a ferrimagnet below 620 °C. The *γ-Fe_2O_3* nanoparticles (4-16 nm) with a relatively narrow size distribution have been obtained by mild oxidation (Me_3NO) of preformed metallic nanoparticles.[111] The same result can be attained by direct introduction of $Fe(CO)_5$ into a heated solution of Me_3NO. The oxidation with air is also used to prepare *γ-Fe_2O_3* nanoparticles. For this purpose, the Fe_3O_4 nanoparticles (9 nm) are boiled in water at pH 12-13.[112]

The most popular route to *γ-Fe_2O_3* nanoparticles is thermal decomposition of Fe^{3+} salts in various media. Rather exotic groups are used in some cases as anions. For example, good results have been obtained by using iron complexes with cupferron.[113] A mechanochemical synthesis of *γ-Fe_2O_3* has been described.[114] An iron powder was milled in a planetary mill with water; this is a convenient one-stage synthesis of maghemite nanoparticles (15 nm).

Additionally, nonspherical Fe_2O_3 nanoparticles, such as nanorods, nanowires, nanobelts, and nanotubes, have also been synthesized and used for investigating their peculiar magnetic properties.[115]

2.4.4.1.2 Fe_3O_4 (Magnetite)

Among all iron oxides, magnetite Fe_3O_4 possess the most interesting properties because of the presence of iron cations in two valence states, Fe^{2+} and Fe^{3+}, in the inverse spinel structure. The cubic spinel Fe_3O_4 is ferrimagnetic at temperatures below 858 K. The route to these particles used most often involves treatment of a solution of a mixture of iron salts (Fe^{2+} and Fe^{3+}) with a base under an inert atmosphere. For example, the addition of an aqueous solution of ammonia to a solution of $FeCl_2$ and $FeCl_3$ (1:2) yields nanoparticles, which are transferred into a hexane solution by treatment with oleic acid.[116] The repeated selective precipitation gives Fe_3O_4 nanoparticles with a rather narrow size distribution. The synthesis can be performed starting only from $FeCl_2$, but in this case, a specified amount of an oxidant ($NaNO_2$) should be added to the aqueous solution apart from alkali. This method allows one to vary both the particle size (6.5-38 nm) and (to a certain extent) the particle shape.[117]

In some cases, thermal decomposition of compounds containing Fe^{3+} ions under oxygen-deficient conditions is accompanied by partial reduction of Fe^{3+} to Fe^{2+}. Thus thermolysis of $Fe(acac)_3$, in diphenyl ether in the presence of small amounts of hexadecane-1,2-diol (probable reducer of a part of Fe^{3+} ions to Fe^{2+}) gives very fine Fe_3O_4 nanoparticles (about 1 nm), which can be enlarged by adding excess $Fe(acac)_3$, into the reaction mixture.[118] Fe_3O_4 nanoparticles can be also prepared in uniform sizes of about 9 nm by autoclave heating the mixture, consisting of $FeCl_3$, ethylene glycol, sodium acetate, and polyethylene glycol.[119] For partial reduction of Fe^{3+} ions, hydrazine has also been recommended.[120] The reaction of $Fe(acac)_3$, with hydrazine is carried out in the presence of a surfactant. This procedure resulted in superparamagnetic magnetite nanoparticles with controlled sizes, 8 and 11 nm.

Thus, Fe_3O_4 nanoparticles with an average size of 3.5 nm have been prepared by thermal decomposition of $Fe_2(C_2O_4)_3 \cdot 5H_20$ at T > 400 °C.[121] Furthermore, the controlled reduction of ultradispersed α-Fe_2O_3 in a hydrogen stream at 723 K (15 min) is a more reliable method of synthesis of Fe_3O_4 nanoparticles. Particles with ca. 13 nm size were prepared in this way.[122]

The stabilization in the water media is interesting for bioapplications, but at the same time a problem also. For solving it cyclodextrin was used to transfer obtained organic ligand stabilized iron oxide nanoparticles to aqueous phase via forming an inclusion complex between surface-bound surfactants and cyclodextrin.[123] In contrast, higher nanoparticles (20 nm < d < 100 nm) are of great interest, mainly for hyperthermia because of their ferrimagnetic behavior at room temperature.

2.4.4.1.3 FeO (Wustite)

Cubic Fe^{2+} oxide is antiferromagnetic (T_c = 185 K) in the bulk state. Joint milling of Fe and Fe_2O_3 powders taken in a definite ratio give nanoparticles (5-10 nm) consisting of FeO and Fe.[124] On heating these particles at temperatures of 250-400 °C, the metastable FeO phase disproportionates to Fe_3O_4 and Fe, while above 550 °C it is again converted into nanocrystalline FeO.[125]

2.4.4.1.4 FeOOH

The oxyhydroxides, nominally FeOOH, include goethite, lepidocrocite, akaganeite, and several other polyrnorphs. They often contain excess water. Ferrihydrite $Fe_5HO_8{\cdot}4(H_20)$ is typically considered a metastable iron oxide that can act as a precursor to the more stable iron oxides such as goethite and hematite.[126] Oxyhydroxides are normally obtained by precipitation from an aqueous solution. The particle size is controlled by initial iron concentration, organic additives, pH, and temperature.

Among the known oxide hydroxides $Fe_2O_3{\cdot}H_2O$, the orthorhombic *α-FeOOH* (goethite) is antiferromagnetic in the bulk state and has T_c = 393 K.[127] Synthetic goethite nanoparticles are typically acicular and are often aggregated into bundles or rafts of oriented crystallites.

β-FeOOH (akagenite) is paramagnetic at 300 K.[128] Akaganeite always has a significant surface area and some amount of excess water, which increases tremendously with the decreasing particle size. Recent studies of nanoakaganite show that at very high surface areas, where the particle size becomes comparable to a few unit cells, akaganeite may contain goethite-like structural features possibly related to the collapse of exposed tunnels.

γ-FeOOH (lipidocrokite) is paramagnetic at 300 K and *δ-FeOOH* (ferroxyhite) is ferromagnetic.[129] Although the bulk *α-FeOOH* is antiferromagnetic, in the form of nanoparticles it has a nonzero magnetic moment due to the incomplete compensation of the magnetic moments of the sublattices. Goethite nanoparticles have been studied by Mössbauer spectroscopy.[130] As a rule, *α-FeOOH* is present in iron nanoparticles as an admixture phase. Ferrihydrite is widespread but the nature of its extensive disorder is still controversial. Because of chemical and structural variability in FeOOH containing nanoparticles, it is also critical to determine their chemical composition, including water content, surface area, and particle size.

2.4.4.2 Cobalt Oxides

Cubic cobalt oxide is antiferromagnetic and has T_N = 291 K. Cobalt monoxide has played an important role in the discovery of the "exchange shift" of the hysteresis curve, first found for

samples consisting of oxidized Co nanoparticles.[131] Data on the dependence of T_N on the particle size were obtained in a study of CoO nanoparticles dispersed in a LiF matrix.[132] The particles obtained by vacuum deposition contained a small metal core, according to powder X-ray diffraction. As the particle size decreased from 3 to 2 nm, T_N decreased from 170 to 55 K. Apparently, the presence of an oxide layer on cobalt nanoparticles can markedly increase the coercive force. For example, the coercive forces (at 5 K) of monodisperse 6 and 13 nm oxidized Co particles obtained by plasma gas condensation in an installation for the investigation of molecular beams were ca. 5 and 2.4 kG, respectively.[133] Unfortunately, the blocking temperature for 6 nm nanoparticles was lower than room temperature (about 200 K); therefore, under normal conditions, their coercive force was equal to zero.

2.4.4.2.1 Co_3O_4

The Co_3O_4 nanoparticles (cubic spinel) with sizes of 15-19 nm dispersed in an amorphous silicon matrix exhibited ferrimagnetic properties at temperatures below 33 K (for bulk samples, T_N = 30 K).[134] A method for controlled synthesis of Co_3O_4 cubic nanocrystallites (10-100 nm) has been developed.[135]

2.4.4.3 Nickel Oxide

Bulk crystals of NiO are antiferromagnetic, the Néel temperature being 523 K, but when the nanoparticles sizes are of the order of a few nanometers, they become superparamagnetic or superantiferromagnetic.[136] NiO possess not only magnetic but also electrical properties. The conductivity increases by 6-8 orders of magnitude in nanosized NiO as compared to that of bulk crystals, something that is attributed to the high density of defects.[137] It has been pointed out that electrodes composed of NiO nanoparticles exhibit a higher capacity and better cyclability than the ordinary ceramic material.[138]

2.5 Protection/Stabilization of Magnetic Nanoparticles

Although there have been many significant developments in the synthesis of magnetic nanoparticles, maintaining the stability of these particles for a long time without agglomeration or precipitation is an important issue. Stability is a crucial requirement for almost any application of magnetic nanoparticles. Especially pure metals, such as Fe, Co, and Ni and their metal alloys, are very sensitive to air. Thus, the main difficulty for the use of pure metals or alloys arises from their instability towards oxidation in air, and the susceptibility towards oxidation becomes higher the smaller the particles are. Therefore, it is necessary to develop efficient strategies to improve the chemical stability of magnetic nanoparticles. The most straightforward method seems to be protection by a layer which is impenetrable, so that oxygen cannot reach the surface of the magnetic particles. Often, stabilization and protection of the particles are closely linked with each other.

All the protection strategies result in magnetic nanoparticles with a core–shell structure, that is, the naked magnetic nanoparticle as a core is coated by a shell, isolating the core against the environment.

The applied coating strategies can roughly be divided into two major groups: coating with organic shells, including surfactant and polymers,[139] or coating with inorganic components, including silica,[140] carbon,[141] precious metals (such as Ag,[142] Au[143]) or oxides, which can be created by gentle oxidation of the outer shell of the nanoparticles, or additionally deposited, such as Y_2O_3.[144] As an alternative, magnetic nanoparticles can also be dispersed/embedded into a dense matrix, typically in polymer, silica, or carbon, to form composites, which also prevents or at least minimizes the agglomeration and oxidation. However, the nanoparticles are then fixed in space relative to each other, which is often not desired. In contrast, individually protected nanocrystals are freely dispersible and stable in a variety of media owing to the protecting shell around them.[145]

2.5.1 Surface Passivation by Mild Oxidation

A very simple approach to protect the magnetic particles is to induce a controlled oxidation of a pure metal core, a technique long known for the passivation of air-sensitive supported catalysts. This oxidation can be achieved by various methods. For example, Peng *et al*. developed a method for oxidizing gas-phase nanoparticles by using a plasma-gas-condensation-type cluster deposition apparatus.[146] Boyen *et al*. demonstrated that very good control over the chemical state of the cobalt nanoparticles was achieved by their exposure to an oxygen plasma.[147] The control of the oxide layer has a tremendous impact on exchange-biased systems, where a well-defined thickness of the ferromagnetic core and the antiferromagnetic shell are desirable. Moreover, a direct correlation of the structure and magnetism in the small particles can be determined. Bönnemann *et al.* developed a mild oxidation method, using synthetic air to smoothly oxidize the as-synthesized cobalt nanoparticles to form a stable CoO outer layer which can stabilize the cobalt nanoparticles against further oxidation.[148]

2.5.2 Surfactant and Polymer Coating

Surfactants or polymers are often employed to passivate the surface of the nanoparticles during or after the synthesis to avoid agglomeration. In general, electrostatic repulsion or steric repulsion can be used to disperse nanoparticles and keep them in a stable colloidal state. The best known example for such systems are the ferrofluids which were invented by Papell in 1965.[149] In the case of ferrofluids, the surface properties of the magnetic particles are the main factors determining colloidal stability. The major measures used to enhance the stability of ferrofluids are the control of surface charge[150] and the use of specific surfactants.[151] For instance, magnetite nanoparticles synthesized through the co-precipitation of Fe^{2+} and Fe^{3+} in ammonia or NaOH solution are usually negatively charged, resulting in agglomeration. To achieve stable colloids, the magnetite nanoparticle precipitate can be peptized (to disperse a precipitate to form a colloid by adding of surfactant) with aqueous tetramethylammonium hydroxide or with aqueous perchloric acid.[150] The magnetite nanoparticles can be acidified with a solution of nitric acid and then further

oxidized to maghemite by iron nitrate. After centrifugation and redispersion in water, a ferrofluid based on positively charged *γ-Fe_2O_3* nanoparticles was obtained, since the surface hydroxy groups are protonated in the acidic medium.[152] Commercially, water- or oil-based ferrofluids are available. They are usually stable when the pH value is below 5 (acidic ferrofluid) or over 8 (alkaline ferrofluid).

In general, surfactants or polymers can be chemically anchored or physically adsorbed on magnetic nanoparticles to form a single or double layer,[153] which creates repulsive (mainly as steric repulsion) forces to balance the magnetic and the van der Waals attractive forces acting on the nanoparticles. Thus, by steric repulsion, the magnetic particles are stabilized in suspension. Polymers containing functional groups, such as carboxylic acids, phosphates, and sulfates, can bind to the surface of magnetite[154] or maghemite. Suitable polymers for coating include poly(pyrrole), poly(aniline), poly(alkylcyanoacrylates), poly(methylidene malonate), and polyesters, such as poly(lactic acid), poly (glycolic acid), poly(*ε*-caprolactone), and their copolymers.[155] Surface-modified magnetic nanoparticles with certain biocompatible polymers are intensively studied for magnetic-field-directed drug targeting, and as contrast agents for magnetic resonance imaging.[156]

Chu *et al.* reported a synthesis of polymer-coated magnetite nanoparticles by a single inverse microemulsion.[157] The magnetite particles were first synthesized in an inverse microemulsion, consisting of water/sodium bis(2-ethylhexylsulfosuccinate)/toluene. Subsequently, water, monomers (methacrylic acid and hydroxyethyl methacrylate), crosslinker (*N*,*N'*-methylenebis(acrylamide)), and an initiator (2,2'-azobis(isobutyronitrile)) were added to the reaction mixture under nitrogen, and the polymerization reaction was conducted at 55 °C. After polymerization, the particles were recovered by precipitation in an excess of an acetone/ methanol mixture (9:1 ratio). The polymer-coated nanoparticles have superparamagnetic properties and a narrow size distribution at a size of about 80 nm. However, the long term stability of these polymer-coated nanoparticles was not addressed. Polyaniline can also be used to coat nanosized ferromagnetic Fe_3O_4 by oxidative polymerization in the presence of the oxidant ammonium peroxodisulfate.[158] The nanoparticles obtained are polydisperse (20–30 nm averaged diameter) and have the

expected core–shell morphology. Asher *et al*. reported that single iron oxide particles (ca. 10 nm) can be embedded in polystyrene spheres through emulsion polymerization to give stable superparamagnetic photonic crystals.[159] Polystyrene coating of iron oxide nanoparticles was also achieved by atom transfer radical polymerization.[160]

Metallic magnetic nanoparticles, stabilized by single or double layers of surfactant or polymer are not air stable, and are easily leached by acidic solution,[161] resulting in the loss of their magnetization. A thin polymer coating is not a good enough barrier to prevent oxidation of the highly reactive metal particles. Polymer coating is thus not very suitable to protect very reactive magnetic nanoparticles.

Another drawback of polymer-coated magnetic nanoparticles is the relatively low intrinsic stability of the coating at higher temperature, a problem which is even enhanced by a possible catalytic action of the metallic cores. Therefore, the development of other methods for protecting magnetic nanoparticles against deterioration is of great importance.

2.5.3 Precious-Metal Coating

Precious metals can be deposited on magnetic nanoparticles through reactions in microemulsion,[162] redox transmetalation,[163] iterative hydroxylamine seeding,[164] or other methods, to protect the cores against oxidation.

Cheon *et al.* reported a synthesis of platinum-coated cobalt by refluxing cobalt nanoparticle colloids (ca. 6 nm) and [Pt-$(hfac)_2$] (hfac = hexafluoroacetylacetonate) in a nonane solution containing $C_{12}H_{25}NC$ as a stabilizer.[163a] After 8 h reflux and addition of ethanol and centrifugation, the colloids are isolated from the dark red-black solution in powder form. These particles are air stable and can be redispersed in typical organic solvents. The reaction byproduct was separated and analyzed as [$Co(hfac)_2$], indicating that the formation of the core–shell structure was driven by redox transmetalation reactions between Co^0 and Pt^{2+}.

Gold seems to be an ideal coating owing to its low reactivity. However, it was found that the direct coating of magnetic particles with gold is very difficult, because of the dissimilar nature of the two surfaces.[165] Progress has been made, though, recently. O'Connor and co-

workers have synthesized gold-coated iron nanoparticles with about 11 nm core size and a gold shell of about 2.5 nm thickness.[163b] These gold coated iron particles are stable under neutral and acidic aqueous conditions. The coating was achieved by a partial replacement reaction in a polar aprotic solvent. Briefly, a yellow solution of $FeCl_3$, dissolved in *N*-methylpyrrolydone (NMP), was added to a dark green NMP solution containing sodium and naphthalene under intensive stirring at room temperature. Thus, the Fe^{3+} ions were reduced by sodium to form the metallic cores. After removal of sodium chloride by centrifugation, and the addition of 4-benzylpyridine as capping agent at elevated temperature, the iron nanoparticles were coated with gold by the addition of dehydrated $HAuCl_4$ dissolved in NMP.

Gold-coated iron nanoparticles could also be prepared by a reverse microemulsion method. The inverse micelles were formed with cetyltrimethylammonium bromide (CTAB) as surfactant, 1-butanol as a co-surfactant, and octane as the continuous oil phase. $FeSO_4$ was reduced by $NaBH_4$, then addition of $HAuCl_4$ coated gold on the iron nanoparticles.[143a]

Zhang *et al.* reported a new method for the preparation of gold coated iron magnetic core–shell nanoparticles by the combination of wet chemistry and laser irradiation. The synthesized iron nanoparticles and gold powder were irradiated by a laser in a liquid medium to deposit the gold shell.[166] The 18 nm body centered cubic (bcc) iron single domain magnetic cores are covered by a gold shell of partially fused approximately 3 nm-diameter fcc gold nanoparticles. The core–shell particles are superparamagnetic at room temperature with a blocking temperature, T_B, of approximately 170 K. After four months of shelf storage in normal laboratory conditions, their magnetization normalized to iron content was measured to be 210 emu/g, roughly 96% of the bulk iron value, which indicates the high stability.

Guo *et al.* have reported a synthesis of gold coated cobalt nanoparticles based on a chemical reduction reaction.[167] The cobalt particles were fabricated using 3-(*N*,*N*-dimethyldodecylammonio) propanesulfonate as the surfactant to prevent agglomeration, and lithium triethylhydridoborate as the reducing agent. The cobalt nanoparticles produced were added to $KAuCl_4$ in tetrahydrofuran (THF) solution under ultrasonication and inert

atmosphere. The gold shell was deposited on the cobalt nanoparticle through reduction of the Au^{3+} by cobalt surface atoms.

Gold coating of magnetic nanoparticles is especially interesting, since the gold surface can be further functionalized with thiol groups. This treatment allows the linkage of functional ligands which may make the materials suitable for catalytic and optical applications.[168]

2.5.4 Silica Coating

A silica shell does not only protect the magnetic cores, but can also prevent the direct contact of the magnetic core with additional agents linked to the silica surface thus avoiding unwanted interactions. For instance, the direct attachment of dye molecules to magnetic nanoparticles often results in luminescence quenching. To avoid this problem, a silica shell was first coated on the magnetic core, and then dye molecules were grafted on the silica shell.[169] Silica coatings have several advantages arising from their stability under aqueous conditions (at least if the pH value is sufficiently low), easy surface modification, and easy control of interparticle interactions, both in solution and within structures, through variation of the shell thickness.

The Stöber method and sol–gel processes are the prevailing choices for coating magnetic nanoparticles with silica.[170] The coating thickness can be tuned by varying the concentration of ammonium and the ratio of tetraethoxysilane (TEOS) to H_2O. The surfaces of silica-coated magnetic nanoparticles are hydrophilic, and are readily modified with other functional groups.[171] The functionalization could introduce additional functionality, so that the magnetic particles are potentially of use in biolabeling, drug targeting, drug delivery. Previous studies involved the coating of hematite (Fe_2O_3) spindles and much smaller magnetite clusters with silica;[172] the oxide cores could subsequently be reduced in the dry state to metallic iron.[173] The advantage of this method is that silica coating was performed on an oxide surface, which easily binds to silica through OH surface groups.

Xia and co-workers have shown that commercially available ferrofluids can be directly coated with silica shells by the hydrolysis of TEOS.[170c] A water-based ferrofluid (EMG 340) was diluted with deionized water and 2-propanol. Ammonia solution and various amounts of

TEOS were added stepwise to the reaction mixture under stirring. The coating step was allowed to proceed at room temperature for about 3 h under continuous stirring. The coating thickness could be varied by changing the amount of TEOS. Since the iron oxide surface has a strong affinity towards silica, no primer was required to promote the deposition and adhesion of silica. Owing to the negative charges on the silica shells, these coated magnetic nanoparticles are redispersible in water without the need of adding other surfactants.

Kobayashi *et al.* described a method for the synthesis of monodisperse, amorphous cobalt nanoparticles coated with silica in aqueous ethanolic solution by using 3-aminopropyltrimethoxysilane and TEOS as the silica precursor.[174] Shi and co-workers have prepared uniform magnetic nanospheres (ca. 270 nm) with a magnetic core and a mesoporous-silica shell.[175] The synthesis involved forming a thin and dense silica coating on hematite nanoparticles by the Stöber process, a second coating, the mesoporous silica shell, was added by a simultaneous sol–gel polymerization of TEOS and n-octadecyltrimethoxysilane. The hematite core can be reduced to the metallic state by H_2.

Though great progress in the field of silica-coated nanoparticles has been made, the synthesis of uniform silica shells with controlled thickness on the nanometer scale still remains challenging. As an alternative, the microemulsion method was also tried.[176] Homogeneous silica-coated Fe_2O_3 nanoparticles with a silica shell of controlled thickness (1.8–30 nm) were synthesized in a reverse microemulsion.[177]

Tartaj *et al.* reported a synthesis of monodisperse air-stable superparamagnetic *α-Fe* nanocrystals encapsulated in nanospherical silica particles of 50 nm in diameter. The iron oxide nanoparticles are embedded in silica by the reverse microemulsion technique, the *α-Fe* is obtained by reduction with hydrogen at 450 °C.[178] Similarly, a reverse micelle microemulsion approach was also reported to coat a layer of silica around spinel ferrite nanoparticles of $CoFe_2O_4$ and $MnFe_2O_4$.[179]

Although metals protected by silica can be synthesized by reduction after synthesis, silica deposition directly on pure metal particles is more complicated because of the lack of OH

groups on the metal surface. An additional difficulty for coating metallic nanoparticles, such as iron and cobalt with silica, which has to be overcome, is that iron and cobalt are readily oxidized in the presence of dissolved oxygen. Therefore, it is necessary to use a primer to make the surface "vitreophilic" (glasslike).[180] This chemistry has been used to coat precious metals.[181] Another possibility would be using stable cobalt nanoparticles, passivated by the gentle oxidation method developed by Bönnemann *et al.*,[148] as starting materials for such silica coating. However, no corresponding report has appeared to date.

From the mentioned examples above, it can be seen that silica coating of magnetic oxide nanoparticles is a fairly controllable process. However, silica is unstable under basic condition, in addition, silica may contain pores through which oxygen or other species could diffuse. Coating with other oxides is much less developed, and therefore alternative methods, especially those which would allow stabilization under alkaline conditions, are needed.

2.5.5 Carbon Coating

Although to date most studies have focused on the development of polymer or silica protective coatings, recently carbon-protected magnetic nanoparticles are receiving more attention, because carbon-based materials have many advantages over polymer or silica, such as much higher chemical and thermal stability as well as biocompatibility.

Right after the discovery of fullerenes, it was found that carbon-encapsulated metal or metal carbide nanocrystallites can be generated by the Krätschmer arc-discharge process.[182] Since then, many studies have shown that in the presence of metal nanoparticles (Co, Fe, Ni, Cr, Au, etc), graphitized carbon structures, such as carbon nanotubes and carbon onions, are formed under arc-discharge, laser ablation, and electron irradiation.[183] The well-developed graphitic carbon layers provide an effective barrier against oxidation and acid erosion. These facts indicate that it is possible to synthesize carbon-coated magnetic nanoparticles, which are thermally stabile and have high stability against oxidation and acid leaching, which is crucial for some applications.[184] Moreover, carbon-coated nanoparticles are usually in the metallic state, and thus have a higher magnetic moment than the corresponding oxides.

Though carbon-coated magnetic nanoparticles have many advantageous properties, such particles are often obtained as agglomerated clusters, owing to the lack of effective synthetic methods, and a low degree of understanding of the formation mechanism. The synthesis of dispersible, carbon-coated nanoparticles in isolated form is currently one of the challenges in this field.

References

[38] P. Moriarty, *Rep. Prog. Phys.*, **2001**, *64*,297.

[39] A.l. Gusev, A.A. Rampel, *Nanokristallicheskie Materialy (Nanocrystalline Materials)*, Moscow: Fizmatlit, **2001**.

[40] Sergey B. Gubin, *"Magnetic Nanoparticles"*, **2009**, Wiley-VCH.

[41] a) A.P. Alivisatos, P.F. Barbara, A.W. Castleman, J. Chang, D.A. Dixon, M.L. Klein, G.L. McLendon, J.S. Miller, M.A. Ratner, P.J. Rossky, S.l. Stupp, M.E. Thompson, *Adv. Mater.*, **1998**, *10*, 1297; (b) T. Sugimoto, *Monodispersed Particles*, Elsevier, **2001**; (c) *"Nanostructured Materials; Selected Synthesis, Methods, Properties and Applications"* Eds., P. Knauth and J. Schoonman, Kluwer, Dordrecht, **2004**; (d) J.P. Wilcoxon, B.L. Abrams, *Chem. Soc. Rev.*, **2006**, *35*, 1162; e) O. Masala, R. Sesadri, *Ann. Rev. Mater. Res.*, **2004**, *34*, 41.

[42] (a) J.T. Lue, *J. Phys. Chem. Solids.* **2001**, *62*, 1599; (b) J. Jortner, C.N.R. Rao, *Pure Appl. Chem.* **2002**, *74*, 1491; (c) N.L. Rosi, C.A. Mirkin, *Chem. Rev.* **2005**, *105*,1547.

[43] (a) V.E. Fertman, *Magnetic Fluids Guide-Book: Properties and Application*, Hemisphere, New York, **1990**; (b) B.M. Berkovsky, V.F. Medvedev, M.S. Krakov, *Magnetic Fluides: Engineering Applications*, Oxford University Press, Oxford, **1993**.

[44] An-Hui-Lu, E.L. Salabas, F. Schuth, *Angew. Chem. Int. Ed.*, **2007**, *46*, 1222.

[45] (a) X. Batlle, A. Labarta, *J. Phys. D*, **2002**, *35*, R15; (b) C. M. Sorensen, *Magnetismin Nanoscale Materials in Chemistry* (Ed.: K. J. Klabunde), Wiley-Interscience Publication, New York, **2001**.

[46] T. Iwaki, Y. Kakihara, T. Toda, M. Abdullah, K. Okuyama, *J. Appl. Phys.*, **2003**, *94*, 6807.

[47] (a) A. Ney, P. Poulopoulos, M. Farle, K. Baberschke, *Phys. Rev. B*, **2000**, *62*, 11336, and references therein; (b) S. Foner, *Rev. Sci. Instrum.*, **1959**, *30*, 548; (c) M. Farle, *Rep. Prog. Phys.*, **1998**, *61*, 755; (d) H. Elbert, *Rep. Prog Phys.*, **1996**, *59*, 1665; (e) J. Stöhr, *J. Magn. Magn. Mater.* **1999**, *200*, 470; (f) B. Hillebrands, G. Güntherodt, *Ultrathin Magnetic Structure*, Vols I and II, Berlin, Springer, **1994**.

[48] R.H. Kodama, *J. Magn. Magn. Mater.*, **1999**, *200*, 359.

[49] M. Respaud, J.M. Broto, H. Rakoto, A.R. Fert, L. Thomas, B. Barbara, M. Verelst, E. Snoeck, P. Lecante, A. Mosset, J. Osuna, T. Ould Ely, C. Amiens, B. Chaudret, *Phys. Rev. B*, **1998**, *57*, 2925.

[50] F. Bødker, S Mørup, S. Linderoth, *Phys. Rev. Lett.*, **1994**, *72*, 282.

[51] (a) W. S. Seo, H.H. Jo, K. Lee, B. Kim, S.J. Oh, J.T. Park, *Angew. Chem.*, **2004**, *116*, 1135; *Angew. Chem. Int. Ed.*, **2004**, *43*, 1115; (b) T. Hyeon, S.S. Lee, J. Park, Y. Chung, H.B. Na, *J. Am. Chem. Soc.*,

2001, *123*, 12798; (c) S.I. Makhlouf, *J. Magn. Magn. Mater.*, **2002**, *246*, 184; (d) Y. Wang, C.-M. Yang, W. Schmidt, B. Spliethoff, E. Bill, F. Schüth, *Adv. Mater.*, **2005**, *17*, 53.

[52] A. Homola, M. Lorenz, C. Mastrangelo, T. Tilbury, *IEEE Trans. Magn.*, **2003**, *22*, 716.

[53] P. M. Paulus, H. Bönnemann, A.M. van der Kraan, F. Luis, J. Sinzig, L.J. de Jongh, *Eur. Phys. J. D*, **1999**, *9*, 501.

[54] J. Hormes, H, Modrow, H. Bönnemann, C.S.S.R. Kumar, *J. Appl. Phys.*, **2005**, *97*, 10R102.

[55] D.A. van Leeuwen, J.M. van Ruitenbeek, L.J. de Jongh, A. Ceriotti, G. Pacchioni, O.D. Häberlen, N. Rösch, *Phys. Rev. Lett.*, **1994**, *73*, 1432.

[56] N. Cordente, M. Respaud, F. Senocq, M-J. Casanove, C. Amiens, B. Chaudret, *Nano Lett.*, **2001**, *1*, 565.

[57] J. Nogués, J. Sort, V. Langlais, V. Skumryev, S. Suriñach, J.S. Muñoz, M.D. Baró, *Phys. Rep*., **2005**, *422*, 65.

[58] E.L. Salabas, A. Rumplecker, F. Kleitz, F. Radu, F. Schüth, *Nano Lett.*, **2006**, *6*, 2977.

[59] V. Skumryev, S. Stoyanov, Y. Zhang, G. Hadjipanayis, D. Givord, J. Nogués, *Nature*, **2003**, *423*, 850.

[60] H. Zeng, J. Li, L. Zhong, S. Sun, *Nature*, **2002**, *420*, 395.

[61] H. Zeng, S. Sun, J. Li, Z. L. Wang, J.P. Liu, *Appl. Phys. Lett.*, **2004**, *85*, 792.

[62] (a) S.P. Gubin, Yu.A. Koksharov, G.B. Khomutov, G.Yu. Yurkov, *Russian. Chem. Rev.*, **2005**, *74*, 489; (b) S.P. Gubin, YU.A. Koksharov, *Neorg. Mater.*, **2002**, *38*, 1287.

[63] S.P. Gubin, *Ros. Khim. Zh.*, **2000**, *44(6)*, 23.

[64] (a) W.J. Zhang, *Nanopart. Res.*, **2003**, *5*,323; (b) D.L. Huber, *Small*, **2005**, *1*, 482.

[65] S. Gangopadhyay, G.C. Hadjipanayis, B. Dale, C.M. Sorensen, K.J. Klabunde, V. Papaefthymiou, A. Kostikas, *Phys. Rev.*, **1992**, *B 45*, 9778.

[66] J.F. Loffler, J.P. Meier, B. Doudin, J.P. Ansermet, W. Wagner, *Phys. Rev.*, **1998**, *B 57*, 2915.

[67] W.A. de Heer, P. Milani, A. Chatelain, *Phys. Rev. Lett.*, **1990**, *65*, 488.

[68] L. Guo, Q.J. Huang, X.Y. Li, S.H. Yang, *Phys. Chem. Chem. Phys.,* **2001**, *3*, 1661.

[69] S.M. Ponder, J.G. Darab, J. Bucher, D. Caulder, l. Craig, L. Davis, N. Edelstein, W. Lukens, H. Nitsche, L. Rao, D.K. Shuh, T.E. Mallouk, *Chem. Mater.*, **2001**, *13*, 479.

[70] A.S. Dehlinger, J.F. Pierson, A Roman, P.H. Bauer, *Suif. Coat. Technol.*, **2003**, *174*, 331.

[71] D.P. Dinega, M.G. Bawendi, *Angew. Chem. Int. Ed. Engl.*, **1999**, *38*, 1788.

[72] O. Kitakami *et al*., *Phys. Rev.*, **1997**, *B 56*, 849.

[73] M. Pileni, *Appl. Suif. Sci.*, **2001**, *171*, 1.

[74] M.P. Pileni, *Langmuir*, **1997**, *13*, 3266.

[75] L. Yiping, G.C. Hadjipanayis, V. Papaefthymiou, A. Kostikas, A. Simopoulos, C.M. Sorensen, K.J. Klabunde, *J. Magn. Magn. Mater.*, **1996**, *164*, 357.

[76] D.L. Peng, K. Sumiyama, T.J. Konno, T. Hihara and S. Yamamuro, *Phys. Rev.*, **1999**, *B 60* , 2093.

[77] L. Bi, S. Li, Y. Zhang, D. Youvei, *J. Magn. Magn. Mater.*, **2004**, *277*, 363.

[78] O. Cintora-Gonzalez, C. Estournes, M. Richard Pionet, J.L. Guille, *Mater. Sci. Eng.*, **2001**, *C 15*, 179.

[79] W.N. Wang, I. Yoshifimi, I. Wuled-Lengorro, K. Okuyama, *Mater Sci. Eng.*, **2004**, *B 111*, 69.

[80] A. Gavirin, C.L. Chen, *J. Appl. Phys.*, **1993**, *73*, 6949.

[81] S. Doppiu, V. Langlais, J. Sort, S. Surinach, M.D. Barò, Y. Zhang, G. Hadjinapayis, J. Nogue's, *Chem. Mater.*, **2004**, *16*, 5664.

[82] C. Estourne's, T. Lutz, J. Happich, T. Quaranta, P. Wissler, J.L. Guille, *J. Magn. Magn. Mater.*, **1997**, *173*, 83.

[83] D. de Caro, J.S. Bradley, *Langmuir*, **1997**, *13*, 3067.

[84] D.H. Chen, S.H. Wu, *Chem. Mater.*, **2000**, *12*, 1354.

[85] K.L. Tsai, J. Dye., *Chem. Mater.*, **1993**, *5*, 540.

[86] A.M. Tishin, Yu.I. Spichkin, *The Magnetocaloric Effect and Its Applications*, Institute of Physics: Bristol, Philadelphia, **2003**.

[87] S. Thongchant, Y. Hasegawa, Y. Wada, S. Yanagia, *Chem. Lett.*, **2001**, *30*, 1274.

[88] S. Thongchant, Y. Hasegawa, Y. Wada, S. Yanagida, *Chem. Lett.*, **2003**, *32*, 706.

[89] J.A. Nelson, L.H. Bennet, M.J. Wagner, *J. Am. Chem. Soc.*, **2002**, *124*, 2979.

[90] D. Johnson, P. Perera, M.J. O'Shea, *J. Appl. Phys.*, *79*, 5299.

[91] T. Sourmail, *Prog. Mater. Sci.*, **2005**, *50*, 816.

[92] X.G. Li, T. Murai, T. Saito, S. Takahashi, *J. Magn. Magn. Mater.*, **1998**, *190*, 277.

[93] B.L. Cushing, V.L. Kolesnichenko, C.J. O'Connor, *Chem. Rev.*, **2004**, *104*, 3893.

[94] X.G. Li, A. Chiba, S. Takahashi, *J. Magn. Magn. Mater.*, **1997**, *170*, 339.

[95] A.M. Afanas'ev, LP. Suzdalev, M.Ya. Gen, V.l. Gol'danskii, V.P. Korneev, E.A. Manykin, *Zh. Eksp. Teor. Fiz.*, **1970**, *58*, 115.

[96] B.K. Rao, S.R. de Debiaggi, P. Jena, *Phys. Rev.*, **2001**, *B 64*, 418.

[97] S. Sun, H. Zeng, *J. Am. Chem. Soc.*, **2002**, *124*, 8204.

[98] S. Sun, E.E. Fullerton, D. Weller, C.B. Murray, *IEEE Trans. Magn.*, **2001**, *37*, 1239.

[99] T. Hyeon, *Chem. Commun.*, **2003**, 927.

[100] M. Chen, J.P. Liu, S. Sun, *J. Am. Chem. Soc.*, **2004**, *126*, 8394.

[101] R.C. O'Handley, *Modem Magnetic Materials: Principle and Applications*, Wiley-Interscience: New York 434, **2000**.

[102] R.M. Cornell, U. Schwertmann, *The Iron Oxides: Structure, Properties, Reactions, Occurrences and Uses*, 2nd Ed.; Wiley-VCH: Weinheim, **2003**.

[103] P. Tartaj, M.P. Morales, S. Veintemillas-Verdaguer, T. Gonzalez-Carren, C.J. Serna, *J. Magn. Magn. Mater.*, **2005**, *290-291*, 28.

[104] C. Feldmann, H.O. Jungk, *Angew. Chem., Int. Ed.*, **2001**, *40*, 359.

[105] R. Vijaya Kumar, Yu. Koltypin, Y.S. Cohen, Y. Cohen, D. Aurbach, O. Palchik, I. Felner, A. Gedanken, *J. Mater. Chem.*, **2000**, *10*, 1125.

[106] D.R. Lovley, *Microbiol. Rev.*, **1991**, *55*, 259.

[107] U. Schwertmann, E. Murad, *Clays Clay Miner.*, **1983**, *31*, 277.

[108] M.F. Hansen, C.B. Koch, S. Morup, *Phys. Rev.*, **2000**, *B 62*, 1124.

[109] L. Zhang, G.. Papaefthymiou, J.Y. Ying, *J. Appl. Phys.*, **1997**, *81*, 6892.

[110] Y.Y. Fu, R.M. Wang, J. Xu, J. Chen, Y. Yan, A.V. Narlikar, H. Zhang, *Chem. Phys. Lett.*, **2003**, *379*, 373.

[111] T. Hyeon, S.S. Lee, J. Park, Y. Chung, H.B. Na, *J. Am. Chem. Soc.*, **2001**, *123*, 12798.

[112] J. Tang, M. Myers, K.A. Bosnick, L.E. Brus, *J. Phys. Chem.*, **2003**, *B 107*, 7501.

[113] J. Rockenberger, E.C. Scher, A.P. Alivisatos, *J. Am. Chem. Soc.*, **1999**, *121*, 11595.

[114] R. Janot, D. Guerard, *J. Alloys Compd.*, **2002**, *333*, 302.

[115] (a) Z. Jing, S. Wu, *Mater. Lett.*, **2004**, *58*, 3637; (b) X.G. Wen, S.H. Wang, Y. Ding, Z.L. Wang, S.H. Yang, *J. Phys. Chem. B*, **2005**, *109*, 215.

[116] T. Fried, G. Shemer, G. Markovich, *Adv. Mater.*, **2001**, *13*, 1158.

[117] I. Nedkov, T. Merodiiska, S. Kolev, K. Krezhov, D. Niarchos, E. Moraitakis, Y. Kusano, J. Takada, *Monatsh. Chem.*, **2002**, *133*, 823.

[118] S. Sun, H. Zeng, *J. Am. Chem. Soc.*, **2002**, *124*, 8204.

[119] X. Wang, J. Zhuang, O. Peng, Y. Li, *Nature*, **2005**, *437*, 121.

[120] Y. Hou, J. Yu, S. Gao, *J. Mater .Chem.*, **2003**, *13*, 1983.

[121] Y.U.F. Krupyanskii, LP. Suzdalev, *Zh. Eksp. Teor. Fiz.*, **1974**, *67*, 736.

[122] R.N. Panda, N.S. Gajbhiye, G. Balaji, *J. Alloys Compd.*, **2001**. *326*, 50.

[123] W.W. Yu, X. Peng, *Angew. Chem. Int. Edn.*, **2002**, *41*, 2368.

[124] J. Ding, W.F. Miao, E. Pirault, R. Street, P.G. McCormick, *J. Alloys Compd.*, **1998**, *161*, 199.

[125] (a) L. Minervini, R.W. Grimes, *J. Phys. Chem. Solids*, **1999**, *60*, 235; (b) K. Tokumitsu, T. Nasu, *Scr. Metall.*, **2001**, *44*, 1421.

[126] U. Schwertmann, J. Friedl, H. Stanjek, D.G. Schulze, *Clay Miner.*, **2000**, *35*, 613.

[127] C.J.W. Koch, M.B. Madsen, S. Morup, *Hyperfine Interact.*, **1986**, *28*, 549.

[128] S. Morup, T.M. Meaz, C.B. Koch, H.C.B. Hansen, *Z. Phys.*, **1997**, *D 40*, 167.

[129] T. Meaz, C.B. Koch, S. Morup, in *Proceedings of the Conference ICAME-95*, Bologna, **1996**, *50*, 525.

[130] M.B. Madsen, S. Morup, *Hyperfine Interact.*, **1988**, *42*, 1059.

[131] M. Kiwi, *J. Magn. Magn. Mater.*, **2001**, *234*, 584.

[132] S. Sako, K. Ohshima, M. Sakai, S. Bandow, *Surf. Rev. Lett.*, **1996**, *3*, 109.

[133] D.L. Peng, K. Sumiyama, T. Hihara, S. Yamamuro, T.J. Konno, *Phys. Rev.*, **2000**, *B 61*, 3103.

[134] M. Sato, S. Kohiki, Y. Hayakawa, Y. Sonda, T. Babasaki, H. Deguchi, M. Mitome, *J. Appl. Phys.*, **2000**, *88*, 2771.

[135] J. Feng, H.C. Zeng, *Chem. Mater.*, **2003**, *15*, 2829.

[136] R.H. Kodama, *J. Magn. Magn. Mater.*, **2000**, *221*, 32.

[137] V. Biju, A.M. Khadar, *J. Mater. Sci.*, **2003**, *38*, 4005.

[138] Z. Fei-bao, Z. Ying-ke, L. Hu-liu, *Mater. Chem. Phys.*, **2004**, *83*, 60.

[139] (a) L. E. Euliss, S.G. Grancharov, S. O'Brien, T.J. Deming, G.D. Stucky, C.B. Murray, G.A. Held, *Nano Lett.*, **2003**, *3*, 1489; (b) X. Liu, Y. Guan, Z. Ma, H. Liu, *Langmuir*, **2004**, *20*, 10278; (c) R. Hong, N.O. Fischer, T. Emrick, V.M. Rotello, *Chem. Mater.*, **2005**, *17*, 4617; (d) Y. Sahoo, H. Pizem, T. Fried, D. Golodnitsky, L. Burstein, C.N. Sukenik, G. Markovich, *Langmuir*, **2001**, *17*, 7907; (e) M. Kim, Y. Chen, Y. Liu, X. Peng, *Adv. Mater.*, **2005**, *17*, 1429.

[140] Y. Kobayashi, M. Horie, M. Konno, B. Rodriguez-Gonzalez, L.M. Liz-Marzan, *J. Phys. Chem. B*, **2003**, *107*, 7420.

[141] A.-H. Lu, W. Li, N. Matoussevitch, B. Spliethoff, H. Bönnemann, F. Schüth, *Chem. Commun.*, **2005**, 98.

[142] N. S. Sobal, M. Hilgendorff, H. Moehwald, M. Giersig, M. Spasova, T. Radetic, M. Farle, *Nano Lett.*, **2002**, *2*, 62.

[143] (a) Q. Liu, Z. Xu, J. A. Finch, R. Egerton, *Chem. Mater.*, **1998**, *10*, 3936; (b) J. Lin, W. Zhou, A. Kumbhar, J. Wiemann, J. Fang, E.E. Carpenter, C.J. O'Connor, *J. Solid State Chem.*, **2001**, *159*, 26.

[144] N.O. Nunez, P. Tartaj, M.P. Morales, P. Bonville, C.J. Serna, *Chem. Mater.*, **2004**, *16*, 3119.

[145] D.K. Kim, M. Mikhaylova, Y. Zhang, M. Muhammed, *Chem. Mater.*, **2003**, *15*, 1617.

[146] D.L. Peng, K. Sumiyama, T. Hihara, S. Yamamuro, T.J. Konno, *Phys. Rev. B*, **2000**, *61*, 3103.

[147] H.-G. Boyen, G. Kästle, K. Zürn, T. Herzog, F. Weigl, P. Ziemann, O. Mayer, C. Jerome, M. Möller, J.P. Spatz, M.G. Garnier, P. Oelhafen, *Adv. Funct. Mater.*, **2003**, *13*, 359.

[148] H. Bönnemann, W. Brijoux, R. Brinkmann, N. Matoussevitch, N.Waldoefner, N. Palina, H. Modrow, *Inorg. Chim. Acta.*, **2003**, *350*, 617.

[149] S.S. Papell, *US Patent 3215572*, **1965**.

[150] R. Massart, *IEEE Trans. Magn.*, **1981**, *MAG-17*, 1247.

[151] (a) K. Raj, R. Moskowitz, *J. Magn. Magn. Mater.*, **1990**, *85*, 107; (b) M. De Cuyper, M. Joniau, *Langmuir*, **1991**, *7*, 647; (c) A. Wooding, M. Kilner, D. Lambrick, *J. Colloid Interface Sci.*, **1992**, *149*, 98.

[152] D. Zins, V. Cabuil, R. Massart, *J. Mol. Liq.*, **1999**, *83*, 217.

[153] (a) L. Shen, P.E. Laibinis, T.A. Hatton, *Langmuir*, **1999**, *15*, 447; (b) M.H. Sousa, F.A. Tourinho, J. Depeyrot, G.J. da Silva, M.C.F.L. Lara, *J. Phys. Chem. B*, **2001**, *105*, 1168.

[154] R.M. Cornell, U. Schertmann, *The Iron Oxides: Structure, Properties, Reactions, Occurrence and Uses*, CH, Weinheim, **1996**.

[155] (a) M. Wan, J. Li, *J. Polymer. Sci.*, **1998**, *36*, 2799; (b) M.D. Butterworth, S.A. Bell, S.P. Armes, A.W. Simpson, *J. Colloid Interface Sci.*, **1996**, *183*, 91; (c) P. Tartaj, M.P. Morales, T. González-Carreno, S. Veintemillas-Verdaguer, C.J. Serna, *J. Magn. Magn. Mater.*, **2005**, *28*, 290; (d) G. Barratt, *Cell. Mol. Life Sci.*, **2003**, *60*, 21.

[156] (a) L.A. Harris, J.D. Goff, A.Y. Carmichael, J.S. Riffle, J.J. Harburn, T.G. St. Pierre, M. Saunders, *Chem. Mater.*, **2003**, *15*, 1367; A.F. Thunemann, D. Schutt, L. Kaufner, U. Pison, H. Möhwald, *Langmuir*, **2006**, *22*, 2351.

[157] P.A. Dresco, V.S., B. Chu, Zaitsev, R.J. Gambino, *Langmuir*, **1999**, *15*, 1945.

[158] J. Deng, X. Ding, W. Zhang, Y. Peng, J. Wang, X. Long, P. Li, A.S.C. Chan, *Polymer*, **2002**, *43*, 2179.

[159] X. Xu, G. Friedman, K. Humfeld, S. Majetich, S. Asher, *Adv. Mater.*, **2001**, *13*, 1681.

[160] (a) C.R. Vestal, Z.J. Zhang, *J. Am. Chem. Soc.*, **2002**, *124*, 14312; (b) Y. Wang, X. Teng, J.-S. Wang, H. Yang, *Nano Lett.*, **2003**, *3*, 789.

[161] D. Farrell, S. A. Majetich, J.P.Wilcoxon, *J. Phys. Chem. B*, **2003**, *107*, 11022.

[162] (a) J. Rivas, R.D. Sánchez, A. Fondado, C. Izco, A.J. García-Bastida, J. García-Otero, J. Mira, D. Baldomir, A. González, I. Lado, M.A. López-Quintela, S.B. Oseroff, *J. Appl. Phys.*, **1994**, *76*, 6564; (b) E.E. Carpenter, C. Sangregorio, C.J. O'Connor, *IEEE Trans. Magn.*, **1999**, *35*, 3496.

[163] (a) J.-I. Park, J. Cheon, *J. Am. Chem. Soc.*, **2001**, *123*, 5743; (b) Z. Ban, Y.A. Barnakov, F. Li, V.O. Golub, C.J. O'Connor, *J. Mater. Chem.*, **2005**, *15*, 4660; (c) Y. Shon, G.B. Dawson, M. Porter, R.W. Murray, *Langmuir*, **2002**, *18*, 3880.

[164] J.L. Lyon, D.A. Fleming, M.B. Stone, P. Schiffer, M.E. Williams, *Nano Lett.*, **2004**, *4*, 719.

[165] (a) S.-J. Cho, J.-C. Idrobo, J. Olamit, K. Liu, N.D. Browning, S.M. Kauzlarich, *Chem. Mater.*, **2005**, *17*, 3181; (b) H. Yu, M. Chen, P.M. Rice, S.X. Wang, R.L. White, S. Sun, *Nano Lett.*, **2005**, *5*, 379; (c) L. Wang, J. Luo, M.M. Maye, Q. Fan, Q. Rendeng, M.H. Engelhard, C. Wang, Y. Lin, C.-J. Zhong, *J. Mater. Chem.*, **2005**, *15*, 1821; (d) D. Caruntu, B.L. Cushing, G. Caruntu, C.J. O'Connor, *Chem. Mater.*, **2005**, *17*, 3398.

[166] J. Zhang, M. Post, T. Veres, Z.J. Jakubek, J. Guan, D. Wang, F. Normandin, Y. Deslandes, B. Simard, *J. Phys. Chem. B*, **2006**, *110*, 7122.

[167] (a) Z. Guo, C.S.S.R. Kumar, L.L. Henry, C.K. Saw, J. Hormes, E.J. Podlaha, *49th Magnetism and Magnetic Materials (MMM) Annual Conference Proceedings*, **2004**, S. 366; (b) Z. Lu, M.D. Prouty, Z. Guo, V.O. Golub, C.S.S.R. Kumar, Y.M. Lvov, *Langmuir*, **2005**, *21*, 2042.

[168] V.L. Colvin, A.N. Goldstein, A.P. Alivisatos, *J. Am. Chem. Soc.*, **1992**, *114*, 5221.

[169] D. Ma, J. Guan, F. Normandin, S. Denommee, G. Enright, T. Veres, B. Simard, *Chem. Mater.*, **2006**, *18*, 1920.

[170] (a) W. Stöber, A. Fink, E.J. Bohn, *J. Colloid Interface Sci.*, **1968**, *26*, 62; (b) T. Tago, T. Hatsuta, K. Miyajima, M. Kishida, S. Tashiro, K. Wakabayashi, *J. Am. Ceram. Soc.*, **2002**, *85*, 2188; (c) Y. Lu, Y. Yin, B.T. Mayers, Y. Xia, *Nano Lett.*, **2002**, *2*, 183; (d) C. Graf, D.L.J. Vossen, A. Imhof, A. Van Blaaderen, *Langmuir*, **2003**, *19*, 6693; (e) A.P. Philipse, M.P.B. van Bruggen, C. Pathmamanoharan, *Langmuir*, **1994**, *10*, 92.

[171] A. Ulman, *Chem. Rev.*, **1996**, *96*, 1533.

[172] (a) M. Ohmori, E. Matijevic, *J. Colloid Interface Sci.*, **1992**, *150*, 594; (b) M.A. Correa-Duarte, M. Giersig, N. A. Kotov, L.M. Liz-Marzán, *Langmuir*, **1998**, *14*, 6430.

[173] M. Ohmori, E. Matijevic, *J. Colloid Interface Sci.*, **1993**, *160*, 288.

[174] Y. Kobayashi, M. Horie, M. Konno, B. Rodriguez-González, L.M. Liz-Marzán, *J. Phys. Chem. B*, **2003**, *107*, 7420.

[175] W. Zhao, J. Gu, L. Zhang, H. Chen, J. Shi, *J. Am. Chem. Soc.*, **2005**, *127*, 8916.

[176] S. Santra, R. Tapec, N. Theodoropoulou, J. Dobson, A. Hebrad, W. Tan, *Langmuir*, **2001**, *17*, 2900.

[177]] D.K. Yi, S.S. Lee, G.C. Papaefthymiou, J.Y. Ying, *Chem. Mater.*, **2006**, *18*, 614.

[178] P. Tartaj, C.J. Serna, *J. Am. Chem. Soc.*, **2003**, *125*, 15754.

[179] C.R. Vestal, Z.J. Zhang, *Nano Lett.*, **2003**, *3*, 1739.

[180] L.M. Liz-Marzán, M. Giersig, P. Mulvaney, *Chem. Commun.*, **1996**, 731.

[181] T. Ung, L.M. Liz-Marzán, P. Mulvaney, *Langmuir*, **1998**, *14*, 3740.

[182] J.H.J. Scott, S.A. Majetich, *Phys. Rev. B*, **1995**, *52*, 12564.

[183] (a) K.H. Ang, I. Alexandrou, N.D. Mathur, G.A.J. Amaratunga, S. Haq, *Nanotechnology*, **2004**, *15*, 520; (b) W. Teunissen, F.M.F. de Groot, J. Geus, O. Stephan, M. Tence, C. Colliex, *J. Catal.*, **2001**, *204*, 169.; (c) T. Hayashi, S. Hirono, M. Tomita, S. Umemura, *Nature*, **1996**, *381*, 772; (d) R. Nesper, A. Ivantchenko, F. Krumeich, *Adv. Funct. Mater.*, **2006**, *16*, 296.

[184] H.B.S. Chan, B.L. Ellis, H.L. Sharma, W. Frost, V. Caps, R.A. Shields, S.C. Tsang, *Adv. Mater.*, **2004**, *16*, 144.

Chapter 3: Superparamagnetic Iron Oxide Nanoparticles

3 Superparamagnetic Iron Oxide Nanoparticles: Some General Remarks

Among all the class of magnetic nanoparticle, Superparamagnetic Iron Oxide Nanoparticles (SPIONs) have recently attracted the attention of the scientific community thanks to their peculiar characteristics.

As previously largely discuss, bulk magnetic materials are composed of regions, called magnetic domains, within which there is an alignment of the magnetic moments. If the volume of the material is reduced, as in the case of SPIONs, a situation in which just one domain is reached occurs and the magnetic properties are no longer similar to bulk materials.

Due to their small volume, SPIONs present superparamagnetic behavior, meaning that the thermal energy may be enough to change spontaneously the magnetization within each nanoparticles. In other words, the magnetic moment of each SPION will be able to rotate randomly just because of the temperature influence. For this reason, in the absence of an electromagnetic field (*Figure 4*) the net magnetic moment of a system containing SPIONs will be zero at high enough temperatures. However, in the presence of a field, there will be a net statistical alignment of magnetic moments, analogous to what happens to paramagnetic materials, except that now the magnetic moment is not that of a single atom but of the SPIONs containing various atoms which can be up to 10^4 times larger than for a paramagnetic material. This property, marked by the lack of remanent magnetization after removal of external fields, enables the SPIONs to maintain their colloidal stability and avoid agglomeration, which is important for biomedical applications.[185]

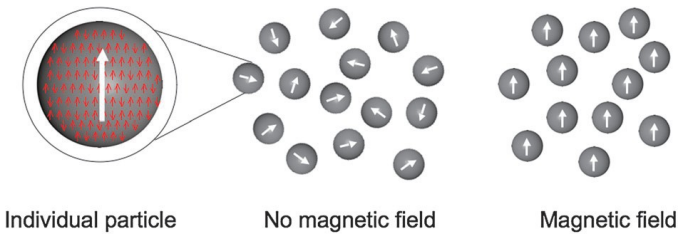

Figure 4 *- Schematic representation of a superparamagnetic particle. Note that although the moments within each particle are ordered (red arrows), the net magnetic moment of a system containing SPIONs will be zero in the zero field and at high enough temperatures. In the presence of a field, there will be a net statistical alignment of magnetic moments.*

For these reasons, the application of an external alternating magnetic field (AMF) to SPIONs leads to the production of energy, in the form of heat, if the magnetic field is able to reorient the magnetic moments of the SPIONs.[186] Such an effect can be exploited to use SPIONs as mediators in magnetic hyperthermia.

In bigger multidomain magnetic nanoparticles, this reorientation is produced through the movement of domain walls, while in small monodomain SPIONs, the reorientation of the magnetic moments can occur due to (i) the rotation of the moment within the SPIONs, overcoming their anisotropy energy barrier (Néel loss), or (ii) the mechanical rotation of the SPIONs that will create frictional losses with the environment (Brown loss) (*Figure 5*). For maghemite γ-Fe_2O_3 SPIONs, below 15 nm, theoretically, Néel relaxation prevails over Brown

relaxation while for larger sizes and low viscosity media, Brown relaxation is the rotation mechanism.[187]

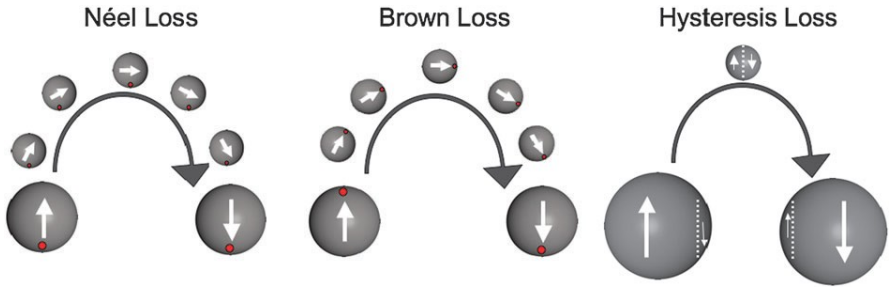

Figure 5 *- (Left) Rotation of the moment within the SPION, overcoming their anisotropy energy barrier that leads to Néel Loss, (centre) mechanical rotation of the SPIONs, that will create frictional losses with the environment and lead to Brown losses and (right) movement of domain walls in multidomain SPIONs that leads to hysteresis loss.*

SPIONs are also able to create small local magnetic fields, which cause a shortening of the relaxation times (T_1 and T_2) of the surrounding protons. This effect is named proton relaxation enhancement and leads to a change of the Nuclear Magnetic Resonance (NMR) signal intensity in its surroundings.

MRI contrast is improved due to the presence of SPIONs acting as contrast enhancing agents. MRI contrast enhancement relies on the different engulfment of magnetic nanoparticles by different cells.[188] It has been shown that the use of SPIONs improves lesion detection and diagnostic accuracy of MRI.[189] T_1 and T_2 are called the longitudinal and transverse proton relaxation times, respectively. The longitudinal relaxation involves redistributing the populations of the nuclear spin states in order to reach the thermal equilibrium distribution. It reflects an exchange of energy, as heat, from the system to its surrounding. T_1 measures the dipolar coupling of the proton moments to their surrounding; thereby isolated protons would show negligible rates of T_1 relaxation. The transverse relaxation is related to the decoherence of the magnetization of the precessing protons due to magnetic interactions with each other and with other fluctuating moments in their surroundings. SPIONs are magnetically saturated at common field strengths used for MRI and their presence produces a marked shortening of T_2 along with a less marked reduction of T_1. Therefore, most of the published examples of the use of SPIONs as contrast agents are based in T_2 weighted

imaging even though the impact on T_1 is significant and often higher compared to paramagnetic chelates.[190]

From a chemical point of view, SPIONs are small synthetic γ-Fe_2O_3 (maghemite) or Fe_3O_4 (magnetite) particles with a core size normally under 15 nm. For more details, refer to *section 2.4.4.1* and references therein.

3.1 Biomedical Application of SPIONs

In order to use SPIONs in biomedical field, a proper surface functionalization is required. Organic molecules that exhibit specific bioactivity must be loaded onto SPION surface and in this thesis the mainly used strategies will be shown *[see Chapter 4]*.

The surface modification by organic molecules has different tasks to fulfill:[191] (i) stabilize the nanoparticles in a biological suspension with a pH around 7.4 and a high salt concentration, (ii) provide functional groups at the surface for further derivatization, and finally (iii) avoid immediate uptake by the reticulendothelial system (RES).[192]

Drug targeting has emerged as one of the modern technologies for drug delivery.[193]

Drug targeting involves *passive*, *active* or *physical* targeting. In *passive* targeting the distribution of the drugs within the body occurs through drug and carrier properties that are unchanged ("Prodrugs'"). *Active* targeting is achieved with mechanisms that allow direct targeting of drugs and/or carriers to specific cells, tissues or organ systems through specific recognition mechanisms. *Physical* targeting allows distribution of drugs and carrier systems through external influences, such as magnets in the case of SPIONs or heat.

SPIONs in combination with an external magnetic field allow delivering particles to the desired target area and fixing them at the local site while the medication is released and acts locally (Magnetic Drug Targeting, MDT).[193,194] *[see section 3.4.2]* Therefore, the dosage of the medication can be reduced and the systemic effect of the drugs kept to a minimum.[193,195]

The possibilities of SPIONs applications have drastically increased in recent years.[194c,195,196] In the clinical area of human medicine, these particles are being used as delivery systems for

drugs,[197] genes[198] and radionuclides.[196b] Furthermore, ferrofluids, as contrast agents in magnetic resonance imaging (MRI) *[see section 3.4.1]*, are routinely applied in the field of diagnostic imaging.[199] SPIONs are also attractive for *in vitro* applications in medical diagnostics, such as research in genetics[198b] and technologies based on immune magnetic separation (IMS) of cells, proteins, DNA/RNA, bacteria, virus and other biomolecules.[200] Furthermore, in recent years, advances were made using SPIONs in clinical studies of cancer therapy in veterinary[201] and human medicine[194a,202] by attacking solid tumors with magnetically targeted 4-epidoxorubicin, or enhancing intraarterial chemotherapy through targeted retention of particles.

Magnetic Fluid Hyperthermia (MFH) is another field where SPIONs are applied to create an increase in temperature by applying an oscillating magnetic field to kill the tumor cells.[203] This type of therapy is already used in human patients in the field of oncology *[see section 3.4.3]*.

One of the promising applications of SPIONs in the future could be focused on the musculoskeletal system in humans and animals.[204] Many of the diseases in the musculoskeletal system are characterized by local inflammatory processes and currently are treated with systemic non-steroidal antiinflammatory drugs (NSAID's)[205] or corticosteroids.[206] Apart from systemic side effects from these drugs, such as gastric ulcers or bleeding tendencies, local access or maintaining of therapeutic drug concentrations may be a problem. SPIONs could serve a major purpose through drug delivery to inflammatory sites to maintain appropriate concentrations while at the same time reducing cost, overall dosage and unwanted side effects. The magnets used in conjunction with SPIONs as drug carriers would allow switching on and off the magnetic field, thus targeting the particles at the local site for time, dosage and elimination.

One of the reasons why the use of SPIONs was limited in the last 2 decades was their insufficient characterization, the inhomogenous morphology and fast elimination through the RES.[195] However, new technologies in synthesis and methods of particle analysis together with more sophisticated coatings optimized properties of SPIONs and thus, their use has become highly attractive for medical applications in diagnostics and therapy.

3.2 Properties and Characteristics of SPIONs for Biomedical Applications

3.2.1 Size of Particles

The size of particles usually refers to the total diameter of the particles including the iron core and the coating. Since the smallest diameter of capillaries in the body is 4 µm,[207] larger particles will be mainly captured and withheld in the lungs.[208] Particles with larger sizes and/or aggregations of small particles thus may be trapped, causing emboli within the capillary bed of the lungs.[209] Depending on their magnetic energy, most nanoparticles have a tendency to aggregate, thus reducing their surface charge. This may lead to precipitation that could prove dangerous if these particles are injected intravenously. Therefore, it is important to know the surface charge and aggregation behavior of the particles in blood.[210]

Most intravenously applied nanoparticles are recognized as ‘‘foreign’’ from the body system and are eliminated immediately through macrophages of the mononuclear phagocytosis system (MPS).[211] Particles smaller than 4 µm are taken up through cells of the reticuloendothelial system, mainly in the liver (60–90%) and spleen (3–10%).[209,211] While it is more likely that small particles up to 100 nm will be phagocytosed through liver cells (openings in the endothelium of liver sinusoids are between 100 and 150 nm), there is a tendency for particles larger than 200 nm to be filtered by the venous sinuses of the spleen.[212] If particles between 30 and 100 nm are intravenously applied, the liver eliminates the larger particles faster from the bloodstream compared to the smaller sizes. Thus, the larger the particles are, the shorter is their plasma half-life-period.[213]

Depending on particle size, uptake may be subdivided in *phagocytosis* (all sizes) or *pinocytosis* (particles < 150 nm).[211,214] Large particles will be only removed by cells capable of phagocytosis, whereas smaller particles can be removed by all types of cells through pinocytosis (all cells are capable of pinocytosis). Phagocytotic activity increases with size of particles.[214]

Under physiologic conditions, particles larger than 10 nm cannot penetrate the endothelium.[195] However, this permeability barrier may be increased under pathologic conditions, such as inflammation or tumor infiltration. There, the penetration threshold can be increased to allow 700 nm particles.[212] This can also be temporarily achieved through the help of medication, immune modulators, heat or radiation.[195]

In conclusion, the uptake of nanoparticles is strongly dependent on particle size as it was proven *in vitro*[215] and *in vivo*.[214,216]

3.2.2 Toxicity of Particles

All pharmaceutical substances intended for use in humans and animals require extensive testing for toxic side effects. This is also true for SPIONs. Apart from acute toxicity, the toxicity of degradation products, stimulation of cells with subsequent release of inflammatory mediators,[214] and toxic effects through the particulate system have to be seriously considered.

A first indication about the toxicity can be obtained by studying tissues from cell cultures histologically after incubation with nanoparticles.[204,217] However, the *cytotoxicity is usually much higher in vitro compared to in vivo*. This may be explained by the fact that degradation products responsible for the toxicity are eliminated continuously from the application site *in vivo*. Therefore, toxicity tests conducted *in vitro* may have limited application.[214]

If suspensions containing nanoparticles are used *in vivo*, they should be hydrophilic and their pH should be close to 7.4.[195] In addition, they should be degraded and eliminated by the body system without residues, otherwise they may accumulate in certain cell compartments, such as liposomes, or tissues from the phagocytosis system (MPS).[214]

One of the feasible toxicity tests *in vivo* is the intraperitoneal application of nanoparticles in mice[218] that allows studying the LD_{50} dosage, the mitotic index (mutagenicity), and the effect of particles on macrophages and other cells (liver, spleen, kidney, peritoneal cells) by means of histology.

The toxicity (acute and subacute toxicity, mutagenicity), and pharmacokinetics (body distribution, metabolism, bioavailability, elimination) of nanoparticles with a median diameter of 80 nm (measured by laser light scattering) was investigated earlier in a large experimental study in dogs as well as mice.[219] The particles tested were planned for later studies centered on MRI diagnostics of liver problems. Before intravenous application, the particles were functionalized with radioactive iron and several parameters were studied: (i) the distribution of radioactivity within different tissues using a special indicator for Fe isotopes, (ii) the relaxation time of liver and spleen in MRI, (iii) the capability to treat a previously induced iron deficit anemia, (iv) pathology of several organ systems by means of histology, (v) chemscreen of blood and urine and (vi) the mutagenicity by means of a special test (Ames Salmonella Microsome Reverse Mutation Assay).

One hour after injection, 82.6% of the particles could be detected in the liver and 6.2% in the spleen. The concentration of radioactive particles was slowly decreased in the liver (plasma half-life 3 days) and the spleen (4 days) and the radioactive iron was incorporated into the hemoglobin of erythrocytes. The mean detection time (T_2) in the MRI was shorter (2 days), since only unchanged particles are capable of inducing enough contrast to be detected. The previously induced anemia, however, was successfully treated within a period of 7 days. No acute or subacute toxic side effects were found in histology or serologic blood tests, although a maximal dosage of 3000 µmol Fe/kg was applied in the dogs and rats. This corresponds to a 150 times higher in dosage compared to what is required for diagnostic liver tests using MRI.

Further *in vivo* tests with SPION based on particles of 100–1000 nm with either dextran, anhydroglucose or carbonate coating, and even clinical tests in humans showed excellent biocompatibility.[194a,202,220]

3.2.3 Surface Charge

The measured surface charge of SPIONs is related to the electrical potential at the shear plane of the double layer, the so-called zeta potential, which is measured through the

electrophoretic motility.[214] Using electrostatic stabilization of the SPIONs, a high zeta potential is needed.

The zeta potential is dependent on electrolyte concentration of the soluble medium *in vitro* and additionally on the adsorbing plasma proteins *in vivo*.[221] If the zeta potential is lower than a given critical value of the particulate system, aggregation and precipitation of the particles occurs.

The surface charge also plays an important role during endocytosis. There should be a slower uptake for negatively charged particles due to the negative ‘‘rejection’’ effect of the negatively charged cell membrane. However, the endocytosis index *in vitro* is minimal with a zeta potential close to zero.[222] In contrast, phagocytosis is increased with a higher surface charge independent of whether the charge is negative or positive.[211]

The higher the surface charge, the shorter is the residence time of SPIONs in the circulatory system.[213]

3.2.4 Protein Adsorption Capacity

If nanoparticles are injected intravenously, immediate interaction with plasma proteins occurs. The adsorption of proteins at the particle surface is called *opsonization*.[223] The amount of adsorbed proteins is based on the size of the molecules and the charge and hydrophobicity of the particle surface. With increasing size, charge and hydrophobicity of the particles, the capacity of protein adsorption increases.[211] Also hydrophobic interactions have an effect on protein adsorption[224] such that dehydration of hydrophobic areas results in entropy gain which in turn facilitates protein adsorption.[225] The adsorbed protein components play an important role in the biodistribution, degradation and elimination of the nanoparticles.[211,226] Proteins that encourage phagocytosis are called *opsonins* (e.g. immunglobulin G (IgG), complement system, fibronectin),[207,227] whereas those inhibiting phagocytosis are called *dysopsonins*.[223,228]

The adsorption of a variety of proteins on nanoparticle systems has been investigated *in vitro* and *in vivo*.[223,229] The opsonins and dysopsonins as well as other inactive proteins of the

blood plasma are responsible for the overall behavior of nanoparticles *in vivo*. Therefore, it is suboptimal to study the adsorption behavior of single proteins with nanoparticles.[223] It is much more effective to study all plasma proteins present in blood by means of two-dimensional polyacrylamide gel electrophoresis.[211,230] With this method, several thousands of plasma proteins can be separated at the same time according to their isoelectric point and molecular weight. The main challenge encountered with this method is to identify the adsorbed proteins in combination with the particles without creating artifacts.[211] Magnetic particles in contrast may relatively easily be separated from blood plasma by means of a magnetic separation technique. Studies elucidating the pattern of protein adsorption on SPIONs with a diameter of 65 nm and carboxydextran coating revealed a 40% IgG and 20% fibronectin adsorption of the overall adsorbed protein. In addition, IgM, IgD, complement factor C3, apolipoprotein A-1 and three further undefined proteins were detected. These particles were quickly eliminated and phagocytosed by Kupffer cells in the liver.

3.3 In Vitro Use of SPIONs

SPIONs have proven to be very useful tools for magnetic separation techniques in clinical use and have replaced other separation technologies.[195,194c,196a,200,231] This is true for immunomagnetic cell separation and purification, as solid phase for immunoassays for isolation, purification and recognition of proteins.[194c,231a,f] In addition they are used for molecular biology, where they were shown to be useful for the isolation, purification, hybridization, synthesis and as markers for DNA/RNA.[194c,196a,231a,d,f] The isolation and detection of microorganisms is easily possible using SPIONs,[196a,231a] as well as efficient gene transfer of nucleotides or gene sequences into cells.[198b]

In medical and clinical diagnostics, the interaction of antigens and antibodies is routinely used to measure concentrations of biological markers. Traditionally, antibodies and/or antigens are immobilized as solid phases on filters, tubular structures, plastic spheres or plates. The use of SPIONs as solid phases for these separation techniques has revolutionized and simplified this field of clinical chemistry through the development of more sensitive, highly efficient and automated immunoassays.[194c,195,231b,g,h,232] Also magnetic beads

consisting of macroporous polymer particles containing iron oxide magnetic particles within the pores (microspheres) are successfully used for this technology of immune magnetic separation (IMS).[200,231d] This technique is an attractive, cost effective alternative for fluorescent activated cell sorting (FACS), which in contrast to IMS is less efficient, slower, requires a high dilution of the cell suspension and also has problems with sterility.[231b] IMS allows detecting very low concentrations of cells (up to 10 cells/ml) and this is an advantage in early diagnostics of cancer in the search of circulating tumor cells in the blood[200,231c] or bone marrow.[195,200,231b,e]

Cells,[194c,200] proteins, nucleic acids,[194c] bacteria, virus, parasites[196a,231b] and fungal agents may be well conserved if separated with IMS, and can be cultured in appropriate culture media afterwards without having to eliminate the particles.[196a]

Most of the commercially available magnetic separation systems function according to the same principle: the surface of the SPIONs is labeled with antibodies against epitopes of cells, bacteria or other target antigens.[233] Thereafter, the labeled particles are mixed with the suspension to be tested. After the antigen and antibody reaction, the labeled, immunomagnetic cell or bacteria suspension is pipetted in a separation container and a magnetic field is applied. While the immunomagnetic labeled cells remain within the container, all other substances are washed out.

Through the development of the so-called ‘‘Microfabricated Flow System’’, the IMS technology was refined to the point where a continuous separation in a one-step procedure and without complicated washings can be achieved.[231b]

SPIONs have also demonstrated their efficiency as non-viral gene vectors that facilitate the introduction of plasmids into the nucleus multifold compared to routinely available standard technologies. As in cell separation, the applied magnetic field allows transporting the genes selectively to the desired local cells within cell cultures. This is possible for the investigation of cell differentiating factors in non-gene manipulated neighboring cells within the same cell culture.[198b]

3.4 In Vivo Applications of SPIONs

3.4.1 Magnetic Resonance Imaging (MRI)

Clinical diagnostics with MRI has become a popular non-invasive method for diagnosing mainly soft tissue or recent cartilage pathologies, because of the different relaxation times of hydrogen atoms.[195,234] SPIONs were developed as contrast agents for MRI and increase the diagnostic sensitivity and specificity due to modifications of the relaxation time of the protons.[195,199b,f,235] The first dextran coated SPIONs were already 10 years ago officially registered as contrast agents for MRI of the liver in Europe.[199c] The efficacy of the SPIONs as contrast agent in various tissues depends on their physicochemical properties, such as size, charge and coating,[213] and can be increased through surface modifications by biologically active substances (antibodies, receptor ligands, polysaccharides, proteins, etc.).[195,199b,236]

The hydrodynamic diameter of the SPION used with MRI varies between 20 and 3500 nm, although intravenously applied particles are relatively small and range between 20 and 150 nm with, or 5–15 nm without coating.[199a,235b] Coatings usually are made from derivates of dextran and poly(ethyleneglycol),[235b] but also starch, albumin, silica, etc.[199a]

Since most of the particles are ingested from cells of the reticulendothelial system (RES), their distribution is most easily made visible in the liver, spleen, bone marrow[237] and lymphnodes.[199a,b,d,235a,d,k,m,238] Renal flow can also be visualized by means of SPIONs.[235f,239,240]

Furthermore, SPIONs were used as oral contrast agents for the diagnosis of gastrointestinal tumors,[199d,e,231d,241] or intravenously for the detection of other tumors in the body system,[199b,c,201b,235l] infarcts in the cardiovascular system,[199d,235c,242] experimentally in cerebral areas [235j,p,243] with increased permeability of the blood brain barrier.[199b,244] SPIONs are also predestined for use as combined carrier systems for drug delivery while at the same time serving as contrast agent.[199b] In this way, the kinetics of the pharmaceutical agent could be followed by means of MRI. In addition, distribution of particles can be influenced through the application of an external magnet.[201b]

3.4.2 Magnetic Drug Targeting (MDT)

One of the major problems in pharmacotherapy is the delivery of drugs to a specific location and maintenance of its location for the desired length of time. The total concentration of drugs could be reduced drastically and side effects could be avoided. Using an external magnetic field, SPIONs functionalized with reversibly bound drugs could be delivered to specific locations and localized in place.[194a,c] The method of MDT is not only dependent on the physical properties, concentration and amount of applied particles, but also on the type of binding of the drugs. In addition, the geometry, size and duration of external magnet application and route of SPIONs injection, as well as vascular supply of the targeted tissues will influence their effect.

The physiological parameters of the patient, such as body weight, blood volume, cardiac output, peripheral resistance of the circulatory system and organ function will also affect the efficiency of the external magnet apart from the possibility to place the magnet in close vicinity to the location.[195,220a] MDT, however, is dependent on this external magnetic field that in most commercially available magnets a penetration depth of a few millimeters into the tissue is achieved. However, newer investigations report about permanent neodymium iron boron magnets in combination with SPIONs of excellent magnetic properties that increase the depth of the magnetic field up to 10–15 cm.[201a,220b]

In vivo SPIONs were successfully applied intravenously and accumulated at specific locations by means of external magnets.[194a,c,198b,201a,b,220a] This is especially attractive for use in cancer therapy, where chemo- or radiotherapy is demonstrating serious, extensive side effects while only having a small therapeutic margin.

3.4.3 Hyperthermia with Magnetic Ferrofluids

Superparamagnetic particles exposed to an alternating magnetic field can be used for heat induction.[192,245] Through the oscillation of the magnetic moment inside the particles the magnetic field energy in the form of heat is liberated and conducted to the tissue environment.[192,195] SPIONs have a much higher rate of specific absorption compared to

larger magnetic particles with several magnetic domains and therefore, are predestinated for use in hyperthermia, where the tissue is heated up to 41–46 °C.[203,245] If the temperature exceeds 56 °C, necrosis, coagulation or carbonization of the tissue is the result; a procedure called ‘‘thermoablation’’.[245,246] For obvious reasons thermoablation is only of limited value in clinical applications.[203a]

In contrast, hyperthermia is highly suitable for cancer therapy, since tumor cells are highly susceptible to elevated temperatures.[192,247] If tumor cells are heated up to 41–45 °C, the tissue damage for normal tissue is reversible while the tumor cells are irreversibly damaged. This can be an advantage when used in combination with therapies such as radio- and chemotherapy.[203b,245,248] Interestingly, hyperthermia seems to induce modifications of the cell surface receptor molecules and thus, tumor cells are recognized by the immune system (killer cells) more easily.[249] Furthermore, the blood brain barrier is reduced for 60 min when temperatures reach 42.5–43 °C promising an improvement in combined chemotherapies of brain tumors.[245]

Conventional hyperthermia treatments including microwaves, ultrasound, radiofrequency, and infrared, have already been successfully used. However, their disadvantage is based on their inability to selectively induce heat formation in specific tumor tissue, inhibition of heat conduction through less heat conductive tissue, such as fat and cranial bone, the invasiveness of the methods, and temperature distribution inhomogeneities.

In many *in vitro* tests with different types of tumor cells and SPIONs, the optimal physical properties of the SPIONs,[250] antibody mediated tumor adhesion,[247,251] particle uptake into tumor cells,[250] duration and strength of the magnetic field[247,250,251] was studied to achieve the most efficient tumor cell inactivation. They were then confirmed in animal experiments *in vivo* (mostly in mice) with experimentally induced tumors.[203,246,248]

Currently, clinical trials in human patients affected with prostate and brain tumors are conducted using local magnetic hyperthermia in combination with radiotherapy.[245]

Apart from cancer therapy, local magnetic hyperthermia could be used for blood coagulation in small vessels,[195] for selective temperature increases in virus infected cells (eg. HIV after

coupling of CD4 glycoproteins to SPIONs)[192] and as a drug delivery mechanism, where substances are coupled to magnetic microspheres or SPIONs.[252]

As a summary, the application of SPIONs for local magnetic hyperthermia is a promising tool for future therapy where selective, efficient and non-invasive methods for heat induction in tissues are warranted.

References

[185] M. Colombo, S. Carregal-Romero, M.F. Casula, L. Gutiérrez, M.P. Morales, I.B. Böhm, J.T. Heverhagen, D. Prosperi, W.J. Parak, *Chem. Soc. Rev.*, **2012**, *41*, 4306-4334.

[186] R.E. Rosensweig, *J. Magn. Magn. Mater.*, **2002**, *252*, 370-374.

[187] J.P. Fortin, C. Wilhelm, J. Servais, C. Menager, J.C. Bacri, F. Gazeau, *J. Am. Chem. Soc.*, **2007**, *129*, 2628-2635.

[188] M.F. Bellin, *Eur. J. Radiol*., **2006**, *60*, 314-323.

[189] M.G.Harisinghani, K.S. Jhaveri, R.Weissleder,W. Schima, S. Saini, P.F. Hahn, P.R. Mueller, *Clin. Radiol.*, **2001**, *56*, 714-725.

[190] (a) U.I. Tromsdorf, O.T. Bruns, S.C. Salmen, U. Beisiegel, H. Weller, *Nano Lett.*, **2009**, *9*, 4434-4440; (b) E. Taboada, E. Rodriguez, A. Roig, J. Oro, A. Roch, R.N. Muller, *Langmuir*, **2007**, *23*, 4583-4588; (c) S. Wagner, J. Schnorr, H. Pilgrimm, B. Hamm, M. Taupitz, *Invest. Radiol.*, **2002**, *37*, 167-177; (d) M. Taupitz, S. Wagner, J. Schnorr, I. Kravec, H. Pilgrimm, H. Bergmann-Fritsch, B. Hamm, *Invest. Radiol.*, **2004**, *39*, 394-405.

[191] T. Neuberger, B. Schöpf, H. Hofmann, M. Hofmann, B. von Rechenberg, *J. Magn. Magn. Mater.*, **2005**, *293*, 483-496.

[192] F. Füssel, *Dissertation*, Aachen: Rheinisch-Westfälische Technische Hochschule Aachen, **1997**.

[193] V.P. Torchilin, *Eur. J. Pharm. Sci.*, **2000**, *11*, S81.

[194] (a) A.S. Lübbe, C. Bergmann, H. Riess, *et al.*, *Cancer Res.*, **1996**, *56*, 4686; (b) A.S. Lübbe, C. Alexiou, C. Bergmann, *J. Surg. Res.*, **2001**, *95*, 200; (c) V. Strom, K. Hultenby, C. Gruttner, *et al.*, *Nanotechnology*, **2004**, *15*, 457; (d) S. Rudge, C. Peterson, C. Vessely, *et al.*, *J. Controlled Release*, **2001**, *74*, 335.

[195] W. Schütt, C. Grüttner, U. Häfeli, *et al*., *Hybridoma*, **1997**, *16*, 109.

[196] (a) O. Olsvik, T. Popovic, E. Skjerve, *et al.*, *Microbiol. Rev.*, **1994**, *7*, 43; (b) W. Schütt, C. Grüttner, J. Teller, *et al.*, *Artif. Organs*, **1998**, *23*, 98. (c) J. Ugelstad, P. Stenstad, L. Kilaas, *et al.*, *Blood Purificat.*, **1993**, *11*, 349.

[197] J. Kreuter, *Habilitationsschrift*, Federal Institute of Technology, Zürich, **1981**.

[198] (a) S.S. Davis, *Trends Biotechnol.*, **1997**, *15*, 217; (b) F. Scherer, M. Anton, U. Schillinger, *et al.*, *Gene Therapy*, **2002**, *9*, 102.

[199] (a) L. Babes, B. Denizot, G. Tanguy, *et al.*, *J. Colloid Interface Sci.*, **1999**, *212*, 474; (b) J.W.M. Bulte, R.A. Books, in: U. Häfeli, *et al.* (Eds.), *Scientific and Clinical Applications of Magnetic Carriers*, Plenum

Press, New York, London, **1997**, p. 527; (c) M. Kresse, S. Wagner, M. Taupitz, in: U. Häfeli, *et al.* (Eds.), *Scientific and Clinical Applications of Magnetic Carriers*, Plenum Press, New York, **1997**, p. 545; (d) D. Poliquen, J.J. Jeune, R. Perdristot, *et al.*, *J. Magn. Reson. Imaging*, **1991**, *9*, 275; (e) P.A. Rinck, G. Myhr, O. Smevik, *et al.*, *Röfo Fortschr. Rontg.*, **1992**, *157*, 533; (f) C. Chambon, O. Clement, A. Le Blanche, *et al.*, *Magn. Reson. Imaging*, **1993**, *11*, 509.

[200] W.S. Prestvik, A. Berge, P.C. Mork, *et al.*, in: U. Häfeli, *et al.* (Eds.), *Scientific and Clinical Application of Magnetic Carriers*, Plenum Press, New York, **1997**, p. 11.

[201] (a) G. Scott, C. Peterson, C. Hohn, *et al.*, *J. Magn. Magn. Mater.*,**1999**, *194*, 132; (b) C. Alexiou, W. Arnold, R. Klein, *et al.*, *Cancer Res.*, **2000**, *60*, 6641.

[202] A.S. Lübbe, C. Bergmann, in: U. Häfeli, *et al.* (Eds.), *Scientific and Clinical Applications of Magnetic Carriers*, Plenum Press, New York, **1997**, p. 457.

[203] (a) A. Jordan, R. Wust, H. Faehling, *et al.*, in: U. Häfeli, *et al.* (Eds.), *Scientific and Clinical Applications of Magnetic Carriers*, Plenum Press, New York, **1997**, p. 569; (b) A. Jordan, R. Scholz, P. Wust, *et al.*, *J. Magn. Magn. Mater.*, **1999**, *201*, 413.

[204] T. Neuberger, *Ph.D. Thesis*, University of Zürich, **2002**.

[205] R.D. Altman, C.J. Lozada, *Osteoarthritis Cartilage*, **1998**, *6 (Suppl. A)*, 22.

[206] (a) D.D. Frisbie, C.E. Kawcak, G.W. Trotter, *et al.*, *Equine Vet. J.*, **1997**, *29*, 349; (b) C.E. Kawcak, R.W. Norrdin, D.D. Frisbie, *et al.*, *Equine Vet. J.*, **1998**, *30*, 66; (c) T. Tobin, in: C. Thomas (Ed.), *Drugs and the Performance Horse*, third ed., Springfield, **1981**, p. 132.

[207] R.F. Schmidt, G. Thews, *Physiologie des Menschen*, 26th ed., Springer, Berlin, **1995**, p. 515.

[208] J. Kreuter, *Factors influencing the body distribution of polyacrylic nanoparticles*, in: P. Buri, A. Gumma (Eds.), *Drug Targeting*, Elsevier, Amsterdam, **1985**.

[209] J. Kreuter, *Pharm. Acta Helv.*, **1983**, *58*, 196.

[210] G. Strom, S.O. Belliot, T. Daemen, *et al.*, *Adv. Drug Deliv. Rev.*, **1995**, *17*, 31.

[211] R.H. Müller, M. Lück, S. Harnisch, *et al.*, in: U. Häfeli, *et al.* (Eds.), *Scientific and Clinical Applications of Magnetic Carriers*, Plenum Press, New York, **1997**, p. 135.

[212] M.M. Moghimi, A.C. Hunter, J.C. Murray, *Pharmacol. Rev.*, **2001**, *53*, 283.

[213] C. Chouly, D. Polyquen, I. Lucet, *et al.*, *J. Microencapsulation*, **1996**, *13*, 245.

[214] S. Maaβen, E. Fattal, R.H. Müller, *et al.*, *STP Pharma Sci.*, **1993**, *3*, 11.

[215] (a) S. Rudt, *Ph.D. Thesis*, University of Kiel, *1992*; (b) M. Lück, *Ph.D. Thesis*, FU Berlin, **1997**.

[216] A. Karino, H. Hayashi, K. Yamada, *et al.*, *J. Pharm. Sci.*, **1987**, *76*, 273.

[217] (a) F.J. Papatheofanis, R. Barmada, *J. Biomed. Mater. Res.*, **1991**, *25*, 761; (b) R.H. Müller, S. Maaβen, H. Weyhers, *et al.*, *J. Drug Targeting*, **1996**, *4*, 161; (c) C.H. Dodd, H.C. Hsu, W.J. Chu, *et al.*, *J. Immunol. Methods*, **2001**, *256*, 89; (d) M. Lewin, N. Carlesso, C.H. Tung, *et al.*, *Nature Biotechnol.*, **2000**, *18*, 410.

[218] (a) Z.G.M. Lacava, R.B. Azevedo, *et al.*, *J. Magn. Magn. Mater.*, **1999**, 194, 90; (b) Z.G.M. Lacava, *J. Magn. Magn. Mater.*, **1999**, *201*, 431.

[219] R. Weissleder, D.D. Stark, B.L. Engelstad, *et al.*, *Am. J. Roentgenol.*, **1989**, *152*, 167.

[220] (a) A.S. Lübbe, C. Bergmann, J. Brock, *et al.*, *J. Magn. Magn. Mater.*, **1999**, *194*, 149; (b) A.A. Kuznetsov, A.R. Harutyunyan, *et al.*, in: U. Häfeli, *et al.* (Eds.), *Scientific and Clinical Applications of Magnetic Carriers*, Plenum Press, New York, **1997**, p. 379.

[221] R.H. Müller, *Zetapotential und Partikelladung in der Laborpraxis*, Bd. 37, Wissenschaftliche Verlagsgesellschaft GmbH, Stuttgart, **1996**.

[222] T. Kissel, M. Roser, *Proceedings of the International Symposium on Controlled Release of Bioactive Materials*, **1991**, *18*, 275.

[223] T.I. Armstrong, M.C. Davies, L. Illum, *J. Drug Targeting*, **1997**, *4*, 389.

[224] T. Blunk, D.F. Hochstrasser, J. Sachez, *et al.*, *Electrophoresis*, **1993**, *14*, 1382.

[225] W. Norde, F.M. Ritchie, G. Nowicka, *et al.*, *J. Colloid Interface Sci.*, **1986**, *112*, 447.

[226] (a) R.H. Müller, S. Herbort, *Nanopartikel—gewebespezifische Arzneiform für Zytostatika*, **1990**, *DAZ 130*, 1509; (b) G. Borchard, J. Kreuter, *Pharm. Res.*, **1996**, *13*, 1055; (c) G. Borchhard, J. Kreuter, *J. Drug Targeting*, **1993**, *1*, 15.

[227] J.J. Hsu, R.L. Juliano, *Biochem. Biophys. Acta*, **1982**, *720*, 411.

[228] H.M. Patel, *Crit. Rev. Ther. Drug Carrier System*, **1992**, *9*, 39.

[229] (a) D.V. Bazile, C. Ropert, P. Huve, *et al.*, *Biomaterials*, **1992**, *13*, 1093; (b) G. Borchard, *Ph.D. Thesis*, J.W. Goethe-Universität, Frankfurt am Main, **1993**; (c) M.E. Norman, P. Williams, L. Illum, *Biomaterials*, **1993**, *14*, 193; (d) J.C. Leroux, F.D. Jaeghere, B. Anner, *et al.*, *Life Sci.*, **1995**, *57*, 695.

[230] T. Blunk, *Ph.D. Thesis*, University Kiel, **1994**.

[231] (a) C. Grüttner, J. Teller, *J.Magn.Magn. Mater.*, **1999**, *194*, 8; (b) G. Blankenstein, in: U. Häfeli, *et al.* (Eds.), *Scientific and Clinical Applications of Magnetic Carriers*, Plenum Press, New York, **1997**, p. 233; (c) P.A. Liberti, C.G. Rao, L.W.M.M. Terstappen, *J. Magn. Magn. Mater.*, **2001**, *225*, 301; (d) J. Ugelstad, A. Berge, T. Ettlingsen, *et al.*, *Prog. Polym. Sci.*, **1992**, *17*, 87; (e) J.G. Treleaven, J. Ugelstad, T. Philip, *et al.*, *Lancet*, **1984**, *14*, 70; (f) M. Bosnes, A. Deggerdal, A. Rian, *et al.*, in: U. Häfeli, *et al.*

(Eds.), *Scientific and Clinical Applications of Magnetic Carriers*, Plenum Press, New York, **1997**, p. 269; (g) J.J. Chalmers, M. Zaborowski, L. Sun, *et al.*, *Biotechnol. Prog.*, **1998**, *14*, 141; (h) K. Menik, M. Nakamura, K. Comella, *et al.*, *Biotechnol. Prog.*, **2001**, *17*, 907.

[232] M. Meza, in: U. Häfeli, *et al*. (Eds.), *Scientific and Clinical Application of Magnetic Carriers*, Plenum Press, New York, London, **1997**, p. 303.

[233] K.E. McCloskey, K. Comella, J.J. Chalmers, *et al.*, *Biotechnol. Bioeng.*, **2001**, *75*, 642.

[234] A. Tanimoto, D. Pouliquen, B.P. Kreft, *et al.*, *J. Magn. Reson. Imaging*, **1994**, *4*, 653.

[235](a) C. Bordat, M. Sich, F. Rety, *et al.*, *J. Magn. Reson. Imaging*, **2000**, *12*, 505; (b) D. Portet, B. Denizot, E. Rump, *et al.*, *J. Colloid Interface Sci.*, **2001**, *238*, 37; (c) L.J.M. Kroft, J. Doornbos, R.J.v.d. Geest, *et al.*, *Magn. Reson. Imaging*, **1998**, *16*, 755; (d) Y. Abe, Y. Yamashita, T. Namimoto, *et al.*, *Radiat. Med.*, **2000**, *18*, 97; (e) D. Artemov, N. Mori, B. Okollie, *et al*., *Magn. Reson. Med.*, **2003**, *49*, 403; (f) N. Beckmann, C. Cannet, *et al.*, *Magn. Reson. Med.*, **2003**, *49*, 459; (g) M. Brauer, *Prog. Neuropsychopharmacol. Biol. Psych.*, **2003**, *27*, 323; (h) B.J. Dardzinski, V.J. Schmithorst, *et al.*, *Magn. Reson. Imaging*, **2001**, *19*, 1209; (i) V. Dousset, C. Delalande, L. Ballarino, *et al.*, *Magn. Reson. Med.*, **1999**, *41*, 329; (j) G. Fleige, C. Nolte, M. Synowitz, *et al.*, *Neoplasia*, **2001**, *3*, 489; (k) R. Guimaraes, O. Clement, J. Bittoun, *et al.*, *Am. J. Roentgenol.*, **1994**, *162*, 201; (l) M. Krause, K.K. Kwong, J. Xiong, *et al.*, *Ophthalmic Res.*, **2002**, *34*, 241; (m) P. Oswald, O. Clement, C. Chambon, *et al.*, *Magn. Reson. Imaging*, **1997**, *15*, 1025; (n) P. Reimer, R. Weissleder, A.S. Lee, *et al.*, *Radiology*, **1990**, *177*, 729; (o) J.M. Rogers, J. Lewis, L. Josephson, *Magn. Reson. Imaging*, **1994**, *12*, 1161; (p) A. Sbarbati, A. Reggiani, E. Lunati, *et al.*, *Neuroimage*, **2000**, *12*, 418; (q) S.A. Schmitz, S.E. Coupland, R. Gust, *et al.*, *Invest. Radiol.*, **2000**, *35*, 460; (r) B.E. VanBeers, J. Pringot, B. Gallez, *J. Radiol.*, **1995**, *76*, 991; (s) R. Weissleder, P. Reimer, A.S. Lee, *et al.*, *Am. J. Roentgenol.*, **1990**, *155*, 1161; (t) R. Weissleder, M. Papisov, *Rev. Magn. Reson. Med.*, **1993**, *4*, 1; (u) R. Weissleder, A. Bogdanov, *et al.*, *Adv. Drug Deliv. Rev.*, **1995**, *16*, 321; (v) G. Wen, X.L. Zhang, R.M. Chang, *et al.*, *Di Yi Jun Yi Da Xue Xue Bao*, **2002**, *22*, 451.

[236] Y. Zhang, S.J. Dodd, K.S. Hendrich, *et al.*, *Kidney Int.*, **2000**, *58*, 1300.

[237] E. Seneterre, R. Weissleder, D. Jaramillo, *et al.*, *Radiology*, **1991**, *179*, 529.

[238] K. Lind, M. Kresse, N.P. Debus, *et al.*, *J. Drug Targeting*, **2002**, *10*, 221.

[239] Q. Ye, D. Yang, M. Williams, *et al.*, *Kidney Int.*, **2002**, *61*, 1124.

[240] J.P. Laissy, J.M. Idee, A. Loshkajian, *et al.*, *J. Magn. Reson. Imaging*, **2000**, *12*, 278.

[241] P.A. Rinck, O. Smevik, G. Nilsen, *et al.*, *Radiology*, **1991**, *178*, 775.

[242] (a) E. Canet, D. Revel, L. Sebbag, *et al.*, *Am. Heart J.*, **1995**, *130*, 949; (b) L.O. Johansson, A. Bjornerud, *et al.*, *J. Magn. Reson. Imaging*, **2001**, *13*, 615; (c) S. Litovsky, M. Madjid, A. Zarrabi, *et al.*, *Circulation*, **2003**, *107*, 1545; (d) D. Nanz, D. Weishaupt, H.H. Quick, *et al.*, *Magn. Reson. Med.*, **2000**, *43*, 645; (e) S.G. Ruehm, C. Corot, P. Vogt, *et al.*, *Circulation*, **2001**, *103*, 415.

[243] A. Moore, E. Marecos, A. Bogdanov, *et al.*, *Radiology*, **2000**, *214*, 568.

[244] V. Rousseau, B. Denizot, D. Pouliquen, *et al.*, *J. Magn. Magn. Mater.*, **1997**, *5*, 213.

[245] A. Jordan, R. Scholz, K. Maier-Hauff, *et al.*, *J. Magn. Magn. Mater.*, **2001**, *225*, 118.

[246] I. Hilger, W. Andrä , R. Hergt, *et al.*, *Radiology*, **2001**, *218*, 570.

[247] M.S. Shinkai, M. Suzuki, S. Iijima, *et al.*, *Biotechnol. Appl. Biochem.*, **1994**, *21*, 125.

[248] D.C.F. Chan, D.B. Kiprotin, P.A. Brunn, in: U. Häfeli, *et al.* (Eds.), *Scientific and Clinical Applications of Magnetic Carriers*, Plenum Press, New York, **1997**, p. 607.

[249] G. Multhoff, C. Bozler, M. Wiesnet, *et al.*, *Int. J. Cancer*, **1995**, *61*, 272.

[250] A. Jordan, R. Scholz, P. Wust, *et al.*, *J. Magn. Magn. Mater.*, **1999**, *194*, 185.

[251] M. Suzuki, M. Shinkai, *et al.*, *Biotechnol. Appl. Biochem.*, **1995**, *1*, 335.

[252] D.C.F. Chan, D.B. Kirpotin, P.A. Brunn, *J. Magn. Magn. Mater.*, **1993**, *122*, 374.

Ph.D. RESEARCH PROJECT

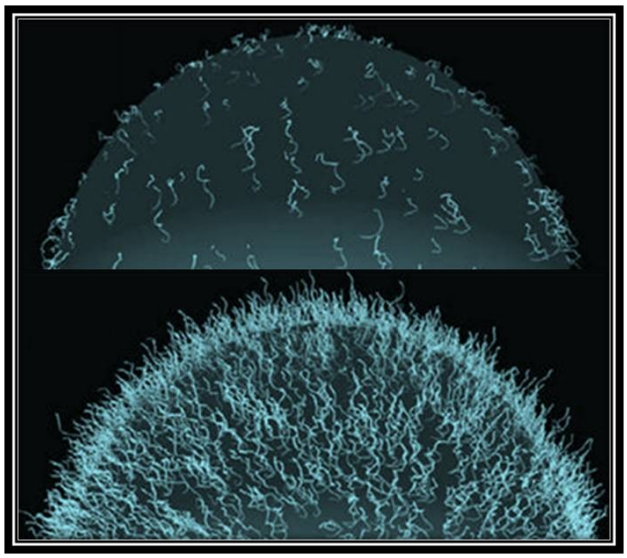

Chapter 4: Surface Functionalization of SPIONs

4 Strategies for SPIONs' Surface Modification

As previously reported, the main difficulty for the use of magnetic nanoparticles in biological fields arises from their chemical instability (oxidation or corrosion phenomena) *[see section 2.5]*, and from the necessity to obtain proper bionanoconjugates able to exhibit the specific biological activity they were designed for, without inducing an immunogenic response *[see section 3.1]*.

These two tasks are complementary; in fact, to prevent oxidation or corrosion of the metallic magnetic core, proper coating are needed. At the same time, to act as bionanoconjugates, the nanoparticles must be coated with specific biomolecules, creating a protective shell around the metallic surface. We can say that often stabilization, protection and desired biological activity of the nanoparticles are closely linked each other.

All the surface modification strategies used with SPIONs consist in a core–shell structure, in which the naked magnetic nanoparticle as a core is coated by a shell, isolating the core itself against the external environment.

The applied coating strategies can roughly be divided into two major groups: coating with organic shells, including surfactant and polymers,[139] as well as biomolecules, or coating with inorganic components (precious metals, silica, carbon).[140,141,142,143,144]

In order to use SPIONs for biomedical applications, the nanoparticle surface must be covered with targeting agents, therapeutic drugs or other functional probes. Hence, the need to develop efficient synthetic strategies for the conjugation of biomolecules onto SPIONs is an important and appealing target.

The strategies used can involve *passive non-covalent adsorption* on the outer particle surface or the formation of a more stable *covalent bond* by using appropriate heterobifunctional linkers,[253] in which one functional group specifically binds the nanoparticle, while the other reacts with the biomolecules in order to form the new bionanoconjugates (*Figure 6*). In theory, these kind of linkers can interact first with the nanoparticle surface leaving the additional functional group able to couple the biomolecule or, *vice versa*, can directly react with the biomolecule and, subsequently, can be supported onto SPIONs.

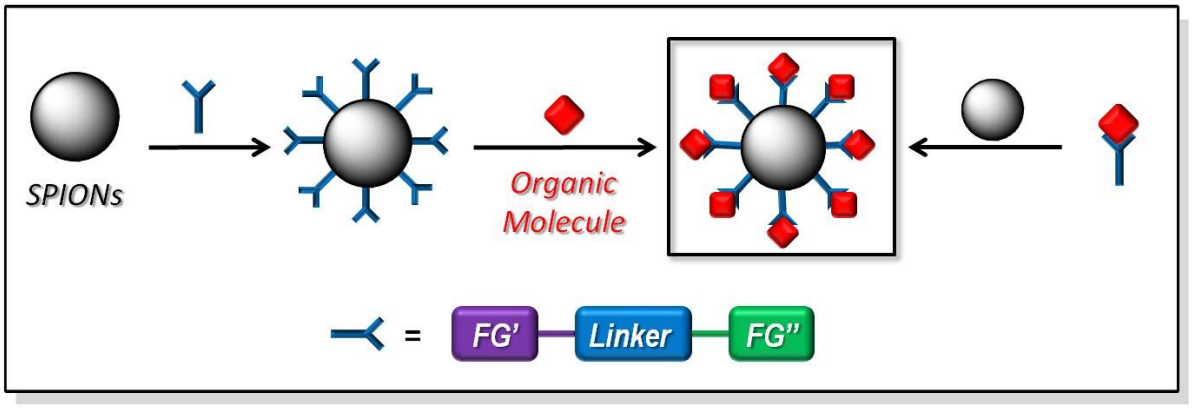

Figure 6 *- The heterobifunctional linker bears two orthogonal functional groups (FG' and FG'') able to selectively react with the SPION surface or with the organic molecule that we want to support on nanoparticle.*

The linker plays a crucial role in the design and synthesis of new nanoconjugates; obviously this molecule acts as a connection between the inorganic magnetic core and the organic biomolecules, but can also acts as protecting shell as well as spacer, with the aim to create an organized distribution of biomolecules on the SPIONs surface.

It's worthy to note that sometimes biomolecules can directly bear a proper functional group able to interact with the nanoparticles, so in these case no linkers are needed.

Otherwise, in order to act their specific bioactivity, some biomolecules need to be quite far away from the SPION surface and the atomic length of the linkers cannot be enough. For these reasons an additional spacer is needed.

4.1 Classical Methodologies for the Surface Modification of SPIONs

As mentioned in *section 4*, the grafting of organic molecules onto the SPION surface consists in the interaction of a proper functional group with the nanoparticles. These interactions are possible thanks to the presence of hydroxyl groups exposed on the SPION surface (*Figure 7*),[152] normally generated by natural passivation during the nanoparticles synthesis.

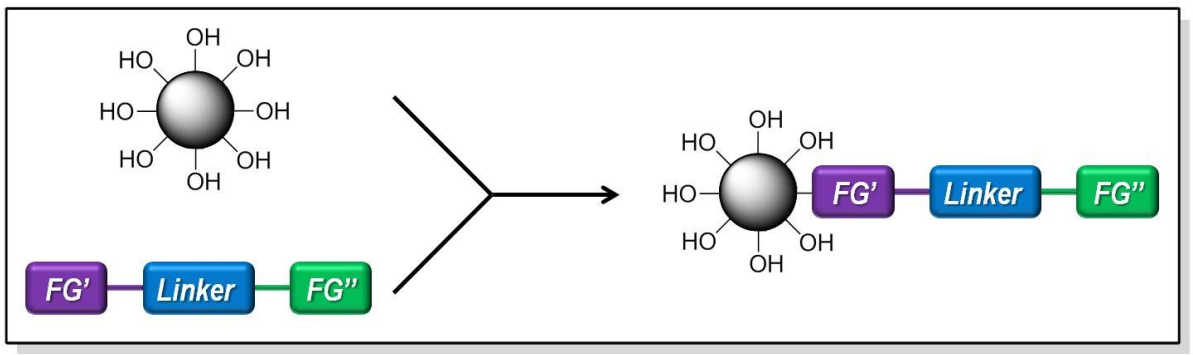

***Figure 7** - Interaction between the first functional group (FG') of an heterobifunctional linker with the surface hydroxyl groups of a SPION.*

To better understand how an organic molecule (either a linker or a biomolecule) can interact with the SPION surface, it's necessary to analyze the nature of the interaction formed.

Two kind of interactions are possible: a *non-covalent adsorption* or a *covalent binding*. These two features will be discussed in the next sections.

4.1.1 Non-Covalent Adsorption of Organic Molecules onto SPIONs

Chemically speaking, SPIONs are nanoparticles composed of mineral iron oxide, with their surface completely covered by hydroxyl groups.

A particle of a mineral oxide in suspension in an aqueous solution tends to polarize and to be electrically charged.[254] Most oxides are amphoteric. Thus, the nature and importance of this charge are a function of pH of the solution surrounding the particle.

For example, in an acidic medium, the particle will be positively charged and the principle of electroneutrality implies the presence of a layer of ions with opposite charge near this particle. The two electric charges compensating each other. If we consider a model in agreement with the Gouy-Chapman theory (the diffuse model of electrical double layer in which the electric potential decreases exponentially away from the surface to the fluid bulk),[255,256] counteranions will be thus located around the particle in a thin diffuse layer, as shown in *Figure 8*.

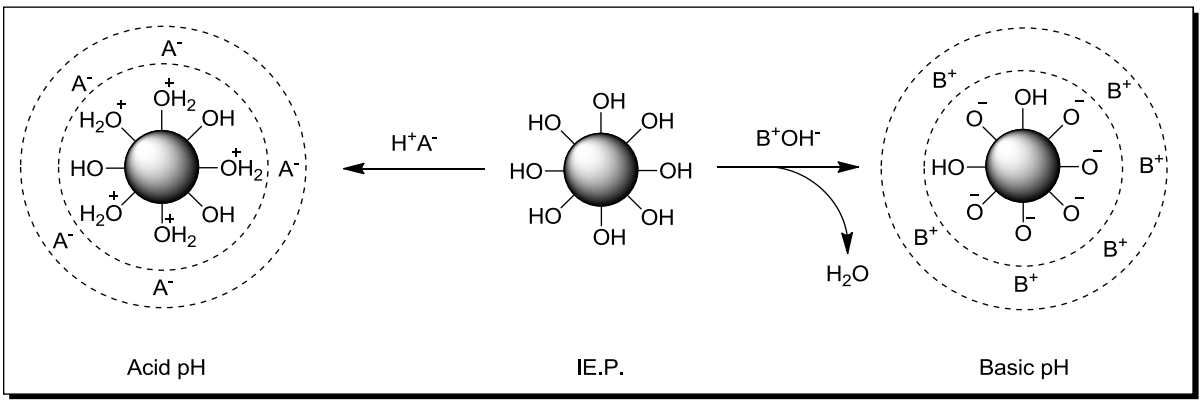

Figure 8 *- Schematic representation of the surface polarization of an oxide particle as a function of the solution pH.*

Schematically, the equation of the surface polarization may be written as follows:

$$\text{S-OH} + \text{H}^+\text{A}^- \rightleftharpoons \text{S-OH}_2^+\text{A}^-$$

where S-OH represents a surface adsorption site and H^+A^- a mineral acid.

In a basic medium, the reverse is true. The particle is negatively charged and is surrounded by compensating cations. The equation of the surface polarization may be written as follows:

$$\text{S-OH} + \text{B}^+\text{OH}^- \rightleftharpoons \text{S-O}^-\text{B}^+ + \text{H}_2\text{O}$$

where B^+OH^- represents a base.

Oxide	***IE.P.***	***Adsorption Capability***
Sb_2O_5	<0.4	
WO_3	<0.5	CATIONS
SiO_2	1.0-2.0	
U_3O_8	≈4	
MnO_2	3.9-4.5	
SnO_2	≈5.5	
TiO_2	≈6	
UO_2	5.7-6.7	CATIONS or
γ-Fe_2O_3	6.5-6.9	ANIONS
ZrO_2	≈6.7	
CeO_2	≈6.75	
Cr_2O_3	6.5-7.5	
α,γ-Al_2O_3	7.0-9.0	
Y_2O_3	≈8.9	
α-Fe_2O_3	8.4-9.0	
ZnO	8.7-9.7	ANIONS
La_2O_3	≈10.4	
MgO	12.1-12.7	

Table 1 *- Isoelectric Points (IE.P.) of various oxides*

One conceives easily that between these two cases, a given value of pH exists at which the particle is overall not charged. This value, which is a characteristic of the oxide corresponds to its zero point of charge, also called *Isoelectric Point* (IE.P.).

Given the IE.P. of an oxide, we may estimate in advance the adsorption capability (anionic or cationic) of particle surface and roughly what the pH range (acidic or basic) of the impregnating solution will be. Nowadays, the IE.P. of a large number of oxides are known and available in literature.[257] Some examples are reported in *Table 1*.

As we can see from the *Table 1*, *γ-Fe_2O_3* SPIONs are amphoteric and can adsorb both cations or anions that are present in the aqueous solution.

This peculiar property can be exploited in order to support biomolecules onto the SPIONs surface by a mild ***non-covalent interaction***. Indeed carboxylic,[258] sulfonic[259] and phosphonic acids,[260] dissolved in organic solvent, can interact with the hydroxyl groups of the iron oxide nanoparticles leading to the formation of carboxylate, sulfonate or phosphonate species in a double layer model as shown in *Figure 9*.

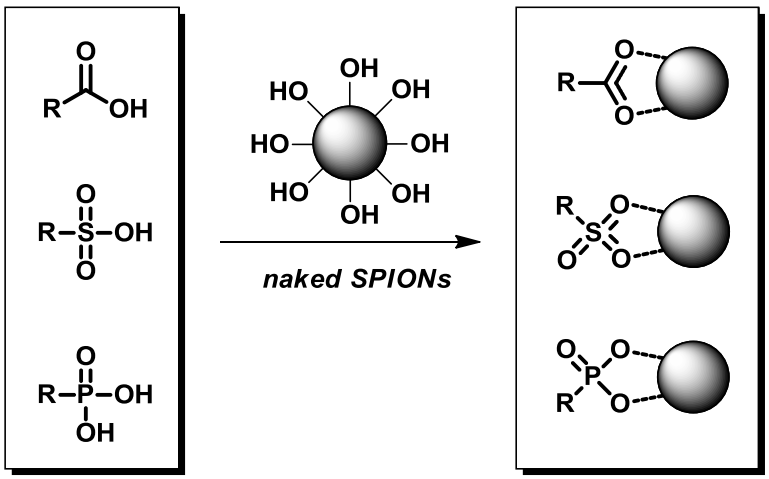

Figure 9 *- Non-covalent adsorption of carboxylic, sulfonic and phosphonic cids onto SPION surface.*

Non-covalent interactions can normally occur with organic acids, while classical organic bases (such as amines) are not able to form the double layer system.

In this research project the use of carboxylate moiety as anchoring group for non-covalent adsorption of biomolecules onto superparamagnetic iron oxide nanoparticles have been successfully exploited *[see section 5.7]*.

4.1.2 Covalent Binding of Organic Molecules onto SPIONs

The surface functionalization of SPIONs can also be carried out by the formation of ***covalent bonds*** between the surface hydroxyl groups of the nanoparticles and a proper functional group present onto an organic molecule, either a simple heterobifunctional linker, an organic spacer or a more complex biomolecule.

As previously reported in *section 2.5.4*, magnetic nanoparticles can be easily coated with a silica shell, thanks to the reaction of TEOS (triethoxysilane) with the nanoparticle surface.[170] In fact, the silane moieties are able to covalently react with the hydroxyl groups exposed on the iron oxide surface, leading to a complete coverage of the external magnetic core.

In an analogous way, covalent surface modification of SPIONs with organic molecules can be easily achieved exploiting the reactivity of siloxane moieties towards the hydroxyl groups present onto the nanoparticle surface.

In fact, alkoxysilanes react with SPIONs *via* a silylation reaction leading to the formation of covalent Fe-O-Si and Si-O-Si bonds.[261] Furthermore, the presence of an additional orthogonal functional group permits to functionalize the nanoparticle surface with a second reactive free functional moiety.

3-Aminopropyl-triethoxysilane (APTES) is the most commonly used alkoxysilane due to the presence of three hydrolysable ethoxysilane moieties able to react with the nanoparticle surface, but also bearing a terminal free amino group capable to further chemical modification (*Figure 10a*).

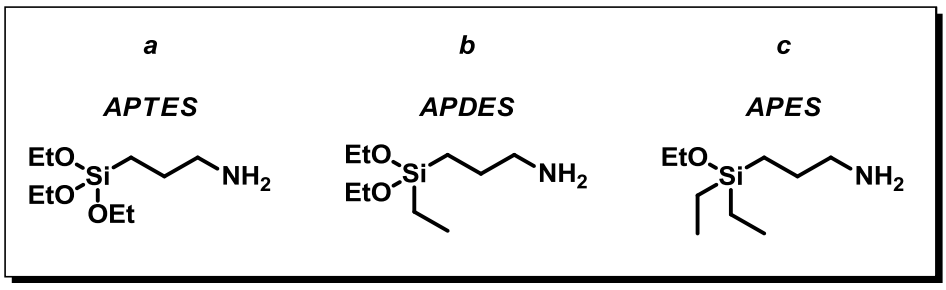

Figure 10 *- Structural formulas of a) 3-aminopropyl-triethoxysilane (APTES), b) 3-aminopropyl-ethyl-diethoxysilane (APDES) and c) 3-aminopropyl-diethyl-ethoxysilane (APES).*

The silylation process is very complex and does not involve a single mechanism. Thus, many different intermediates are possible.[262]

Varying the nature of the alkoxysilane coating reagent, it's possible to easily tune the final loading of the organic molecules covalently grafted onto the SPION surface, tuning at the same time the surface density of the additional free functional groups (e.g. free NH_2 moieties).

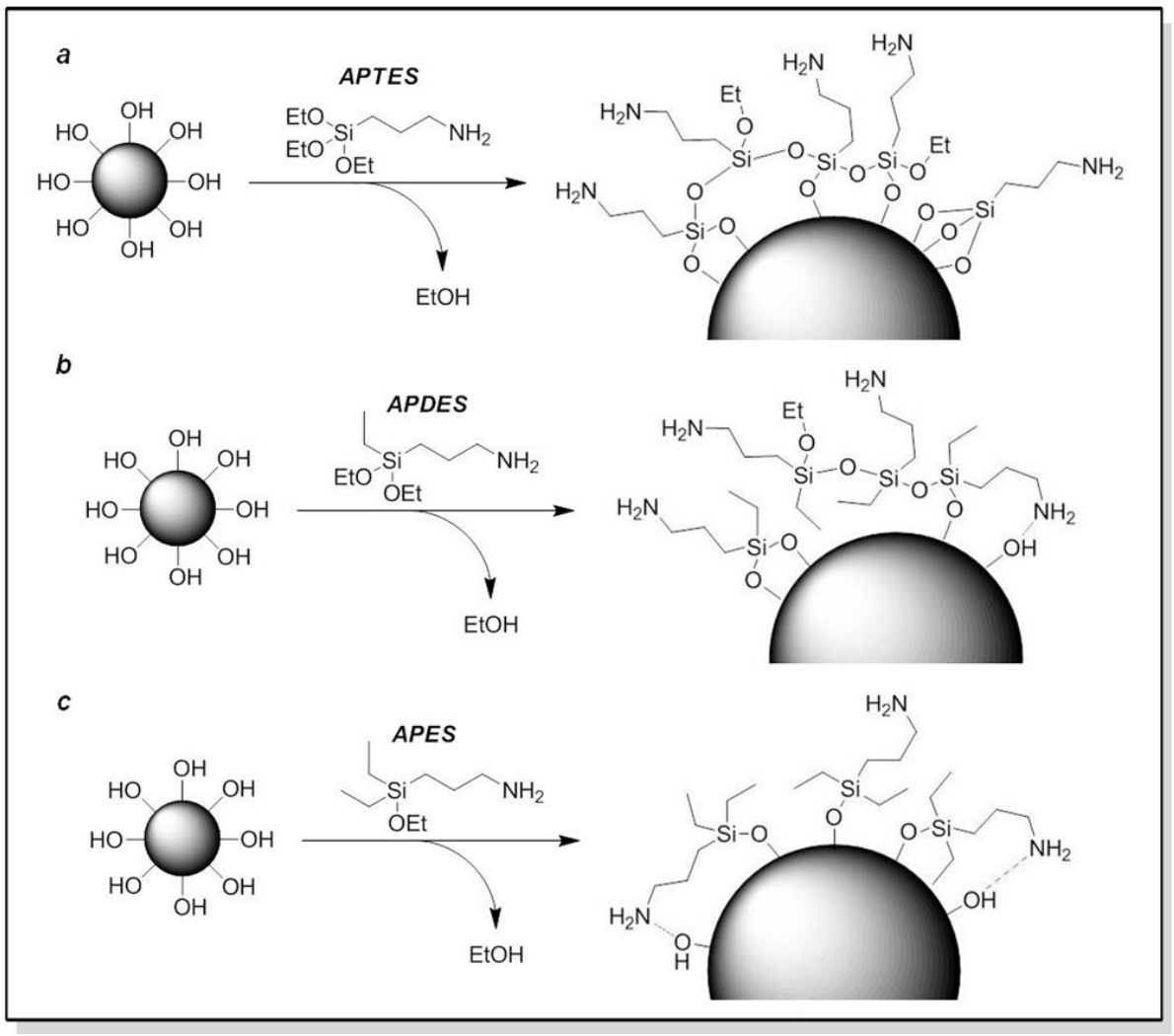

Figure 11 *- Schematic examples of possible SPIONs surface after coating with a) APTES, b) APDES and c) APES alkoxysilanes. It's to note that free amino moieties can form hydrogen bonds with free OH surface groups.*

As schematically reported in *Figure 11*, using the same concentration of three different alkoxysilanes for the covalent surface functionalization of SPIONs, different results can be obtained.

The polycondensation process was outstanding for the APTES molecule (*Figure 11a*) thanks to its three ethoxy groups, which contributed to a large amino group density. When the 3-aminopropyl-ethyl-diethoxysilane (APDES, *Figures 10b* and *11b*) or 3-aminopropyl-diethyl-ethoxysilane (APES, *Figure 10c* and *11c*) were used the loading and the free-amino group density were lower due to the presence of ethyl groups that cause steric hindrances onto the particle surface, reducing the number of formed Fe-O-Si bond, as well as the capability to cross-link (Si-O-Si).

A decrease in the amino group density may also be related to hydrogen bond formation between the anchored amino moieties and neighbor surface hydroxyl groups.[261]

As said before, APTES is one of the most used heterobifunctional linker for the covalent surface modification of SPIONs; the obtained silicon coating prevents from corrosion phenomena and the terminal free amino group can be chemically derivatized in order to anchor different kind of biomolecules onto SPIONs.

4.2 The Discovery of a New Covalent Surface Modification: Anchoring of Isocyanates onto SPIONs

During this Ph.D. research work, both *non-covalent* and *covalent* surface interactions were investigated in order to obtain new bionanoconjugates. Specifically, we were interested in the search for new heterobifunctional linkers able to covalently bind the SPIONs surface, as an alternative to the previously used linker APTES (*Figure 10a*).

In this work, commercially available *γ-Fe_2O_3* maghemite SPIONs (Alfa Aesar) with an average diameter of 10±2 nm were used.

Generally, APTES functionalized nanoparticles can be easily synthesized as reported in *Scheme 1*.[263]

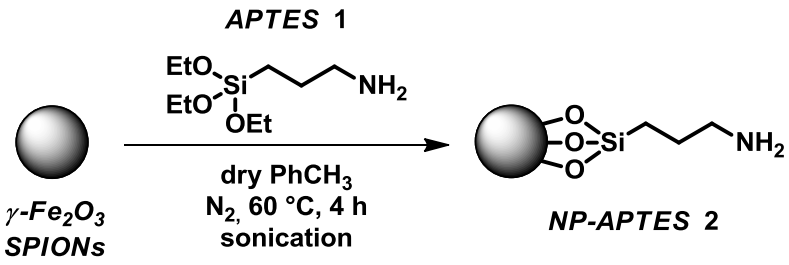

Scheme 1 *- Synthesis of APTES functionalized SPIONs.*

APTES **1** is added to a suspension of naked maghemite SPIONs under sonication; after 4 hours at 60 °C it is possible to isolate the corresponding NP-APTES **2**. The free amino-groups can be used to bind proper biomolecules as itself or after a functional group interconversion.

Using the same strategy, we decided to use the 3-(triethoxysylil)propyl isocyanate (TESPI) **3**, instead of APTES **1**, in order to obtain a new nanoconjugates bearing free NCO-groups on the surface (*Scheme 2*).

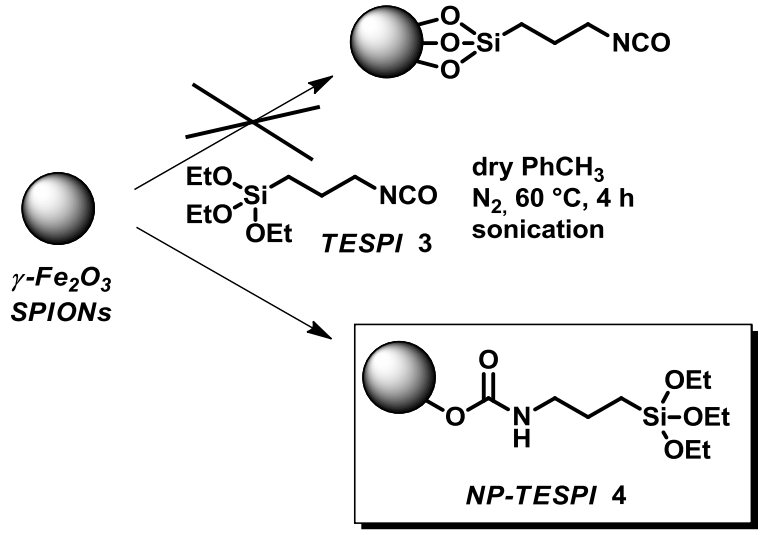

Scheme 2 *- Reaction between SPIONs and TESPI.*

Unexpectedly, we didn't obtain the desired product in which the alkoxysilane reacted with the SPION surface. From FTIR spectroscopy (*Figure 12*) and elemental analysis (E.A.) we have deduced that the isocyanate group of TESPI **3** had interacted with the SPION surface leading to a new species of nanoconjugate. Our hypothesis was that the NCO moiety reacted with the surface OH-groups of the nanoparticle, forming carbamate-like bond, affording the new nanoconjugate NP-TESPI **4** (*Scheme 2*).

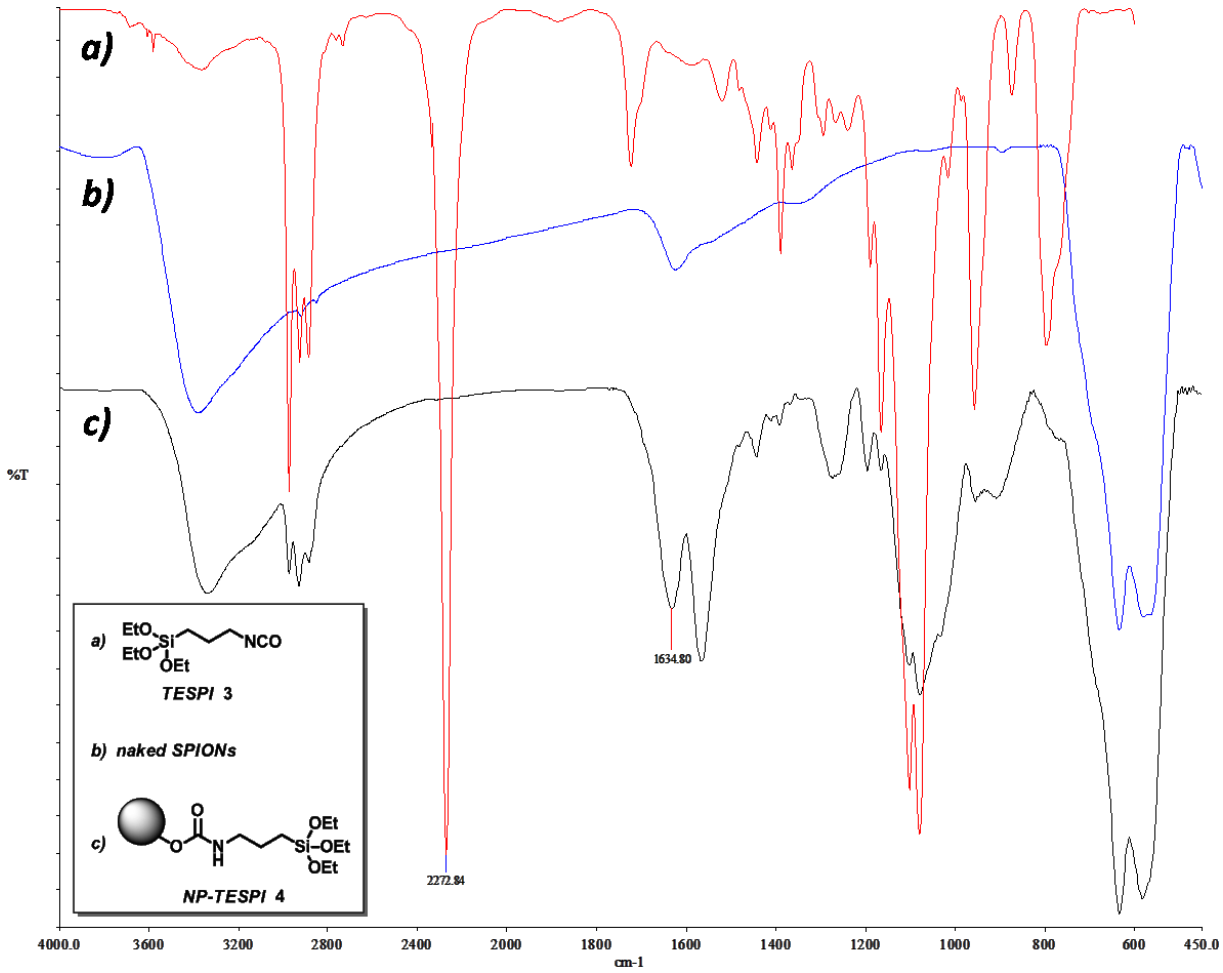

Figure 12 *- FT-IR spectra of a) TESPI* **3***, b) naked SPIONs and c) NP-TESPI* **4***. In spectrum c) is clearly visible the peak at 1635 cm^{-1} referred to the carbamate-like C=O stretching, while the NCO band at 2273 cm^{-1} is absent.*

This unexpected result led us to further investigate the reactivity of the isocyanate group towards the SPION surface.

To the best of our knowledge, only two examples of the use of an isocyanate moiety as the anchoring group onto nanoparticle materials are reported in literature; in particular, Ma *et al.* reported the use of isophorone diisocyanate in reaction with the silanol groups on the surface of nanosilica with formation of a carbamate-like bond,[264] while Ou *et al.* reported the covalent interaction of toluene-2,4-diisocyanate with the hydroxyl groups that cover the

titania nanoparticles.[265] Since in these papers no depth studies were made to demonstrate the formation of a carbamate bond between the isocyanate group and the nanoparticles surface, and nothing is reported in literature about iron oxide nanoparticle grafting with isocyanates, we decided to deep investigate this new anchoring methodology.

In fact, the generality of the grafting of isocyanate molecules onto SPIONs surface, could be exploited as a new anchoring system and a new class of heterobifunctional linkers for SPIONs could be proposed.

The scope of this new possible anchoring strategy was evaluated preparing a small library of new nanoconjugates starting from commercially available (**5**-**9**) or easily synthesizable (**10**) differently substituted isocyanates, reported in *Figure 13*.

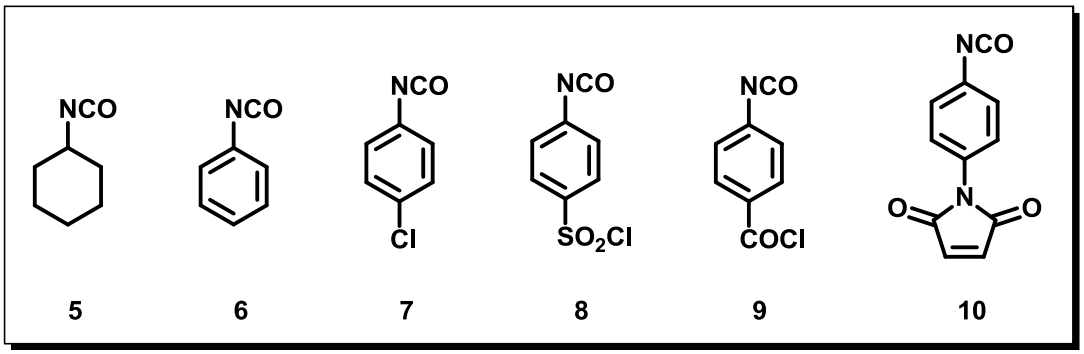

Figure 13

Isocyanates **8**-**10** were endowed with a second functional group which, in principle, could be used to support organic molecules to the SPIONs surface through the linker.

As said before, the (*p*-maleimido)phenyl isocyanate (PMPI) **10** can be easily synthesized as reported in literature and its synthesis is shown in *Scheme 3*.[266]

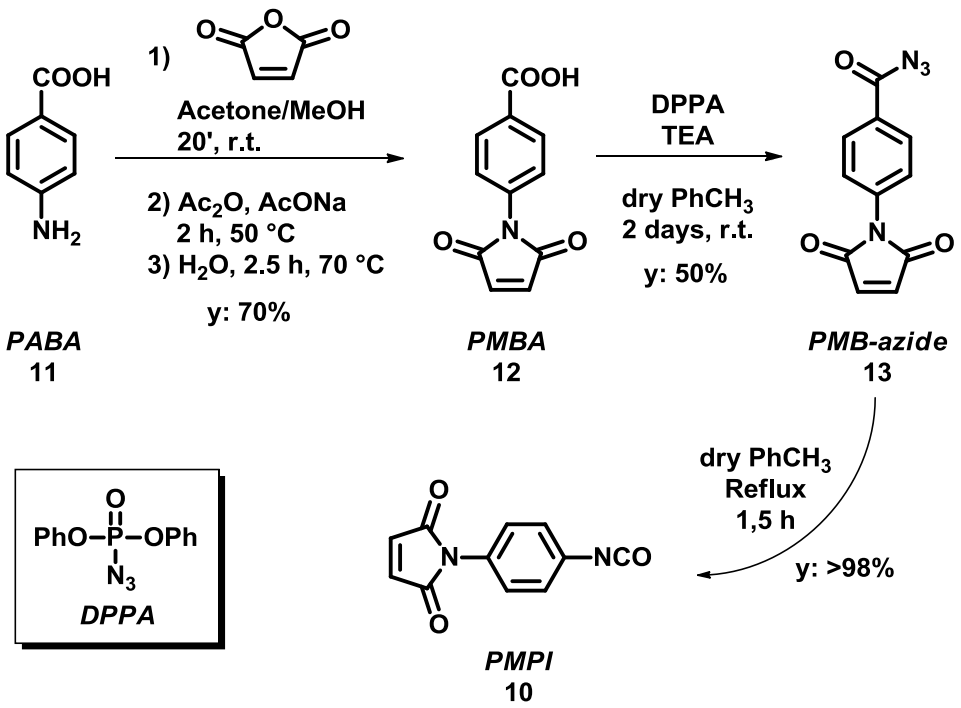

Scheme 3 *- Synthesis of PMPI* **10***.*

Starting from the commercially available (*p*-amino)benzoic acid (PABA) **11** it is possible to obtain the (*p*-maleimido)benzoic acid (PMBA) **12** in 70% yield by reaction with maleic anhydride in a three step procedure. PMBA **12** is directly converted in the corresponding (*p*-maleimido)benzoyl azide (PMB-azide) **13** using diphenylphosphoryl azide (DPPA) in the presence of triethylamine; after chromatographic purification, pure **13** is recovered in 50% yield. Then, the labile acyl azide **13** undergoes a Curtius rearrangement affording the desired PMPI **10** in quantitative yield.

To overcome the limiting step (in terms of yield and reaction time) of conversion of carboxylic acid **12** into the acyl azide **13**, we set up the alternative two step procedure reported in *Scheme 4*. First, **12** was converted into the corresponding (*p*-maleimido)benzoyl chloride (PMB-Cl) **14** by refluxing in thionyl chloride and then, the obtained acyl chloride was reacted with sodium azide in order to form the PMB-azide **13** in 70% yield after chromatographic purification.

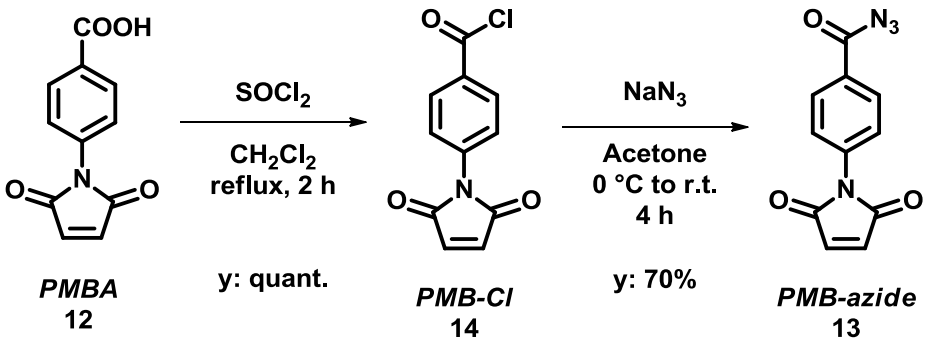

Scheme 4 *- Alternative synthesis of PMB-azide* **13**.

In order to verify the formation of the carbamate bond between –NCO containing molecules **5**-**10** and SPIONs, but also the reproducibility of our innovative grafting methodology, a general protocol for the synthesis of new nanoconjugates has been set up.

The general procedure used to anchor isocyanates **5**-**10** onto the naked SPIONs is shown in *Scheme 5*.

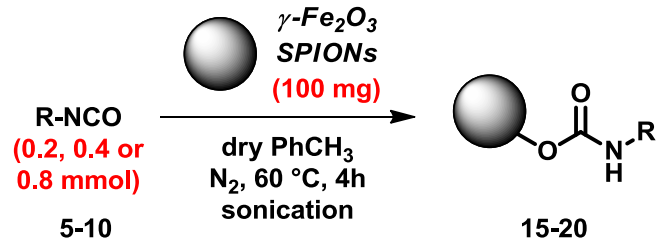

Scheme 5 *- Standard procedure for the synthesis of new carbamate-based nanoconjugates.*

The proper isocyanate (0.2, 0.4 or 0.8 millimoles) was added to a suspension of 100 mg of naked SPIONs in dry toluene, under sonication at 60 °C for 4 hours. The resulting suspension was then centrifugated at 5000 round per minute for 10 minutes; the supernatant was eliminated and the solid residue was washed with fresh toluene (3x5 ml) and diethyl ether (3x5 ml) affording the desired nanoconjugates **15**-**20** (*Figure 14*).

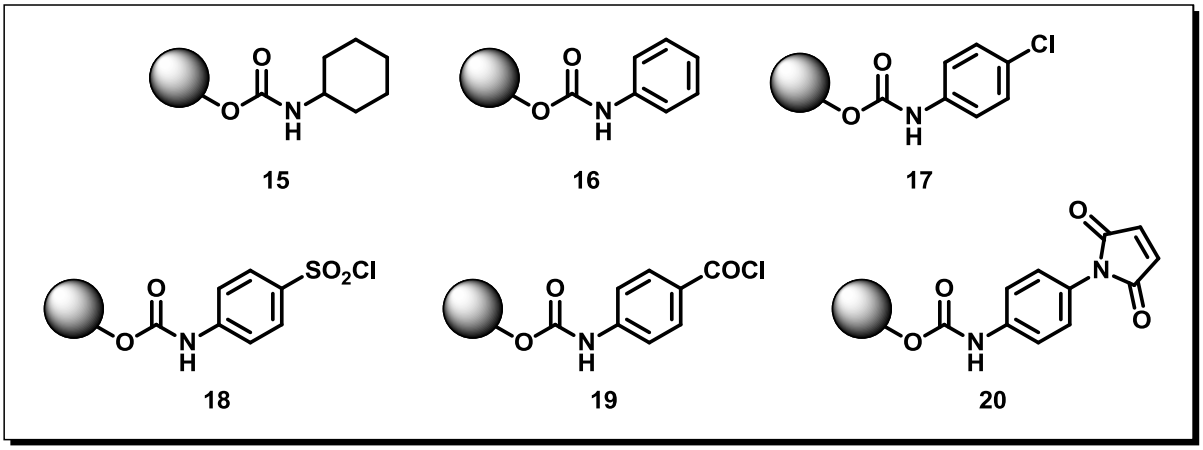

Figure 14

All nanoconjugates were characterized by elemental analysis (E.A.) and infrared spectroscopy (FTIR), while only some of them have been further characterized by High Resolution Magic Angle Spinning NMR technique (HR-MAS NMR). The results obtained confirmed us the formation of a stable carbamate-like bond between the isocyanate group of the organic molecules and the surface hydroxyl groups of the nanoparticles. These results will be fully discussed in the next sections.

4.2.1 Elemental Analysis Characterization: Determination of the Final Loading

In organic chemistry elemental analysis (E.A.) refers to the determination of the mass fractions of carbon, hydrogen and nitrogen of a sample. This information is important to help determine the structure of an unknown molecule, as well as to help ascertain the structure and purity of a synthesized compound. The most common form of CHN analysis is accomplished by combustion analysis. In this technique, a sample is burned in an excess of oxygen, and various traps collect the combustion products (carbon dioxide, water, and nitric oxide). The masses of these combustion products can be used to calculate the composition of the unknown sample. The analysis of results is performed by determining the ratio of elements from within the sample, and working out a chemical formula that fits with those results.

All of the nanoconjugates **15**-**20** were submitted to E.A., from which the chemical formula of the organic residues anchored onto the SPIONs surface was confirmed *[for analytical data referred to the experimental part, section 4.6.2]*.

The sum of the percentages in weight of carbon, hydrogen and nitrogen obtained from the analysis, together with the percentages of other elements calculated on a molar basis from nitrogen, has provided us a first value of loading expressed as percentage in weight of the organic part anchored onto nanoparticle surface. This total percentage of organic part [***Tot % org***] corresponds to the quantity in milligrams of the organic residue *per* 100 milligrams of nanoconjugates. From the molecular weight of the anchored molecule is therefor possible to express the final loading as millimoles of organic part *per* gram of nanoparticles [***mmol/g*** $_{NPs}$], in an analogous way that's normally used with solid phase supports.

The synthetic protocol used to synthesize nanoconjugates **15**-**20**, was set up in order to verify the reproducibility of the methodology and the possibility to tune the quantity of organic molecule grafted onto the SPIONs surface. For these reasons the final loading of each nanoconjugate was determined by E.A. and the results obtained in the three series of test reactions with 0.2, 0.4 and 0.8 millimoles of isocyanates *per* 100 milligrams of naked nanoparticles are shown in *Table 2, Table 3* and *Table 4*, respectively.

R-NCO	***Nanoconjugate***	**0.2 mmol of NCO / 100 mg NPs**	
		Tot % org	*mmol/g$_{NPs}$*
5	**15**	13.83	1.10
6	**16**	15.36	1.28
7	**17**	16.62	1.08
8	**18**	17.54	0.80
9	**19**	22.17	1.21
10	**20**	14.42	0.67
Average Loading		***16.66***	***1.02***

Table 2 *- Final loading for nanoconjugates* **15**-**20** *in the reaction with 0.2 millimoles of isocyanate per 100 milligrams of naked SPIONs.*

R-NCO	*Nanoconjugate*	**0.4 mmol of NCO / 100 mg NPs**	
		Tot % org	*mmol/g_{NPs}*
5	**15**	26.69	2.11
6	**16**	26.55	2.21
7	**17**	29.83	1.93
8	**18**	19.74	0.90
9	**19**	25.74	1.41
10	**20**	31.07	1.44
Average Loading		***26.60***	***1.67***

Table 3 *- Final loading for nanoconjugates* **15**-**20** *in the reaction with 0.4 millimoles of isocyanate per 100 milligrams of naked SPIONs.*

R-NCO	*Nanoconjugate*	**0.8 mmol of NCO / 100 mg NPs**	
		Tot % org	*mmol/g_{NPs}*
5	**15**	51.47	4.08
6	**16**	43.80	3.65
7	**17**	40.33	2.61
8	**18**	21.75	0.99
9	**19**	35.01	1.92
10	**20**	51.81	2.41
Average Loading		***40.70***	***2.61***

Table 4 *- Final loading for nanoconjugates* **15**-**20** *in the reaction with 0.8 millimoles of isocyanate per 100 milligrams of naked SPIONs.*

As shown in tables, an average loading of 16.66% (1.02 mmol/g_{NPs}), 26.60% (1.67 mmol/g_{NPs}) and 40.70% (2.61 mmol/g_{NPs}) was calculated for the three cases.

In *Figure 15* is reported a loading comparison (in total percentage in weight of loaded organic molecule) of the nanoconjugates **15**-**20** and of the calculated average loading for the three sets of reaction with different ratio of starting isocyanate. We can see that for each nanoconjugate, the loading increases with a good linearity increasing the amount of the corresponding isocyanate. In the case of nanoconjugate **18**, the loadings are quite lower probably due to the extreme lability of the corresponding starting isocyanate **8**.

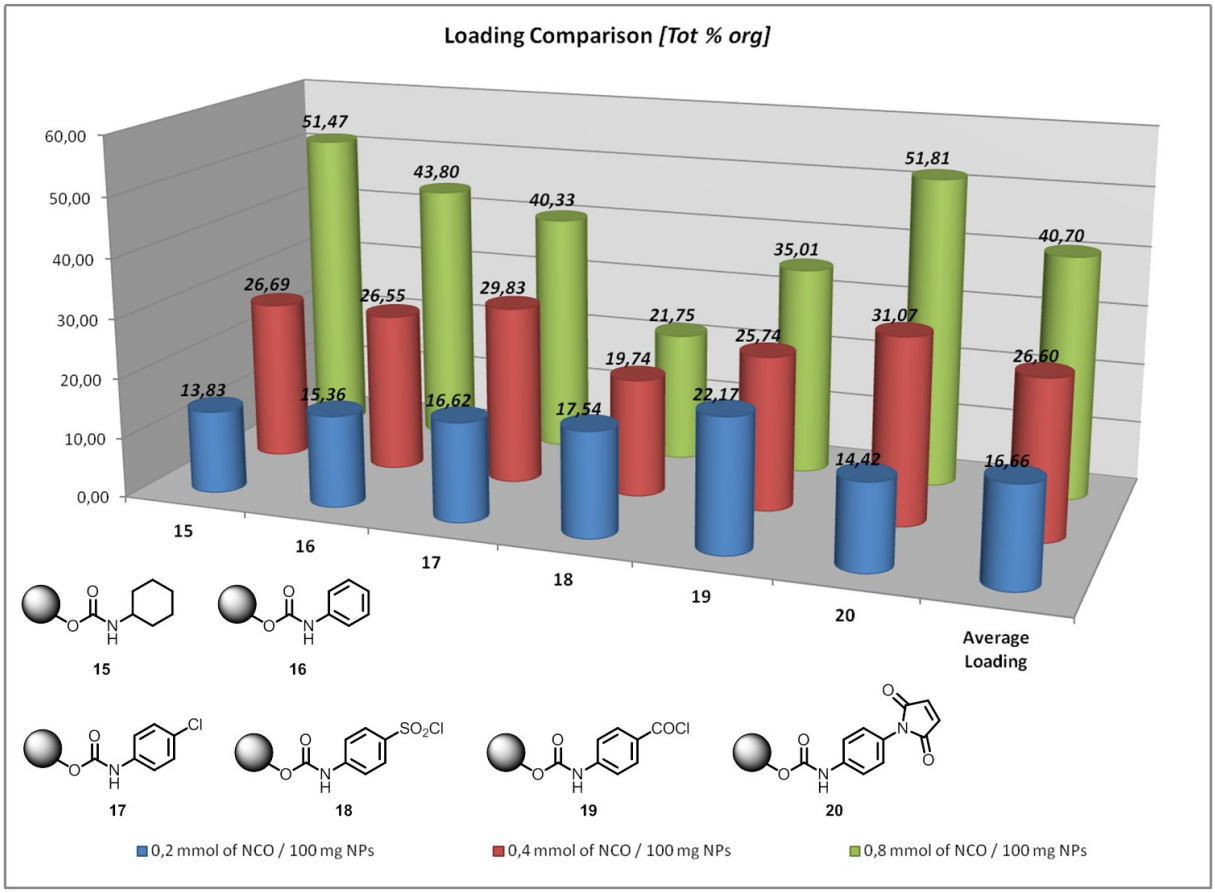

Figure 15 *- Loading comparison of nanoconjugates* **15**-**20***, express as total percentage in weight of organic part loaded onto SPIONs (Tot % org).*

The same considerations can be done for the data reported in *Figure 16*, where the loadings are expressed as millimoles of organic part *per* gram of functionalized nanoparticles.

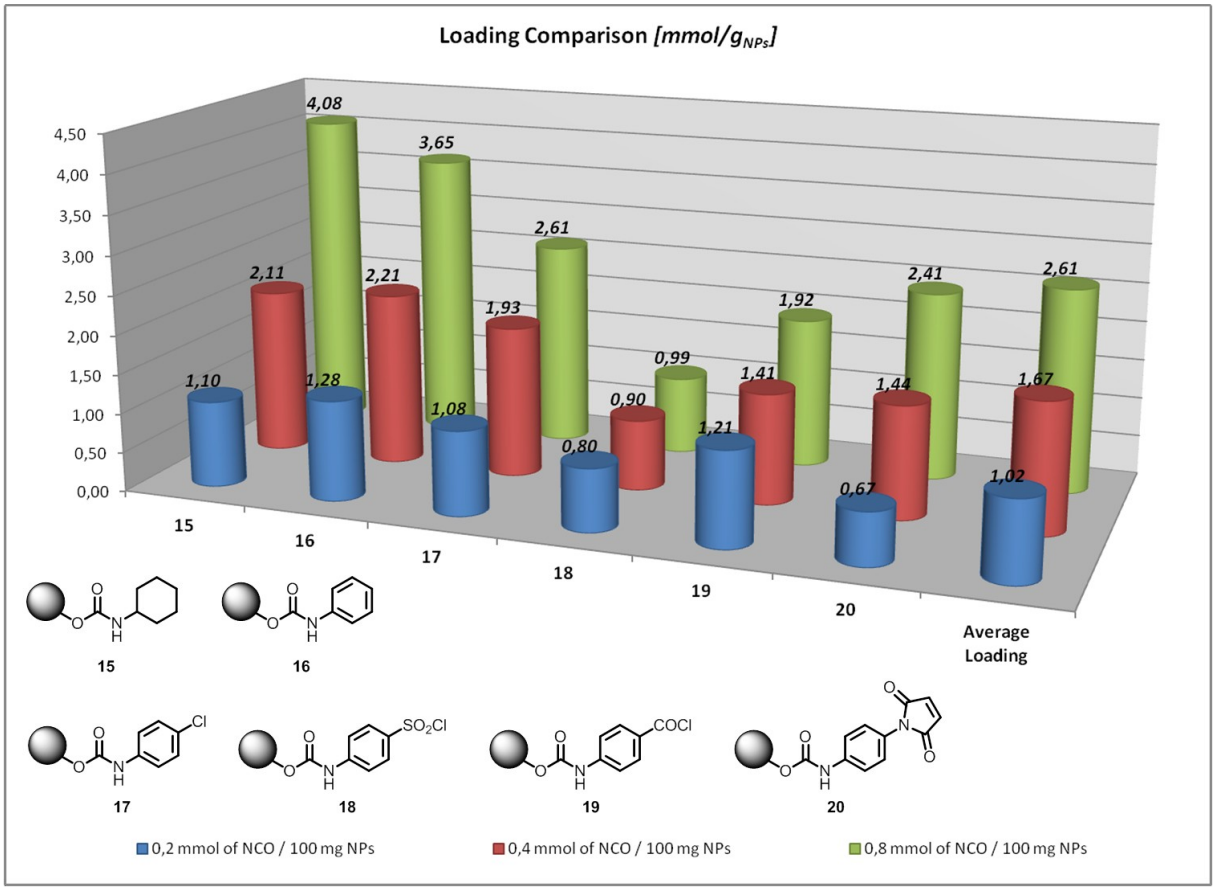

Figure 16 *- Loading comparison of nanoconjugates* **15**-**20***, express as millimoles of organic part per gram of functionalized nanoparticles (mmol/g$_{NPs}$).*

The reproducibility of the reactions of isocyanate with SPIONs was confirmed in the ase of PMPI **10**. In fact, three experiments in which 0.8 millimoles of **10** were reacted with 100 milligrams of naked SPIONs, afforded the nanoconjugate **20** with approximately the same loading values (*Table 5*).

Entry	**0.8 mmol of PMPI / 100 mg NPs**	
	Tot % org	*mmol/g$_{NPs}$*
A	51.81	2.41
B	52.12	2.42
C	51.11	2.38

Table 5 *- Reproducibility of the loading in the synthesis of nanoconjugate* **20***.*

As previously said, the loadings increase with a good linearity. In the graph reported in *Figure 17*, the average loadings expressed in [*Tot % org*] and [*mmol/g$_{NPs}$*] are reported with their linear regression trend lines.

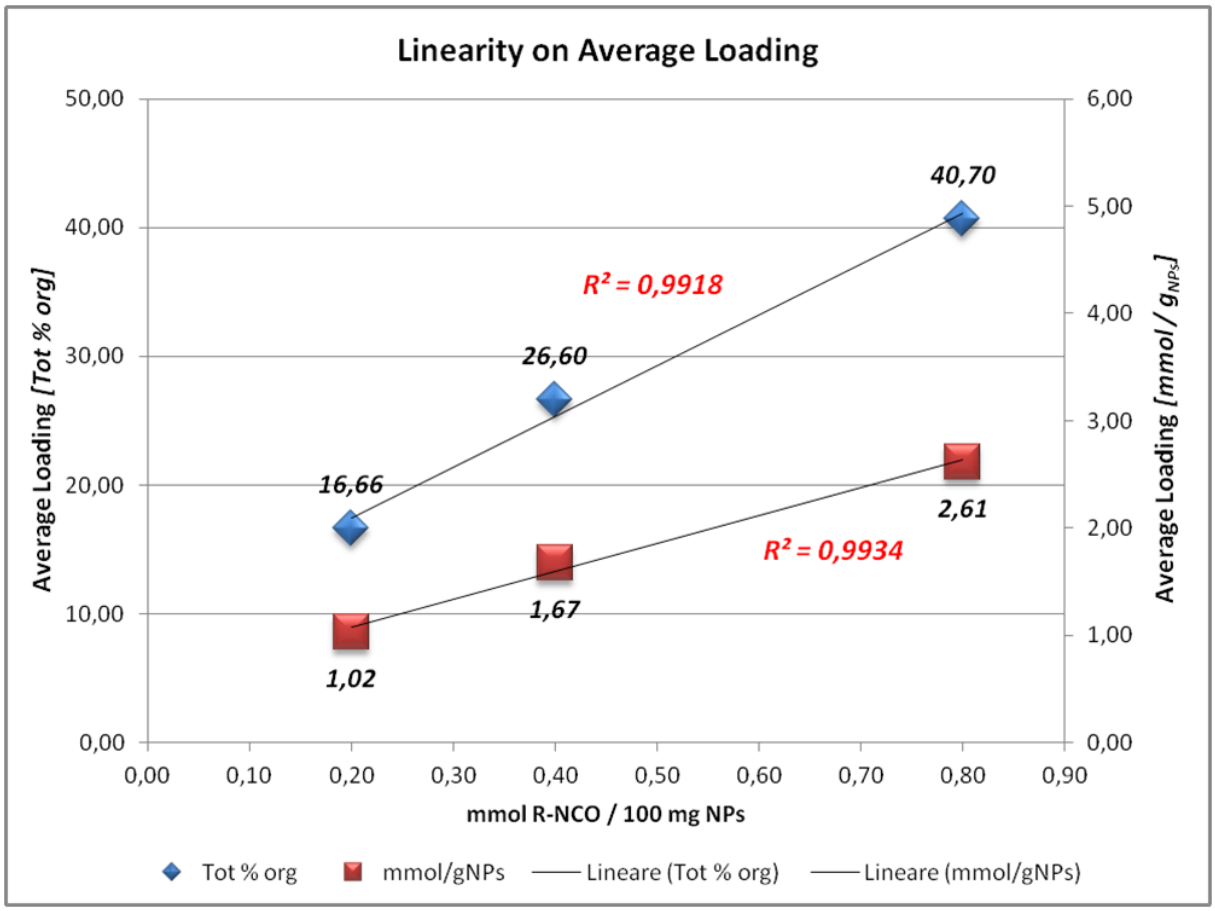

Figure 17 *- Linear regressions on average loading values.*

The correlation coefficients R^2 determined on the average loading values are higher than 0.99, confirming the excellent linearity in which the grafting of isocyanates onto SPION surface happens.

We can conclude that from E.A. it was possible to confirm that the organic residues anchored onto the SPIONs surface correspond to the expected chemical formula. Furthermore, the reproducibility of the methodology was demonstrated and the final loadings increase with the increasing amount of the starting isocyanate with an excellent linearity, proving that's is possible, in principle, to easily tune the desired final loading of a

nanoconjugate, just modifying the ratio between the amount of the starting NCO-molecule and the naked SPIONs.

4.2.2 Infrared Spectroscopy: Demonstration of a Carbamate-like Bond Formation

Fourier Transform Infrared Spectroscopy (FTIR) is a common technique used in organic chemistry to characterize chemical compounds exploiting the vibrational modes of an "IR active" molecule. FTIR was already used in sampling transmission mode to characterize magnetite and maghemite nanoparticles, also in the presence of organic coating.[258a,267]

In order to prove the grafting of isocyanate molecules onto the SPIONs surface by the formation of a carbamate-like bond, the naked SPIONs, the starting isocyanates **5**-**10** and the corresponding nanoconjugates **15**-**20** were analyzed by FTIR.

Spectra were acquired on a Spectrum One FTIR spectrophotometer (Perkin Elmer) in the range 4000-450 cm^{-1} in transmittance mode. 0.5 mg of sample were diluted in 150 mg FTIR grade KBr and ground in an agate mortar. KBr was previously dried at 125°C under vacuum. Then mixed powder was pressed at 9 tons for 3 min to obtain slim semitransparent tablet. Spectra were recorded selecting 64 scans and 4 cm^{-1} resolution. The background of pure KBr was separately recorded using the same conditions and automatically subtracted from sample spectra.

Spectra of starting isocyanate were acquired in transmittance mode in the range 4000-600 cm^{-1} using NaCl windows as support and selecting 4 scans and 4 cm^{-1} resolution.

In *Figure 18* is reported the FTIR spectrum of naked SPIONs in which are clearly visible the strong broad band at high wavenumber (about 3380 cm^{-1}) due to the presence of the nanoparticles surface hydroxyl groups and the strong Fe-O absorption from 650-500 cm^{-1}.

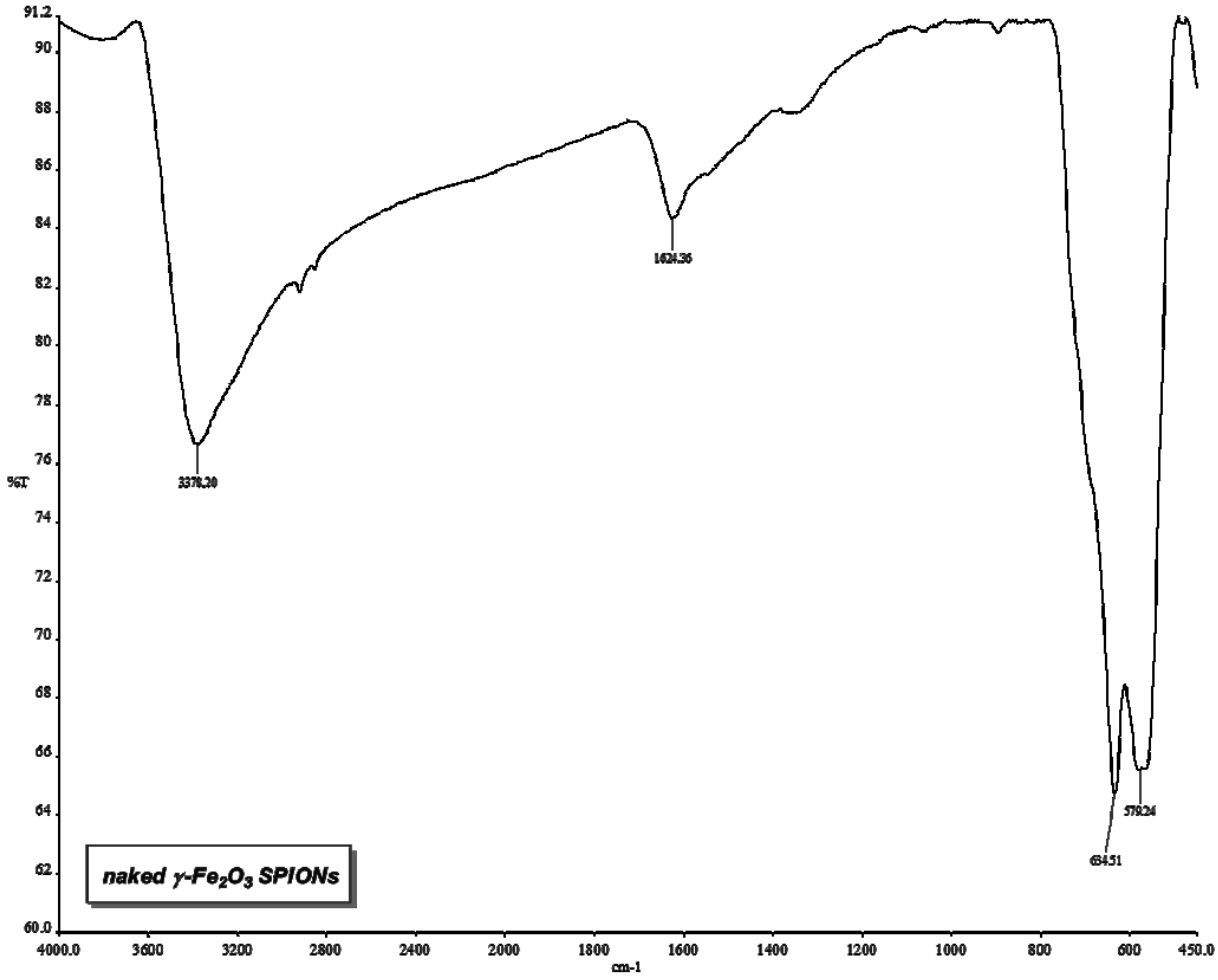

Figure 18 *- FTIR spectrum of naked SPIONs*

In the next figures are reported the superimposed spectra of the starting isocyanates (red line), the naked SPIONs (blue line) and the corresponding obtained nanoconjugates (black line).

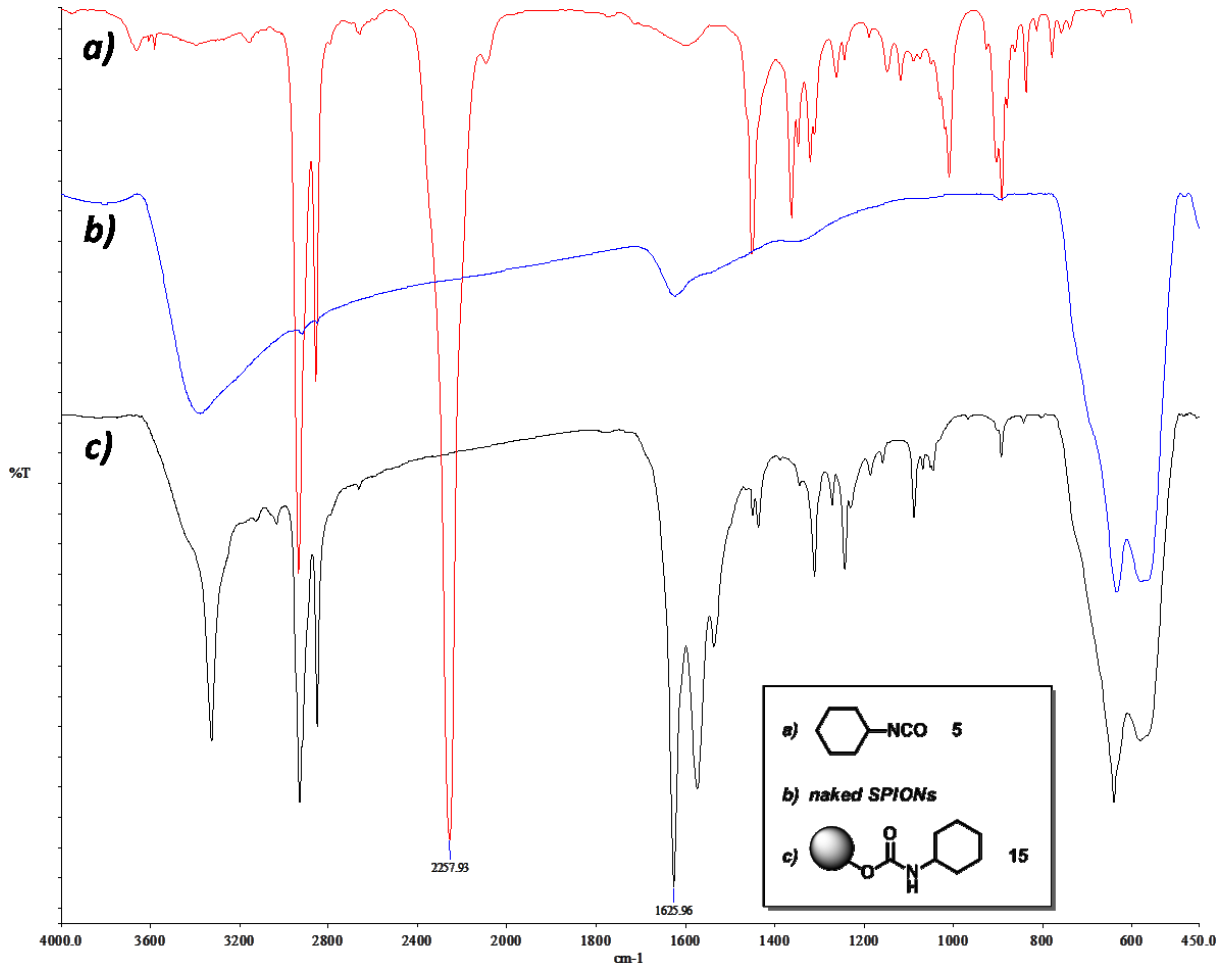

Figure 19 *- FTIR spectra of a) cyclohexyl isocyanate* **5** *(red line), b) naked SPIONs (blue line) and c) nanoconjugate* **15** *(black line). The labeled peak at 2258 cm^{-1} in spectrum a), corresponding to NCO stretching, is no longer visible in spectrum c), in which are instead clearly visible all the vibrational bands related to the C-H bonds and at 1626 cm^{-1} the sharp peak of carbamate C=O stretching. At about 3300 cm^{-1}, the stretching of carbamate N-H bond is also present.*

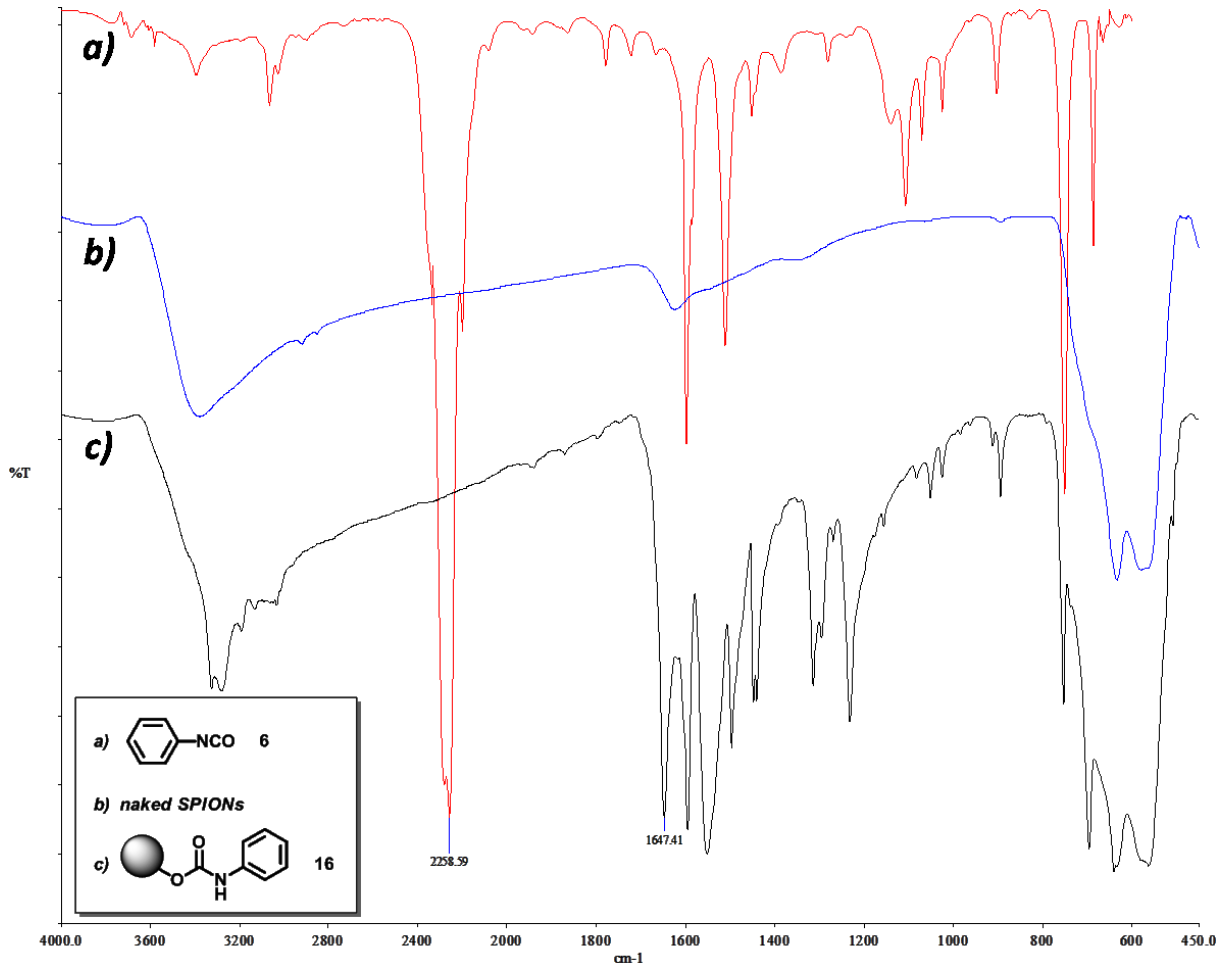

Figure 20 *- FTIR spectra of a) phenyl isocyanate* **6** *(red line), b) naked SPIONs (blue line) and c) nanoconjugate* **16** *(black line). The labeled peak at 2259 cm^{-1} in spectrum a), corresponding to NCO stretching, is no longer visible in spectrum c), in which are instead clearly visible all the vibrational bands related to the C-H and C=C bonds and at 1647 cm^{-1} the sharp peak of carbamate C=O stretching. At about 3300 cm^{-1}, the stretching of carbamate N-H bond is also present.*

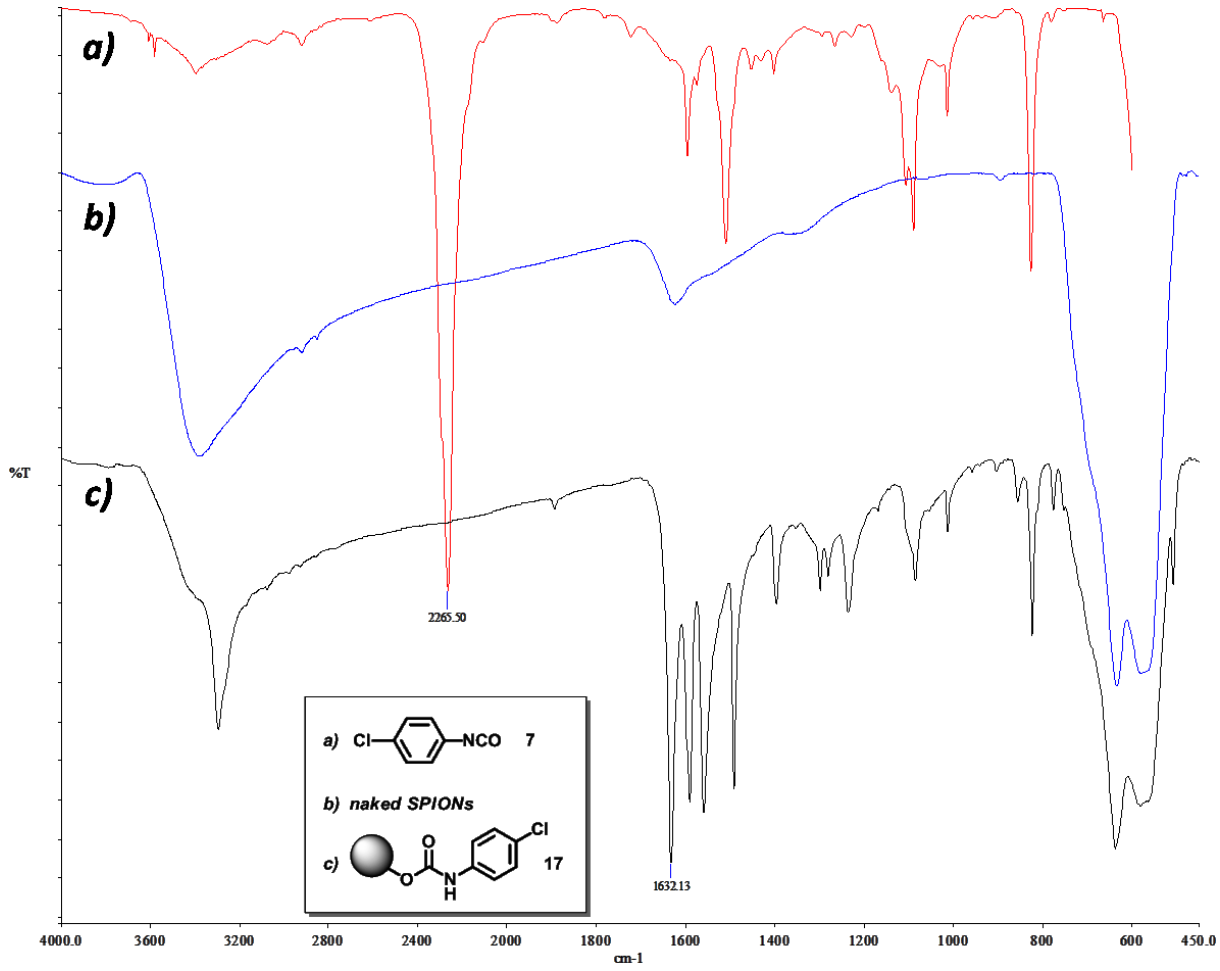

Figure 21 *- FTIR spectra of a) p-chlorophenyl isocyanate* **7** *(red line), b) naked SPIONs (blue line) and c) nanoconjugate* **17** *(black line). The labeled peak at 2265 cm^{-1} in spectrum a), corresponding to NCO stretching, is no longer visible in spectrum c), in which are instead clearly visible all the vibrational bands related to the C-H and C=C bonds and at 1632 cm^{-1} the sharp peak of carbamate C=O stretching. At about 3300 cm^{-1}, the stretching of carbamate N-H bond is also present.*

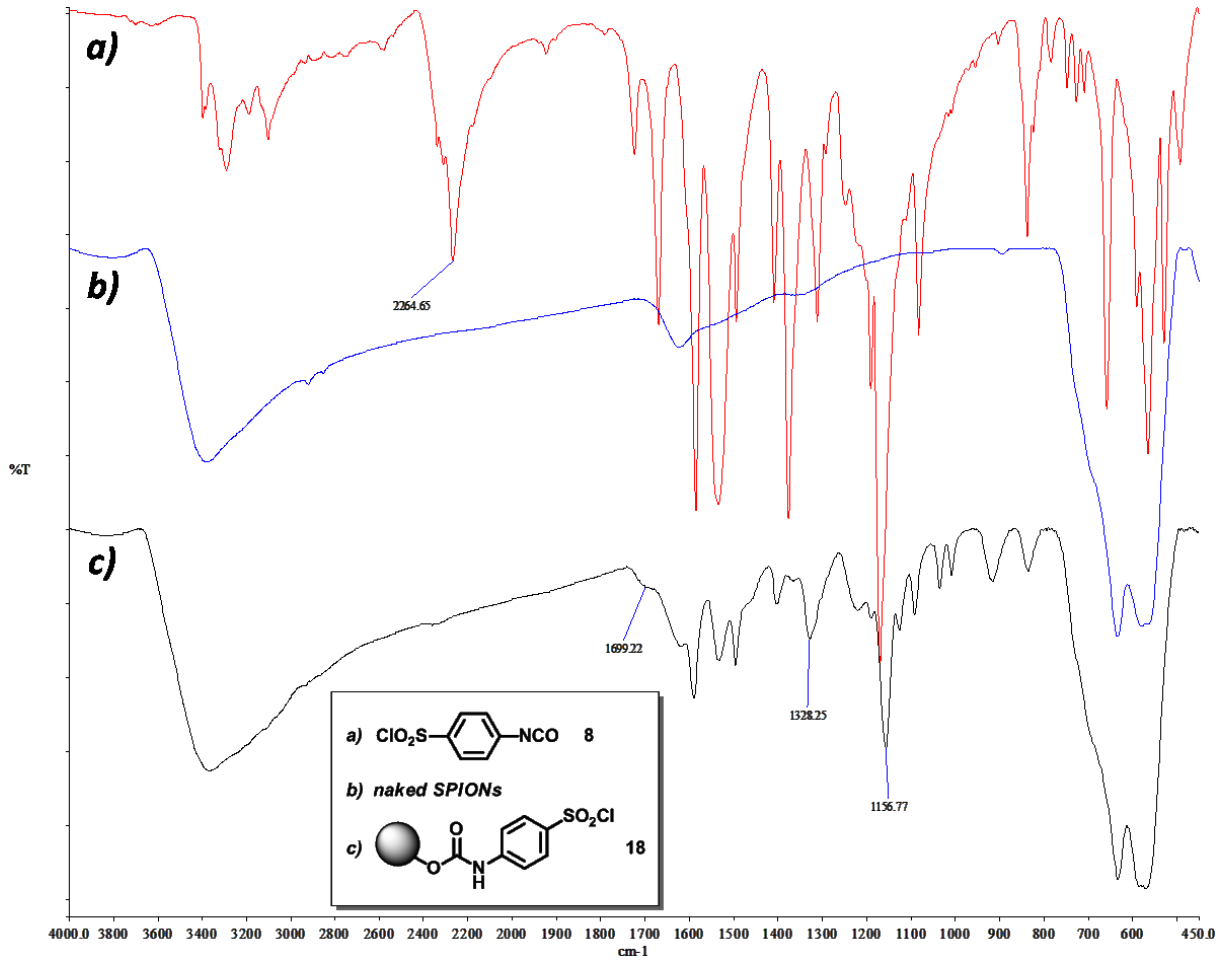

Figure 22 *- FTIR spectra of a) (p-chlorosulfonyl)phenyl isocyanate* **8** *(red line), b) naked SPIONs (blue line) and c) nanoconjugate* **18** *(black line). The labeled peak at 2265 cm^{-1} in spectrum a), corresponding to NCO stretching, is no longer visible in spectrum c), in which are instead clearly visible all the vibrational bands related to the C-H and C=C bonds, the classical stretching of O=S=O moiety at 1328-1157 cm^{-1} and at 1699 cm^{-1} the shouldered peak of carbamate C=O stretching.*

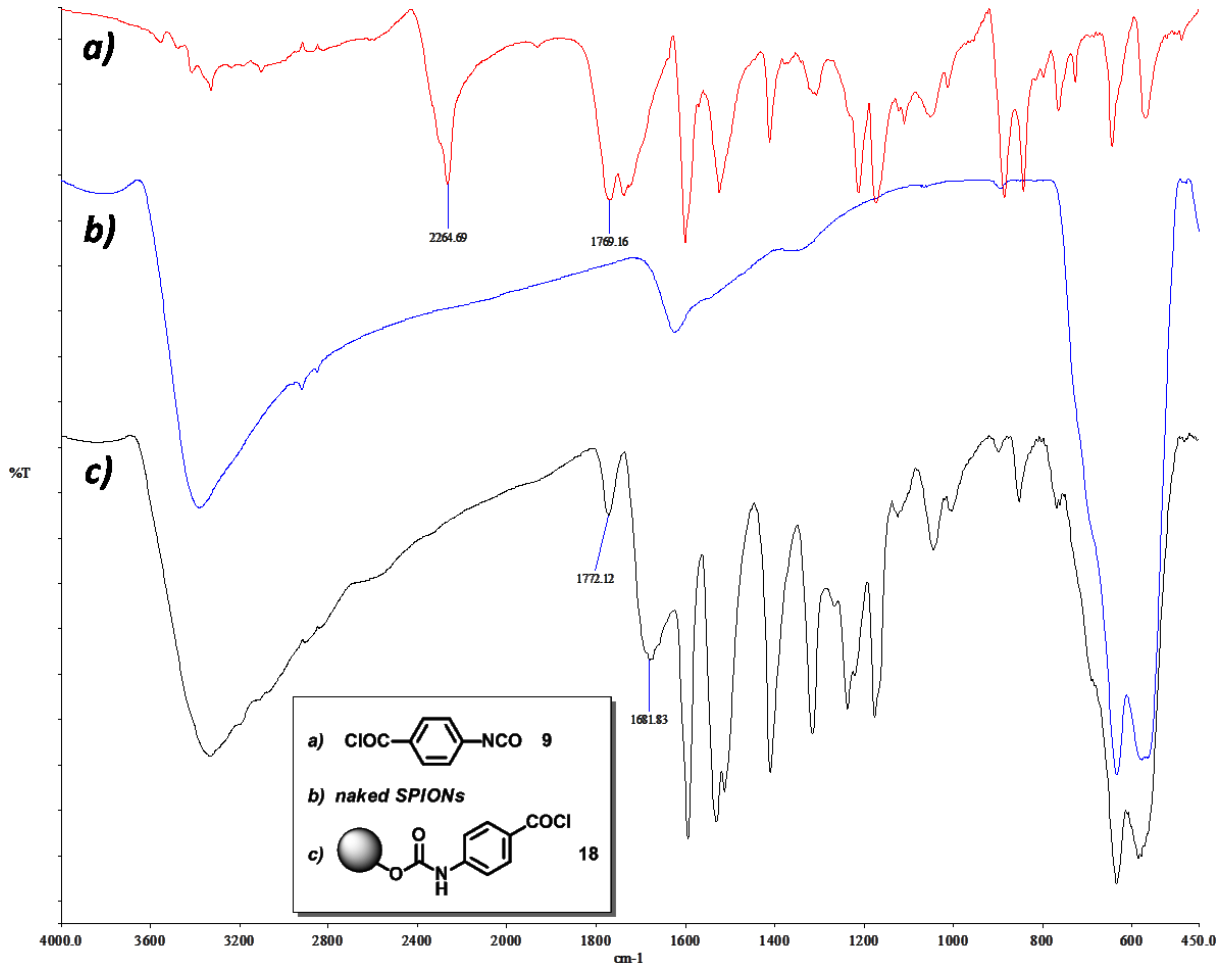

Figure 23 *- FTIR spectra of a) (p-isocyanate)benzoyl chloride* **9** *(red line), b) naked SPIONs (blue line) and c) nanoconjugate* **19** *(black line). The labeled peak at 2265 cm^{-1} in spectrum a), corresponding to NCO stretching, is no longer visible in spectrum c), in which are instead clearly visible all the vibrational bands related to the C-H and C=C bonds, the classical stretching of chloroacyl moiety at about 1770 cm^{-1} and at 1682 cm^{-1} the peak of carbamate C=O stretching.*

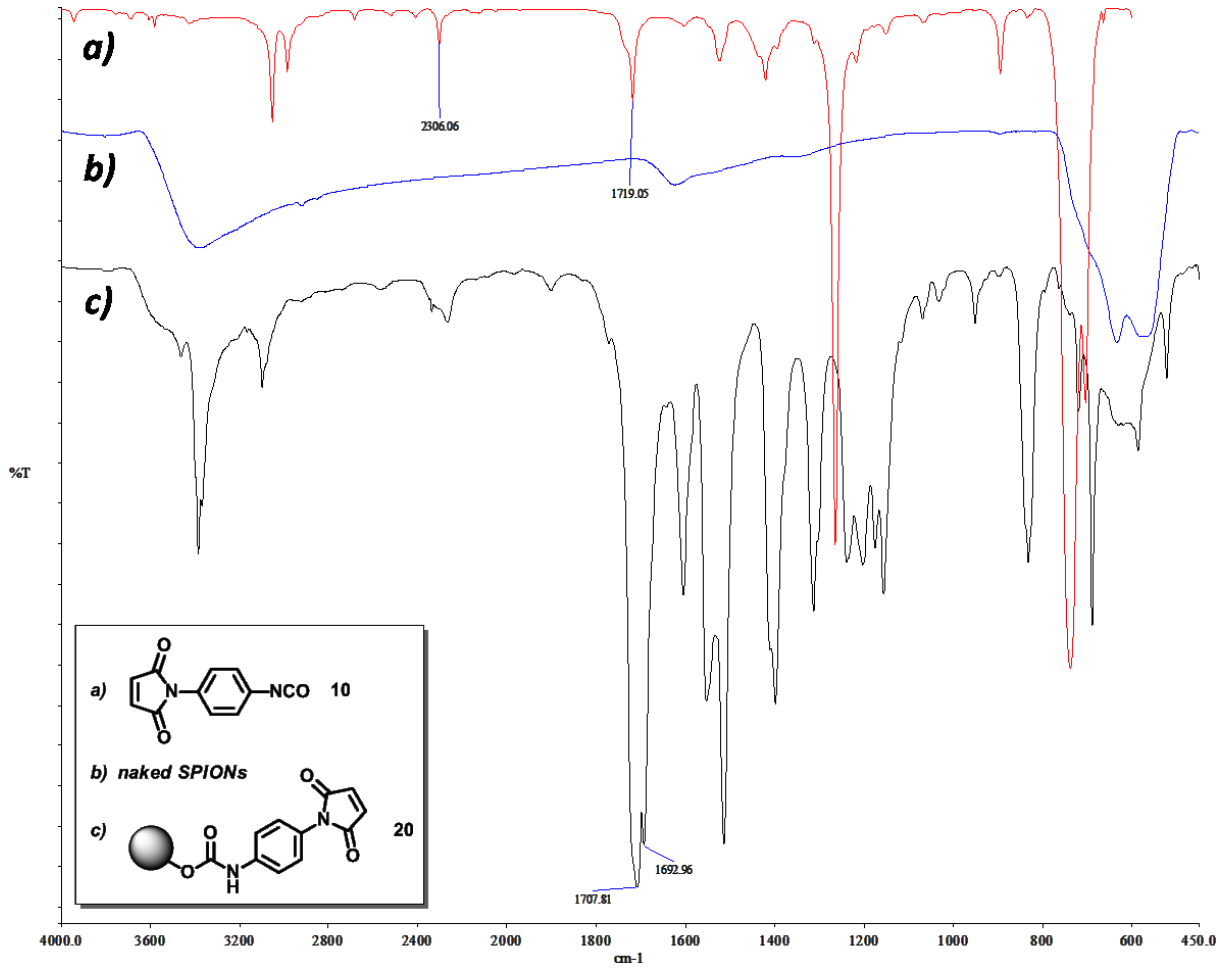

Figure 24 *- FTIR spectra of a) (p-maleimido)phenyl isocyanate PMPI* **10** *(red line), b) naked SPIONs (blue line) and c) nanoconjugate* **20** *(black line). The labeled peak at 2306 cm^{-1} in spectrum a), corresponding to NCO stretching, is no longer visible in spectrum c), in which are instead clearly visible all the vibrational bands related to the C-H and C=C bonds, the maleimido C=O stretching peak at about 1710 cm^{-1} and at 1693 cm^{-1} the sharp peak of carbamate C=O stretching. At about 3300 cm^{-1}, the stretching of carbamate N-H bond is also present.*

As an example, we can discuss the FTIR spectra shown in *Figure 20*, in which the phenyl isocyanate **6** and the corresponding nanoconjugate **16** were reported.

Spectrum a) shows at 2259 cm^{-1} a typical strong band of isocyanate group stretching. This peak is absent in coated nanoparticle spectrum c) that, on the contrary, shows a peak at 1647 cm^{-1}; this peak is due to C=O stretching of new carbamate group, formed in nanoparticles-isocyanate interaction. The presence of iron justifies signal shift at lower

frequency compared to a totally organic carbamate. The peak at 3326 cm^{-1} is related to the carbamate N-H stretching, absent in a) e b) and partially covered by broad band of nanoparticles surface hydroxyl groups.

Moreover in c) bands in the region of 1594-1497 cm^{-1} are associated with C=C of aromatic ring stretching and with N-H deformation, while in the region 1314-1230 cm^{-1} signal are related to C-O and Ar-N stretching. Both naked and coated nanoparticles spectra show clearly strong Fe-O absorption from 650 to 500 cm^{-1}. *[For the complete attribution of vibrational bands of each compounds referred to the experimental part, section 4.6.2.]*

The same considerations can be done for each nanoconjugates.

In *Table 6* are summarized the wavenumber for the C=O vibrational stretching bands of the starting isocyanate **5**-**10** and the corresponding nanoparticle-carbamate derivatives **15**-**20**.

R-NCO	***Nanoconjugate***	***Stretching [cm^{-1}]***		***Figure***
		-N=C=O	*C=O carbamate*	
5	**15**	2258	1626	19
6	**16**	2259	1647	20
7	**17**	2265	1632	21
8	**18**	2265	1699	22
9	**19**	2265	1682	23
10	**20**	2306	1693	24

Table 6 *- C=O Stretching values of starting isocyanate and corresponding nanoconjugates.*

It's worthy to note that the final loading of a nanoconjugate plays a crucial role in the resolution of the FTIR spectrum. The three series of reaction performed for the synthesis of nanoconjugate **20** (0.2, 0.4 and 0.8 millimoles of PMPI **10** *per* 100 mg of naked SPIONs) were characterized by FTIR, and their spectra are reported in *Figure 25*.

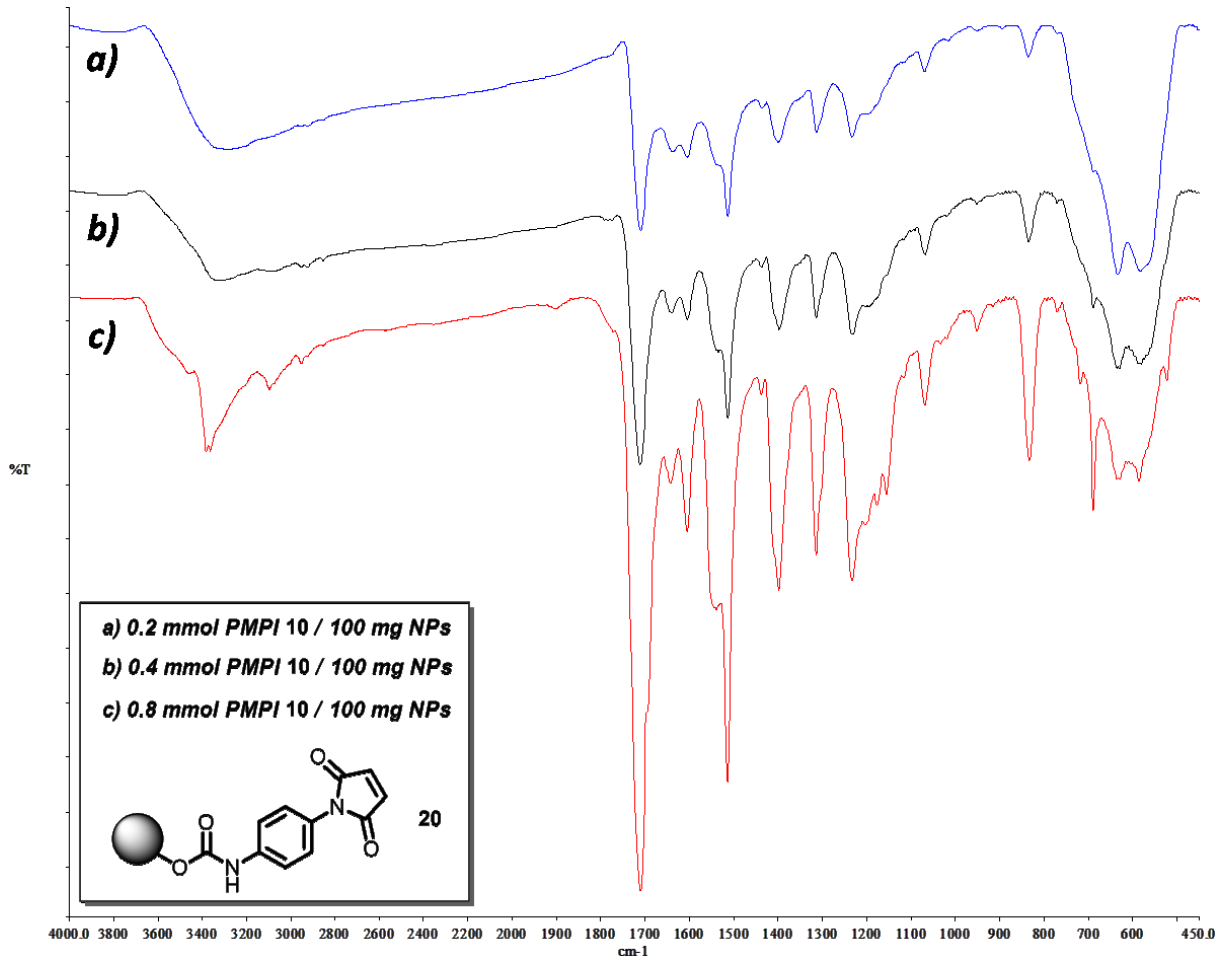

Figure 25 *- FTIR spectra of nanoconjugate* **20** *obtained reacting a) 0.2 mmol PMPI* **10** */ 100 mg NPs (blue line), b) 0.4 mmol PMPI* **10** */ 100 mg NPs (black line) and c) 0.8 mmol PMPI* **10** */ 100 mg NPs (red line). The loading of* **20** *increases from a) to c). Final loading: a) 14.41% (0.62 mmol/g_{NPs}), b) 31.07% (1.34 mmol/g_{NPs}) and c) 51.81% (2.24 mmol/g_{NPs}).*

Increasing the final loading, the resolution of the peaks related to the vibrational modes of the organic molecule anchored onto the SPIONs surface increases. In *Figure 25* is clearly shown how the intensity of the peaks related to the organic molecule increases (*e.g.* the carbamate N-H stretching at ca. 3300 cm^{-1} becomes more visible increasing the final loading of the nanoconjugate **20**), while the strong absorption bands of the iron oxide become weaker.

We can conclude that FTIR spectroscopy helps to point out the interaction between the isocyanate group and the SPIONs surface, confirming the formation of a carbamate bond for all products. Furthermore, FTIR spectroscopy has proved to be the choice technique for the analysis of these kind of nanoconjugates.

4.2.3 High Resolution Magic Angle Spinning NMR: a Further Confirmation of the Covalent Adsorption of Isocyanates onto SPIONs

The High Resolution Magic Angle Spinning (HR-MAS) probes have been designed to perform solution type experiments, while spinning the sample at the magic angle (54.7°) and are able to work with gel samples and semisolid matrices; they have been used successfully for the characterization of gels,[268] biopsies,[269] nanocrystalline proteins,[270] metabolic phenotypes of entire microorganisms[271] and also with intact tissues, with a spectral resolution comparable to that observed with extract solutions.[272]

As just described in previous works, ^{1}H-NMR resolved spectra of a ligands bound to a paramagnetic nanocrystal, like SPIONs, are difficult to perform for many reasons: the large broadening effects caused by the paramagnetic material,[273] that also measurably changes the nuclear magnetic resonance relaxation properties of nearby protons in aqueous solution, at distances up to ca. 50 μm;[274] the decreased mobility of the ligands on the surface, as well as the paramagnetism of the iron oxide, in addition to an inherent broadness in the spectra, causes the lack of splitting in the peaks and, in order to obtain a ^{1}H-NMR spectrum with conventional NMR probes, with a minimal resolution, the solution has to be extremely dilute.[275]

Working in this direction, some ^{1}H spectra were initially reported with a quite good signal shape[273,275] but the resolution was still not enough to clearly show the multiplet's structure, also with very diluted and simple molecules.

By the way, it was shown[263,276] that the HR-MAS NMR technique, could be a powerful tool to overcome problems such as the low resolution of the ^{1}H spectra not only against the

chemical shift anisotropy problem, but also decreasing the paramagnetic effects, allowing the characterization of the structures of different organic ligands bound to superparamagnetic iron oxide nanoparticles (both Fe_2O_3 or Fe_3O_4 SPIONs) producing resolved ^1H spectra with structured NMR signals.

We have just effectively used this NMR technique in a precedent work[277] analyzing Peptide Nucleic Acid (PNA) strands linked on magnetic maghemite nanoparticles and producing sets of ^1H resolved spectra.

In this thesis we have applied again this analytic tool performing different kind of NMR experiments, in order to characterize some of the obtained nanoconjugates and, at the same time, with the aim to give an additional prove of the carbamate bond formation.

In *Table 7*, the HR-MAS experiments performed on nanoconjugates **15**-**17** and **20** are summarized proving the versatility of this technique, while nanoconjugates **18** and **19** were not characterized with NMR spectroscopy due to the lability of the additional -SO_2Cl and -COCl moieties.

Nanoconjugate	**HR-MAS experiments**
15	^1H, ^{13}C, COSY, HSQC
16	^1H, ^{13}C
17	^1H, ^{13}C
20	^1H, DOSY

Table 7 *- HR-MAS experiments performed on some nanoconjugates.*

The NMR spectrometer with the HR-MAS facility, located in the Big Instrument Center (C.I.G.A.), of University of Milan, is an FT-NMR *Avance*^{TM} *500* (*Bruker Italia S.r.l.*) with a superconducting ultrashield magnet of 11.7 Tesla (^1H frequency: 500.13 MHz).

The probe is doubly tuned (^1H and ^{13}C), in addition to a 2H lock channel. All three channels are operating via a single NMR transmit/receive solenoid coil located inside the MAS turbine. The probe is capable of performing either direct or indirect (inverse) detection experiments.

The probe allows to perform high resolution MAS experiments at spinning rates of up to 15 KHz, with 4 mm zirconia oxide rotors, for liquid or liquid-like samples; in our study the spinning rates were optimized between 5 KHz and 12 KHz speed values to rich a compromise between the needing to have the spinning side bands out of the ^{1}H spectrum, the best resolution behaviour and the minimum presence of turbulence or rotational artifacts.

All the samples were diluted in deuterated methyl sulfoxide (few milligrams in 150-200 µl DMSO-d_6 100%); the saturated solutions (do to the low solubility of γ-Fe_2O_3 nanoconjugates) of nanoparticles dispersion, after different cycles of vortex/sonication, were decanted by night leaving to precipitate the large aggregates and the upper suspension was then collected for NMR analysis. A dilution at different levels was sometimes necessary to find the concentration limit before the broadening of the NMR signals. The sample temperature it's speed rotation dependent and was so varying from 30 to 35 °C, in different experiments performed.

In *Figure 26* is reported the ^{1}H HR-MAS NMR spectrum of nanoconjugate **15**. A high resolved spectrum was obtained with 4 KHz speed in which are clearly visible the ten CH_2 protons of the cyclohexyl ring (labeled as 4-8) and a dublet at 5.58 ppm related to the presence of the aliphatic carbamate NH proton (2).

In *Figure 27* the ^{13}C HR-MAS NMR spectrum is shown. Also in this case all the carbons of the cyclohexyl ring are present at high field, while a deshielded peak at 157 ppm confirms the presence of a carbamate C=O carbon atom (1).

In proton spectrum is no visible the peak related to the CH proton (3) and for this reason COSY and HSQC experiments were performed; the results are here reported in *Figure 28* and *Figure 29*, respectively.

In the COSY spectrum, the peak of water shows a double correlation with the NH proton (2) and with the most shielded multiplet referred to the CH_2 protons of the ring, indicating that proton (3) lays under the water signal. This hypothesis was confirmed by HSQC analysis in which a direct correlation between the water signal and the tertiary carbon (3) at 48 ppm was observed.

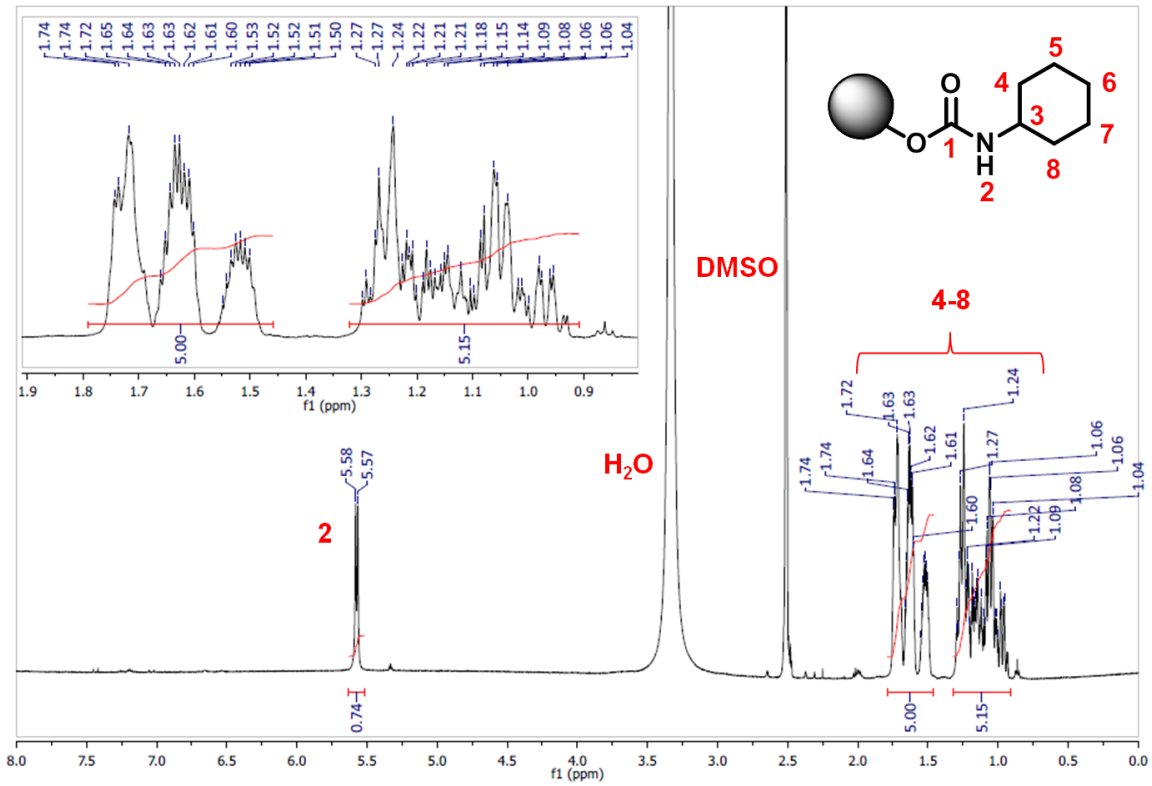

Figure 26 *- ^{1}H HR-MAS NMR spectrum of nanoconjugate* **15** *in DMSO (4 KHz speed).*

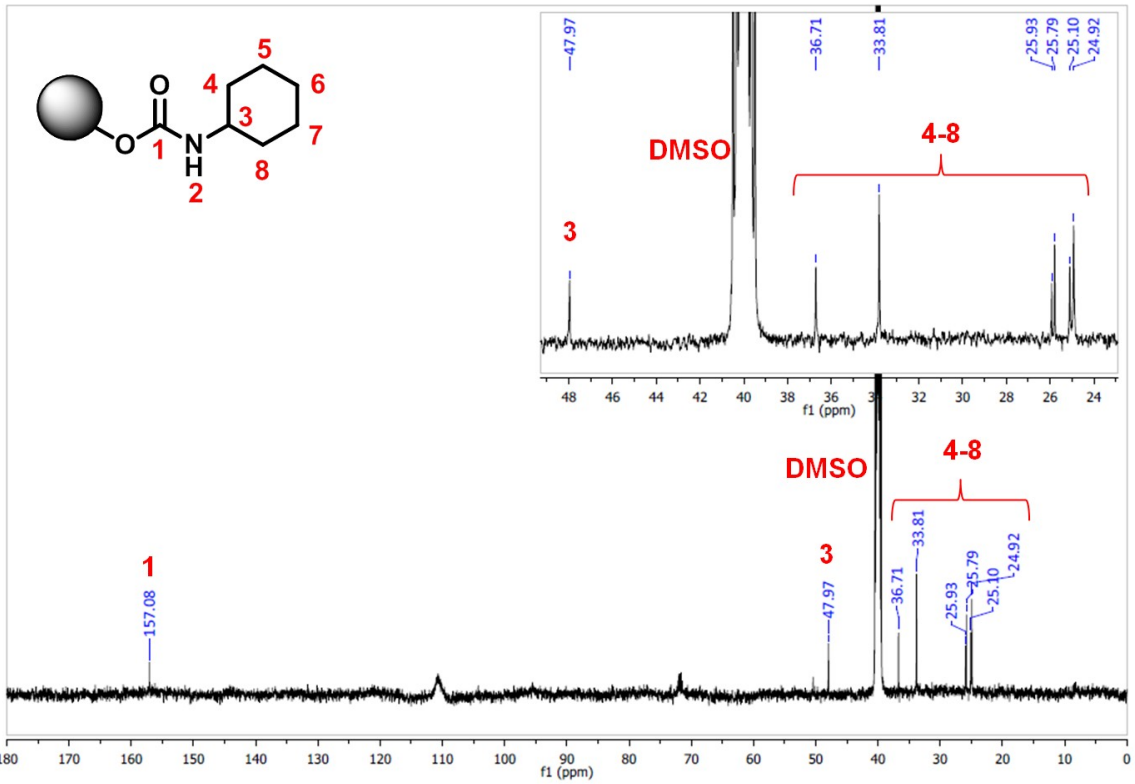

Figure 27 *- ^{13}C all decoupled HR-MAS NMR spectrum of nanoconjugate* **15** *in DMSO (4 KHz speed).*

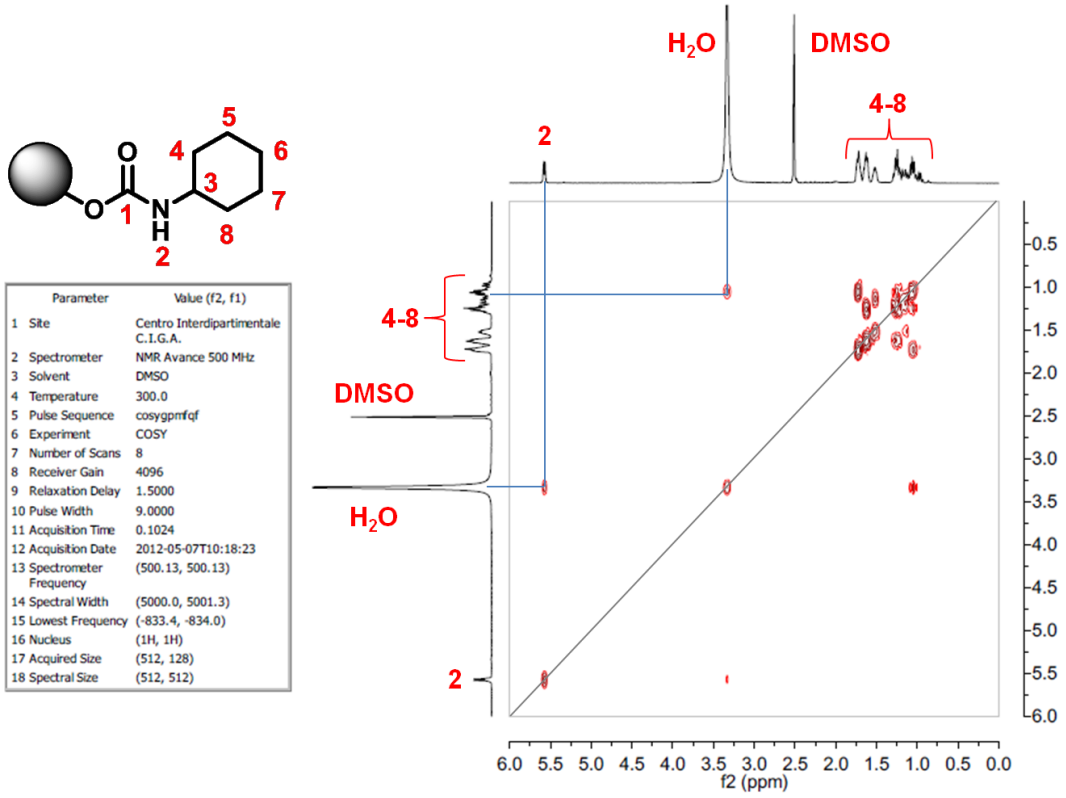

	Parameter	Value (f2, f1)
1	Site	Centro Interdipartimentale C.I.G.A.
2	Spectrometer	NMR Avance 500 MHz
3	Solvent	DMSO
4	Temperature	300.0
5	Pulse Sequence	cosygpmfqf
6	Experiment	COSY
7	Number of Scans	8
8	Receiver Gain	4096
9	Relaxation Delay	1.5000
10	Pulse Width	9.0000
11	Acquisition Time	0.1024
12	Acquisition Date	2012-05-07T10:18:23
13	Spectrometer Frequency	(500.13, 500.13)
14	Spectral Width	(5000.0, 5001.3)
15	Lowest Frequency	(-833.4, -834.0)
16	Nucleus	(1H, 1H)
17	Acquired Size	(512, 128)
18	Spectral Size	(512, 512)

Figure 28 *- COSY HR-MAS NMR spectrum of nanoconjugate* **15** *in DMSO (4 KHz speed).*

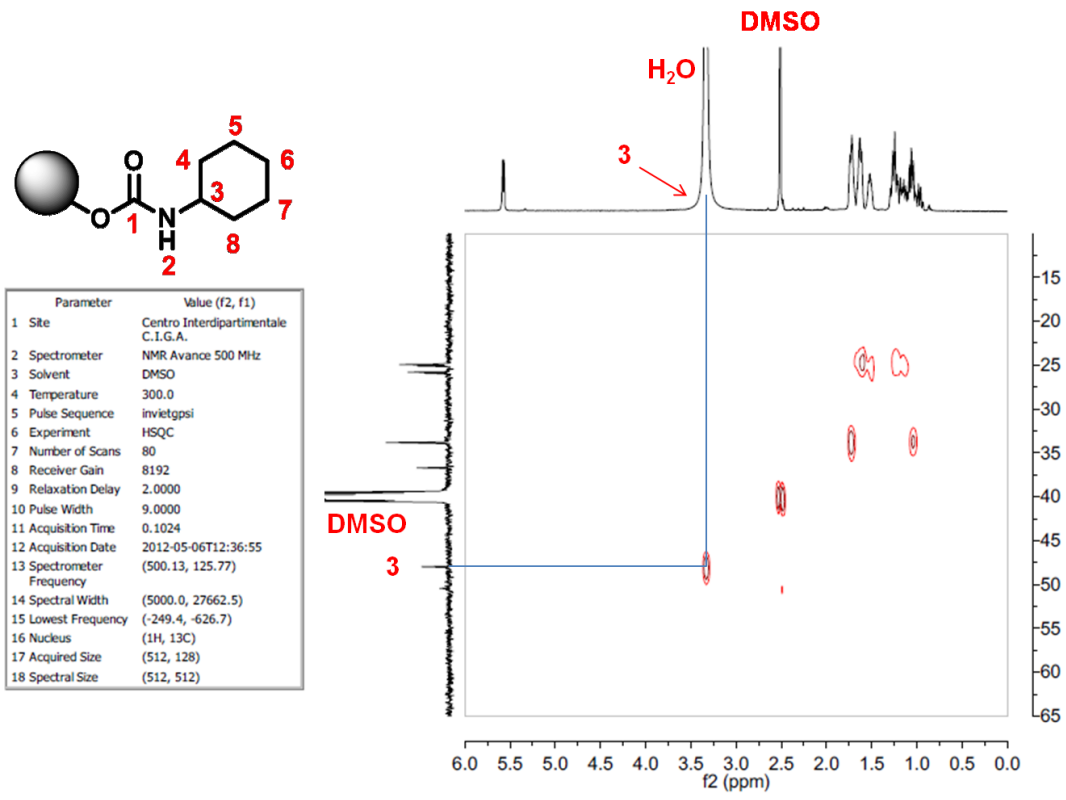

	Parameter	Value (f2, f1)
1	Site	Centro Interdipartimentale C.I.G.A.
2	Spectrometer	NMR Avance 500 MHz
3	Solvent	DMSO
4	Temperature	300.0
5	Pulse Sequence	invietgpsi
6	Experiment	HSQC
7	Number of Scans	80
8	Receiver Gain	8192
9	Relaxation Delay	2.0000
10	Pulse Width	9.0000
11	Acquisition Time	0.1024
12	Acquisition Date	2012-05-06T12:36:55
13	Spectrometer Frequency	(500.13, 125.77)
14	Spectral Width	(5000.0, 27662.5)
15	Lowest Frequency	(-249.4, -626.7)
16	Nucleus	(1H, 13C)
17	Acquired Size	(512, 128)
18	Spectral Size	(512, 512)

Figure 29 *- HSQC HR-MAS NMR spectrum of nanoconjugate* **15** *in DMSO (4 KHz speed).*

The proton and the carbon NMR spectra of nanoconjugate **16** are reported in *Figure 30* and *Figure 31*.

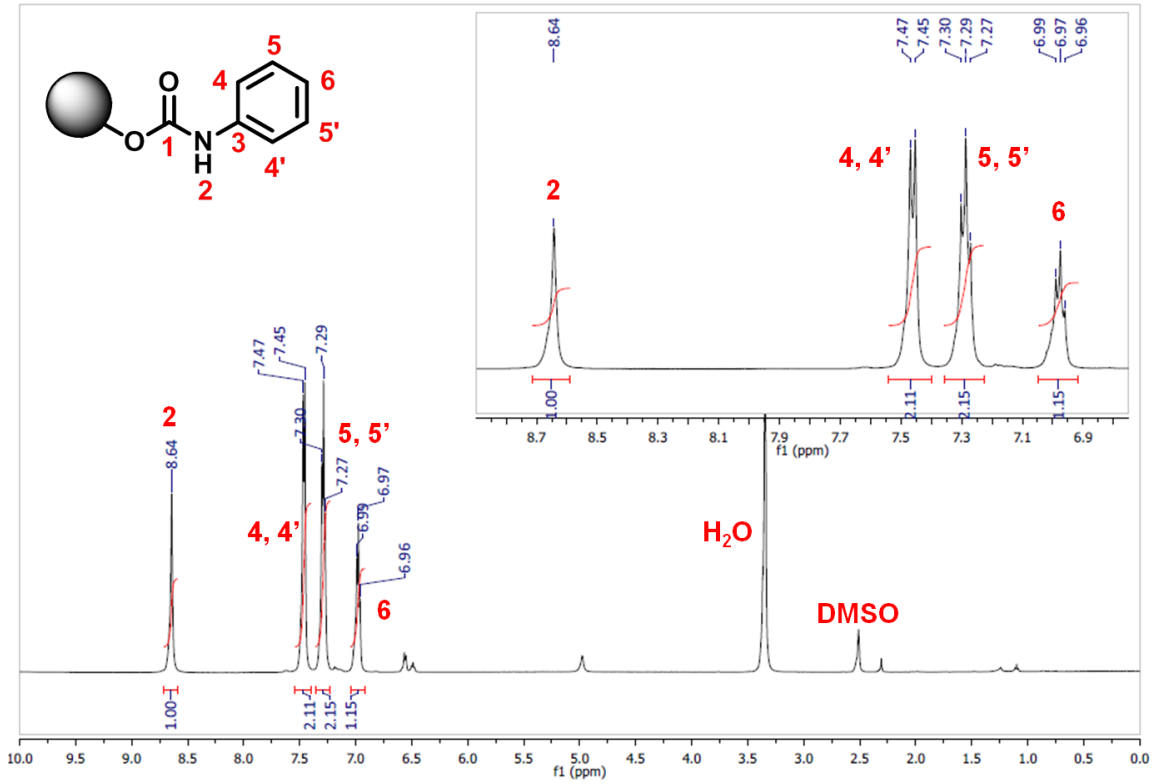

Figure 30 *- ^{1}H HR-MAS NMR spectrum of nanoconjugate* **16** *in DMSO (6 KHz speed).*

In ^{1}H spectrum the peaks of the monosubstituted aromatic ring are present (4-6), together with a singlet deshielded peak at 8.64 ppm related to the NH aromatic carbamate proton (2).

From ^{13}C spectrum is possible to further confirm the formation of a carbamate bond thanks to the presence of a quaternary strong deshielded carbon peak at 153 ppm (1).

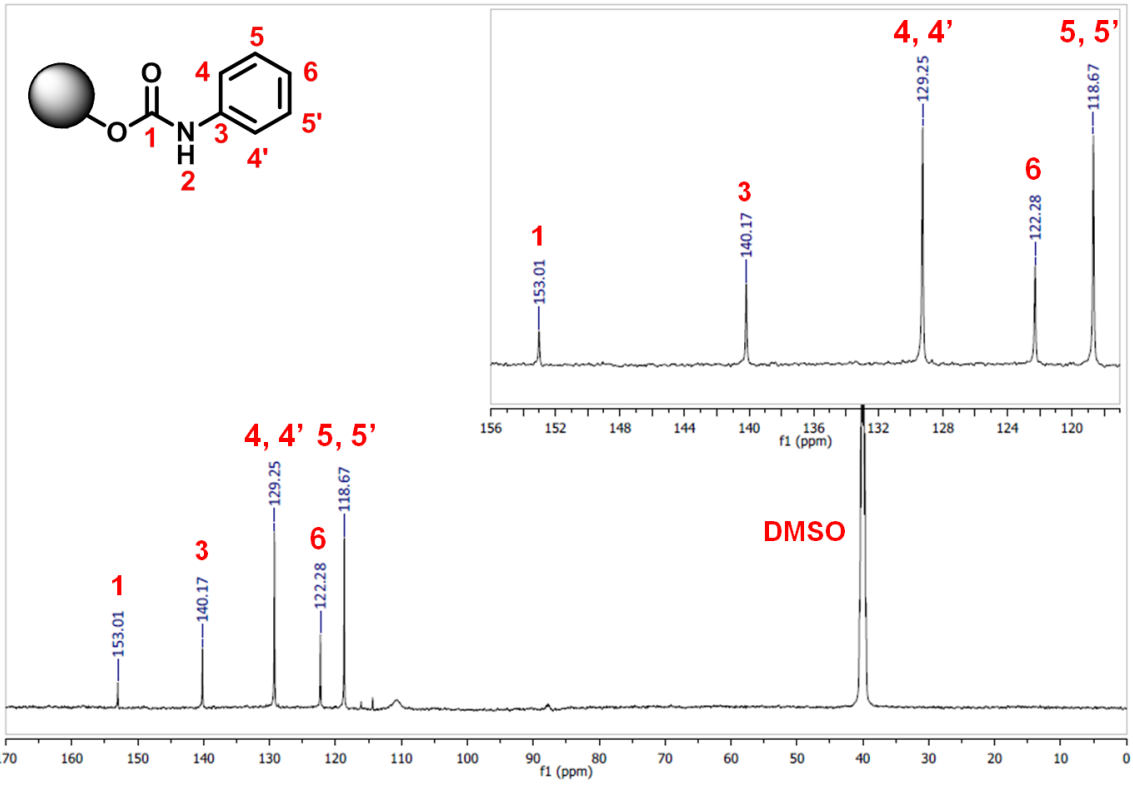

Figure 31 - *^{13}C all decoupled HR-MAS NMR spectrum of nanoconjugate* **16** *in DMSO (6 KHz speed).*

To demonstrate the importance of the spinning rates, in *Figure 32* is shown the resolution behavior with the MAS speed increasing in different HR-MAS experiments performed on nanoconjugate **16**.

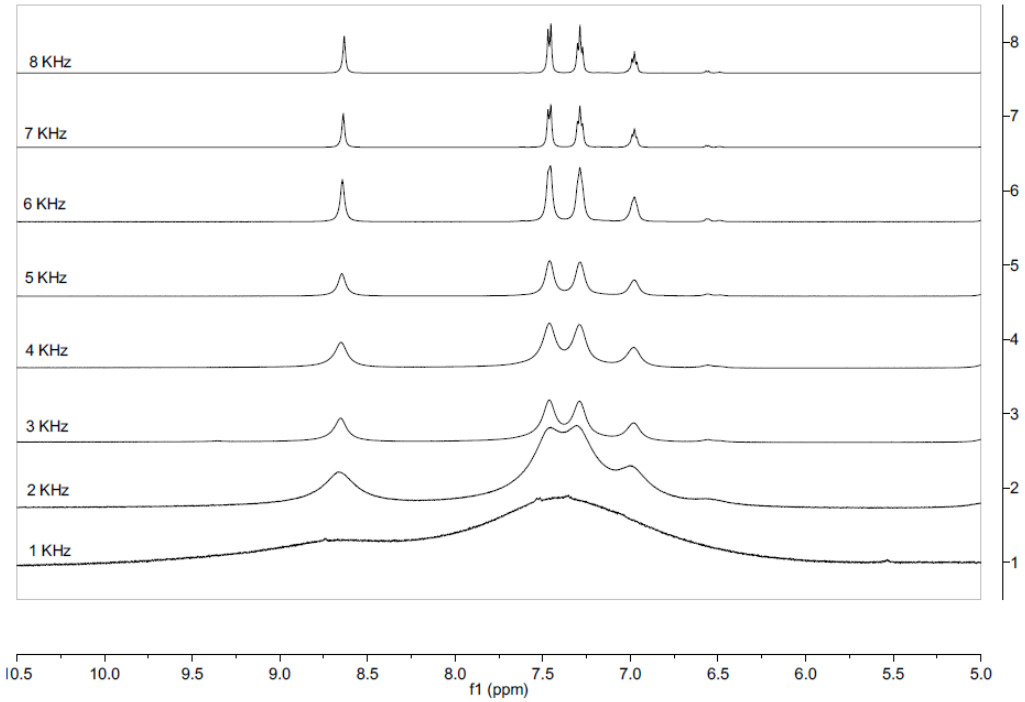

Figure 32 *- Array plot of expanded region of nanoconjugate* **16** *^{1}H spectra acquired at different MAS speed rotations.*

Also for nanoconjugate **17** ^{1}H and ^{13}C spectra were acquired confirming the formation of the covalent interaction between the starting isocyanate and the nanoparticle surface. The carbamate NH singlet proton (2) at 8.83 ppm and the aryl carbamate C=O carbon peak at 153 ppm (1) are clearly visible, as well as all the other peaks related to the proton AB system and CH carbons of disubstituted aromatic ring (*Figure 33* and *Figure 34*). An array plot of an expanded region of the proton spectra at different speed rate was also shown (*Figure 35*), demonstrating how MAS technique can resolved spectra also in presence of superparamagnetic metallic core.

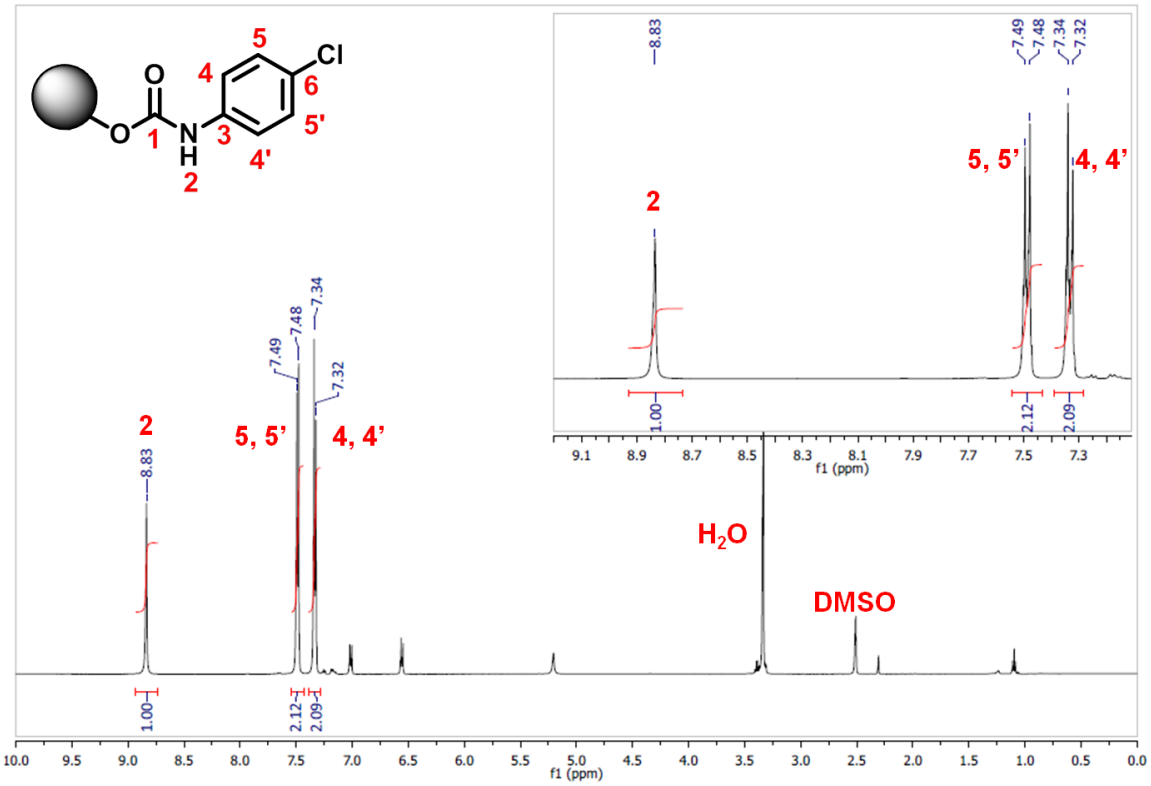

Figure 33 - *^{1}H HR-MAS NMR spectrum of nanoconjugate* **17** *in DMSO (6 KHz speed).*

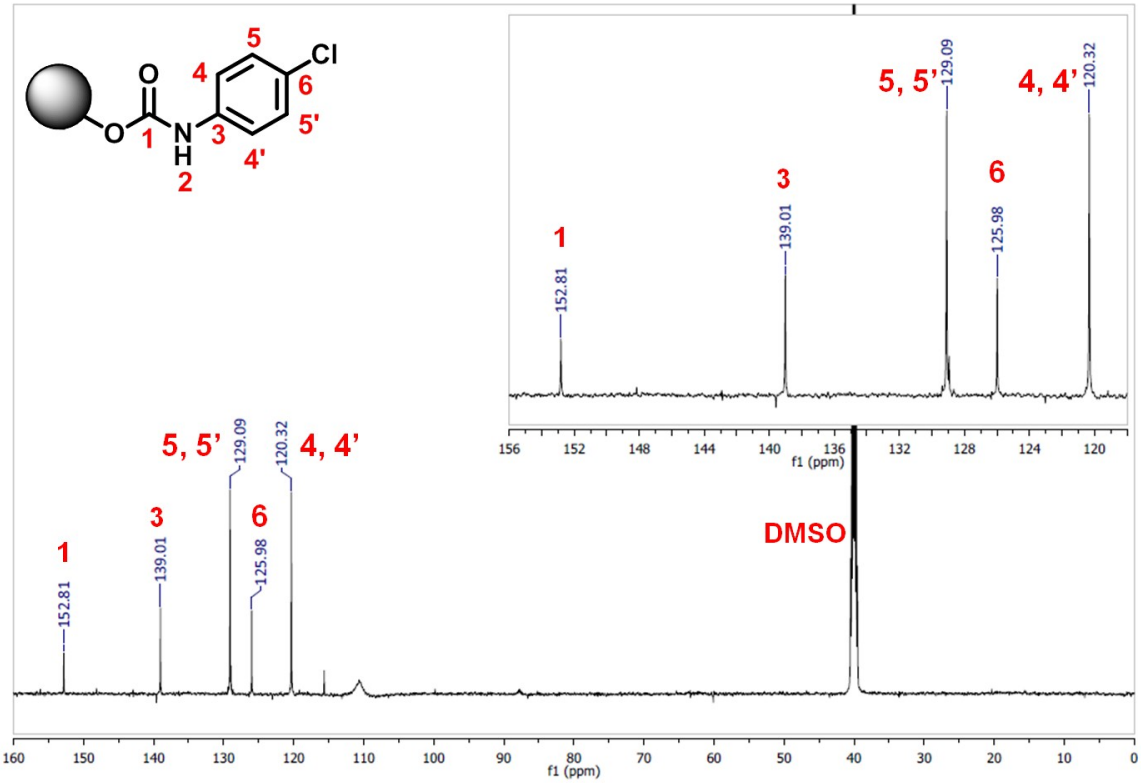

Figure 34 - *^{13}C all decoupled HR-MAS NMR spectrum of nanoconjugate* **17** *in DMSO (6 KHz speed).*

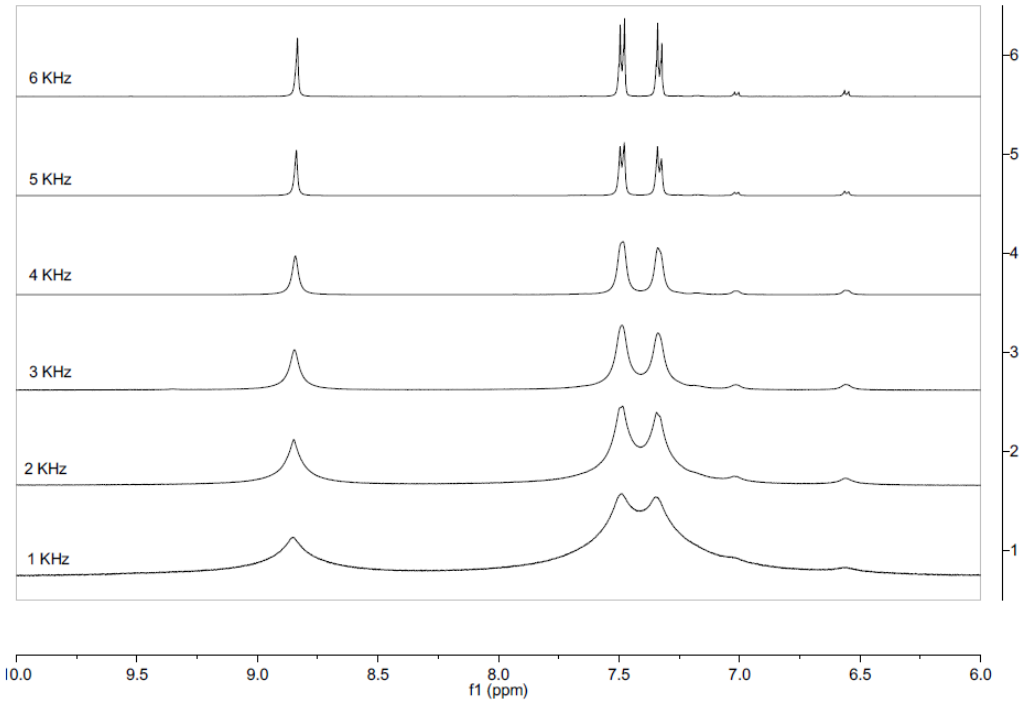

Figure 35 *- Array plot of expanded region of nanoconjugate* **17** *^{1}H spectra acquired at different MAS speed rotations.*

Proton HR-MAS spectrum of nanoconjugate **20**, reported in *Figure 36*, clearly shows the AB system of the disubstituted phenyl ring and the singlet of the two CH protons of the maleimido moiety; the singlet at 8.94 ppm is related to the proton resonance of the carabamate NH hydrogen atom (1).

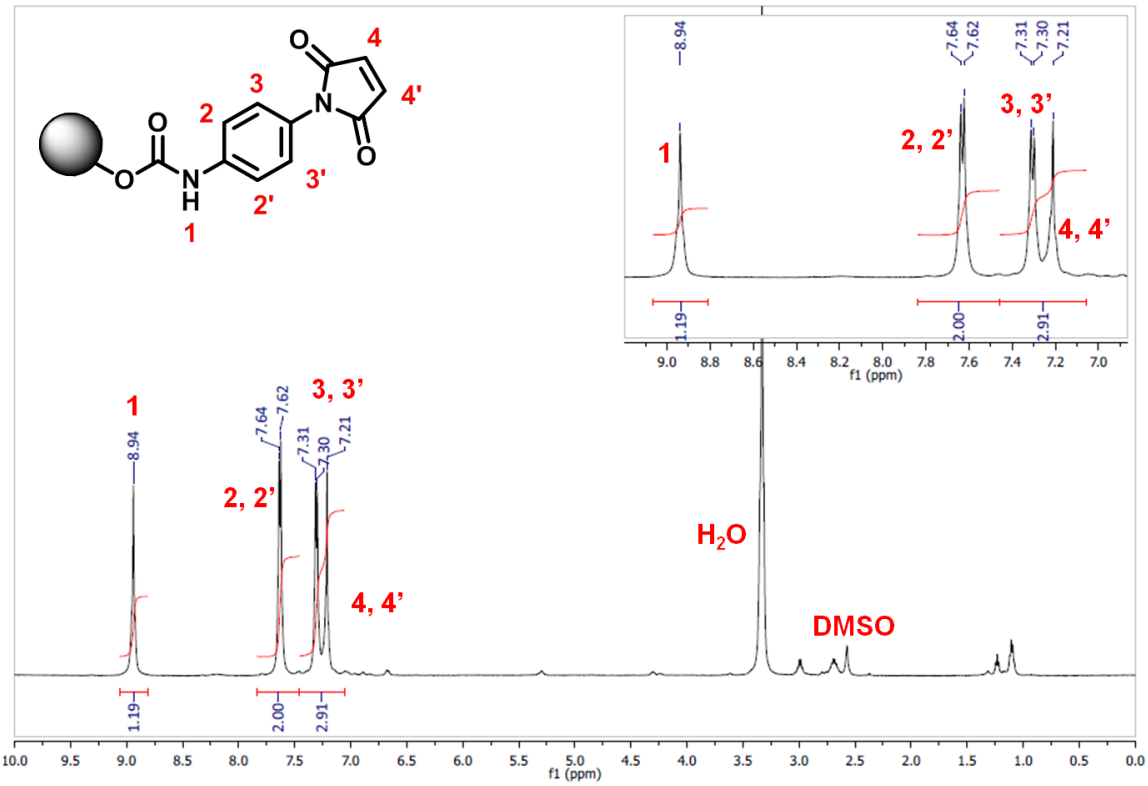

Figure 36 *- ^{1}H HR-MAS NMR spectrum of nanoconjugate* **20** *in DMSO (12 KHz speed).*

On this nanoconjugate, preliminary DOSY experiments were also performed.

4.2.3.1 Diffusion Ordered Nuclear Magnetic Resonance Spectroscopy (DOSY)

Self-diffusion is the random translational motion of molecules driven by their internal kinetic energy.[278] Translational diffusion and rotational diffusion can be distinguished. Diffusion is related to molecular size, as becomes apparent from the Stokes-Einstein equation: $D = {k_B T}/{f}$, where D is the diffusion coefficient, k_B is the Boltzmann constant, T is the temperature, and f is the friction coefficient.

If the solute is considered to be a spherical particle with an effective hydrodynamic radius (i.e. Stokes radius) r_S in a solution of viscosity η, then the friction coefficient is given by: $f = 6\pi\,\eta\,r_s$.

Using the pulsed-field gradient (PFG) method, motion is measured by evaluating the attenuation of a spin echo signal.[279] The attenuation is achieved by the dephasing of nuclear spins due to the combination of the translational motion and the imposition of gradient pulses. In contrast to relaxation methods, no assumptions concerning the relaxation mechanisms are necessary.

The PFG NMR sequence (*Figure 37*) is the simplest for measuring diffusion.[279] During application of the gradient, which is along the direction of the static spectrometer field, B_0, the effective magnetic field for each spin is dependent on its position. Therefore, the precession frequency is also position dependent which leads to the development of position dependent phase angles. The 180° pulse changes the direction of the precession. Hence, the second gradient of equal magnitude will cancel the effects of the first and refocus all spins, provided that no change of position, with respect to the direction of the gradient, has occurred. If there is a change of position, the refocusing will not be complete. This results in a remaining dephasing which is proportional to the displacement during the period Δ between the two gradients. Since diffusion is a random motion, there is a distribution of gradient-induced phase angles. These random phase shifts are averaged over the ensemble of spins contributing to the observed NMR signal. Hence, this signal is not phase shifted but attenuated, with the degree of attenuation depending on the displacement.

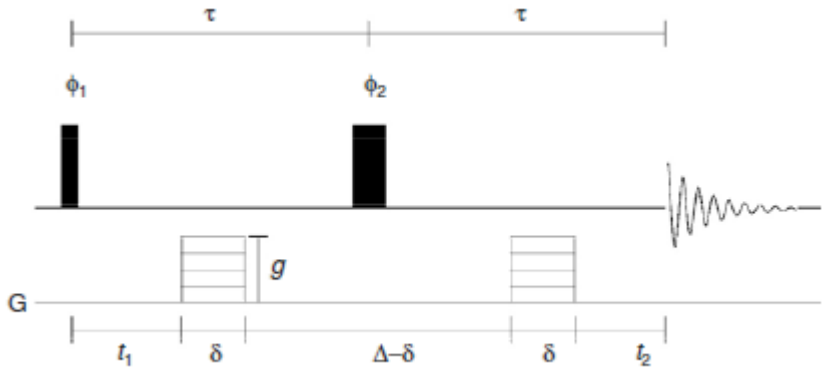

Figure 37 *- The Stejskal and Tanner pulsed field gradient NMR sequence. Narrow and wide filled bars correspond to 90° and 180° pulses, respectively. Open bars with horizontal stripes correspond to pulsed-field gradients whose strength is varied during the experiment. The pulse phases are* $\boldsymbol{\phi_1 = x}$ *and* $\boldsymbol{\phi_2 = y}$*. Phase cycling can be included to remove spectrometer artifacts.*

The signal intensity *S(2τ)* after the total echo time *2τ* is given by:

$$S(2\tau) = S(0)\exp\left(-\frac{2\tau}{T_2}\right)exp\left[-\gamma^2 g^2 D\delta^2\left(\Delta - \frac{\delta}{3}\right)\right] = S(2\tau)_{g=0}exp\left[-\gamma^2 g^2 D\delta^2\left(\Delta - \frac{\delta}{3}\right)\right]$$

where *S*(0) is the signal intensity immediately after the 90° pulse, T_2 is the spin-spin relaxation time of the species, *γ* is the gyromagnetic ratio of the observed nucleus, *g* is the strength of the applied gradient, and *δ* and *Δ* are the length of the rectangular gradient pulses and the separation between them, respectively. Typically, *δ* is in the range of 0.5-5 ms, the diffusion time *Δ* is in the range of milliseconds to seconds, and *g* is up to 20 T/m.

To determine diffusion coefficients, a series of experiments is performed in which either *g*, *δ*, or *Δ* is varied while keeping *τ* constant to achieve identical attenuation due to relaxation. Normally, the gradient strength *g* is incremented in subsequent experiments. Non-linear regression of the experimental data can be used for the determination of *D*.

Nowadays, the LED (Longitudinal Eddy current Delay or Longitudinal Encode-Decode) pulse sequence (*Figure 38*) is most often used for measuring diffusion since it allows eddy currents to decay and uses bipolar gradients which enables double effective strength as well as compensation for imperfections. This sequence is not affected by spin-spin coupling since it is based on the stimulated echo sequence.

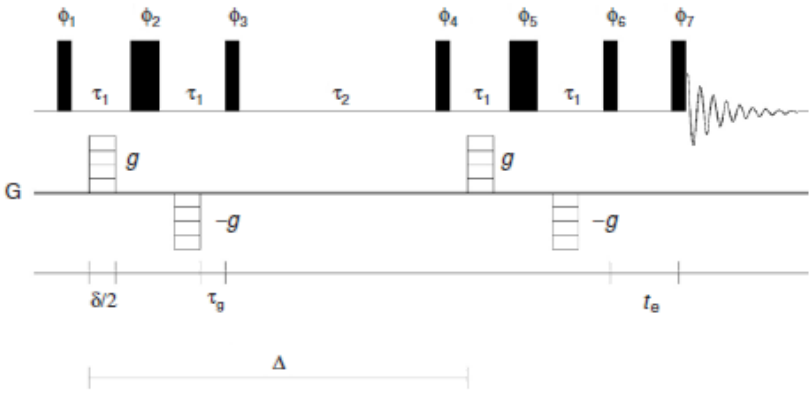

Figure 38 *- The LED pulse sequence using bipolar gradients. Narrow and wide filled bars correspond to 90° and 180° pulses, respectively.*

The signal intensity of the LED sequence is given by:

$$S = S_{g=0} exp\left[-\gamma^2 g^2 D\delta^2 \left(\Delta - \frac{\delta}{3} - \frac{\tau_g}{2}\right)\right]$$

In the chemical shift dimension, Fourier transformation (FT) is applied as usual. For each frequency *υ*, the signal can (in general) have contributions from several components (1,…*n*) which individually decay with their respective diffusion coefficient:

$$S(g,\upsilon) = \sum_{i=1}^{n} S_i\,(0,\upsilon) exp\left[-\gamma^2 g^2 D_i\delta^2 \left(\Delta - \frac{\delta}{3}\right)\right]$$

The individual diffusion coefficients D_i and the signal intensities $S_i(0,\upsilon)$ have to be extracted in order to construct the diffusion spectra. The name DOSY (Diffusion Ordered Spectroscopy) refers to the presentation of the data obtained in PFG or LED NMR measurements where the chemical shift is plotted in one (or two) dimension and the diffusion coefficient in the other dimension. This presentation allows the identification of signals belonging to one component (or at least to components showing the same diffusion coefficient).[280]

To better understand how DOSY techniques can help in the characterization of a mixture of compounds, as well as the data obtained are presented, in *Figure 39* is reported the ^{13}C DOSY spectrum of a mixture of glucose, sucrose and sodium dodecyl sulfate (SDS) as an explicative example.[281] Diffusion coefficient *D* increasing from down to up in the 2D map of *Figure 39*.

Greater the diffusion coefficient *D* (expressed in square meters *per* second [m^2/s]), higher the speed rate of the diffusion of the molecule in solution.

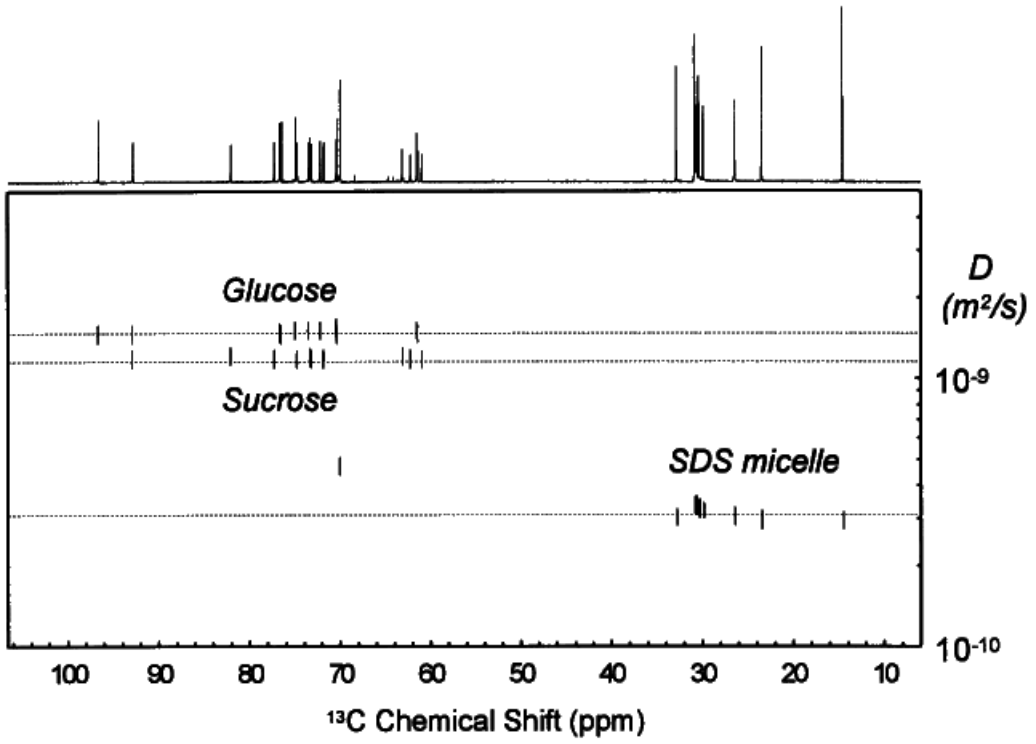

Figure 39 *- ^{13}C INEPT-DOSY for a mixture containing glucose, sucrose, and SDS in D_2O. Dotted lines show average diffusion coefficients of each component. The 1D ^{13}C INEPT spectrum of the mixture is shown at the top.*

A preliminary DOSY study in MAS experiments was performed on nanoconjugate **20**, in order to investigate how the presence of a strong magnetic field can influence the diffusion coefficient of an organic molecule anchored onto a superparamagnetic metallic core.

We have already demonstrated that MAS techniques can lead to well resolved spectra regardless of the presence of the metallic core exposed to a magnetic field.

Despite the nanoconjugates are bigger molecular entities and thus lower diffusion coefficient are expected, the presence of an external static strong magnetic field, added to the pulse field gradients can in theory accelerate the diffusion motion of these superparamagnetic systems.

In *Figure 40*, the DOSY spectrum of **20** is shown and a single set of diffusion signals are present with an average diffusion coefficient of ca. 7.0e-9 m^2/s. Diffusion coefficient *D* increasing in this case from up to down in the 2D map of *Figure 40*.

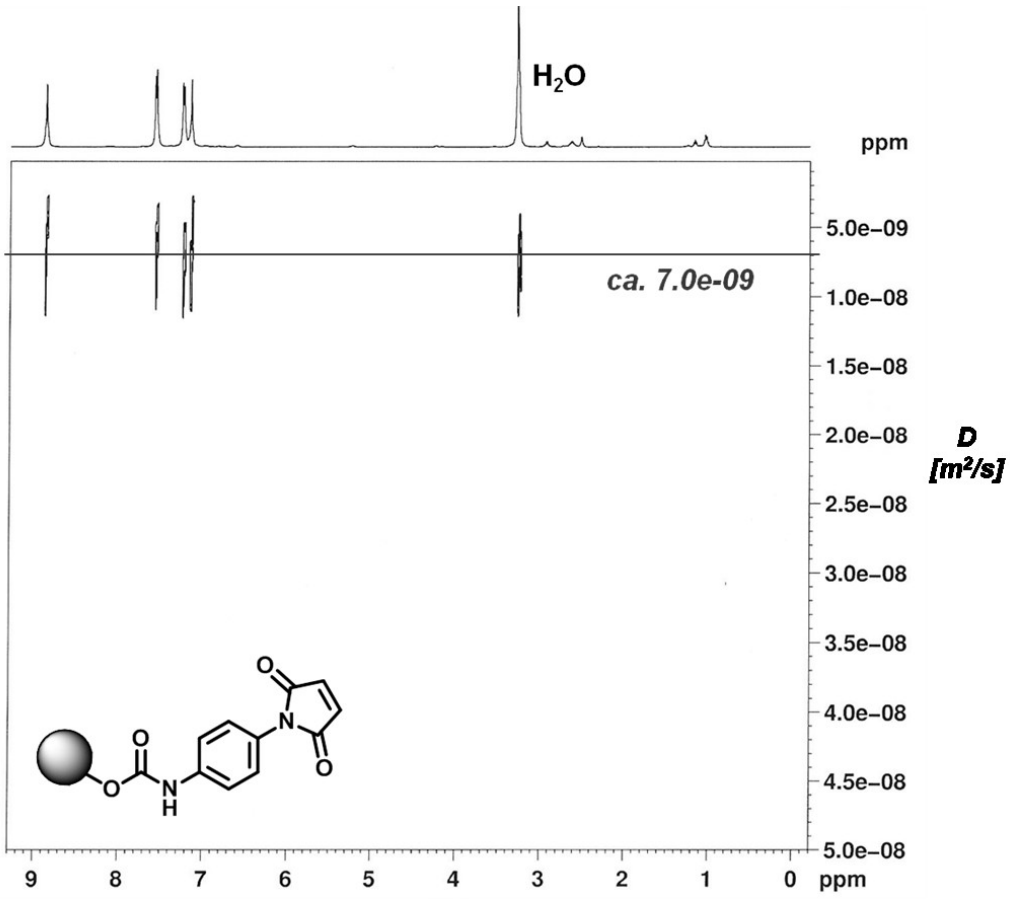

Figure 40 *- ^{1}H-DOSY of nanoconjugate* **20***.*

To evaluate how this value is affected by the presence of the metallic superparamagnetic core surrounded by the magnetic field, we decided to compare the obtained diffusion coefficient with the one determined by DOSY experiment performed on the most similar organic compound not grafted on nanoparticles.

For this reason, starting from the PMPI **10** has been synthesized the corresponding bis-urea **21**, just adding few amounts of water to a solution of **10** in DMSO.[266] The recovered urea was then analyzed by ^{1}H HR-MAS NMR (*Figure 41*) and its diffusion coefficient was determined by HR-MAS DOSY experiment (*Figure 42*).

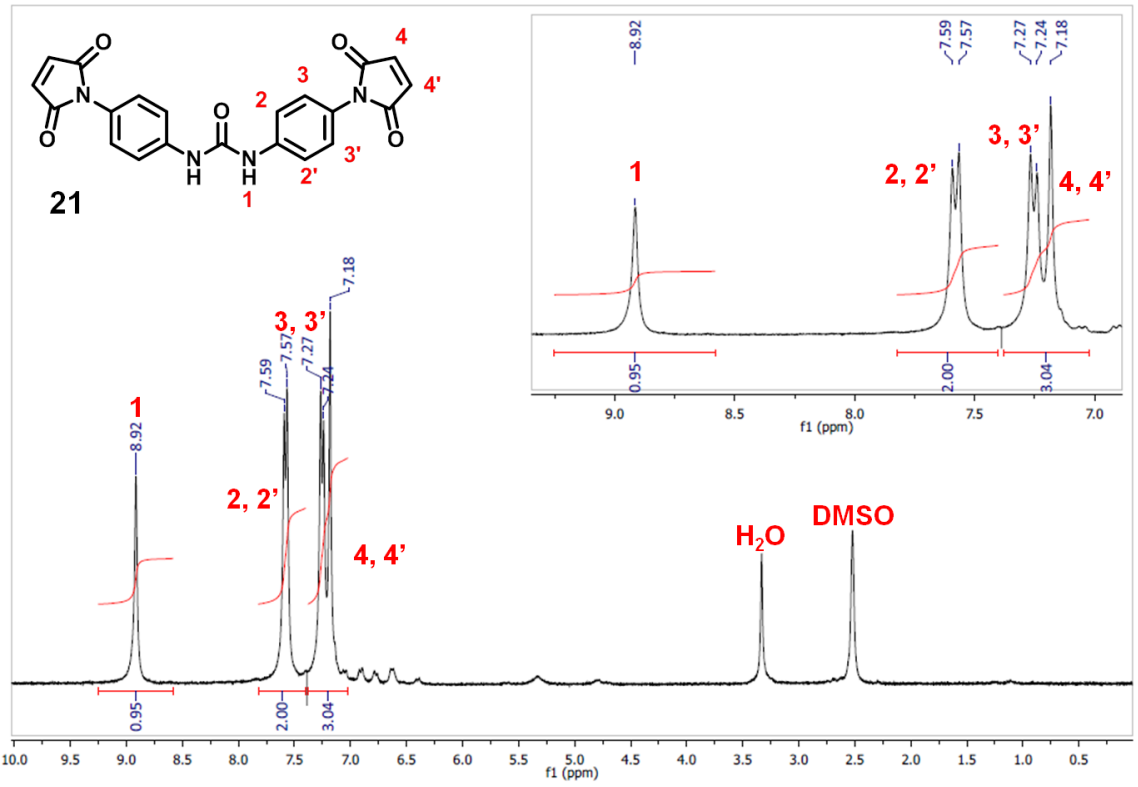

Figure 41 *- [1]H HR-MAS of the bis[(p-maleimido)phenyl] urea* **21** *in DMSO (12 KHz speed).*

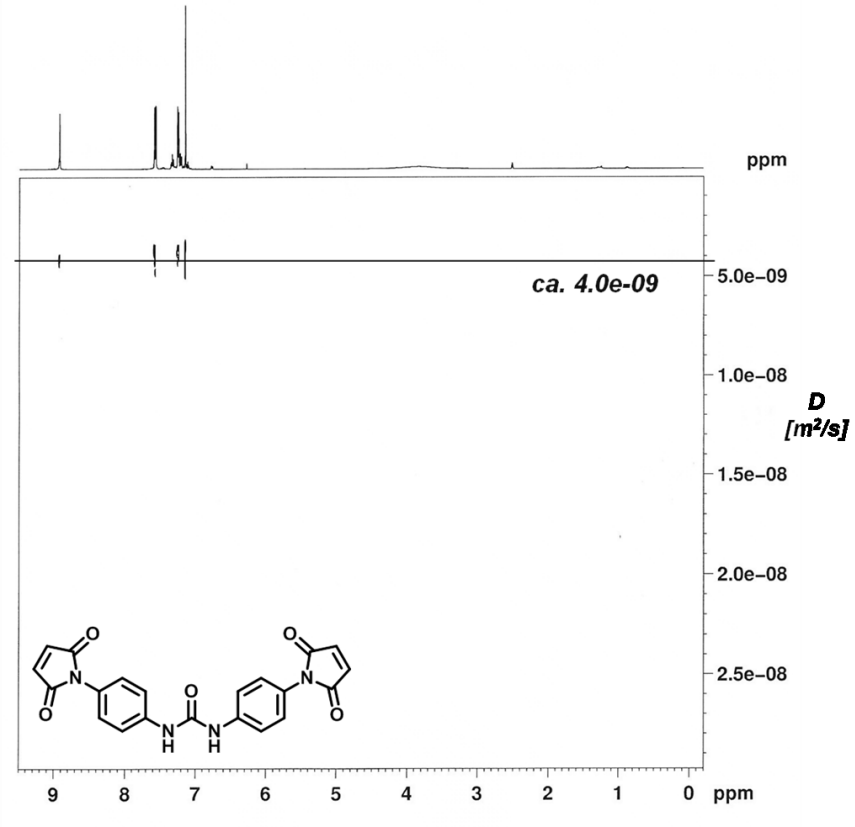

Figure 42 *- [1]H-DOSY of bis[(p-maleimido)phenyl] urea* **21**.

The chemical shifts of the urea proton signals are quite the same of that obtained for nanoconjugate **20**, confirming the nature of the organic residue onto the SPIONs surface, while the diffusion coefficient for the free **21** in DMSO solution is ca. 4.0e-9 m^2/s, lower than the value obtained for the analogue nanoconjugate **20**. This result may confirm that the magnetic core induce an acceleration in the diffusive phenomenon caused by the stronger influence of the NMR magnetic fields (static and pulsed ones).

In addition ^{1}H-DOSY HR-MAS NMR experiment was also acquired for a mixture of **20** and **21**, in ratio 2:1 in DMSO (*Figure 43*). The ratio of the two species in the mixture was chosen in order to obtain almost the same intensity signal.

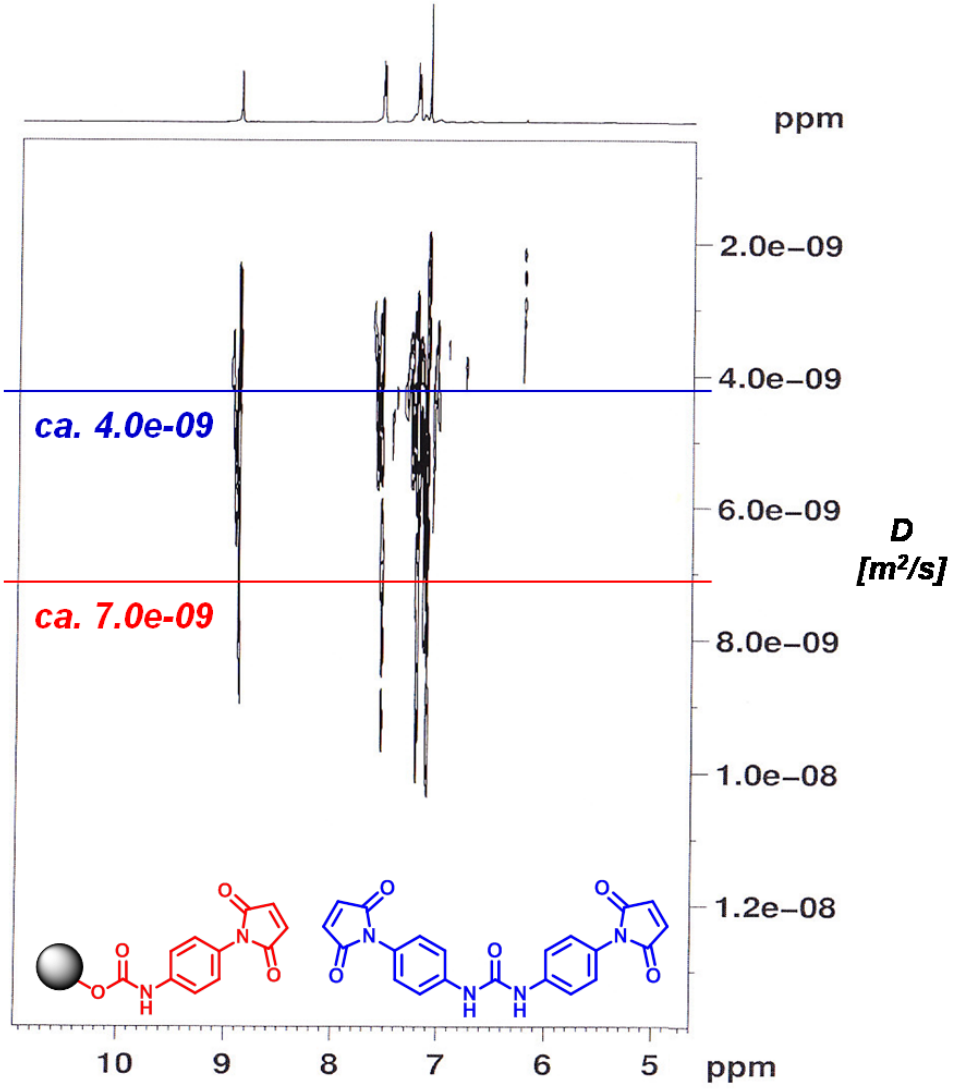

Figure 43 *- ^{1}H-DOSY of a mixture of nanoconjugate* **20** *and bis[(p-maleimido)phenyl] urea* **21** *in DMSO (ratio 2:1).*

Having almost the same chemical shift, **20** and **21** gave practically a superimposed proton projection spectrum on the upper horizontal axis, while in the bidimensional area can be recognized two sets of signals (easily visible in the signal at about 7.6 ppm, where a net interruption is present). The diffusion coefficients of the two species were also confirmed.

These are only preliminary results in the use of DOSY experiments for the characterization of magnetic nanoconjugates, so further work must be done.

Concerning the general use of the HR-MAS technique, we can conclude that the results obtained demonstrate the grafting of isocyanate molecules onto the SPIONs surface, leading to the formation of a carbamate bond. The MAS tool has proved to be versatile and furthermore, can be used to overcome all the problems related to the presence of a superparamagnetic core. Very nice spectra were obtained and preliminary DOSY experiments were performed.

4.3 Non-Covalent versus Covalent Surface Interactions

Having established the easy anchoring of isocyanates onto the SPIONs surface by the formation of a carbamate bond, we decided to compare the efficiency of this new grafting methodology with the already known non-covalent adsorption of carboxylic acid and with the most used linker based on siloxane interaction.

For this purpose we started comparing the loadings of nanoconjugates **16** and **20** (obtained by anchoring the phenyl isocyanate **6** and the (*p*-maleimido)phenyl isocyanate **10**, respectively) *versus* the loadings of the nanoconjugates **23** and **24** that have been synthesized starting from the corresponding carboxylic compounds, the benzoic acid **22** and the (*p*-maleimido)benzoic acid **12** (*Figure 44*). Functionalized nanoparticles **23** and **24** bear the same organic residue of the analogous nanoconjugates **16** and **20**, but differ from the anchoring group.

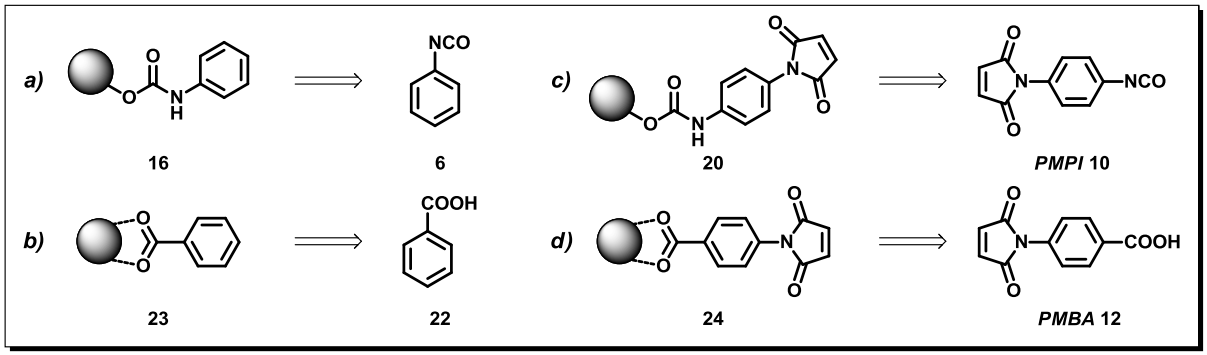

Figure 44 *- Synthesis of comparable nanoconjugates* **16***,* **20***,* **23** *and* **24***. In a) and c)* **16** *and* **20** *are formed by covalent interaction between the starting isocyanates* **6** *and* **10** *with SPIONs, while in b) and d) a non-covalent adsorption were used to obtain nanoconjugate* **23** *and* **24** *from the corresponding carboxylic acids* **22** *and* **12***.*

In order to obtain comparable loading values for the nanoconjugates **23** and **24**, the same synthetic protocol used for the grafting of isocyanates onto SPIONs, previously shown in *Scheme 5*, was applied. Thus, 0.2, 0.4 and 0.8 millimoles of carboxylic acids **22** e **12** were added to a suspension of 100 milligrams of naked SPIONs in toluene. After 4 hours at 60 °C under sonication, the desired functionalized nanoparticles **23** and **24** were isolated. The loadings were determined by E.A. and FTIR spectra were acquired demonstrating the anchoring of the organic carboxylic acid by a non-covalent adsorption with formation of a carboxylate species (a strong sharp peak at ca. 1600 cm^{-1} was obtained for both the nanoconjugates, corresponding to the $O=C-O^-$ stretching).

In *Table 8* and *Table 9* are reported the loading values obtained from E.A. of nanoconjugates **23** and **24**, compared with the ones obtained for compounds **16** and **20** in the three series of reaction performed increasing the amount of the organic ligand.

Ligand	*Nanoconjugate*	**0,2 mmol of Ligand / 100 mg NPs**		*Interaction*
		Tot % org	*mmol/g_{NPs}*	
6	**16**	15,36	1,28	*Covalent*
22	**23**	6,96	0,58	*Non-Covalent*

Ligand	*Nanoconjugate*	**0,4 mmol of Ligand / 100 mg NPs**		*Interaction*
		Tot % org	*mmol/g_{NPs}*	
6	**16**	26,55	2,21	*Covalent*
22	**23**	7,64	0,63	*Non-Covalent*

Ligand	*Nanoconjugate*	**0,8 mmol of Ligand / 100 mg NPs**		*Interaction*
		Tot % org	*mmol/g_{NPs}*	
6	**16**	43,80	3,65	*Covalent*
22	**23**	8,22	0,68	*Non-Covalent*

Table 8 *- Loading values obtained from elemental analysis for the nanoconjugate* **23** *(non-covalent adsorption), compared with the final loadings of nanoconjugate* **16** *(covalent interaction).*

Ligand	*Nanoconjugate*	**0,2 mmol of Ligand / 100 mg NPs**		*Interaction*
		Tot % org	*mmol/g_{NPs}*	
10	**20**	14,42	0,67	*Covalent*
12	**24**	12,63	0,58	*Non-Covalent*

Ligand	*Nanoconjugate*	**0,4 mmol of Ligand / 100 mg NPs**		*Interaction*
		Tot % org	*mmol/g_{NPs}*	
10	**20**	31,07	1,44	*Covalent*
12	**24**	13,11	0,61	*Non-Covalent*

Ligand	*Nanoconjugate*	**0,8 mmol of Ligand / 100 mg NPs**		*Interaction*
		Tot % org	*mmol/g_{NPs}*	
10	**20**	51,81	2,44	*Covalent*
12	**24**	14,52	0,67	*Non-Covalent*

Table 9 *- Loading values obtained from elemental analysis for the nanoconjugate* **24** *(non-covalent adsorption), compared with the final loadings of nanoconjugate* **20** *(covalent interaction).*

From the loading values obtained, we can note that the covalent grafting of isocyanates leads to higher loading compared with the non-covalent interaction of carboxylic acids and in *Figure 45* and *Figure 46* these values are summarized. Furthermore, only a slight increase in final loading was observed increasing the amount of the starting carboxylic ligand.

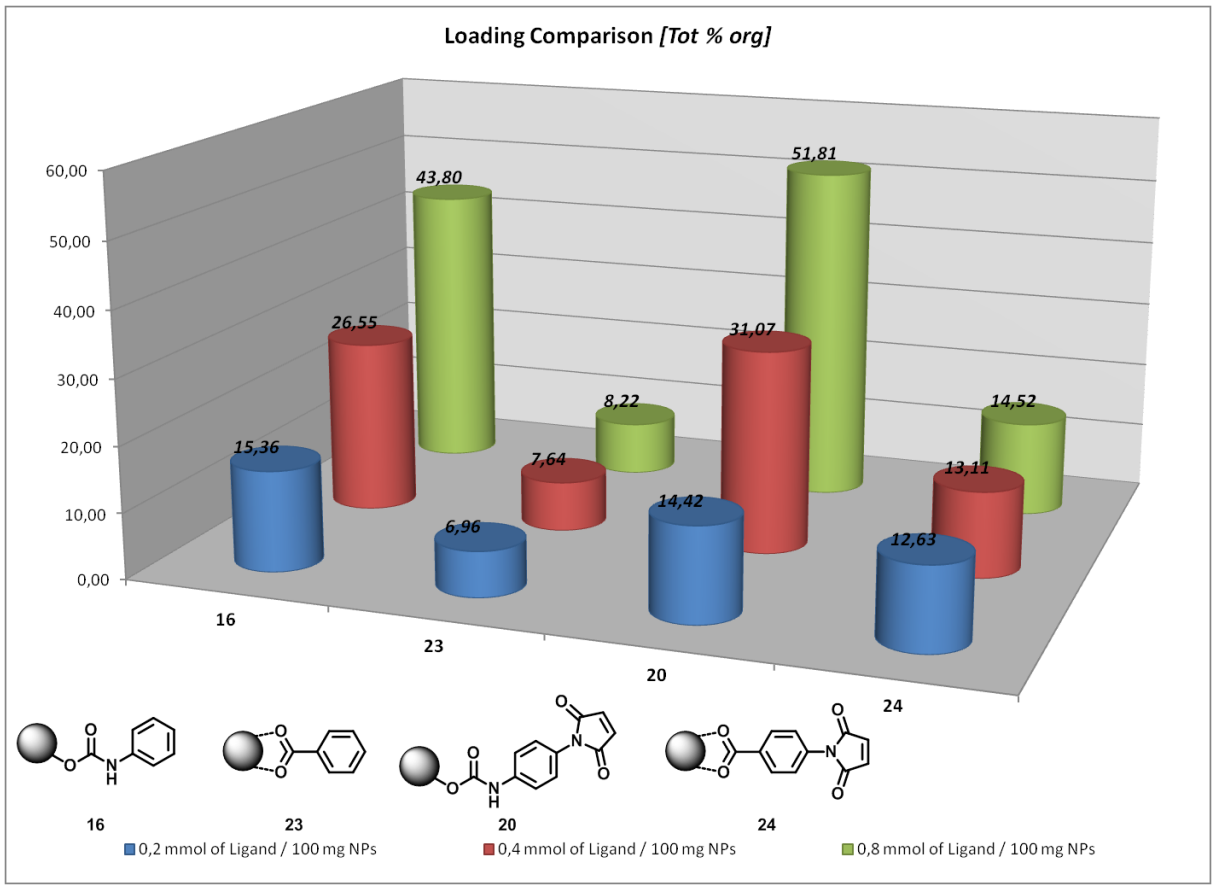

Figure 45 *- Loading comparison of nanoconjugates* **16** *and* **20** *(covalent interaction) versus* **23** *and* **24** *(non-covalent adsorption), express as total percentage in weight of organic part loaded onto SPIONs [Tot % org].*

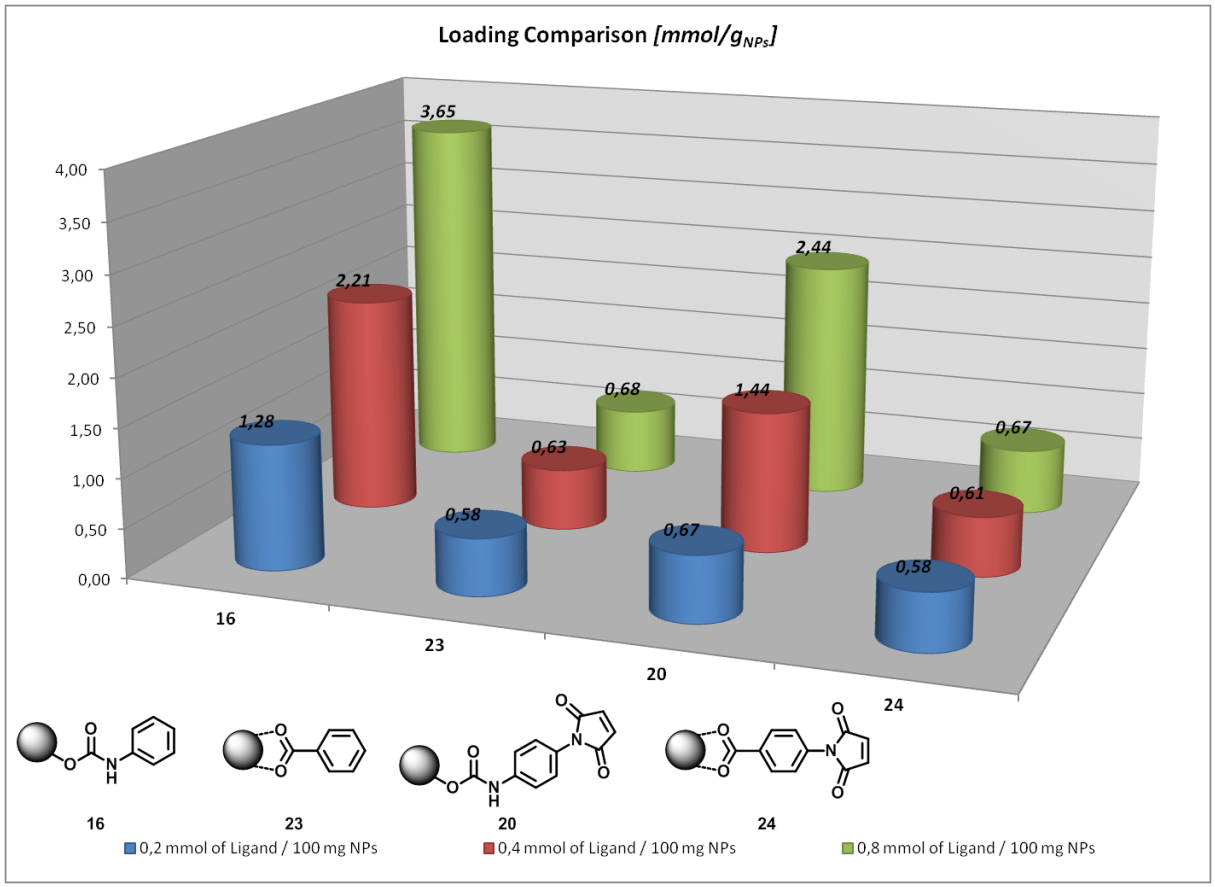

Figure 46 *- Loading comparison of nanoconjugates* **16** *and* **20** *(covalent interaction) versus* **23** *and* **24** *(non-covalent adsorption), express as millimoles of organic part per gram of functionalized nanoparticles [mmol/g$_{NPs}$].*

The same approach was used to compare the amount of isocyanate loaded onto SPIONs against the covalent silylation of APTES **1** (*Figure 47*).

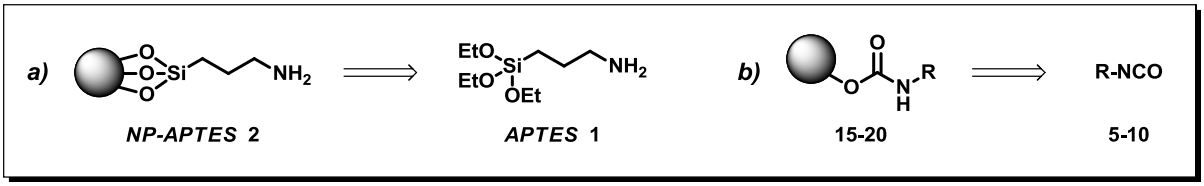

Figure 47 *– Synthetic approach for the synthesis of a) nanoconjugates* **2**, *from the corresponding alkoxysylane APTES* ***1*** *and b) nanoconjugates* **15**-**20**, *from starting isocyanates* **5**-**10**. *The loading values obtained for the silyloxy-derivative will be compared with the average loading calculate for the new grafting methodology.*

Nanoconjugate **2** was therefore synthesized accordingly to *Schemes 1* and *5*, using 0.2, 0.4 and 0.8 millimoles of **1** *per* 100 milligrams of naked nanoparticles. The functionalized SPIONs were analyzed by E.A. and the loadings obtained were compared with the average loading found for the isocyanate covalent interaction (*Tables 2-4*). The results are reported in *Table 10* and summarized in *Figure 48*.

Ligand	***Nanoconjugate***	**0,2 mmol of Ligand / 100 mg NPs**		***Interaction***
		Tot % org	*mmol/g_{NPs}*	
1	**2**	5,27	0,39	*Covalent*
Average Loading with R-NCO		16,66	1,02	*Covalent*
Ligand	***Nanoconjugate***	**0,4 mmol of Ligand / 100 mg NPs**		***Interaction***
		Tot % org	*mmol/g_{NPs}*	
1	**2**	7,59	0,56	*Covalent*
Average Loading with R-NCO		26,6	1,67	*Covalent*
Ligand	***Nanoconjugate***	**0,8 mmol of Ligand / 100 mg NPs**		***Interaction***
		Tot % org	*mmol/g_{NPs}*	
1	**2**	13,02	0,97	*Covalent*
Average Loading with R-NCO		40,7	2,61	*Covalent*

Table 10 *- Loading values obtained from elemental analysis for the nanoconjugate* **2** *(Si-O covalent interaction), compared with the average loading calculated on nanoconjugate* **15-20** *(carbamate covalent interaction).*

Also in this case, lower loading values were obtained for covalent Si-O bond formation respect to the carbamate bond interaction. Increasing the amount of alkoxysilane, an increase in the final loading was observed for nanoconjugate **2**, which reached the 13% with 0.8 mmol of ligand. This value however is significantly lower than the one obtained when the isocyanate was grafted onto the nanoparticles surface.

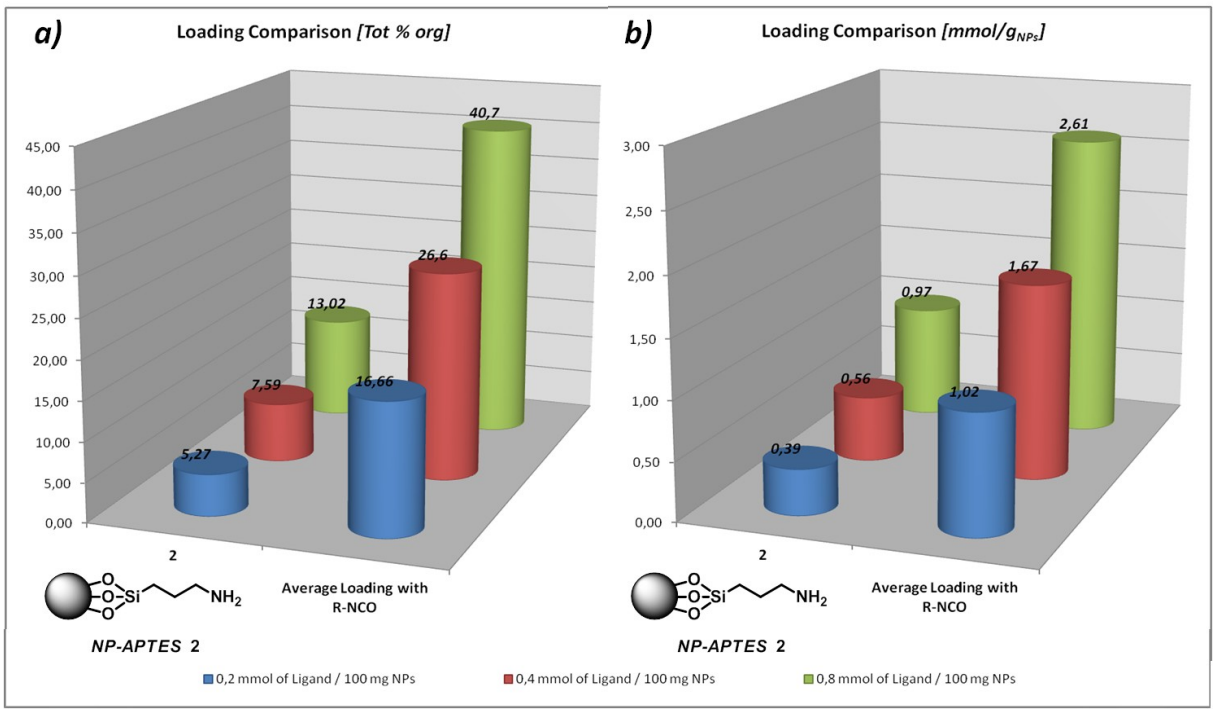

Figure 48 *- Loading comparison of nanoconjugate* **2** *(Si-O covalent interaction) versus the average loading calculated on nanoconjugate* **15-20** *(carbamate covalent interaction).*

We may conclude this section by stating that the new methodology developed in this research leads to significantly higher loading values if compared to the classical non-covalent adsorption of carboxylic acids and also respect to the main used covalent silylation of nanoparticles.

4.4 The Use of Properly Functionalized Isocyanates as Heterobifunctional Linkers

The outstanding functionalization of SPIONs with isocyanates, with formation of a covalent carbamate bond, led us to further investigate the possibility of use these organic molecules as heterobifunctional linkers.

The concepts related to the synthetic strategy that involves proper functionalized organic molecules as linker, were already widely explained *[see section 4]*.

From the beginning of this research work, we decided to study this new functionalization methodology with the final aim of conjugating bioactive molecules onto the SPIONs surface thanks to the use of specifically designed linkers.

For this reason, isocyanates **8**-**10** were chosen in order to obtain the corresponding nanoconjugates **18**-**20**, that bear an additional reactive functional group.

The chlorosulfonyl and the chloroacyl moieties are highly reactive towards amines and alcohols, affording the corresponding amides and esters, while the maleimido group is a classical Michael acceptor able to react with strong nucleophiles, as thiols and amines.

The first step was to demonstrate that the -SO_2Cl and -COCl groups are not reactive towards the nanoparticles surface. Indeed, the functionalization reaction consists in the direct addition of the isocyanates **8** and **9** in a suspension of naked SPIONs in dry toluene so, in principle, a possible competitive reaction can occur with formation of the corresponding esters with the surface hydroxyl groups.

To verify this possibility, blank reactions were performed with tosyl chloride **25** and benzoyl chloride **26** (*Scheme 6* and *Scheme 7*, respectively).

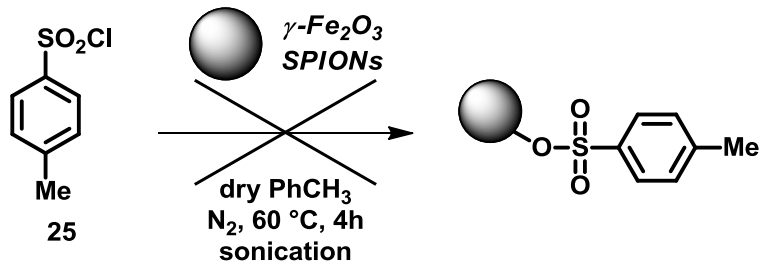

Scheme 6 *- Blank reaction between tosyl chloride* **25** *and naked SPIONs.*

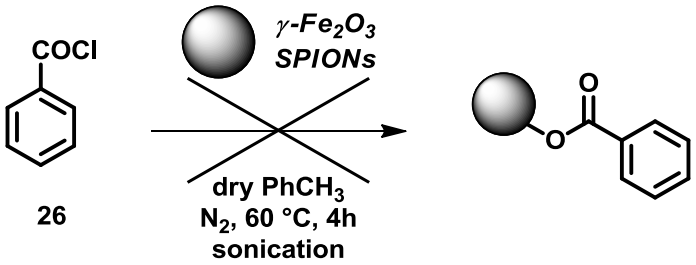

Scheme 7 *- Blank reaction between benzoyl chloride* **26** *and naked SPIONs.*

The recovered nanoparticles were analyzed by E.A. and FTIR spectroscopy, but no significant interaction with the SPIONs surface was detected. The total percentages of organic part were lower than 4 % and, as shown in FTIR spectra reported in *Figure 49* and *Figure 50*, no relevant peaks were present. The only intense vibrational bands are related to the strong absorption of iron oxide nanoparticles and few peaks (with very low intensity) can be associated to an unspecific interaction of sulfonic and carboxylic acid that may be formed by partial hydrolysis of the chlorosulfonyl and chloroacyl moieties in the reaction conditions.

To prove the formation of a non-covalent interaction between the COOH group arising from partial hydrolysis of **26** and the nanoparticles, we decided to perform the reaction previously shown in *Scheme 7*, in the presence of water in order to generate *in situ* the corresponding benzoic acid **22** (*Scheme 8*). From this reaction we obtained the nanoconjugate **23**, that has been already synthesized starting from the corresponding carboxylic acid **22** *[see Figure 44b]*.

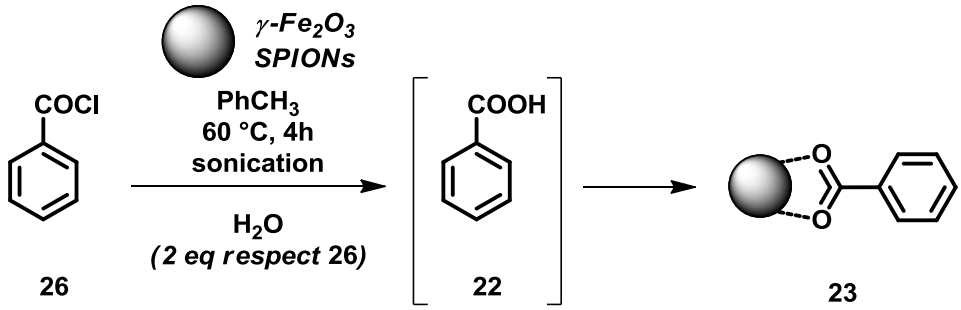

Scheme 8 *- Blank reaction between benzoyl chloride* **26** *and naked SPIONs in presence of water. The hydrolyzed compound* **22** *was generated in situ and directly reacted with nanoparticles, affording* **23***.*

In *Figure 50c* is clearly visible the strong sharp peak related to the non-covalent adsorption of the carboxylate molecule onto the SPIONs surface, as well as all the vibrational bands related to the aromatic ring.

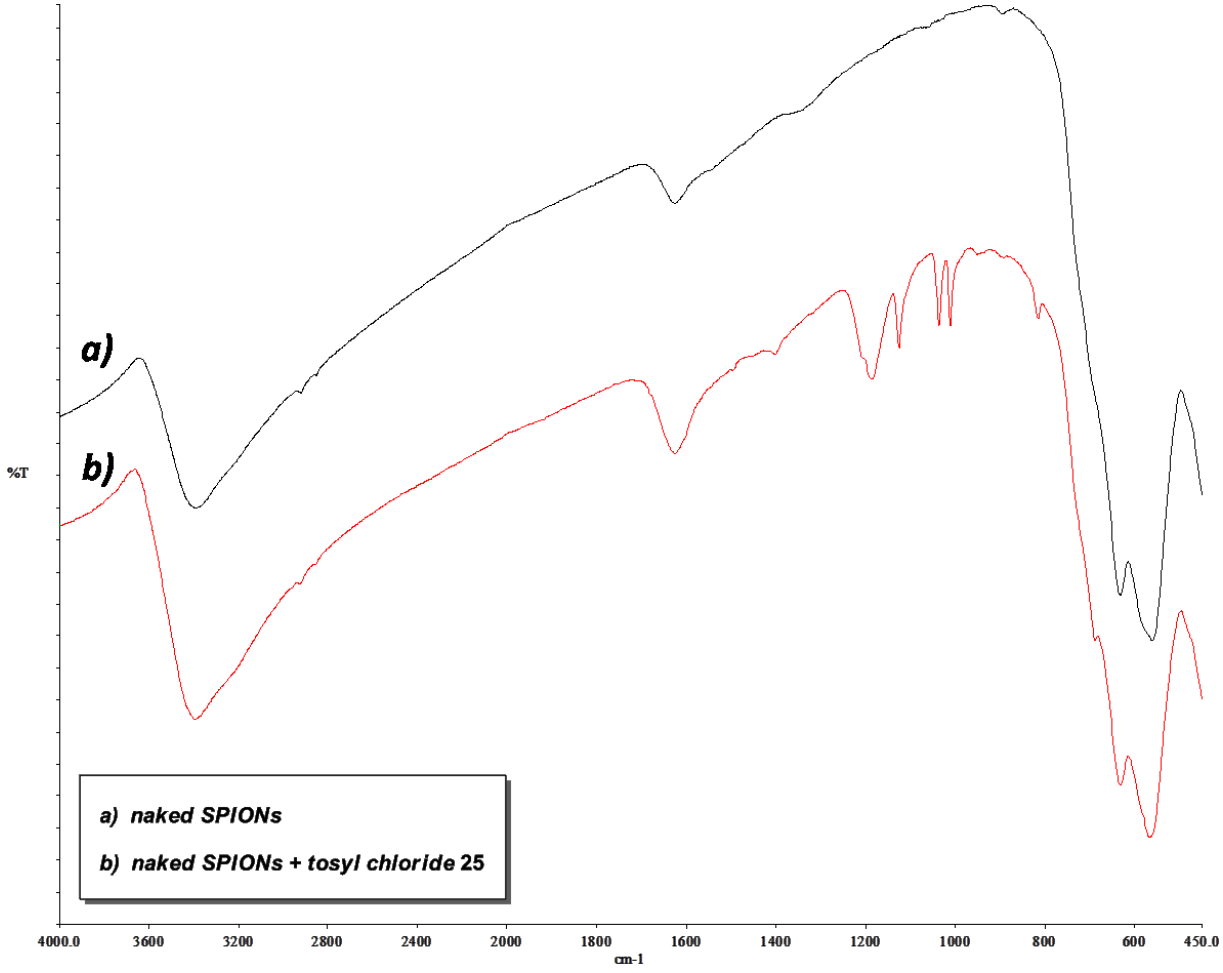

Figure 49 *- FTIR spectra of a) naked SPIONs (black line) and b) nanoparticles obtained by reaction with tosyl chloride* **25** *(red line). In spectrum b) in the range of 1200-1000 cm^{-1} are present some peaks that can be referred to the chemisorption of sulfonic acid onto the SPIONs surface.*

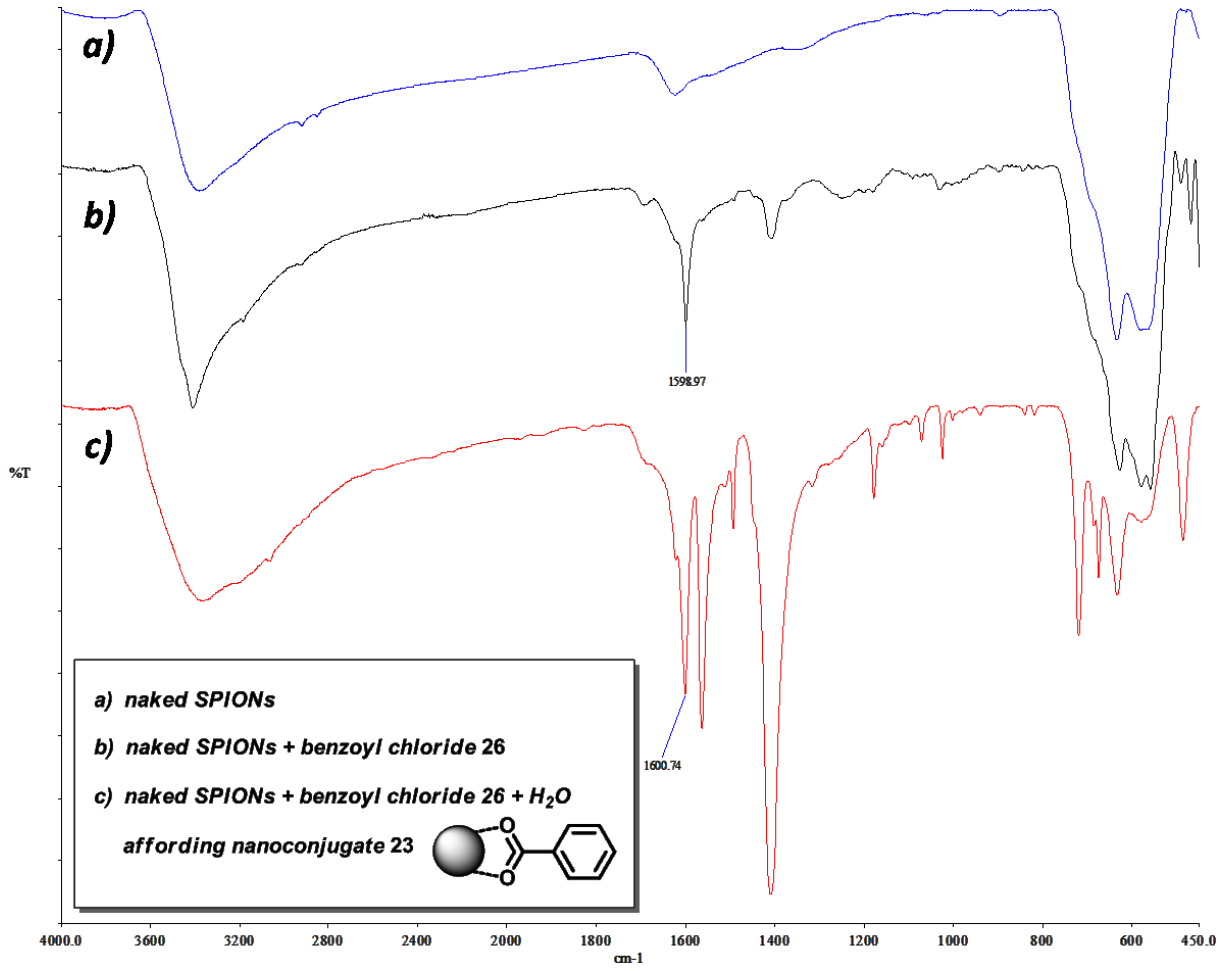

Figure 50 *- FTIR spectra of a) naked SPIONs (blue line), b) nanoparticles obtained by reaction with benzoyl chloride* **26** *(black line) and c) nanoconjugate* **23** *obtained by reacting naked SPIONs with* **26** *in presence of water. In spectrum b) the peak at 1599 cm^{-1} is related to the formation of a non-covalent interaction with formation of a carboxylate species. This is probably due to the partial hydrolysis of* **26** *in the reaction condition. In spectrum c) the unspecific adsorption of the completely hydrolyzed* **26** *(with in situ formation of benzoic acid* **22***) is clearly visible. To note the strong sharp peak at 1600 cm^{-1} referred to the carboxylate species.*

Having established that the chlorosulfonyl and the chloroacyl moieties are not able to directly bind the SPIONs surface leading to ester-derivatives, we decided to use the (*p*-chlorosulfonyl)phenyl isocyanate **8** and the (*p*-isocyanate)benzoyl chloride **9** as heterobifunctional linkers. Working in inert atmosphere with dry solvent, it is possible to

prevent the hydrolysis of -SO_2Cl and -COCl groups, as already demonstrated by FTIR spectroscopy on nanoconjugates **18** and **19** *[see Figure 22 and 23, respectively]*.

To further prove the presence of the chlorine atom, Beilstein tests were performed on **18** and **19**, resulting in an intense and bright green flame typical of halogens.

The reactivity of nanoconjugates **18** and **19** was then tested reacting them with *n*-butylamine, in order to form the corresponding sulfonamide and amide derivatives **27** and **28** respectively, as shown in *Scheme 9* and *Scheme 10*.

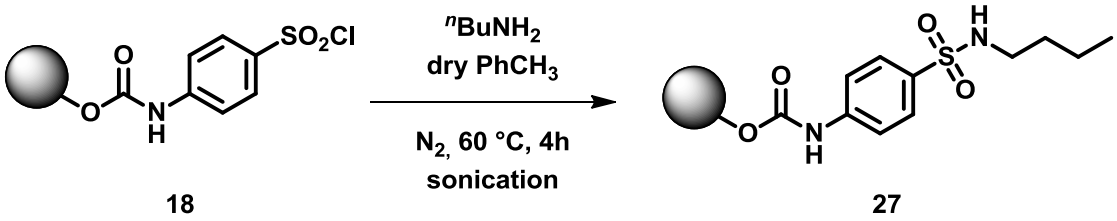

18 **27**

Scheme 9 *- Synthesis of n-butylsulfonamide* **27***.*

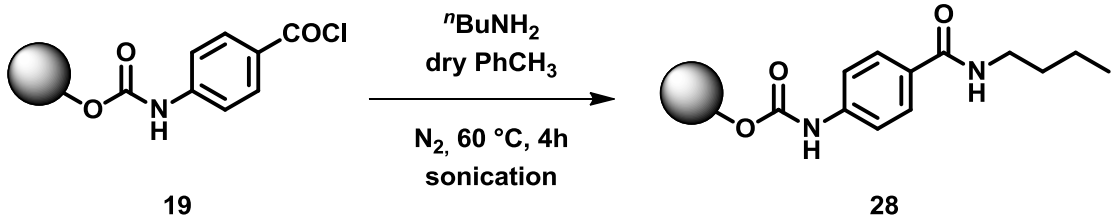

19 **28**

Scheme 10 *- Synthesis of n-butylamide* **28***.*

E.A. and FTIR spectroscopy (*Figure 51* and *Figure 52*) confirm the formation of the desired product, proving the possibility of use these systems as heterobifunctional linkers for the covalent binding of biomolecules onto SPIONs.

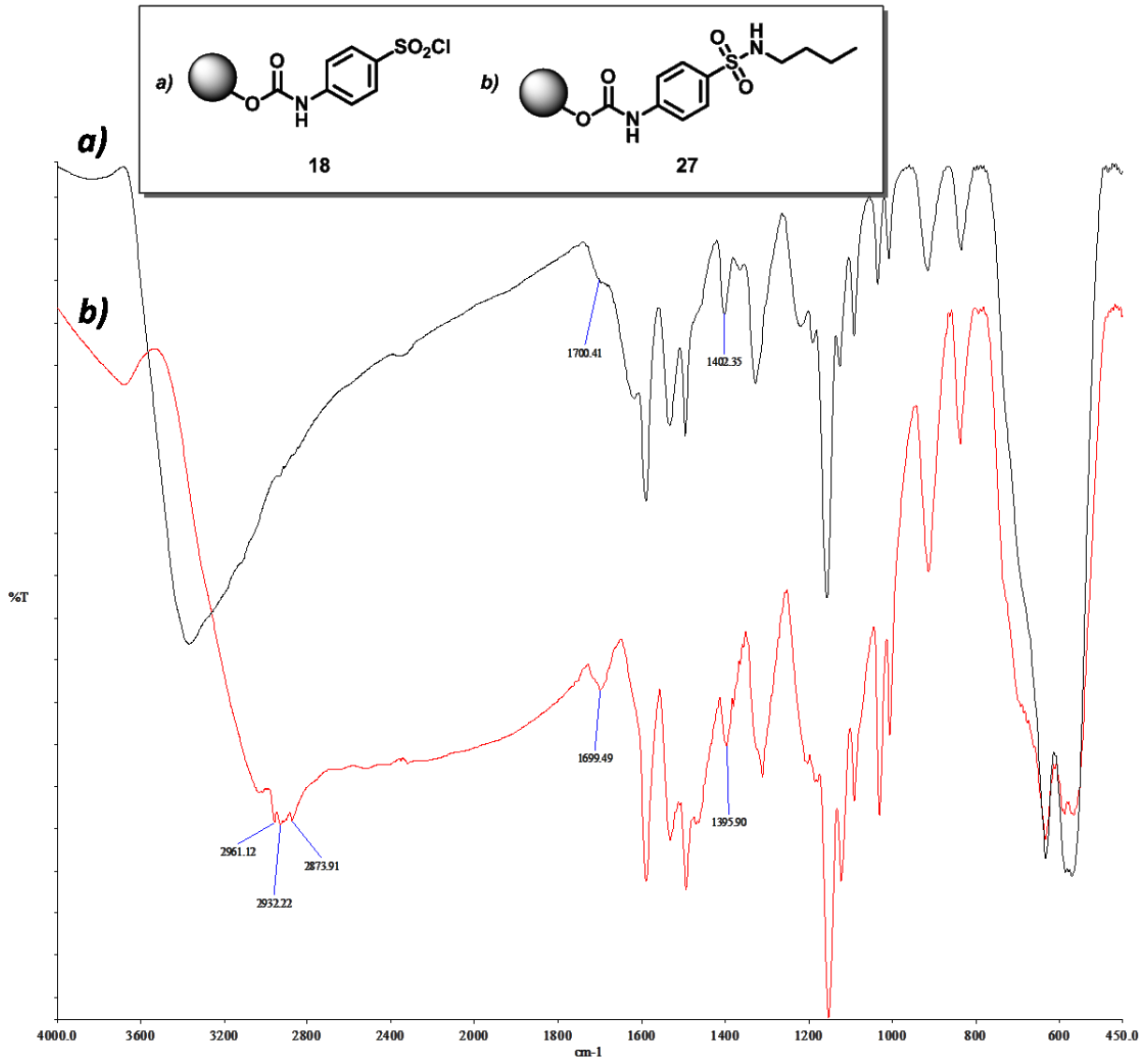

Figure 51 *- FTIR spectra of a) nanoconjugate* **18** *(black line) and b) nanoconjugate* **27** *(red line). In spectrum b) are clearly visible the stretchings at high wavenumber related to C-H bonds of the butyl chain. It's also clearly visible the C=O band of the carbamate and a significant modification in the vibrational bands in the range of 1600-1400 cm^{-1} referred to the presence of the sulfonamide bond and to the bending of N-H and C-H bonds.*

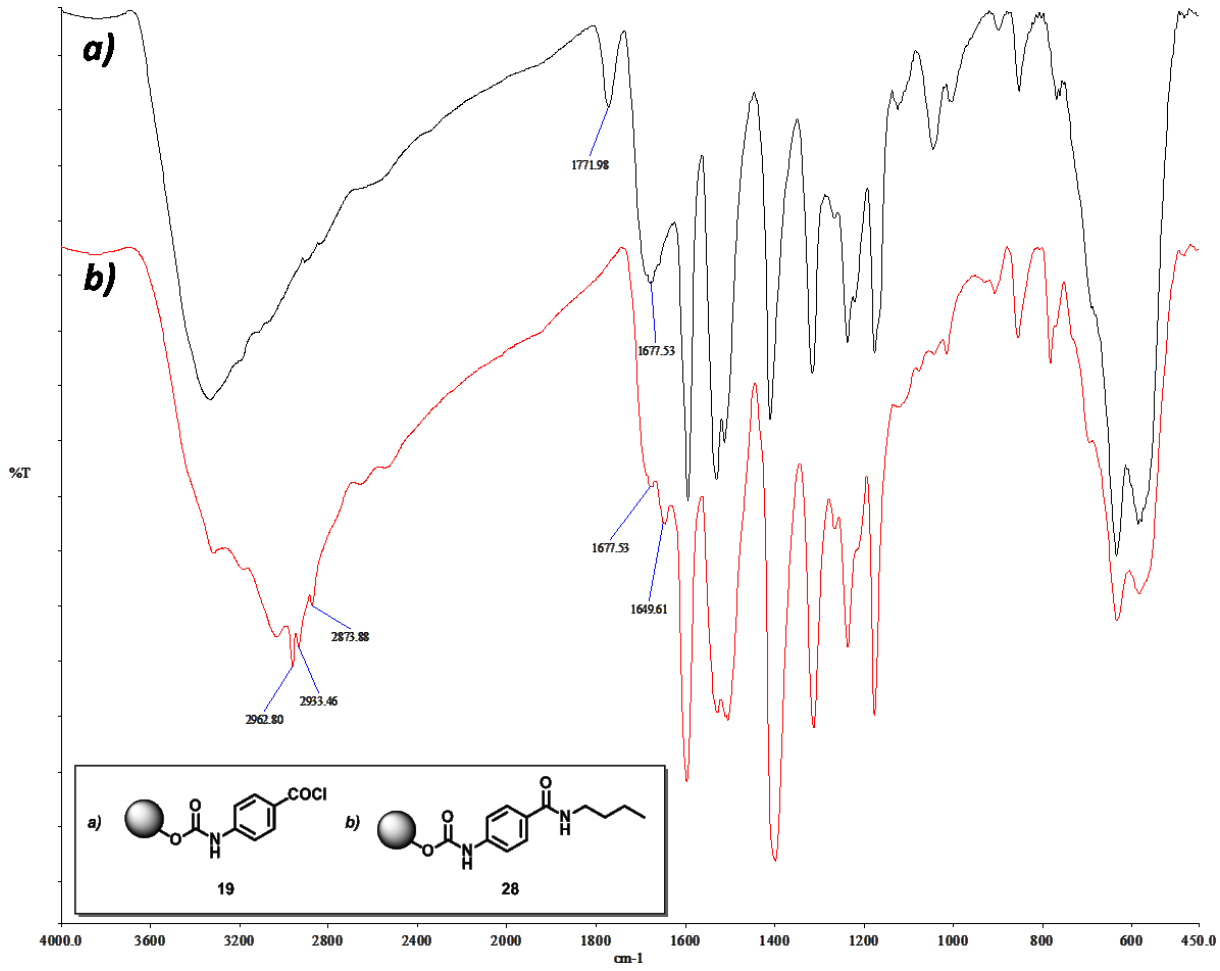

Figure 52 *- FTIR spectra of a) nanoconjugate* **19** *(black line) and b) nanoconjugate* **28** *(red line). In spectrum b) are clearly visible the stretchings at high wavenumber related to C-H bonds of the butyl chain. Are also clearly visible the C=O band of the carbamate (1677 cm^{-1}) and the stretching of the C=O amide moiety (1649 cm^{-1}), while the peak related to the Cl-C=O at 1772 cm^{-1} in spectrum a) disappeared in spectrum b).*

As reported in *section 4.2.1*, the loading of nanoconjugate **18** are quite lower with respect to other compounds due to the extreme lability of the starting isocyanate **8**. For this reason we decided to synthesized the *n*-butylsulfonamide nanoconjugate **27** exploiting an inverse synthetic strategy, reported in *Scheme 11*.

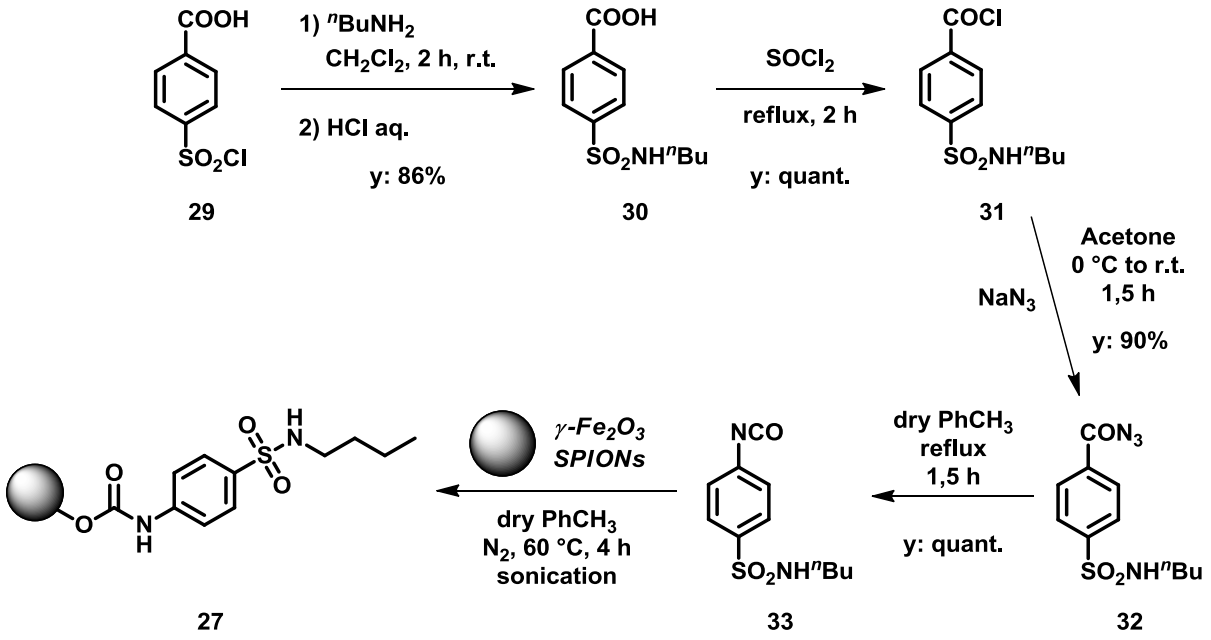

Scheme 11 *- Synthesis of nanoconjugate* **27** *exploiting an inverse synthetic strategy.*

Starting from the commercially available (*p*-chlorosulfonyl)benzoic acid **29**, the corresponding sulfonamide **30** was easily obtained in 86% yield by reaction with an excess of *n*-butylamine; the acyl chloride **31** was then obtained in quantitative yield by refluxing **30** in thionyl chloride. **31** was then reacts with sodium azide affording the acyl azide **32** in 90% yield after chromatographic purification. Eventually, **32** underwent the Curtius rearrangement leading to the corresponding isocyanate **33** in quantitative yield.
Then, 0.4 millimoles of **33** were reacted with 100 milligrams of naked SPIONs using the same synthetic protocol set up for the synthesis of carbamate nanoconjugates. E.A. and FTIR spectroscopy confirmed the formation of the desired product.

The loading obtained using this synthetic strategy can be compared with the previously obtained by the direct amidation on nanoparticle, as shown in *Figure 53*.

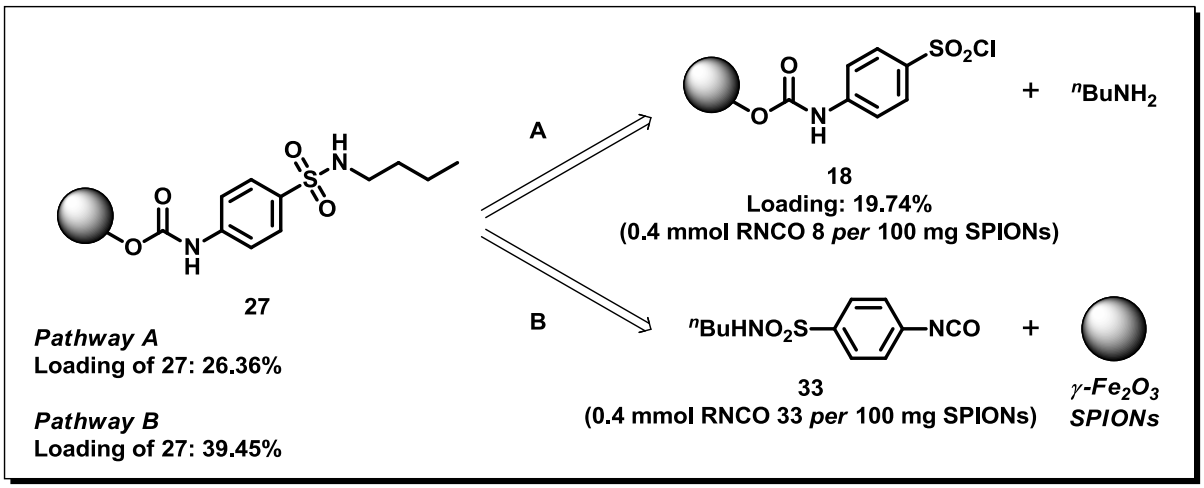

Figure 53 *- Synthetic strategies for the synthesis of nanoconjugate* **27***. Pathway A: direct amidation of nanoconjugate* **18***. Pathway B: direct grafting of functionalized isocyanate* **33** *onto SPIONs.*

The final loading of **27** in pathway A is strictly dependent from the loading of the starting nanoconjugate **18** (that is in turn dependant from the lability of the corresponding isocyanate **8**).

In the case of pathway B, the final loading of **27** is only dependant on the efficiency of the grafting methodology. Using 0.4 millimoles of isocyanate **33** per 100 milligrams of SPIONs, the loading is 39.45%, corresponding to 1.55 mmol/g_{NPs}, value that is perfectly in match with the average loading calculated for nanoconjugate **15**-**20** synthesized with the same reagents ratio and reaction conditions, equal to 1.67 mmol/g_{NPs} *[see Table 3, section 4.2.1]*.

So, we have proved the versatility and reproducibility of the isocyanate grafting methodology but also the versatility of the isocyanate-based heterobifunctional linkers, that can be chemically modified directly onto the SPIONs (pathway A) or before the anchoring (pathway B), exploiting classical organic reactions.

Concerning the nanoconjugate **20**, the maleimido group cannot interact itself with the nanoparticle surface, so it can be used without any problem as unreactive functional group during the grafting of the corresponding isocyanate **10**.

The maleimido moiety is widely used, especially in biological field, as reactive functional group for the anchoring on different substrates of a variable kind of molecules such as proteins, antibodies, fluorophores, drugs or specific markers.

Generally, these kind of compounds bear thiol groups (mercaptan chains, as well as cysteine residues) able to react with the maleimido moiety by a Michael addition, leading to the formation of a new C-S bond. Thus, the *PMPI* **10** can be exploited as heterobifunctional linker thanks to the presence of two functional groups with orthogonal reactivity (*Figure 54*).

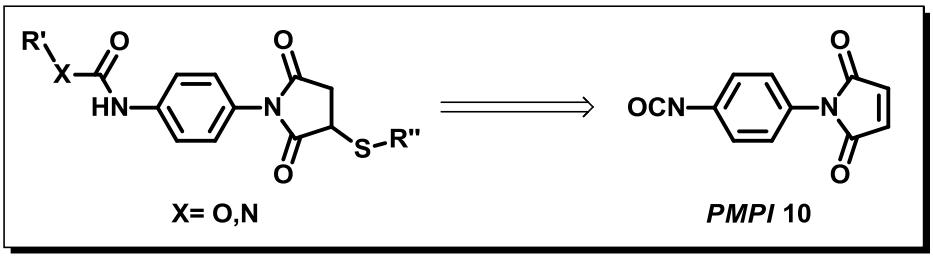

Figure 54 *- Use of PMPI* **10** *as heterobifunctional linker. The isocyanate group reacts with amines or alcohols leading to carbamates and ureas, while the maleimido moiety can react with thiols by Michael additions.*

So, the possibility to cover the SPIONs with maleimido residues, exploiting the selective reactivity of the isocyanate group towards the nanoparticle surface, have opened new way for the synthesis of a new class of conjugates between magnetic NPs and biomolecules.

To check the reactivity of the maleimido group once anchored onto SPIONs, nanoconjugate **20** was first reacted with the commercially available 1-dodecanthiol, (*Scheme 12*). We have chosen this molecule in order to obtain a high infrared response thanks to the presence of the long aliphatic chain, while the new C-S bond has no significant vibrational modes.

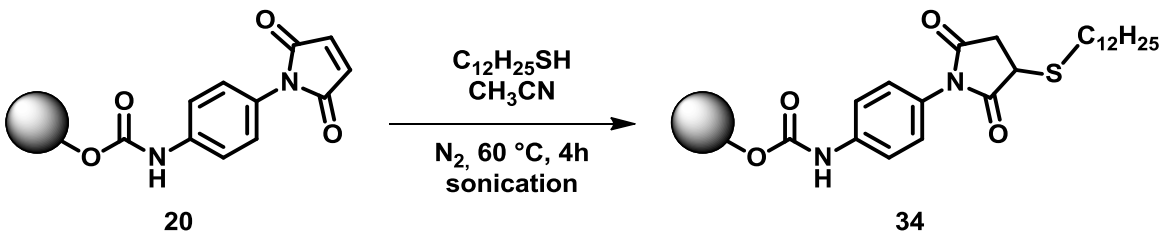

Scheme 12 *- Michael addition of 1-dodecanthiol on* **20***, affording the new nanoconjugate* **34***.*

FTIR spectroscopy confirms the formation of the Michael adduct **34**, as clearly visible in *Figure 55*.

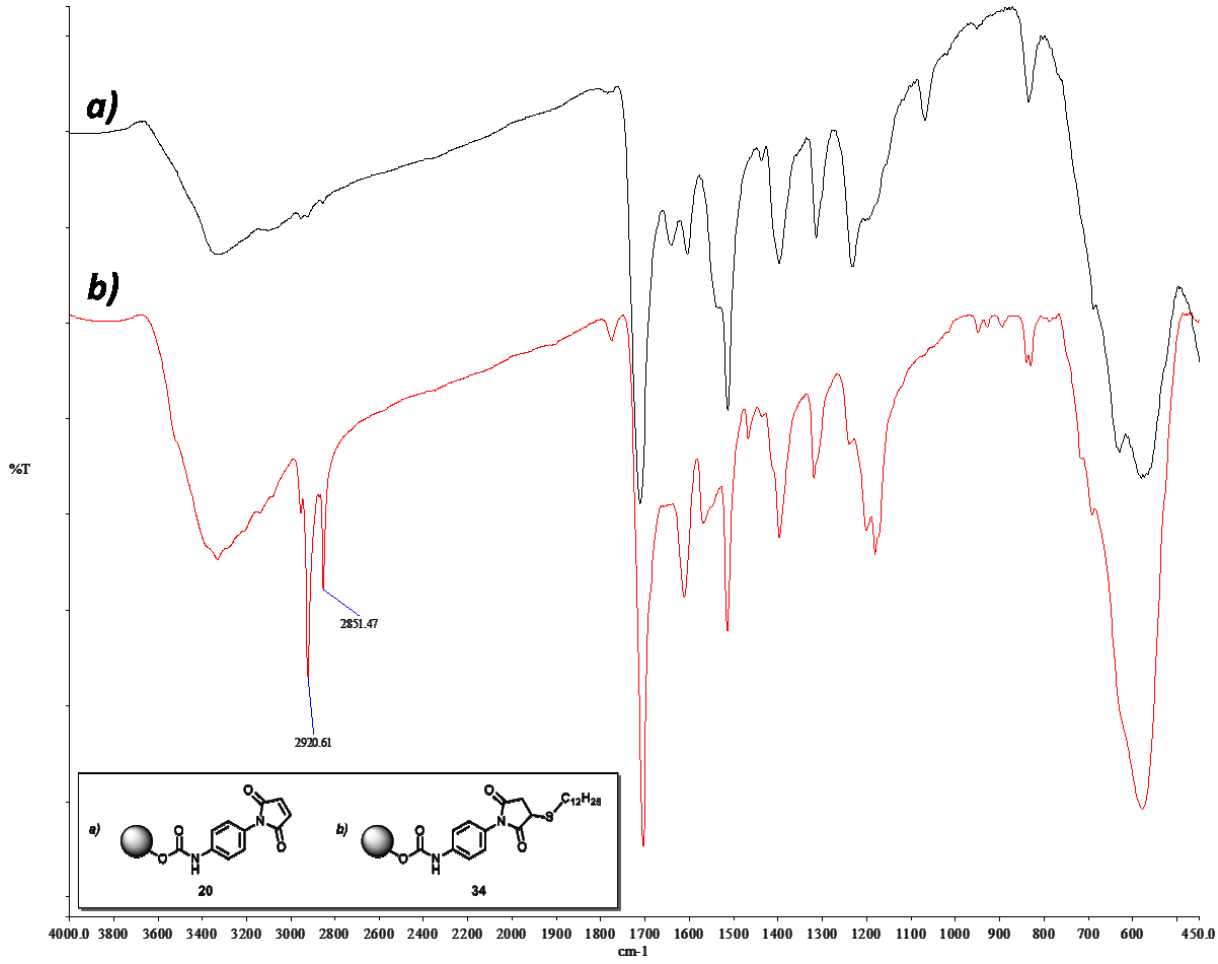

Figure 55 *- FTIR spectra of a) nanoconjugate* **20** *(black line) and b) nanoconjugate* **34** *(red line). In spectrum b) are clearly visible the stretching peaks at high wavenumber related to C-H bonds of the dodecyl chain. The peaks at about 1200 cm^{-1} also became more structured thanks to the presence of strong bending modes of C-H aliphatic bonds.*

Many biomolecules, such as peptides, nucleic acid mimics, proteins or antibodies, already bear thiol groups in their chemical structure. Otherwise, a cysteine residue can be easily introduced.

So, a second test reaction was performed on nanoconjugate **20** with *N*-acetyl-cysteine (*N*-Ac-Cys-OH) as Michael donor (*Scheme 13*).

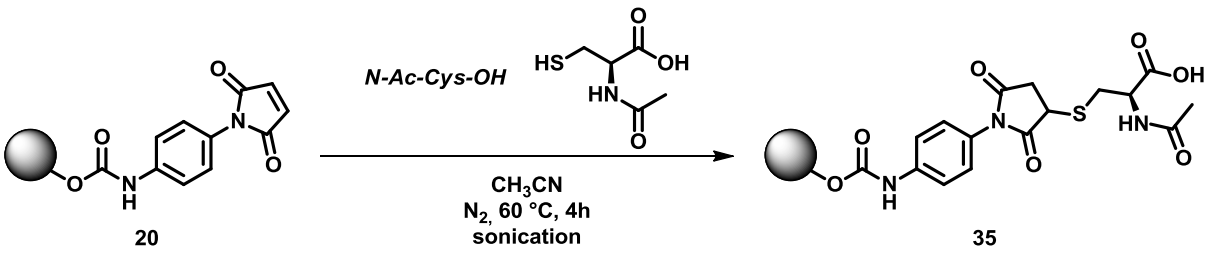

Scheme 13 *- Michael addition of N-Ac-Cys-OH on* **20***, affording the new nanoconjugate* **35**.

Functionalized nanoparticles were isolated and characterized, confirming the formation of the desired nanoconjugate **35**.

Given the results obtained, we can conclude that isocyanate-based heterobifunctional linkers can be easily used for the supporting of organic molecules onto SPIONs. Nanoconjugates **18**-**20** have so proved to be good candidates for this purpose.

4.5 Conclusions

In this chapter we have seen how the mechanism of both non-covalent and covalent interaction of organic molecules with SPIONs surface is the crucial factor in the synthesis of specifically designed nanoconjugates.

During this Ph.D. research work, a new covalent grafting methodology, not reported in the literature, has been developed, by exploiting the reactivity of isocyanates toward nanoparticles. A small library of new nanoconjugates were obtained starting from commercially or easily synthesizable isocyanates and deep characterization studies were performed.

By E.A. we were able to demonstrate how the final loading can be tuned in order to obtain a proper surface distribution of organic molecules. FTIR spectroscopy has clearly shown the formation of a carbamate species, that was further demonstrated by performing HR-MAS NMR experiments.

Having established the easy anchoring of isocyanates onto SPIONs, we compared this new methodology with the already well known grafting of organic molecules by formation of

carboxylate non-covalent adsorption and of classical covalent silylation reaction, demonstrating that it is possible to obtain higher loading using the carbamate bond formation.

Some of the nanoconjugates bear an additional functional group, opening the way for the use of isocyanate-based molecules as heterobifunctional linkers for the covalent binding of biomolecules onto SPIONs, as will be shown in *section 5.8*.

4.6 Experimental Section

4.6.1 Materials and Methods

All reagents and solvents were purchased in higher grade from commercial suppliers and used without further purification, unless otherwise stated. Dry solvents over molecular sieves and other solvents (P.A., ACS reagent) were obtained from Sigma Aldrich. Unless otherwise specified, all the reactions were performed in an inert atmosphere under dry conditions.

γ-Fe_2O_3 SPIONs were purchased from Alpha Aesar and stored away from moisture.

All weightings of reagents were carried out with analytical balance Mettler Toledo AB135-S/FACT.

TLC were run on Kieselgel 60 F254 plates (Fluka), while column chromatography were carried out using silica gel 60 (70-230 mesh, Merck). Automated flash chromatography were done using SPX instrument from Biotage® with pre-packed columns.

To dry the nanoparticles was used a rotating vacuum dryer from Büchi. Once dried, the nanoparticles are stored in a desiccator filled with anhydrous salts.

A sonicator Elma Elmasonic S 30H was used to perform reactions with nanoparticles.

Elemental Analysis were performed in the division of Inorganic, Metallorganic and Analytical Chemistry, from the Department of Chemistry in the University of Milan with a Perkin Elmer instrument.

Infrared spectra of nanoconjugates were acquired on a Spectrum One FTIR spectrophotometer (Perkin Elmer) in the range 4000-450 cm^{-1} in transmittance mode. 0.5 mg of nanoparticles were diluted in 150 mg FTIR grade KBr and ground in an agate mortar. KBr was previously dried at 125°C under vacuum. Then mixed powder was pressed at 9 tons for 3 min to obtain slim semitransparent tablet. Spectra were recorded selecting 64 scans and 4 cm^{-1} resolution. The background of pure KBr was separately recorded using the same conditions and automatically subtracted from sample spectra. Spectra of non-supported organic molecules were acquired in transmittance mode in the range 4000-600 cm^{-1} using NaCl windows as support and selecting 4 scans and 4 cm^{-1} resolution. These analysis were performed in collaboration with the Professor Stradi's reaserch group in the Laboratory of Instrumental Analysis of the division of Organic Chemistry "A. Marchesini", Department of Pharmaceutical Science in University of Milan.

^{1}H, ^{13}C and 2D NMR experiments were recorded on Bruker AMX300 and Bruker Fourier300 instruments (both with ^{1}H frequency: 300 MHz) , and the chemical shifts (δ) are reported in parts per million relative to solvent peak.

HR-MAS NMR experiments were acquired with a spectrometer located in the Big Instrument Center (C.I.G.A.), of University of Milan. The instrument is an FT-NMR *Avance*^{TM} *500* (*Bruker Italia S.r.l.*) with a superconducting ultrashield magnet of 11.7 Tesla (^{1}H frequency: 500.13 MHz). The probe is doubly tuned (^{1}H and ^{13}C), in addition to a 2H lock channel. All three channels are operating via a single NMR transmit/receive solenoid coil located inside the MAS turbine. The probe is capable of performing either direct or indirect (inverse) detection experiments. The probe allows to perform high resolution MAS experiments at spinning rates of up to 15 KHz, with 4 mm zirconia oxide rotors, for liquid or liquid-like samples; in our study the spinning rates were optimized between 4 KHz and 12 KHz speed values to rich a compromise between the needing to have the spinning side bands out of the ^{1}H spectrum, the best resolution behaviour and the minimum presence of turbulence or rotational artifacts. All the samples were diluted in deuterated methyl sulfoxide (few milligrams in 150-200 µl DMSO-d_6 100%); the saturated solutions (do to the low solubility of *γ-*Fe_2O_3 nanoconjugates) of nanoparticles dispersion, after different cycles of vortex/sonication,

were decanted by night leaving to precipitate the large aggregates and the upper suspension was then collected for NMR analysis. A dilution at different levels was sometimes necessary to find the concentration limit before the broadening of the NMR signals. The sample temperature it's speed rotation dependent and was so varying from 30 to 35 °C, in different experiments performed. The chemical shifts (δ) are reported in parts per million relative to solvent peak.

Acquisition parameters of standard ^{1}H zg NMR sequence were: 90° pulse ^{1}H of 9.0 µs, spectral width: sw = 6 KHz (corresponding to 11 ppm), acquisition size: td = 16K, acquisition time: aq = 1.3 s, relaxation delay: d1 = 10 s and a number of scans: ns = 24.

Acquisition parameters of ^{13}C *inverse gated* (^{1}H all decoupled) NMR sequence were: 90° pulse ^{13}C of 9.75 µs, spectral width: sw = 25 KHz (corresponding to 200 ppm), acquisition size: td = 16K, acquisition time: aq = 0.32 s, relaxation delay: d1 = 4 s and a number of scans: ns = 10700.

4.6.2 Experimental Procedures

4.6.2.1 Synthesis of NP-APTES **2**

3-Aminopropyl-triethoxysilane (APTES) **1** (0.2, 0.4 or 0.8 mmol) was added to a suspension of naked SPIONs (100 mg) in dry $PhCH_3$ (5 ml), previously sonicated at 60 °C for 30'; the mixture was stirred, under sonication, at 60 °C for 4 h. After this time the obtained suspension was centrifugated at 5000 r/min for 10' and the supernatant was removed. The solid residue was first washed with fresh $PhCH_3$ (3x5 ml), then with Et_2O (2x5 ml) and vortex/sonication/centrifugation were cyclic repeated for each washing. Functionalized NPs were dried on air for a night and then in a rotating vacuum drier for a day, to afford **2** as a brown powder. Positive Kaiser test confirm the presence of free amino groups on the nanoparticle surface. ***Loadings from E.A.:*** 5.27% (equal to 0.39 mmol/g_{NPs}) [0.2 mmol of **1**/100mg_{NPs}]; 7.59% (equal to 0.56 mmol/g_{NPs}) [0.4 mmol of **1**/100mg_{NPs}]; 13.02% (equal to 0.97 mmol/g_{NPs}) [0.8 mmol of **1**/100mg_{NPs}]. ***^{1}H HR-MAS NMR (D_2O presat, 4 KHz, 500 MHz):*** δ= 0.55-0.61 (m, 2H, CH_2-Si), 1.64-1.70 (m, 2H, CH_2), 2.86-2.96 (m, 2H, CH_2-N). ***FTIR (cm^{-1}) in trasmittance (blank KBr):*** 3390 (υ, N-H), 2930 (υ, C-H), 1550 (δ, N-H), 1490, 1002 (υ, Si-O), 580 (υ, Fe-O).

4.6.2.2 Synthesis of NP-TESPI **4**

3-(Triethoxysylil)propyl isocyanate (TESPI) **3** (0.8 mmol) was added to a suspension of naked SPIONs (100 mg) in dry $PhCH_3$ (5 ml), previously sonicated at 60 °C for 30'; the mixture was stirred, under sonication, at 60 °C for 4 h. After this time the obtained suspension was centrifugated at 5000 r/min for 10' and the supernatant was removed. The solid residue was first washed with fresh $PhCH_3$ (3x5 ml), then with Et_2O (2x5 ml) and vortex/sonication/centrifugation were cyclic repeated for each washing. Functionalized NPs were dried on air for a night and then in a rotating vacuum drier for a day, to afford **4** as a brown powder. ***Loadings from E.A.:*** 32.80% (equal to 1.32 mmol/g_{NPs}). ***FTIR (cm^{-1}) in trasmittance (blank KBr):*** 3335 (υ, N-H), 2974-2885 (υ, C-H), 1634 (υ, C=O carbamate), 1566 (δ, N-H), 1443, 1274, 1103, 1078 (υ, Si-O), 1032, 955.

4.6.2.3 Synthesis of (p-Maleimido)benzoic Acid, PMBA **12**

Commercially available *p*-aminobenzoic acid, PABA **11** (4.26 g, 31 mmol, 1 eq) was suspended in 30 ml of acetone and solubilized by the addition of 5 ml of methanol. A solution of maleic anhydride (3.66 g, 37 mmol, 1.2 eq) in 10 ml of acetone was added dropwise and the resulting precipitate stirred for 20'. The material was suction filtered, washed with acetone, and vacuum-dried to afford a yellow powder (6.36 g). This material was dissolved in acetic anhydride (13 ml), treated with sodium acetate (1.08 g), and then heated with stirring at 50 °C for 2 h. The volatiles were then removed in vacuo, and the resulting residue was taken up in 150 ml of water and heated at 70 °C for 2.5 h. The resulting white precipitate was suction filtered, washed with water, and vacuum-dried overnight to afford compound **12** (4.7 g, 70%). Analysis by silica TLC (10% MeOH in DCM as eluent, visualized by UV absorption and/or iodine vapor staining) showed one spot at *Rf* 0.8. It was used without further purification. ***^{1}H-NMR ($CDCl_3$ + DMSO-d6, 300 MHz):*** δ= 10.0-8.5 (br s, 1H, CO_2H), 7.95 (d, J = 9 Hz, 2H, Ar-H ortho to maleimide), 7.32 (d, J = 9 Hz, 2H, Ar-H ortho to carboxylic acid), 6.8 (s, 2H, maleimide vinyl). ***MS (FAB, 3-nitrobenzyl alcohol):*** m/z 218 (M^+ + 1).

4.6.2.4 Synthesis of (p-Maleimido)benzoyl Chloride, PMB-Cl **14**

p-Maleimidobenzoic acid, PMBA **12** (500 mg, 2.30 mmol) was suspended in 2 ml of DCM and then 10 ml of thionyl chloride were added, leading to a yellowish solution. After refluxing for 2 h, the solution was vacuum-dried to afford a yellow powder, corresponding to desired product **14** (540 mg, quantitative yield). It was used without further purification. ***^{1}H-NMR (DMSO-d6, 300 MHz):*** δ= 8.05 (d, J = 8.7 Hz, 2H, Ar-H ortho to maleimide), 7.51 (d, J = 8.7 Hz, 2H, Ar-H ortho to acyl chloride), 7.22 (s, 2H, maleimide vinyl).

4.6.2.5 Synthesis of (p-Maleimido)benzoyl Azide, PMB-azide **13***, starting from* **12**

A stirred suspension of compound **12** (4.3 g, 20 mmol, 1 eq) in 150 ml of dry toluene was treated with triethylamine (3.04 ml, 22 mmol, 1.1 eq) and then DPPA (4.7 ml, 22 mmol, 1.1 eq). After stirring at room temperature for 2 days, the volatiles were removed in vacuo, and the resulting residue was chromatographed on silica with DCM as eluent. The product **13**, elutes as a pale yellow band and is isolated upon evaporation of solvent to afford a pale yellow crystalline mass (2.14 g, 50%). A recrystallized sample from DCM showed the following behavior in a melting point apparatus: 115-120 °C, sample appears to "pop"; 125-130 °C decomposition with vigorous gas evolution. Analysis by silica TLC (DCM as eluent, visualized by UV absorption and/or iodine vapor staining) showed one spot at *Rf* 0.45. ***^{1}H NMR (CDCl$_3$, 300 MHz):*** δ= 8.0 (d, J = 8 Hz, 2H, ArCH ortho to maleimide), 7.45 (d, J = 8 Hz, 2H, ArCH ortho to acyl azide), 6.75 (s, 2H, maleimide vinyl). ***FTIR (cm^{-1}) in trasmittance (blank KBr):*** 3110, 2160 (υ C=O acyl azide), 1720, 1690, 1600, 1510, 1400, 1380, 1310, 1275, 1210, 1180, 1150, 1120, 1070, 1040, 1010, 850, 830, 690. ***MS (FAB, 3-nitrobenzyl alcohol):*** m/z 215 (M^+ + 1).

4.6.2.6 Synthesis of (p-Maleimido)benzoyl Azide, PMB-azide **13***, starting from* **14**

To a stirred suspension of compound **14** (500 mg, 2.12 mmol, 1 eq) in 5 ml of acetone at 0 °C were added 3 ml of DCM, in order to obtain a yellowish solution. Solid NaN_3 (689 mg, 10.60 mmol, 5 eq) was added in three portions. The suspension was stirred at 0 °C and then raised to room temperature. After stirring at r.t. for 4 h, the volatiles were removed in vacuo, and the resulting residue was chromatographed by automated flash chromatography on pre-packed silica column with DCM as eluent. The product **13**, elutes as a pale yellow band and is isolated upon evaporation of solvent to afford a pale yellow crystalline mass (359 mg, 70%). The product was characterized, confirming the data reported in *procedure 4.6.2.5*.

4.6.2.7 Synthesis of (p-Maleimido)phenyl Isocyante, PMPI **10**

A solution of compound **13** (300 mg, 1.24 mmol) in dry toluene (10 ml) is refluxed under nitrogen for 1.5 h and then evaporated in vacuo. This quantitatively affords compound **10** as yellow micro needles (265 mg). ***Mp:*** 121-123 °C. This compound should be stored in a sealed vial, protected from light and moisture, in a freezer. ***^{1}H-NMR (CDCl$_3$, 300 MHz):*** δ= 7.2 (d, J =

9 Hz, 2H, ArCH ortho to maleimide), 7.02 (d, J = 9 Hz, 2H, ArCH ortho to isocyanate), 6.7 (s, 2H, maleimide vinyl). ***FTIR (cm^{-1}) in trasmittance (blank KBr):*** 3380, 3360, 3120, 3080, 2306 (υ, C=O isocyanate), 1720, 1690 shoulder, 1520, 1390, 1150, 830, 690.

4.6.2.8 Synthesis of NP-Cyclohexyl Carbamate 15

Cyclohexyl isocyanate **5** (0.2, 0.4 or 0.8 mmol) was added to a suspension of naked SPIONs (100 mg) in dry $PhCH_3$ (5 ml), previously sonicated at 60 °C for 30'; the mixture was stirred, under sonication, at 60 °C for 4 h. After this time the obtained suspension was centrifugated at 5000 r/min for 10' and the supernatant was removed. The solid residue was first washed with fresh $PhCH_3$ (3x5 ml), then with Et_2O (2x5 ml) and vortex/sonication/centrifugation were cyclic repeated for each washing. Functionalized NPs were dried on air for a night and then in a rotating vacuum drier for a day, to afford **15** as a brown powder. ***Loadings from E.A.:*** 13.83% (equal to 1.10 mmol/g_{NPs}) [0.2 mmol of **5**/100mg_{NPs}]; 26.69% (equal to 2.11 mmol/g_{NPs}) [0.4 mmol of **5**/100mg_{NPs}]; 51.47% (equal to 4.08 mmol/g_{NPs}) [0.8 mmol of **5**/100mg_{NPs}]. ***^{1}H HR-MAS NMR (DMSO-d6, 4 KHz, 500 MHz):*** δ= 5.57 (d, J = 5, 1H, NH carbamate), 3.33 (signal covered by water, assigned by 2D experiments, 1H, CH-N), 1.74-0.93 (m, 10H, CH_2). ***^{13}C all decoupled HR-MAS NMR (DMSO-d6, 4 KHz, 125 MHz):*** δ= 157.08 (C=O carbamate), 47.97 (CH), 36.71 (CH_2), 33.81 (CH_2), 25.79 (CH_2), 25.10 (CH_2), 24.92 (CH_2). ***FTIR (cm^{-1}) in trasmittance (blank KBr):*** 3326 (υ, N-H), 2928, 2850 (υ, C-H), 1626 (υ, C=O carbamate), 1573 (δ, N-H), 1311, 1243 (υ, C-O and C-N), 1088 (δ, C-H), 640-562 (υ, Fe-O).

4.6.2.9 Synthesis of NP-Phenyl Carbamate 16

Phenyl isocyanate **6** (0.2, 0.4 or 0.8 mmol) was added to a suspension of naked SPIONs (100 mg) in dry $PhCH_3$ (5 ml), previously sonicated at 60 °C for 30'; the mixture was stirred, under sonication, at 60 °C for 4 h. After this time the obtained suspension was centrifugated at 5000 r/min for 10' and the supernatant was removed. The solid residue was first washed with fresh $PhCH_3$ (3x5 ml), then with Et_2O (2x5 ml) and vortex/sonication/centrifugation were cyclic repeated for each washing. Functionalized NPs were dried on air for a night and then in a rotating vacuum drier for a day, to afford **16** as a brown powder. ***Loadings from E.A.:*** 15.36% (equal to 1.28 mmol/g_{NPs}) [0.2 mmol of **6**/100mg_{NPs}]; 26.55% (equal to 2.21 mmol/g_{NPs}) [0.4 mmol of **6**/100mg_{NPs}]; 43.80% (equal to 3.65 mmol/g_{NPs}) [0.8 mmol of **6**/100mg_{NPs}]. ***^{1}H HR-MAS NMR (DMSO-d6, 6 KHz, 500 MHz):*** δ= 8.64 (s, 1H, NH carbamate), 7.46 (d, J = 10, 2H, ArCH ortho to carbamate), 7.29 (m, J_A = 5, J_B = 10, 2H, ArCH meta to carbamate), 6.97 (m, J_A = 5, J_B = 10, 1H, ArCH para to carbamate). ***^{13}C all decoupled HR-MAS NMR (DMSO-d6, 6 KHz, 125 MHz):*** δ= 153.01 (C=O carbamate), 140.17 (ArCH-N), 129.25

(ArCH ortho to carbamate), 122.28 (ArCH para to carbamate), 118.67 (ArCH meta to carbamate). ***FTIR (cm^{-1}) in trasmittance (blank KBr):*** 3326 (υ, N-H), 3282, 3192 (υ, ArC-H), 1647 (υ, C=O carbamate), 1594, 1551 (δ, N-H), 1497, 1447, 1439 (υ, C=C), 1314, 1231 (υ, C-O and C-N), 753, 696 (δ, C-H out of plane), 640-560 (υ, Fe-O).

4.6.2.10 Synthesis of NP-(p-Chloro)phenyl Carbamate **17**

(*p*-Chloro)phenyl isocyanate **7** (0.2, 0.4 or 0.8 mmol) was added to a suspension of naked SPIONs (100 mg) in dry $PhCH_3$ (5 ml), previously sonicated at 60 °C for 30'; the mixture was stirred, under sonication, at 60 °C for 4 h. After this time the obtained suspension was centrifugated at 5000 r/min for 10' and the supernatant was removed. The solid residue was first washed with fresh $PhCH_3$ (3x5 ml), then with Et_2O (2x5 ml) and vortex/sonication/centrifugation were cyclic repeated for each washing. Functionalized NPs were dried on air for a night and then in a rotating vacuum drier for a day, to afford **17** as a brown powder. ***Loadings from E.A.:*** 16.62% (equal to 1.08 mmol/g_{NPs}) [0.2 mmol of **7**/100mg_{NPs}]; 29.83% (equal to 1.93 mmol/g_{NPs}) [0.4 mmol of **7**/100mg_{NPs}]; 40.33% (equal to 2.61 mmol/g_{NPs}) [0.8 mmol of **7**/100mg_{NPs}]. ***^{1}H HR-MAS NMR (DMSO-d6, 6 KHz, 500 MHz):*** δ= 8.83 (s, 1H, NH carbamate), 7.48 (d, J = 10, 2H, ArCH meta to carbamate), 7.33 (d, J = 10, 2H, ArCH ortho to carbamate). ***^{13}C all decoupled HR-MAS NMR (DMSO-d6, 6 KHz, 125 MHz):*** δ= 152.81 (C=O carbamate), 139.01 (ArCH-N), 129.09 (ArCH meta to carbamate), 125.98 (ArCH-Cl), 120.32 (ArCH ortho to carbamate). ***FTIR (cm^{-1}) in trasmittance (blank KBr):*** 3294 (υ, N-H), 1632 (υ, C=O carbamate), 1590, 1559 (δ, N-H), 1491, 1439 (υ, C=C), 1395, 1298, 1236 (υ, C-O and C-N), 1085, 1012 (υ, ArCH-Cl), 823 (δ, C-H out of plane), 637-561 (υ, Fe-O).

4.6.2.11 Synthesis of NP-(p-Chlorosulfonyl)phenyl Carbamate **18**

(*p*-Chlorosulfonyl)phenyl isocyanate **8** (0.2, 0.4 or 0.8 mmol) was added to a suspension of naked SPIONs (100 mg) in dry $PhCH_3$ (5 ml), previously sonicated at 60 °C for 30'; the mixture was stirred, under sonication, at 60 °C for 4 h. After this time the obtained suspension was centrifugated at 5000 r/min for 10' and the supernatant was removed. The solid residue was first washed with fresh $PhCH_3$ (3x5 ml), then with Et_2O (2x5 ml) and vortex/sonication/centrifugation were cyclic repeated for each washing. Functionalized NPs were dried on air for a night and then in a rotating vacuum drier for a day, to afford **18** as a brown powder. ***Beilstein test:*** positive (bright green flame). ***Loadings from E.A.:*** 17.54% (equal to 0.80 mmol/g_{NPs}) [0.2 mmol of **8**/100mg_{NPs}]; 19.74% (equal to 0.90 mmol/g_{NPs}) [0.4 mmol of **8**/100mg_{NPs}]; 21.75% (equal to 0.99 mmol/g_{NPs}) [0.8 mmol of **8**/100mg_{NPs}]. ***FTIR (cm^{-1}) in trasmittance (blank KBr):*** 3294 (υ, N-H), 1699 (υ, C=O carbamate), 1589, 1533 (δ, N-H), 1495, 1402 (υ, C=C), 1328 (asym υ, SO_2), 1156 (sym υ, SO_2), 633-556 (υ, Fe-O).

4.6.2.12 Synthesis of NP-(p-Chloroacyl)phenyl Carbamate **19**

(*p*-Isocyanate)benzoyl chloride **9** (0.2, 0.4 or 0.8 mmol) was added to a suspension of naked SPIONs (100 mg) in dry $PhCH_3$ (5 ml), previously sonicated at 60 °C for 30'; the mixture was stirred, under sonication, at 60 °C for 4 h. After this time the obtained suspension was centrifugated at 5000 r/min for 10' and the supernatant was removed. The solid residue was first washed with fresh $PhCH_3$ (3x5 ml), then with Et_2O (2x5 ml) and vortex/sonication/centrifugation were cyclic repeated for each washing. Functionalized NPs were dried on air for a night and then in a rotating vacuum drier for a day, to afford **19** as a brown powder. ***Beilstein test:*** positive (bright green flame). ***Loadings from E.A.:*** 22.17% (equal to 1.21 mmol/g_{NPs}) [0.2 mmol of **9**/100mg_{NPs}]; 25.74% (equal to 1.41 mmol/g_{NPs}) [0.4 mmol of **9**/100mg_{NPs}]; 35.01% (equal to 1.92 mmol/g_{NPs}) [0.8 mmol of **9**/100mg_{NPs}]. ***FTIR (cm^{-1}) in trasmittance (blank KBr):*** 3297 (υ, N-H), 1772 (υ, C=O acyl chloride), 1681 (υ, C=O carbamate), 1593, 1531, 1512 (δ, N-H), 1410 (υ, C=C), 1316, 1237 (υ, C-O and C-N), 1176 (δ, C-H), 634-579 (υ, Fe-O).

4.6.2.13 Synthesis of NP-(p-Maleimido)phenyl Carbamate **20**

(*p*-Maleimido)phenyl isocyanate PMPI **10** (0.2, 0.4 or 0.8 mmol) was added to a suspension of naked SPIONs (100 mg) in dry $PhCH_3$ (5 ml), previously sonicated at 60 °C for 30'; the mixture was stirred, under sonication, at 60 °C for 4 h. After this time the obtained suspension was centrifugated at 5000 r/min for 10' and the supernatant was removed. The solid residue was first washed with fresh $PhCH_3$ (3x5 ml), then with Et_2O (2x5 ml) and vortex/sonication/centrifugation were cyclic repeated for each washing. Functionalized NPs were dried on air for a night and then in a rotating vacuum drier for a day, to afford **20** as a brown powder. ***Loadings from E.A.:*** 14.42% (equal to 0.67 mmol/g_{NPs}) [0.2 mmol of **10**/100mg_{NPs}]; 31.07% (equal to 1.44 mmol/g_{NPs}) [0.4 mmol of **10**/100mg_{NPs}]; 51.81% (equal to 2.41 mmol/g_{NPs}) [0.8 mmol of **10**/100mg_{NPs}]. ***^{1}H HR-MAS NMR (DMSO-d6, 12 KHz, 500 MHz):*** δ= 8.94 (s, 1H, NH carbamate), 7.63 (d, J = 10, 2H, ArCH ortho to carbamate), 7.31 (d, J = 10, 2H, ArCH meta to carbamate), 7.21 (s, 2H, maleimide vinyl). ***^{1}H HR-MAS DOSY NMR (DMSO-d6, 12 KHz, 500 MHz):*** D ≈ 7.0e-9 m^2/s. ***FTIR (cm^{-1}) in trasmittance (blank KBr):*** 3383 (υ, N-H), 3096 (υ, ArC-H), 1707 (υ, C=O imide), 1692 (υ, C=O carbamate), 1605, 1552 (δ, N-H), 1513 (υ, C=C), 1398 (υ, Ar-N), 1313 (υ, C-N imide), 1239-1175 (υ, C-O and C-N), 831 (δ, C-H), 689-559 (υ, Fe-O).

4.6.2.14 Synthesis of N,N'-bis(p-Maleimidophenyl)urea **21**

A stirred room temperature solution of PMPI **10** (100 mg, 0.47 mmol) in DMSO (2 ml) was treated dropwise with 100 µl of water. After 5 min, excess water was added (10 ml) to precipitate the product, which was isolated by suction filtration. After vacuum-drying, compound **21** was obtained as a white powder (175 mg, 93% yield). ***^{1}H HR-MAS NMR (DMSO-d6, 12 KHz, 500 MHz):*** δ= 8.92 (s, 1H, NH carbamate), 7.58 (d, J = 10, 2H, ArCH ortho to carbamate), 7.25 (d, J = 10, 2H, ArCH meta to carbamate), 7.18 (s, 2H, maleimide vinyl). ***^{1}H HR-MAS DOSY NMR (DMSO-d6, 12 KHz, 500 MHz):*** D ≈ 4.0e-9 m^2/s. ***MS (EI):*** m/z 402 (M^+).

4.6.2.15 Synthesis of NP-Phenyl Carboxylate **23**

Benzoic acid **22** (0.2, 0.4 or 0.8 mmol) was added to a suspension of naked SPIONs (100 mg) in dry $PhCH_3$ (5 ml), previously sonicated at 60 °C for 30'; the mixture was stirred, under sonication, at 60 °C for 4 h. After this time the obtained suspension was centrifugated at 5000 r/min for 10' and the supernatant was removed. The solid residue was first washed with fresh $PhCH_3$ (3x5 ml), then with Et_2O (2x5 ml) and vortex/sonication/centrifugation were cyclic repeated for each washing. Functionalized NPs were dried on air for a night and then in a rotating vacuum drier for a day, to afford **23** as a brown powder. ***Loadings from E.A.:*** 6.96% (equal to 0.58 mmol/g_{NPs}) [0.2 mmol of **22**/100mg_{NPs}]; 7.64% (equal to 0.63 mmol/g_{NPs}) [0.4 mmol of **22**/100mg_{NPs}]; 8.22% (equal to 0.68 mmol/g_{NPs}) [0.8 mmol of **22**/100mg_{NPs}]. ***FTIR (cm^{-1}) in trasmittance (blank KBr):*** 3369 (υ, FeO-H), 3058-2929 (υ, ArC-H), 1599 (υ, CO_2^-), 1524,1447, 1404 (υ, C=C), 1176, 1025, 634-564 (υ, Fe-O).

4.6.2.16 Synthesis of NP-(p-Maleimido)phenyl Carboxylate **24**

(*p*-Maleimido)benzoic acid PMBA **12** (0.2, 0.4 or 0.8 mmol) was added to a suspension of naked SPIONs (100 mg) in dry $PhCH_3$ (5 ml), previously sonicated at 60 °C for 30'; the mixture was stirred, under sonication, at 60 °C for 4 h. After this time the obtained suspension was centrifugated at 5000 r/min for 10' and the supernatant was removed. The solid residue was first washed with fresh $PhCH_3$ (3x5 ml), then with Et_2O (2x5 ml) and vortex/sonication/centrifugation were cyclic repeated for each washing. Functionalized NPs were dried on air for a night and then in a rotating vacuum drier for a day, to afford **24** as a brown powder. ***Loadings from E.A.:*** 12.63% (equal to 0.58 mmol/g_{NPs}) [0.2 mmol of **12**/100mg_{NPs}]; 13.11% (equal to 0.61 mmol/g_{NPs}) [0.4 mmol of **12**/100mg_{NPs}]; 14.52% (equal to 0.67 mmol/g_{NPs}) [0.8 mmol of **12**/100mg_{NPs}]. ***FTIR (cm^{-1}) in trasmittance (blank KBr):*** 3326 (υ, FeO-H), 3075 (υ, ArC-H), 1709 (strong υ, C=O imide), 1604 (strong υ, CO_2^-), 1515 (υ, C=C),

139o (υ, Ar-N), 1319-1298 (υ, C-N imide), 1178 (υ, C-O and C-N), 828 (δ, C-H), 634-583 (υ, Fe-O).

4.6.2.17 Blank Reaction between SPIONs and Tosyl Chloride 25

Tosyl chloride **25** (153 mg, 0.8 mmol) was added to a suspension of naked SPIONs (100 mg) in dry $PhCH_3$ (5 ml), previously sonicated at 60 °C for 30'; the mixture was stirred, under sonication, at 60 °C for 4 h. After this time the obtained suspension was centrifugated at 5000 r/min for 10' and the supernatant was removed. The solid residue was first washed with fresh $PhCH_3$ (3x5 ml), then with Et_2O (2x5 ml) and vortex/sonication/centrifugation were cyclic repeated for each washing. Functionalized NPs were dried on air for a night and then in a rotating vacuum drier for a day. The recovered nanoparticles (brown powder) were analyzed by E.A. and FTIR spectroscopy. ***Loadings from E.A.:*** lower than 4%, no match with any chemical formula. ***FTIR (cm^{-1}) in trasmittance (blank KBr):*** 3390 (strong and broad υ, FeO-H), 1626 (residual absorption of CO_2 and water), 1187-1126 (weak sym υ, SO_2), 633-568 (strong υ, Fe-O).

4.6.2.18 Blank Reaction between SPIONs and Benzoyl Chloride 26

Benzoyl chloride **26** (92 µl, 0.8 mmol) was added to a suspension of naked SPIONs (100 mg) in dry $PhCH_3$ (5 ml), previously sonicated at 60 °C for 30'; the mixture was stirred, under sonication, at 60 °C for 4 h. After this time the obtained suspension was centrifugated at 5000 r/min for 10' and the supernatant was removed. The solid residue was first washed with fresh $PhCH_3$ (3x5 ml), then with Et_2O (2x5 ml) and vortex/sonication/centrifugation were cyclic repeated for each washing. Functionalized NPs were dried on air for a night and then in a rotating vacuum drier for a day. The recovered nanoparticles (brown powder) were analyzed by E.A. and FTIR spectroscopy. ***Loadings from E.A.:*** lower than 4%, no match with any chemical formula. ***FTIR (cm^{-1}) in trasmittance (blank KBr):*** 3390 (strong and broad υ, FeO-H), 1599 (υ, COO^- from hydrolysis of acyl chloride), 1412 (weak υ, C=C), 633-568 (strong υ, Fe-O).

4.6.2.19 Blank Reaction between SPIONs and Benzoyl Chloride 26*, in Presence of Water: Synthesis of NP-Phenyl Carboxylate* 23

Benzoyl chloride **26** (92 µl, 0.8 mmol, 1 eq) was added to a suspension of naked SPIONs (100 mg) in $PhCH_3$ (5 ml), previously sonicated at 60 °C for 30'. Water (29 µl, 1.6 mmol, 2 eq) was added dropwise to the mixture under sonication. After 4 h at 60 °C, the obtained suspension

was centrifugated at 5000 r/min for 10' and the supernatant was removed. The solid residue was first washed with fresh $PhCH_3$ (3x5 ml), then with Et_2O (2x5 ml) and vortex/sonication/centrifugation were cyclic repeated for each washing. Functionalized NPs were dried on air for a night and then in a rotating vacuum drier for a day. The recovered nanoparticles (brown powder) were analyzed by E.A. and FTIR spectroscopy, confirming the formation of nanoconjugate **23**. ***Loadings from E.A.:*** 7.93% (equal to 0.66 mmol/g_{NPs}). ***FTIR (cm^{-1}) in trasmittance (blank KBr):*** 3369 (υ, FeO-H), 3058-2929 (υ, ArC-H), 1599 (υ, CO_2^-), 1524,1447, 1404 (υ, C=C), 1176, 1025, 634-564 (υ, Fe-O).

4.6.2.20 Synthesis of NP-[p-(N-butylsulfamoyl)phenyl] Carbamate 27

n-Butylamine (45 µl, 0.45 mmol, 5 eq) was added to a suspension of functionalized nanoparticles **18** (100 mg, loading 19.74% equal to 0.90 mmol/g_{NPs}, 1 eq) in dry $PhCH_3$ (5 ml), previously sonicated at 60 °C for 30'; the mixture was stirred, under sonication, at 60 °C for 4 h. After this time the obtained suspension was centrifugated at 5000 r/min for 10' and the supernatant was removed. The solid residue was first washed with fresh $PhCH_3$ (3x5 ml), then with Et_2O (2x5 ml) and vortex/sonication/centrifugation were cyclic repeated for each washing. Functionalized NPs were dried on air for a night and then in a rotating vacuum drier for a day, to afford **27** as a brown powder. ***Loadings from E.A.:*** 26.36% (equal to 1.03 mmol/g_{NPs}). ***FTIR (cm^{-1}) in trasmittance (blank KBr):*** 2961-2874 (υ, aliphatic C-H), 1699 (υ, C=O carbamate), 1589, 1532 (υ, C=C), 1493, 1396 (δ, SO_2N-H), 1311 (asym υ, SO_2NH), 1152 (sym υ, SO_2NH), 1122, 1031 (δ, C-H), 633-558 (υ, Fe-O).

4.6.2.21 Synthesis of NP-[p-(N-butylcarbamoyl)phenyl] Carbamate 28

n-Butylamine (95 µl, 0.96 mmol, 5 eq) was added to a suspension of functionalized nanoparticles **19** (100 mg, loading 35.01% equal to 1.92 mmol/g_{NPs}, 1 eq) in dry $PhCH_3$ (5 ml), previously sonicated at 60 °C for 30'; the mixture was stirred, under sonication, at 60 °C for 4 h. After this time the obtained suspension was centrifugated at 5000 r/min for 10' and the supernatant was removed. The solid residue was first washed with fresh $PhCH_3$ (3x5 ml), then with Et_2O (2x5 ml) and vortex/sonication/centrifugation were cyclic repeated for each washing. Functionalized NPs were dried on air for a night and then in a rotating vacuum drier for a day, to afford **28** as a brown powder. ***Loadings from E.A.:*** 31.80% (equal to 1.45 mmol/g_{NPs}); the loading was lower than the expected, may due to the losses of highly functionalized nanoparticles that remain in the supernatant during the isolation process. By the way, CHN values perfectly match the expected chemical formula. ***FTIR (cm^{-1}) in trasmittance (blank KBr):*** 3324 (υ, N-H carbamate), 3193 (υ, N-H amide), 3037 (υ, ArC-H),

2962-2874 (υ, aliphatic C-H), 1678 (υ, C=O carbamate), 1649 (υ, C=O amide), 1596, 153o (υ, C=C), 1505 (δ, N-H), 1398, 1313, 1237 (υ, C-O and C-N), 1176 (δ, C-H), 632-577 (υ, Fe-O).

4.6.2.22 Synthesis of (p-Butylsulfamoyl)benzoic Acid **30**

The commercially available (*p*-chlorosulfonyl)benzoic acid **29** (253 mg, 1.15 mmol, 1 eq) was suspended in 5 ml of DCM at room temperature. *n*-Butylamine (680 µl, 6.90 mmol, 6 eq) was added dropwise, leading to the formation of a yellowish solution. After 2 h under stirring, an aqueous solution of HCl 1M was added till pH 1. The aqueous phase was extracted with AcOEt (2x5 ml) and the combined organic phases were washed with water (3x5 ml), dried on anhydrous Na_2SO_4 and filtered. The solvent was removed under reduced pressure, affording a white crystalline product, corresponding to **30** (254 mg, 86%). No further purifications were needed. ***Mp:*** 216-217 °C (Et_2O). ***^{1}H-NMR (DMSO-d6, 300 MHz):*** δ= 13.42 (s, 1H, CO_2H), 8.12 (d, J = 6 Hz, 2H, Ar-H ortho to carboxylic acid), 7.90 (d, J = 6 Hz, 2H, Ar-H ortho to sulfonamide), 7.74 (t, 1H, NH sulfonamide), 2.76 (q, 2H, CH_2-N), 1.32 (m, 2H, CH_2), 1.22 (m, 2H, CH_2), 0.79 (t, 3H, CH_3).

4.6.2.23 Synthesis of (p-Butylsulfamoyl)benzoyl Chloride **31**

(*p*-Butylsulfamoyl)benzoic acid **30** (250 mg, 0.97 mmol) was suspended in 5 ml of DCM at room temperature and then 10 ml of thionyl chloride were added, leading to a colorless solution. After refluxing for 2 h, the solution was vacuum-dried to afford a white powder, corresponding to desired product **31** (265 mg, quantitative yield). It was used without further purification. ***^{1}H-NMR (DMSO-d6, 300 MHz):*** δ= 8.21 (d, J = 6 Hz, 2H, Ar-H ortho to acyl chloride), 8,01 (d, J = 6 Hz, 2H, Ar-H ortho to sulfonamide), 7.78 (t, 1H, NH sulfonamide), 2.76 (q, 2H, CH_2-N), 1.32 (m, 2H, CH_2), 1.22 (m, 2H, CH_2), 0.79 (t, 3H, CH_3); no residual peak of carboxylic acid was present.

4.6.2.24 Synthesis of (p-Butylsulfamoyl)benzoyl Azide **32**

To a stirred solution of compound **31** (265 mg, 0.96 mmol, 1 eq) in 8 ml of acetone at 0 °C, solid NaN_3 (312 mg, 4.81 mmol, 5 eq) was added in three portions. The suspension was stirred at 0 °C for 30' and then raised to room temperature. After stirring at r.t. for 1.5 h, the volatiles were removed in vacuo, and the resulting residue was chromatographed by automated flash chromatography on pre-packed silica column with methylene chloride as eluent. The product **32** is isolated upon evaporation of solvent to afford a white powder (243 mg, 90%). Analysis by silica TLC (pure DCM as eluent, visualized by UV absorption and/or

iodine vapor staining) showed one spot at *Rf* 0.50. ***^{1}H NMR ($CDCl_3$, 300 MHz):*** δ= 8.16 (d, J = 9 Hz, 2H, Ar-H ortho to acyl azide), 7.95 (d, J = 9 Hz, 2H, Ar-H ortho to sulfonamide), 4.55 (t, 1H, NH sulfonamide), 2.99 (q, 2H, CH_2-N), 1.45 (m, 2H, CH_2), 1.30 (m, 2H, CH_2), 0.85 (t, 3H, CH_3). ***FTIR (cm^{-1}) in trasmittance (NaCl windows):*** 3288, 2965, 2938, 2868, 2190, 2145 (υ C=O acyl azide), 1687, 1432, 1399, 1330, 1256, 1162, 1090, 997, 890, 750, 679.

4.6.2.25 Synthesis of (p-Butylsulfamoyl)phenyl Isocyante 33

A solution of compound **32** (243 mg, 0.861 mmol) in dry toluene (5 ml) is refluxed under nitrogen for 1.5 h and then evaporated in vacuo. This quantitatively affords compound **33** as white needles (218 mg). This compound should be stored in a sealed vial, protected from light and moisture, in a freezer. ***^{1}H-NMR ($CDCl_3$, 300 MHz):*** δ= 7.83 (d, J = 6 Hz, 2H, ArCH ortho to isocyanate), 7.22 (d, J = 6 Hz, 2H, ArCH ortho to sulfonamide), 4.55 (broad s, 1H, NH sulfonamide), 2.95 (q, 2H, CH_2-N), 1.45 (m, 2H, CH_2), 1.30 (m, 2H, CH_2), 0.85 (t, 3H, CH_3). ***^{13}C all decoupled NMR ($CDCl_3$, 75 MHz):*** δ= 137.90 (Cq), 137.41 (Cq), 128.89 (ArCH), 125.81 (Cq, C=O isocyanate), 125.47 (ArCH), 43.08 (CH_2-N), 31.72 (CH_2), 19.80 (CH_2), 13.65 (CH_3). ***FTIR (cm^{-1}) in trasmittance (NaCl windows):*** 3274, 3103, 3069, 2956, 2933, 2872, 2278 (υ, C=O isocyanate), 1647, 1589, 1515, 1425, 1321, 1285, 1157, 1108, 875, 838, 758, 660.

4.6.2.26 Synthesis of NP-[p-(N-butylsulfamoyl)phenyl] Carbamate 27, *starting from* 33

(*p*-Butylsulfamoyl)phenyl isocyanate **33** (102 mg, 0.4 mmol) was added to a suspension of naked SPIONs (100 mg) in dry $PhCH_3$ (5 ml), previously sonicated at 60 °C for 30'; the mixture was stirred, under sonication, at 60 °C for 4 h. After this time the obtained suspension was centrifugated at 5000 r/min for 10' and the supernatant was removed. The solid residue was first washed with fresh $PhCH_3$ (3x5 ml), then with Et_2O (2x5 ml) and vortex/sonication/centrifugation were cyclic repeated for each washing. Functionalized NPs were dried on air for a night and then in a rotating vacuum drier for a day, to afford **27** as a brown powder. ***Loadings from E.A.:*** 39.45% (equal to 1.55 mmol/g_{NPs}). It's to note the the loading obtained is higher than the one obtained for the same compound synthesized by amidation of previously functionalized nanoparticles *[see procedure 4.6.2.20]* ***FTIR (cm^{-1}) in trasmittance (blank KBr):*** 3336 (υ, SO_2N-H), 3271 (υ, N-H carbamate), 2957-2872 (υ, aliphatic C-H), 1699 (υ, C=O carbamate), 1589, 1532 (υ, C=C), 1493, 1396 (δ, SO_2N-H), 1327-1311 (asym υ, SO_2NH), 1157 (sym υ, SO_2NH), 1122, 1031 (δ, C-H), 631-551 (υ, Fe-O).

4.6.2.27 Synthesis of NP-[p-(3-(dodecylthio)-2,5-dioxopyrrolidin-1-yl)phenyl] Carbamate **34**

1-Dodecanthiol (232 µl, 0.964 mmol, 10 eq) was added to a suspension of functionalized nanoparticles **20** (40 mg, loading 51.81% equal to 2.41 mmol/g_{NPs}, 1 eq) in CH_3CN (5 ml), previously sonicated at 60 °C for 30'; the mixture was stirred, under sonication, at 60 °C for 4 h. After this time the obtained suspension was centrifugated at 5000 r/min for 10' and the supernatant was removed. The solid residue was first washed with fresh CH_3CN (3x5 ml), then with Et_2O (2x5 ml) and vortex/sonication/centrifugation were cyclic repeated for each washing. Functionalized NPs were dried on air for a night and then in a rotating vacuum drier for a day, to afford **34** as a brown powder. ***FTIR (cm^{-1}) in trasmittance (blank KBr):*** 3394 (υ, N-H), 3102 (υ, ArC-H), 2921-2852 (υ, aliphatic C-H), 1707 (υ, C=O imide), 1692 (υ, C=O carbamate), 1605, 1552 (δ, N-H), 1513 (υ, C=C), 1398 (υ, Ar-N), 1313 (υ, C-N imide), 1239-1175 (υ, C-O and C-N), 1176 (δ, C-H), 831 (δ, C-H out of plane), 689-559 (υ, Fe-O).

4.6.2.28 Synthesis of NP-[p-(3-((R)-N-acetylcysteine)-2,5-dioxopyrrolidin-1-yl)phenyl] Carbamate **35**

(*R*)-*N*-acetylcysteine (78.66 mg, 0.482 mmol, 10 eq) was added to a suspension of functionalized nanoparticles **20** (20 mg, loading 51.81% equal to 2.41 mmol/g_{NPs}, 1 eq) in CH_3CN (5 ml), previously sonicated at 60 °C for 30'; the mixture was stirred, under sonication, at 60 °C for 4 h. After this time the obtained suspension was centrifugated at 5000 r/min for 10' and the supernatant was removed. The solid residue was first washed with fresh CH_3CN (3x5 ml), then with Et_2O (2x5 ml) and vortex/sonication/centrifugation were cyclic repeated for each washing. Functionalized NPs were dried on air for a night and then in a rotating vacuum drier for a day, to afford **35** as a brown powder. ***Loadings from E.A.:*** 60.32% (equal to 1.60 mmol/g_{NPs}); the loading was lower than the expected, may due to the losses of highly functionalized nanoparticles that remain in the supernatant during the isolation process. By the way, CHN values perfectly match the expected chemical formula. ***FTIR (cm^{-1}) in trasmittance (blank KBr):*** 3360 (broad υ, CO_2H and N-H), 3073 (υ, ArC-H), 2970-2923 (υ, aliphatic C-H), 1777 (υ, C=O amide), 1709 (υ, C=O imide), 1692 (shoulder, C=O carbamate), 1604, 1549 (δ, N-H), 1512 (υ, C=C), 1393 (υ, Ar-N), 1314 (υ, C-N imide), 1233-1180 (υ, C-O and C-N), 1175 (shoulder δ, C-H), 834 (δ, C-H out of plane), 689-585 (υ, Fe-O).

References

[253] R.P. Moerschell, *US 2008/0070802 A1*, **2008**.

[254] J.P. Brunelle, *Pure & Appl. Chem.*, **1978**, *50*, 1211-1229.

[255] (a) G. Gouy, *Comt. Rend.*, **1909**, *149*, 654; (b) G. Gouy, *J. Phys.*, **1910**, *4(9)*, 457.

[256] D.L. Chapman, *Phil. Mag.*, **1913**, *6(25)*, 475.

[257] G.A. Parks, *Chem. Rev.*, **1965**, *65*, 177-198.

[258] (a) S. Yu, G.M. Chow, *J. Mater. Chem.*, **2004**, *14*, 2781-2786; (b) F. Dilnawaz, A. Singh, C. Mohanty, S.K. Sahoo, *Biomaterials*, **2010**, *31*, 3694-3706.

[259] (a) S.A. Corr, Y.K. Gun'ko, R. Tekoriute, C.J. Meledandri, D.F. Brougham, *J. Phys. Chem C*, **2008**, *112(35)*, 13324-13327; (b) E. Camponeschi, J. Walker, H. Garmestani, R. Tannenbaum, *J. Non-Crystalline Solids*, **2008**, *354(34)*, 4063-4069; (c) L. Zhang, W. Zhang, Z. Sun, *Jinan Daxue Xuebao, Ziran Kexueban*, **2010**, *24(1)*, 40-43.

[260] (a) M.A. White, J.A. Johnson, J.T. Koberstein, N.J. Turro, *J. Am. Chem. Soc.*, **2006**, *128*, 11356-11357; (b) Y. Lalatonne, M. Moteil, H. Jouni, J.M. Serfaty, O. Sainte-Catherine, N. Lièvre, S. Kusmia, P. Weinmann, M. Lecouvey, L. Motte, *J. Osteoporosis*, **2010**, ID: 747852.

[261] R.A. Bini, R.F.C. Marques, F.J. Santos, J.A. Chaker, M. Jafelicci Jr., *J. Magn, Magn. Mater.*, **2012**, *324*, 534-539.

[262] (a) C. Zhang, B. Wangler, B. Morgenstern, H. Zentgraf, *Langmuir*, **2007**, *2*, 1427; (b) S. Campelj, D. Makovec, M.J. Drofenik, *J. Magn. Magn. Mater.*, **2009**, *321*, 1346; (c) Z. Xu, Q. Liu, J.A. Finch, *Applied Surface Science*, **1997**, *120*, 269; (d) I.J. Bruce, T. Sen, *Langmuir*, **2005**, *21*, 7029.

[263] L. Polito, D.Monti, E. Caneva, E. Delnevo, G. Russo, D. Prosperi, *Chem. Commun.*, **2008**, 621-623.

[264] G. Ma, W. Liu, X. Liu, J. Wu, T. Yan, B. Xu, *Progress in Organic Coating*, **2011**, *71*, 83-88.

[265] B. Ou, D. Li, Q. Liu, Z. Zhou, G. Chen, P. Liu, *Journal of Macromolecular Science, Part A: Pure and Applied Chemistry*, **2012**, *49*, 149-153.

[266] M.E. Annunziato, U.S. Patel, M. Ranade, P.S. Palumbo, *Bioconjugate Chem.*, **1993**, *4*, 212-218.

[267] L. Hu, A. Percheron, D. Chaumont, C-H. Brachais, *J. Sol-Gel Sci. Technol.*, **2011**, *60*, 198-205.

[268] H. Händel, E. Gesele, G. Gottschall, K. Albert, *Angew. Chem., Int.Ed.*, **2003**, *42*, 438-442.

[269] L.L. Cheng, M.J. Ma, L. Becerra, T. Ptak, I. Tracey, A. Lackner, R.G. Gonzalez, *Proc. Natl. Acad. Sci. U.S.A.*, **1997**, *94*, 6408-6413.

[270] W.T. Franks, B.J. Wylie, H.L.F. Schmidt, A.J. Nieuwkoop, R.M. Mayrhofer, G.J. Shah, D.T. Graesser, C.M. Rienstra, *Proc.Natl. Acad. Sci. U.S.A.*, **2008**, *105*, 4621-4626.

[271] B.J. Blaise, J. Giacomotto, B. Elena, M.E. Dumas, P. Toulhoat, L. Segalat, L. Emsley, *Proc. Natl. Acad. Sci. U.S.A.*, **2007**, *104*, 19808-19812.

[272] *NMR Biomedicine*, **2005**, *18,* 242-251.

[273] A.L. Willis, N.J. Turro, S. O'Brien, *Chem. Mater.*, **2005**, *17*, 5970-5975.

[274] L.O. Sillerud, A.F. McDowell, N.L. Adolphi, R.E. Serda, D.P. Adams, M.J. Vasile, T.M. Alam, *J. of Magnetic Resonance*, **2006**, *181*, 181-190.

[275] M.A. White, J.A. Johnson, J.T. Koberstein, N.J. Turro, *J. Am. Chem. Soc.*, **2006**, *128*, 11356-11357.

[276] L Polito, M. Colombo, D. Monti, S. Melato, E. Caneva, D. Prosperi, *J. Am. Chem. Soc.*, **2008**, *130(38)*, 12712-12724. ".

[277] G. Prencipe, S. Maiorana, P. Verderio, M. Colombo, P. Fermo, E. Caneva, D. Prosperi, E. Licandro; *Chem. Commun.*, **2009**, *40*, 6017-6019.

[278] W.S. Price, *Concepts Magn. Reson.*, **1997**, *9*, 299.

[279] W.S. Price, *Concepts Magn. Reson.*, **1998**, *10*, 197.

[280] C.S. Johnson, *Progress in Nuclear Magnetic Resonance Spectroscopy*, **1999**, *34*, 203–256.

[281] D. Wu, A. Chen, C.S. Johnson Jr., *J. Magn. Reson. A*, **1996**, *123*, 215.

Chapter 5: New SPION-PNA Nanoconjugates

5 Synthesis of New SPION-PNA Nanoconjugates for Biomedical Applications

In this chapter will be discussed the synthesis of specifically modified Peptide Nucleic Acids (PNAs) and their conjugation with superparamagnetic iron oxide nanoparticles (SPIONs), both by non-covalent adsorption or covalent interaction with the nanoparticles surface. After an introduction about what PNAs are, their general properties, characteristics and applications, the discussion will be focused on the synthesis of new SPION-PNA nanoconjugates *[see sections 5.7 and 5.8]*.

5.1 Peptide Nucleic Acids

Peptide Nucleic Acids (PNAs), first introduced in 1991 by Nielsen and co-workers[282] at Copenhagen University, are a remarkable example of a simple, neutral and achiral whole backbone replacement, that has suppressed, in many ways, other attempts to mimic the

native nucleic acid structures in terms of molecular recognition properties. PNAs are synthetic nucleic acid analogues with an achiral pseudopeptide backbone in which the phosphodiester backbone is replaced by repetitive units of *N*-(2-aminoethyl)glycine. On the backbone the purine and pyrimidine bases are attached via a methyl carbonyl linker (*Figure 56*).

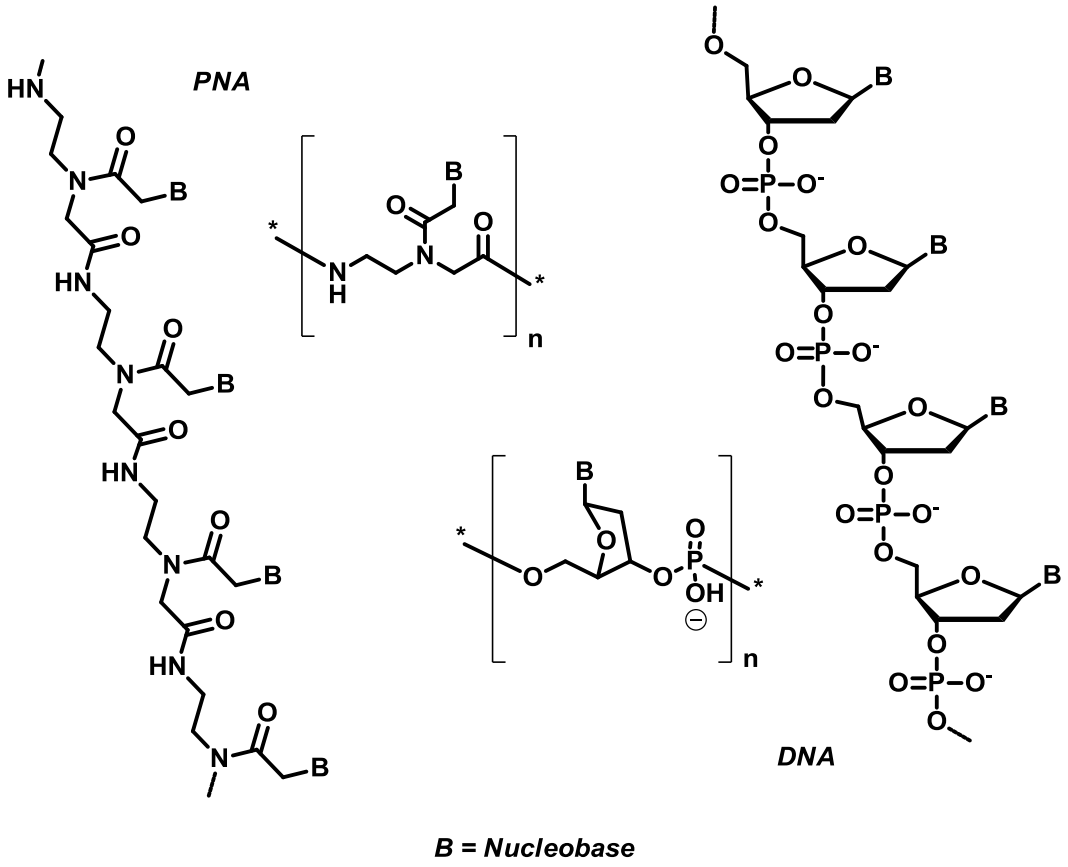

Figure 56 *- PNA (blue) versus DNA (black) oligomeric structures. In squared brackets are shown the repeating units.*

The PNA backbone maintains approximately the same length per repeating unit as in DNA or RNA. The appended nucleobases projects from the backbone to form stable double or triple helical complexes with target nucleic acids.[283] The internucleobase distance in PNA is conserved, so that it can bind to the target DNA or RNA sequences with high sequence specificity and affinity. Therefore, chemical terms they are neither proteins nor nucleic acids. The amide (or peptide) bonds in PNA are sufficiently different from the α-amino acid peptide bonds present in proteins, resulting that PNA is biologically stable. These non-natural

characteristics make PNA oligomers highly resistant to protease and nuclease attacks.[284] Because PNAs have a neutral backbone, hybridization with target nucleic acids is not affected by the interstrand negative charge electrostatic repulsions.[285] In addition, the absence of a repetitive charged backbone prevents PNAs from binding to proteins that normally recognize polyanions, avoiding a major source of nonspecific interactions.

5.1.1 PNA Interactions with Single Strand Nucleic Acids

5.1.1.1 Duplex

PNAs are able to hybridize to both complementary DNA and RNA targets in a sequence-specific manner to form PNA/DNA[286] (*Figure 57*) or PNA/RNA duplex structures, according to Watson-Crick hydrogen binding rules (*Figure 58*).[283,287,288].

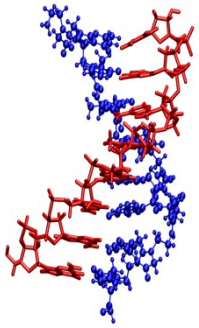

Figure 57 *- PNA/DNA duplex.*

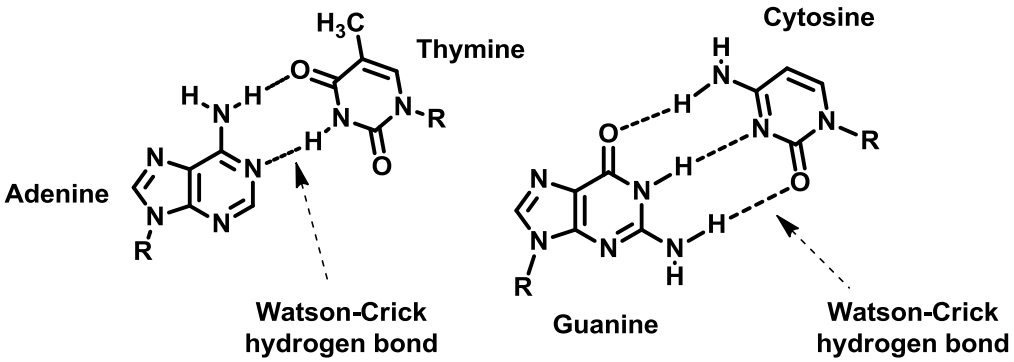

Figure 58 *- PNA/DNA duplex Watson-Crick hydrogen bonding paring rules.*

PNAs bind DNA/RNA in either parallel or antiparallel modes, the later being slightly preferred over the former. The antiparallel mode refers to the instance when the PNA 'N' terminus lies towards the 3'-end and the 'C' terminus lies towards the 5'-end of the complementary DNA/RNA oligonucleotides. Likewise, the parallel mode of binding is said to occur when the PNA 'N' terminus lies towards the 5'-end and the 'C' terminus towards the 3'-end of the complementary DNA/RNA oligonucleotide (*Figure 59*).

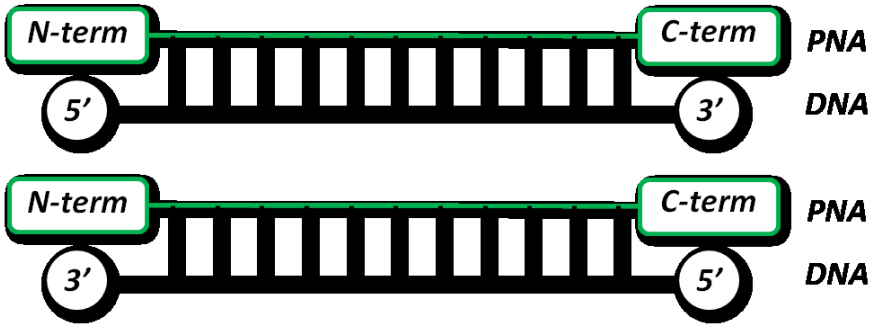

Figure 59 *- PNA/DNA binding in parallel (top) and antiparallel (bottom) modes.*

5.1.1.2 Triplex

Homopyrimidinic PNAs strongly bind to target homopurine nucleic acids and sequence specifically, forming of 2:1 PNA_2/DNA triplex (Figure 60).[289]

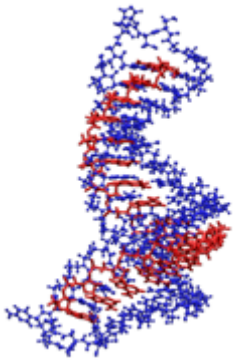

Figure 60 *- PNA/DNA triplex.*

This complex can be formed thanks to the ability of the homopyrimidine strand to bind PNA/DNA duplex by Hoogsteen hydrogen bonding scheme (*Figure 61*).

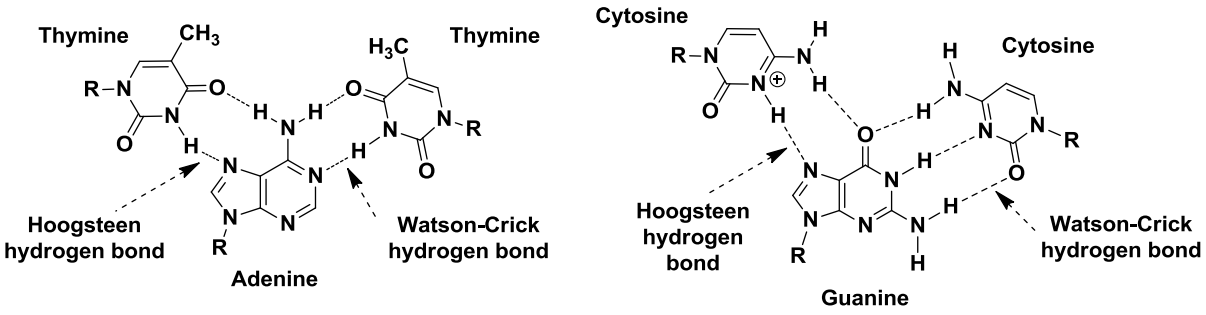

Figure 61 *- PNA/DNA triplex Hoogsteen and Watson-Crick hydrogen bonding paring rules.*

5.1.1.3 Quadruplex

G-quadruplexes are four-stranded structures formed from DNA sequences that contain stretches of contiguous guanine bases, usually in the presence of alkali metal cations.[290] G-quadruplex DNA has been recently in focus because of its putative existence and its biological function at telomeres, which affects replication,[291,292] and in promoter sites influencing transcription.[293] The guanine bases in G-quadruplexes form G-tetrads where four G bases hydrogen bond via the Hoogsteen sites in a cyclic fashion (*Figure 62*).

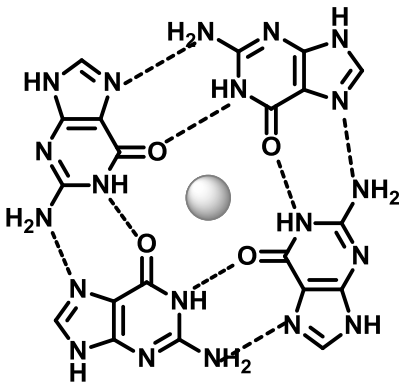

Figure 62 *- G-quadruplex in presence of an alkali metal cation.*

In 2003 Prof. Datta reported[294] that homologous G-rich PNA and DNA oligomers hybridize to form a PNA_2-DNA_2 quadruplex. The hybrid quadruplex exhibits high thermodynamic stability and expands the range of molecular recognition motifs for PNA beyond duplex and triplex formation. After this study many research groups have reported the synthesis of PNA based G-quadruplex structures with different topologies,[295,296] for instance a PNA_4 G-quadruplex,[297] a structure obtained from PNA-DNA chimeras[298] and even a PNA/RNA quadruplex.[299]

5.1.2 PNA Interactions with Double Strands Nucleic Acids

The interaction of single-stranded PNA with double-stranded DNA is interesting not only because of his potential applications in antigene strategy but also for the possible use of PNA in different biotechnological applications (as discussed later). Various modes of interaction are possible, depending on sequences and conditions. *Figure 63* illustrates the triplex and duplex invasion modes, in which the targeting PNA breaks up the double helix and complexes with the complementary DNA strand.

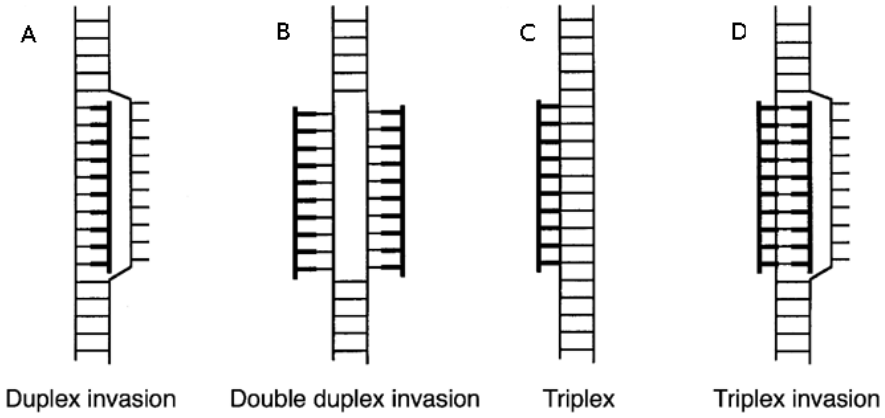

Figure 63 *- Duplex and triplex invasion modes.*

Duplex invasion (*Figure 63A*) can result if the target DNA is a homopyrimidine and the PNA has a homopurine sequence. Instead, if the DNA target is a homopurine sequence, it can result a very stable triplex invasion (*Figure 63D*) complex. Synthesizing pyrimidine-PNAs as a palindrome sequence with a flexible linker in the middle creates a so-called bisPNA or "PNA clamp", allowing triplex formation in optimal directions with the Watson-Crick base pairing in an antiparallel and Hoogsten bonding in a parallel orientation.[300,301] However, the triplex invasion complex is very slow to form at neutral pH, unless the cytosines in the "Hoogsteen-pairing" strand are exchanged to pseudo-isocytosines, also called J bases.[300] For practical applications, the rate of formation can be increased by using cationic PNAs (e.g., with extra lysines linked) or by linking the PNA to an intercalating molecule such as 9-aminoacridine.[302] The most successful method to obtain a double-duplex invasion (*Figure 63B*) is to use a pseudo-complementary PNA (pcPNA) in which nucleobases adenine (A) and thymine (T) in conventional PNA are replaced with modified bases 2,6-diaminopurine (D) and 2-thiouracil (Us).[303]

5.1.3 Stability of PNAs and PNA Complexes

Compared to normal DNA and RNA oligonucleotides, PNAs are much more stable inside cells. PNAs are very resistant to nuclease and protease digestion since nuclease cannot digest their altered backbones.[284] Furthermore, duplexes between PNA and DNA or RNA are in general more thermally stable than the corresponding DNA/DNA or DNA/RNA duplexes.[304,305] The stability of PNA/DNA duplexes was studied by differential scanning calorimetry.[306] PNA/DNA duplexes show increased stability when the purines are in the PNA strand. It is also observed that the thermal stability of PNA/PNA duplexes exceeds that of PNA/RNA duplexes, that are already more stable than PNA/DNA duplexes. As a general rule, the ***Melting Temperature Tm*** (the temperature at which half of the PNA or DNA strands are in the double-helical state and half are in the random coil state) of a PNA/DNA duplex is 1 °C higher per base pair than the Tm of the corresponding DNA/DNA duplex. Very important, the stability of PNA/DNA duplexes are almost unaffected by the ionic strength of the medium.[283] PNA/DNA/PNA triplexes exhibit extraordinarily high stability (the thermal stability for a decamer is typically up to 70 °C).

5.1.4 Solubility of PNAs

As it said, PNAs are charge-neutral compounds and hence have poor water solubility compared with DNA. Neutral PNA molecules tend to aggregate, depending on the sequence of the oligomer. PNA solubility is also related to the length of the oligomer and to the purine/pyrimidine ratio.[304] Some recent modifications, including the incorporation of positively charged lysine residues (carboxyl-terminal or backbone modification in place of glycine), have shown improvements in solubility.[307] Negative charges may also be introduced, especially in PNA/DNA chimeras, which will enhance the water solubility.[308]

5.2 PNA Applications

This chapter will briefly discuss, some possible applications of PNAs. The potential applications of PNAs can be divided in three different field: diagnostics, molecular biology and therapy.

It is important to notice that new techniques are continuously being developed and that this chapter could not be exhaustive. However, some techniques are very important because they represent "historically" steps in the development and use of PNAs.

5.2.1 Diagnostics

PNAs have found application in the detection of genetic mutations and in the analysis of mismatches in the Watson-Creek hydrogen bonding. Their particular affinity towards DNA and RNA, their high sequence specificity and their capacity to perform strand displacements make PNAs powerful tools for diagnostic purposes.

One of the best features of PNAs is the possibility to detect the Single Nucleotide Polymorphism (SNP) by measuring the variations of the melting temperature. Some techniques have been developed for this target, for example the PCR and capillary electrophoresis.[309]

5.2.1.1 Single Base Polymorphism: "PCR Clamping"

The Polymerase Chain Reaction (PCR) technique is considered one of the most valuable step in the detection of genetic diseases. The high specificity of PNA to bind DNA, the greater stability of PNA-DNA duplexes than DNA-DNA ones and the inefficiency of PNA to act as primer for DNA polymerases are the bases for this novel techniques.

This strategy includes a distinct annealing step involving the PNA targeted against one of the PCR primer sites. This step is carried out at a higher temperature than that for conventional PCR primer annealing where the PNA is selectively bound to the DNA molecule. The PNA/DNA complex formed at one of the primer sites effectively blocks the formation of a PCR product.[310] PNA is also able to discriminate between fully complementary and single mismatch targets in a mixed target PCR. Sequence-selective blockage by PNA allows suppression of target sequences that differ by only one base pair. Also, this PNA clamping was able to discriminate three different point mutations at a single position.[311]

5.2.1.2 Screening for Genetic Mutations by Capillary Electrophoresis

In capillary electrophoresis, the separation is generally carried out using a long, thin fused silica capillary (typically 50–80 cm long, inner diameter 10–300 mm). A portion of the coating, closed at one end of the capillary, is removed to allow optical detection of the analyte. The analyte passes the detection window during a separation process and can be visualized by online, automated, UV, or laser-induced fluorescence (LIF) detection systems. Capillary electrophoresis is capable of analyzing minute amounts of sample (typically in the order of picograms to femtograms). However, it is not possible to analyze more than one sample at a time, which is regarded as the major disadvantage compared to slab gel electrophoresis.

A new diagnostic method for the detection of genetic mutations using PNA as a probe for capillary electrophoresis has been reported by Carlsson *et al*.[312] The method is sensitive enough to detect a single mismatch in the sample DNA. The model system consisted of four 50-mer, single-stranded DNA fragments representing a part of the cystic fibrosis transmembrane conductance regulator gene, one wild-type and three mutant sequences, and a 15-mer PNA probe having a sequence complementary to the wild-type oligomer.

The probe PNA only binds the fully matched DNA, and the presence of this duplex is detected using free solution capillary electrophoresis. Separation of full-match from mismatch duplexes was accomplished at a high temperature (70 °C) and 50 mM ionic strength. At this temperature and ionic strength, only the hybrid duplex carrying the wild-type DNA sequences remains stable, while the hybrid complex carrying single mismatch DNA will be melted. Free PNA binds to the capillary wall and is not detected.[312]

Another application involves the use of fluorescent labelled PNAs. PNA probes with fluorescent tags offer sensitive detection and require only a very low concentration of the sample. At high temperatures (as described above), the LIF detection system will generate a signal for the bound PNAs, since free PNA is efficiently removed. Maybe it will be possible in the future to establish a universal screening strategy for any genetic disease with a known spectrum of mutations by developing a PNA probe library, possibly using multiple

fluorescent tags for multiplex testing of one or more exons. Other electrophoretic techniques (also in gel phase) are possible: the RNA binding properties of PNAs have also been characterized using capillary gel electrophoresis.[313,314]

5.2.1.3 PNA as a Probe for Nucleic Acid Biosensor

The DNA biosensor technology holds promises for a rapid and cost-effective detection of specific DNA sequences. A single-stranded nucleic acid probe is immobilized onto optical, electrochemical, or mass-sensitive transducers to detect the complementary (or mismatch) strand in a sample solution. The response from the hybridization event is converted into a useful electrical signal by the transducer. The use of PNAs based probes is a powerful alternative to DNAs based ones in different techniques.

5.2.1.3.1 BIAcore (Biomolecular Interaction Analysis)

The main background of this technique is the effect called SPR (*Surface Plasmon Resonance*). The PNA hybridization and corresponding mismatch analysis can be studied using a BIAcore instrument, which can evaluate a real-time biomolecular interaction analysis using optical detection technology. The real-time interactions are monitored on a sensor (surface) chip, which constitutes the core part of a BIAcore instrument. The probe molecule is attached directly to the surface and the analyte molecule is free in solution. The detection principle in BIA uses surface plasmon resonance. The response signal of the BIAcore apparatus is proportional to the change in the refractive index at the surface and is assumed to be proportional to the mass of substance bound to the chip (*Figure 64*).[315]

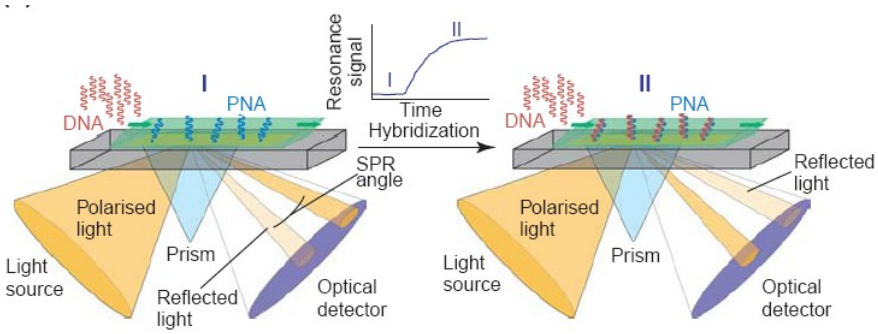

Figure 64 *- Schematic representation of BIAcore.*

Jensen *et al.* used this technique to study the interactions between PNA and DNA or RNA. The sensor chip used in this case was basically a thin gold surface covered with a layer of dextran and containing streptavidin chemically coupled to the dextran. A biotinylated PNA probe was immobilized on the surface by using the strong coupling between biotin and streptavidin. The amount of bound substance (fully complementary as well as various singly mismatched RNA and DNA oligonucleotides) was measured as a function of time when a solution containing the complementary strands passed over the chip surface. In this way both the association (*annealing*) and dissociation (*melting*) kinetics could be studied.[316]

5.2.1.3.2 QCM (Quartz Crystal Microbalance)

The quartz crystal microbalance has been used for some time to monitor the mass or the thickness of thin films deposited on surfaces, to study gas adsorption and the deposition on surfaces in the monolayer and submonolayer regimes[317]. Only recently, this sensitive mass measuring device has begun to be used in the area of biochemistry and biotechnology, such as for studying the hybridization of nucleic acids on surface.[318,319,320] The resonant frequency of the crystal changes due to a minute weight increases on the surface. It is expected that immobilized PNA strands (or probes) would show an improved distinction between the closely related target sequences compared to an immobilized DNA probe. A recent report by Wang and co-workers on quartz crystal microbalance biosensor, based on peptide nucleic acid probes, showed that the system can differentiate between a full complementary and single mismatch oligonucleotide. A rapid and sensitive detection of mismatch sequences is possible by monitoring the frequency/time response of the PNA-QCM biosensor. The PNA probes used in the above-mentioned study, which formed the monolayer onto the gold QCM surface, contained a cysteine attached to the PNA core with the help of an ethylene glycol unit.[321] The remarkable specificity of the immobilized probe provides a rapid hybridization with corresponding oligonucleotides. Such a mismatch sensitivity of PNA-immobilized QCM biosensors could be of great importance for diagnostic applications, particularly for genetic screening and diagnosis of malignant diseases.

5.2.1.3.3 MALDI-TOF Mass Spectrometry

MALDI-TOF mass spectrometry has been used successfully in PNA-based diagnostic research to study discrimination of single-nucleotide polymorphisms (SNPs) in human DNA. The human genome and the mitochondrial DNA contain many SNPs that may be linked to diseases.[322] Rapid and accurate screening of important SNPs, based on high-affinity binding of PNA probes to DNA, is possible by using MALDI-TOF mass spectroscopy. The captured, single-stranded DNA molecules are PCR-amplified and thereafter hybridized with PNA probes in an allele-specific fashion. MALDI-TOF can rapidly and accurately detect (identify) these hybridized PNA probes. This provides a straightforward, rapid, accurate, and specific detection of SNPs in amplified DNA.[323] The detection of multiple point mutations using allele-specific, mass-labelled PNA hybridization probes is also possible by using a direct MALDI-TOF-MS analysis method.[324] The mass spectra will show peaks of distinct masses corresponding to each allele, and in this way a mass spectral 'fingerprint' of each DNA sample can be obtained.[309] This technique can also be applied to analyse microarrays (*Figure 65*).

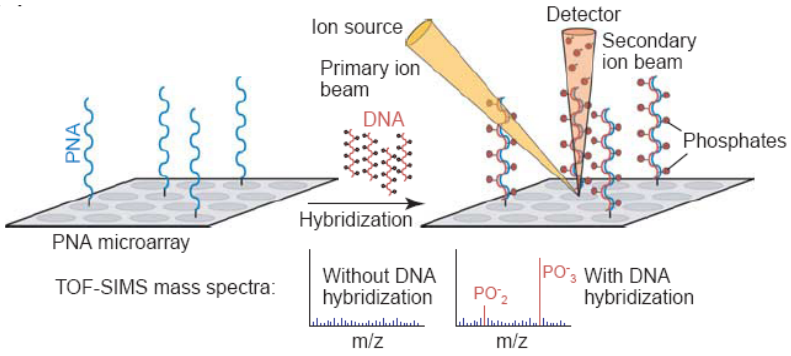

Figure 65 *- Application of MALDI-TOF in the analysis of microarrays.*

5.2.1.3.4 Potentiometric Measurements

Wang *et al.*[325] have also reported the use of PNA as a recognition probe for the electrochemical detection of the hybridization event using chronopotentiometric measurements. The method consists of four steps: probe (PNA) immobilization onto the transducer surface, hybridization, indicator binding, and chronopotentiometric transduction. A carbon paste electrode contains the immobilized DNA or PNA probe. The hybridization

experiment was carried out by immersing the electrode into the stirred buffer solution containing a desired target, followed by measurement of signal. It is important to remember that similar techniques could be used to prepare microarray with electrochemical detection systems.

5.2.1.4 Microarray

Microarrays are small chips carrying on their surface row and column of ordered molecular probes (*spot*). Each of them is able to bind a specific target molecule. The success of microarrays in screening *m*RNA expression profiles of thousands of genes simultaneously has prompted researchers in bioorganic chemistry to explore this format for screening small molecules. From an analytical perspective, the prospect of screening thousand of analytes in a few microlitres is attractive. Microarrays can be prepared by several techniques including photolithography, contact printing and inkjet to generate arrays with densities ranging from 1000 to 500 000 features per square centimetre. To date, a number of chemistries have been developed to derivatize glass surfaces to immobilize proteins, oligosaccharides, and small molecules in the microarray format. Many of these methods require the attachment of the protein or small molecule to the glass slide and likewise require that screening with the biological sample would also be performed on the surface. A supramolecular attachment, based on sequence specific hybridization of peptide nucleic acid (PNA), allows the use of the libraries as a mixture in solution that can then be converted to an organized microarray in one step by a self-sorting process.[326]

The microarray could be treated with the sample and the entity of the response of every single spot leads to the determination of the sample structure. This technique is already successfully applied for nucleic acids sequences screening: in this case the complementary DNA sequences of all known polymorphism are spotted on the chip (*Figure 66*).[327]

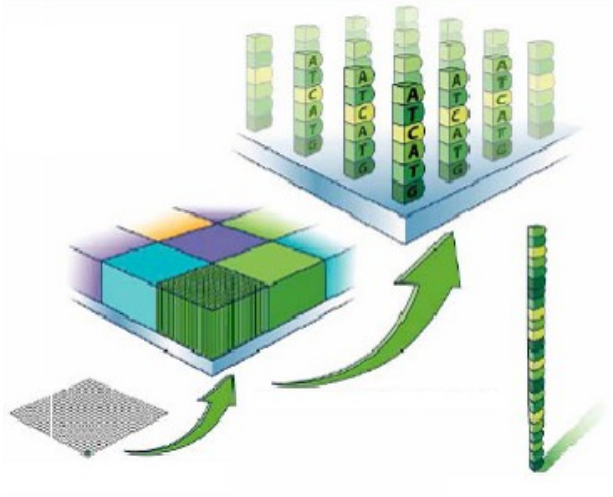

Figure 66 *- Schematic representation of microarrays.*

The microarrays technology is very interesting in biochemistry especially because it can be miniaturized; this feature makes the microarray the best choice to study the interaction between proteins and ligands or to check enzymatic activities in biological unpurified mixtures.

PNAs can represent an useful and advantageous probe, especially for their peculiar chemical, physical and biochemical properties. Different type of PNA based microarrays have been developed, with a variety in terms of its modes of action, especially with respect to detection.[328]

5.2.2 Tools in Molecular Biology

PNAs show good features to be used as new tools in molecular biology. Some example are illustrated in the following sections.

5.2.2.1 PCR

The polymerase chain reaction (PCR) has been widely used for various molecular genetic applications including the amplification of variable number of tandem repeat (VNTR) loci for the purpose of genetic typing.[309] However, in some cases preferential amplification of small allelic products relative to large allelic products may be problematic. This results in an incorrect typing in a heterozygous sample.[329] PNA has been used to achieve an enhanced amplification of VNTR locus D1S80.[330] Small PNA oligomers are used to block the template,

and the latter becomes unavailable for intra- and interstrand interaction during reassociation. On the other hand, the primer extension is not blocked; during this extension, the polymerase displaces the PNA molecules from the template and the primer is extended toward completion of reaction. This approach shows the potential of PNA application for PCR amplification where fragments of different sizes are more accurately and evenly amplified. Since the probability of differential amplification is less, the risk of misclassification is greatly reduced. Misra *et al.* demonstrated that PNA–DNA chimera lacking the true phosphate backbone are capable of acting as primers for polymerase reactions catalyzed by DNA polymerases.[331,332] The chimera $(PNA)_{19}$-TPG-OH, consisting of a 19 base PNA part linked to a single phosphate-containing dinucleotide (TPG-OH) with a free 3'-OH terminus, when annealed with a complementary RNA or DNA template strand works as an efficient primer to catalyze the addition of nucleotide by polymerase enzymes. The primer is also recognized by reverse transcriptase and by the Klenow fragment of *E. coli* DNA polymerase I. The results suggested that the diameter of the duplex region rather than the presence of phosphate backbone of the template primer is the critical factor for a proper template-primer reaction and accommodating the enzyme within the binding domain. It also appears that the primer phosphate backbone may not be essential, at least not in this case, for the polymerase recognition and binding.

5.2.2.2 PNA Hybridization as Alternative to Southern Hybridization

Southern hybridization is perhaps one of the most widely used techniques in molecular biology. Despite its great potential to predict both size and sequence information and information regarding the genetic context, there are certain disadvantages of this process. It requires a laborious multistep washing procedure and sometimes the sequence discrimination between closely related species. PNA pre-gel hybridization simplifies the process of Southern hybridization by reducing the required time, as the cumbersome post separation, probing, and washing steps are eliminated. Labelled (fluoresceinated) PNA oligomers are used as probes and allowed to hybridize to a denatured DNA sample at low ionic strength. The mixture is thereafter subjected directly to electrophoresis for size separation and single stranded DNA fragments separated on the basis of length. The charge-

neutral PNA allows hybridization at low ionic strength and renders higher mobility to the complex, compared to the excess unbound PNA. The DNA-PNA hybrids are blotted (transferred) onto a nylon membrane, dried, UV cross-linked, and detected using standard chemiluminescent techniques.[333] Alternatively, the bound PNA can be detected by using capillary electrophoresis, which uses the direct fluorescence detection method. Under the same conditions, a normal DNA–DNA duplex will tend to disrupt, here as the PNA-DNA duplex will remain intact due o the strong binding of PNA to DNA. This allows specific sequence detection with simultaneous size separation of the target DNA following a simple and straightforward protocol. Consequently, the analysis is much faster than conventional the Southern hybridization technique.[309]

5.2.2.3 PNA-Assisted Rare Cleavage

The DNAs of bacteria have specific sites that are the target of restriction enzymes and methylases. Methylases are particular enzymes that can add a methyl group to a specific DNA site to protect that site against the cutting by some endonucleases.

Peptide nucleic acids, in combination with methylases and other restriction endonucleases, can act as rare genome cutters.[334] The method is called PNA-Assisted Rare Cleavage (PARC) technique. It uses the strong sequence-selective binding of PNAs, preferably bis-PNAs, to short homopyrimidine sites on large DNA molecules, e.g., yeast or λ DNA.[309] The PNA target site is experimentally designed to overlap with the methylation/restriction enzyme site on the DNA, so that a bound PNA molecule will efficiently shield the host site from enzymatic methylation whereas the other unprotected methylation/restriction sites will be methylated. After the removal of bis-PNA, followed by restriction digestions, it is possible to cleave the whole DNA by enzymes into limited number of pieces.[334] DNA is efficiently protected from enzymatic digestion due to methylation in most of the sites except for those previously bound to PNA. Thus, short PNA sequences, particularly positively charged bis-PNAs, in combination with various methylation/restriction enzyme pairs can constitute an extraordinary new class of genome rare cutters.

5.2.2.4 Artificial Restriction Enzyme

S1 nuclease cleaves single-stranded nucleic acids releasing 5'-phosphoryl mono- or oligonucleotides. It removes the single-stranded overhangs of DNA fragments and can be used in RNA transcript mapping and construction of unidirectional deletions. PNA in combination with S1 nuclease can work as an "artificial restriction enzyme" system. Homopyrimidine PNA oligomers hybridize to the complementary targets on dsDNA via a strand invasion mechanism, leading to the formation of looped-out non complementary DNA strands. The enzyme nuclease S1 can degrade this single-stranded DNA part into well defined fragments. If two PNAs are used for this purpose and allowed to bind to two adjacent targets on either the same or opposite DNA strands, it will essentially open up the entire region, making the substrate accessible for the nuclease digestion and thereby increasing the cleavage efficiency.[335]

5.2.2.5 Determination of Telomere Size

The conventional method for the determination of telomere length involves Southern blot analysis of genomic DNA and provides a range for the telomere length of all chromosomes present. The modern approach uses fluorescein-labelled oligonucleotides and monitor *in situ* hybridization to telomeric repeats. However, a more delicate approach resulting in better quantitative results is possible by using fluorescein-labelled PNAs, as shown by Lansdorp *et al*.[336] This PNA-mediated approach permits accurate estimates of telomeric length. *In situ* hybridization of fluorescein-labelled PNA probes to telomeres is faster and requires a lower concentration of the probe compared to its DNA counterpart. Low photobleaching and an excellent signal-to-noise ratio make it possible to quantitate telomeric repeats on individual chromosomes in this way. Experiments suggest that variations of this approach can possibly be applied to other repetitive sequences.

5.2.2.6 Nucleic Acids Purification

Based on its unique hybridization properties, PNAs can also be used to purify target nucleic acids. PNAs carrying six histidine residues have been used to purify target nucleic acids using

nickel affinity chromatography.[337] Also, biotinylated PNAs in combination with streptavidin-coated magnetic beads may be used to purify *Chlamydia trachomatis* genomic DNA directly from urine samples. However, it appears that this simple, fast, and straightforward "purification by hybridization" approach has certain drawbacks. It requires the knowledge of the target sequence and depends on a capture oligomer to be synthesized for each different target nucleic acid. Such target sequences for the short pyrimidine PNA, i.e., the most efficient probe for strand invasion, are prevalent in large nucleic acids. Thus, short PNAs can also be used as generic capture probes for purification of large nucleic acids. It has been shown that a biotintagged PNA-thymine heptamer could be used to efficiently purify human genomic DNA from whole blood by a simple and rapid procedure.[309]

5.2.2.7 Gene Expression Induction

Although most of the focus on PNA applications have revolved around antisense strategies, several groups have studied the ability of PNAs to turn on gene expression. When PNA triplex structures are formed on one strand of the DNA duplex, the opposing DNA strand is displaced to form a D-loop. When sufficiently large, this D-loop resembles a transcriptional bubble or an initiation/elongation loop. Using bacterial and rat spleen-cell nuclear extracts and triplex-forming PNAs that bound to adjacent sites on a DNA template, Møllegaard and colleagues found that transcription was more efficient if two adjacent PNAs were bound to the same strand of DNA, thus giving rise to a 26 base D-loop. In this case, transcript initiation sites mapped to a site just downstream of PNA binding.[338,339]

More recently, the work from the Wang laboratory has extended these findings and has shown that PNAs can be used in cultural cells to activate endogenous gene expression.[340] Using promoter-less GFP reporter constructs containing homopurine PNA target sites just upstream of the GFP initiation codon, Wang was able to demonstrate specific transcriptional initiation in vitro using HeLa cell extracts. In these experiments, designed to explore gene therapy approaches for sikle cell disease and thalassemias, the homopurine target sequence was from the 300 region of the human Gγ-globin promoter. As seen by Møllegaard,[338] transcript start sites mapped to the PNA target site and used the D-loop strand as template. When the PNAs were hybridized to the reporter plasmid under low salt conditions and

microinjected into the nuclei of cells, GFP expression was detected within 20 h of injection. By contrast, no GFP expression was detected in cells microinjected with plasmid alone. Wang also demonstrated that K562 erythroleukemia cells could be efficiently transfected with PNAs using electroporation and inducing the endogenous γ-globin gene threefold over background. Upregulation of γ-globin gene expression, normally suppressed in adults to <1%, can help in the treatment of β-thalassemia disease, in which it may partially act in place of the mutated defective γ-globin. Moreover, this induction was clearly a specific effect of the PNAs since the start sites for the transcripts mapped to both the endogenous promoter and to the PNA binding sites, 300 bp upstream. Thus, despite the presence of physiological salt concentrations and potential chromatin structures, the PNAs were able to bind to their target sites in the chromosome and promote transcription initiation, providing proof of principle for this approach of gene therapy. It is somewhat surprising that γ-globin transcription was induced not only at the PNA binding site, but also from its native promoter region.[340] Probably the transcription of the γ-globin gene from the sequences upstream also makes the native promoter more accessible for RNA polymerase. In the cellular context PNA-mediated arrest of transcription is interpreted as an inability of the transcription machinery to dissociate PNA/DNA or PNA_2/DNA helices, more specifically, by the inability of the DNA helicase to unwind these structures. Indeed, specific studies show that bis-PNAs can significantly reduce DNA unwinding activity of the UL9 helicase.[341,342]

5.2.3 Gene Therapy

Peptide nucleic acids have promise as candidates for gene therapeutic drugs design. They require well identified targets and a well-characterized mechanism for their cellular delivery. In principle, two general strategies can be adapted to design gene therapeutic drugs. Oligonucleotides or their potential analogs are designed to recognize and hybridize to complementary sequences in a particular gene whereby they should interfere with the transcription of that particular gene (antigene strategy, *Figure 67*).

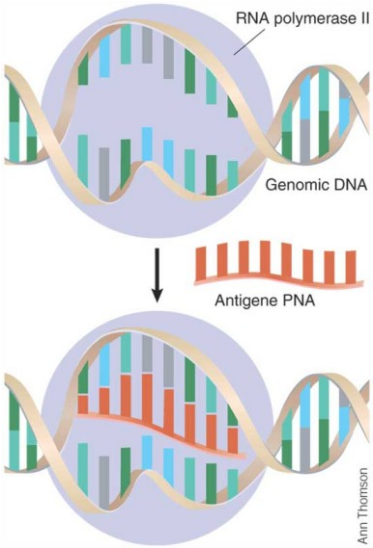

Figure 67 *- Antigene strategy.*

Alternatively, nucleic acid analogs can be designed to recognize and hybridize to complementary sequences in *m*RNA and thereby inhibit its translation (antisense strategy, *Figure 68*). PNAs are chemically and biologically stable molecules and have significant effects on replication, transcription, and translation processes, as revealed from *in vitro* experiments. Moreover, no sign of any general toxicity of PNA has so far been observed.[309]

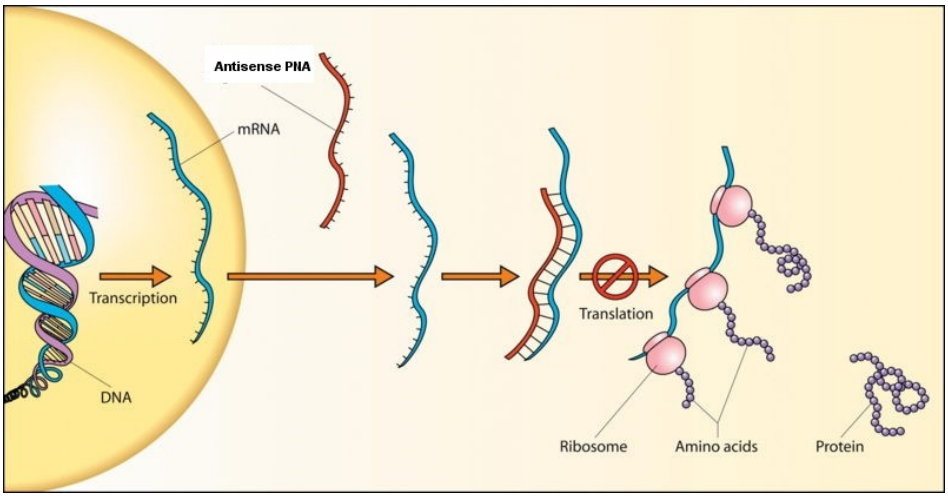

Figure 68 *- Antisense strategy.*

5.2.3.1 Antigene Strategy

Peptide nucleic acids should be capable of arresting transcriptional processes thanks to of their ability to form a stable triplex structure or a strand-invaded or strand displacement complex with DNA. Such complexes can create a structural hindrance to block the stable

function of RNA polymerase and thus are capable of working as antigene agents. Evidence from *in vitro* studies supports the idea that such complexes are indeed capable of affecting the process of transcription involving both prokaryotic and eukaryotic RNA polymerases. PNA targeted against the promoter region can form a stable PNA-DNA complex that restricts the DNA access of the corresponding polymerase. PNA strand displacement complexes, located far downstream from the promoter, can also efficiently block polymerase progression and transcription elongation and thereby produce truncated RNA transcripts; the PNA (DNA poly-purine) target must be present in the gene of interest.[343] Nielsen *et al.* have demonstrated that even an 8-mer PNA (T8) is capable of blocking phage T3 polymerase activity.[344] The presence of a PNA target within the promoter region of IL-2Ra gene has been used to understand the effect of PNA binding to its target on this gene expression.[345,346] The PNA_2/DNA triplex arrests transcription *in vitro* and it is capable of acting as an antigene agent. Unfortunately one of the major obstacles to use PNA as an antigene agent is that the strand invasion or the formation of strand displacement complex is rather slow at physiological salt concentrations.[347] Several modifications of PNA have shown improvements in terms of binding. Modifications of PNA by chemically linking the ends of the Watson-Crick and Hoogsteen PNA strands to each other, introducing pH-independent pseudoisocytosines into the Hoogsteen strand,[348] incorporating intercalators,[349] or positively charged lysine residues[348,350] in PNA strands can drastically increase the association rates with dsDNA. Lee *et al.* have demonstrated that PNA, as well as the PNA-DNA chimera, complementary to the primary site of the HIV-I genome can completely block priming by tRNA3Lys.[351] Consequently, *in vitro* initiation of the reverse transcription by HIV-1 RT is blocked. Thus, oligomeric PNAs targeted to various critical regions of the viral genome are likely to have a strong therapeutic potential for interrupting multiple steps involved in the replication of HIV-1.[351] It has been found that under physiological salt conditions, binding of PNA to supercoiled plasmid DNA is faster compared to linear DNA.[350] This result is relevant to the fact that the transcriptionally active chromosomal DNA usually is negatively supercoiled, so it can be better target for PNA binding *in vivo*. It has also been found that the binding of PNA to dsDNA is enhanced when the DNA is being transcribed. This transcription-mediated PNA binding occurs about threefold as efficiently when the PNA target is situated on the non-

template strand instead of the template strand. As transcription mediates template strand-associated $(PNA)_2$/DNA complexes, which can arrest further elongation, the action of RNA polymerase results in repression of its own activity, i.e., suicide transcription.[352] These findings are highly relevant for the possible future use of PNA as an antigene agent. We wish to refer to reports describing the ability of PNA to activate transcription, although this is not actually related to its antigene effect. Møllegaard *et al.*[338] have efficiently demonstrated that the looped-out single-stranded structure formed as a result of strand invasion is also capable of acting as efficient initiation sites for *Escherichia coli* and mammalian RNA polymerases in which the polymerase might start transcription using the single-stranded loop as a template.[346] This is consistent with the affinity of RNA polymerase for single-stranded DNA and its ability to transcribe single-stranded DNA.

The nuclear localisation signal (NLS) of SV40 has been shown to translocate 17-mer anti-myc PNA over the plasma membrane into the cytosol and further convey into nuclei of Burkitt's lymphoma derived cell-lines. A 17-mer antigene PNA, that is complementary to a unique sequence located at the start of the second exon of c-myc, was delivered into BRG and BJAB cells by both NLS peptide and peptide with a scrambled NLS sequence. However, the nuclear transport of PNA was achieved only with a PKKKRKV peptide that corresponds to the active/wild type NLS (NLSwt).[353] Inside the nuclei the rhodamine-labelled PNA-NLS was visualised as a small number of highly fluorescing bright spots associated with clumped chromatin material. Twenty four hours after application of 10 μM antimyc NLSwt-PNA constructs, MYC expression was inhibited by 75% and cell viability decreased by 25%, respectively. MYC expression in treated cells decreased progressively and after 72 h the protein concentration was below the level of detection. The level of myc *m*RNA was reduced by 35% after 7 h of treatment and by 60% after 18 h, suggesting that MYC expression was also inhibited at the level of transcription. However, reduction of protein concentration upon PNA-NLSwt construct treatment seems to slightly precede the decrease in the *m*RNA concentration. This discrepancy can be explained by general difficulties in quantifying exactly the Western and Northern blot analyses. On the other hand, this hints that antimyc PNA-NLSwt acts not only on a transcriptional, but on a translational level as well.

The potential applicability of receptor mediated intracellular translocation of PNA (from cytosol into the nucleus) was demonstrated in prostatic carcinoma cells. Dihydrotestosterone coupled to anti-gene PNA induced nuclear uptake in LNCaP cells that express the androgen receptor gene (AR), but not in DU145 cells where its receptor gene is silent. The cellular/cytoplasmic uptake of rhodamine labelled antimyc PNA is, however, detectable in both cell-lines, but in DU145 cells the uptake is strictly cytoplasmic only.[354] Coupling of dihydrotestosterone adds hydrophobicity to PNA oligomer molecules and that seems to facilitate the uptake of PNA by cells, as compared to unmodified PNA.

5.2.3.2 Antisense Strategy

In the antisense strategy the target of the PNA strand is the *m*RNA (instead the antigene where the target is the DNA double strand). The basic mechanism of the antisense effect by oligodeoxynucleotides is considered to be either a ribonuclease H (RNase H) mediated cleavage of the RNA strand in oligonucleotide-RNA heteroduplex or a steric blockage in the oligonucleotide-RNA complex of the translation machinery.[355] Oligodeoxynucleotide analogs such as phosphorothioates activate RNase H and thus hold promise of working as antisense agents.[356] However, they also exhibit some non-specificity in their action. PNA/RNA duplexes, on the other hand, cannot act as substrates for RNase H. Normally, the peptide nucleic acid antisense effect is based on the steric blocking of either RNA processing, transport into cytoplasm, or translation. It has been concluded from the results of *in vitro* translation experiments involving rabbit reticulocyte lysates that both duplex- (mixed sequence) and triplex-forming (pyrimidine-rich) PNAs are capable of inhibiting translation at targets overlapping the AUG start codon.[355] Triplex-forming PNAs are able to hinder the translation machinery at targets in the coding region of mRNA. However, the translation elongation arrest requires a $(PNA)_2$–RNA triplex and thus needs a homopurine target of 10-15 bases. In contrast, duplex-forming PNAs are incapable of doing the same. Triplex-forming PNAs can inhibit translation at initiation codon targets and ribosome elongation at codon region targets.

Mologni *et al.* showed effects of three different types of antisense on the *in vitro* expression of PML/RARα gene.[357] The first one was complementary to the first AUG (initiation) site. The

second could bind to a sequence in the coding region that includes the second AUG, the starting site for the synthesis of an active protein. The third PNA was targeted against the 59-untranslated region (UTR) of the *m*RNA, the point of assembly of the translation machinery. Together, these three PNAs could efficiently inhibit translation even at a concentration much below the critical concentration used for each individual. The result suggests that the PNA targeting of RNA molecules like PML/RARα requires the effective blocking of different sequences on the 59 part of the messenger. A 59-UTR PNA target can also be used as efficiently as an initiation (AUG) target to achieve an antisense activity of PNA, and a more effective translation inhibition can be achieved by combining PNA directed toward 59-UTR and AUG regions.

Triple helix-forming PNAs can also hinder the translation process. Bis-PNA or clamp-PNA structures are capable of forming internal triple helical constructs. In principle, if targeted against the coding region of *m*RNA, PNA_2/RNA triple helix-forming derivatives can also cause a stop in translation, which can be easily verified by the detection of a truncated protein.[355] However, this methodology requires a sequence optimization for each new target. Recent studies show that *E. coli* cells are somewhat permeable for PNA molecules. Good and Nielsen [358,359] have shown that it is possible to achieve PNA antisense effects in the 'leaky' mutant strains of *E. coli*. PNAs targeted against the AUG region of the *m*RNA corresponding to β-galactosidase and β-lactamase genes were indeed capable of down-regulating the expression of these two genes.[358] Another study demonstrated the effect of two bis-PNAs, targeted against the homopurine stretches in *r*RNA, either in the peptidyl transferase center or in the α-sarcin loop, in inhibiting the ribosome function in a cell-free system.[359] The translation was arrested at submicromolar range of PNA concentration. The growth of a mutant strain of *E. coli*, namely, AS19, was also inhibited by using the same PNAs at low micromolar concentration.

5.2.3.3 Inhibition of Replication

It is also possible by using PNA to inhibit the elongation of DNA primers by DNA polymerase. Further, the inhibition of DNA replication should be possible if the DNA duplex is subjected to strand invasion by PNA under physiological conditions or if the DNA is single stranded

during the replication process. Efficient inhibition of extrachromosomal mitochondrial DNA, which is largely single-stranded during replication, has been demonstrated by Taylor *et al*.[360] The PNA-mediated inhibition of the replication of mutant human mitochondrial DNA is a novel (and also potential) approach toward the treatment of patients suffering from ailments related to the heteroplasmy of mitochondrial DNA. Here wild-type and mutated DNA are both present in the same cell. Experiments have shown that PNA is capable of inhibiting the replication of mutated DNA under physiological conditions without affecting the wild-type DNA in mitochondria.

5.2.3.4 Interaction of PNA with enzymes

It was observed that PNAs are able to interact with several enzymes.

5.2.3.4.1 RNase H

Despite their remarkable nucleic acid binding properties, PNAs are not generally capable of stimulating RNase H activity on duplex formation with RNA. However, recent studies have shown that DNA/PNA chimeras are capable of stimulating RNase H activity. On formation of a chimeric RNA double strand, PNA/DNA can activate the RNA cleavage activity of RNase H. Cleavage occurs at the ribonucleotide parts basepaired to the DNA part of the chimera. Moreover, this cleavage is sequence specific in such a way that certain sequences of DNA/PNA chimeras are preferred over others.[361] They are also reported to be taken up by cells to a similar extent as corresponding oligonucleotides. Thus, PNA/DNA chimeras appear by far the best potential candidates for antisense PNA constructs.

5.2.3.4.2 Polymerase and reverse transcriptase

In general, there is no direct interaction of PNA with either DNA polymerase or reverse transcriptase. However, different groups have shown indirect involvement of PNA in inhibiting these enzyme functions (activity) under *in vitro* conditions. For example, PNA oligomers are capable of terminating the elongation of oligonucleotide primers by either binding to the template strand or directly competing with the primer for binding to the template. Primer extension by MMLV reverse transcriptase has been shown to be inhibited

by introducing a PNA oligomer.[345] In another experiment, Nielsen *et al.*[362]demonstrated that the primer extension catalyzed by *Taq*-polymerase can be terminated by incorporating a PNA oligomer (PNA-H(t)10) into the system. The latter can bind to a (dA)10 sequence in the template and thereby terminate the primer extension. Moreover, uncharged PNA primers with only a single 59-amino-29,59-dideoxynucleoside at the carboxyl terminus can be recognized by the Klenow fragment for DNA pol I and VentDNA polymerase (*Thermococcus litoralis*), and a linear amplification is possible with the use of an excess of PNA-DNA primer and suitable thermostable polymerases.[363] Moreover, the reverse transcription of *gag* gene of HIV I is also inhibited *in vitro* by PNAs.[364] The inhibition has been achieved by using a bis-PNA construct, which is more efficient than the corresponding mono PNA construct.[357] Also, the reverse transcription can be completely inhibited by a pentadecameric antisense PNA, using a molar ratio of 10:1 (PNA/RNA), without any noticeable RNase H cleavage of the RNA.[364]

5.2.3.4.3 Telomerase

Human telomerase, a ribonucleoprotein complex consisting of a protein with DNA polymerase activity and an RNA component, synthesizes $(TTAGGG)_n$ repeats at the 39 end of DNA strands. PNA oligomers that are complementary to the RNA primer binding site can inhibit the telomerase activity. Studies have shown that the telomerase inhibition activity of PNA is better than that of corresponding activity of phosphorothioate oligonucleotides. This is mainly due to a higher binding affinity of PNA compared to phosphorothioates.[365] Corey and co-workers have demonstrated an efficient inhibition of telomerase after lipid-mediated delivery of template- and nontemplate- directed PNA into the cell.[366]

5.2.3.5 Mutagen Action of PNA

One consequence of the tight binding of triplex-forming oligonucleotides and PNAs to cellular homopurine DNA targets is that they can induce DNA repair pathways within the cell. Thus, the PNA_2/DNA complex can be interpreted by the cell to be a DNA lesion in need of repair. One possible outcome of this is the production of site-specific mutants at, or proximal to, the site of PNA binding.[367] Faruqi ad co-workers reported that PNAs with

binding affinities of around 10^{-7} M were able to be taken up by streptolysin-O permeabilized murine fibroblast, bind to their target sites within SupF1 reporter gene integrated into the genome, and induce point mutations or single base deletions or insertions in the target sequence or within 5 bp of the site.[368]

The frequency of mutagenesis observed with the PNAs was $8x10^{-4}$, compared to a background mutagenesis frequency of $9x10^{-5}$. Similar results have been obtained with tightly binding triplex-forming phosphorothioates, leading to the prediction that triplex complexes in general can induce transcription-coupled DNA repair pathways.[369] Presently, this mutagenic capacity is being developed as a technique to selectively mutagenize and repair single point mutations that are crucial in certain genetic diseases, including sickle cell disease.[339]

5.3 Modified PNAs

The major limitations of the therapeutic applications of PNAs are their poor solubility in aqueous media due to self-aggregation and an insufficient cellular uptake. In order to improve PNA solubility in aqueous media, the cellular uptake, the binding selectivity towards RNA versus DNA, or to stabilise duplex or triplex structures, several analogues have been synthesised over the years.[370]

5.3.1 PNAs with Modified Nucleobases

Inhibition of gene expression by antisense or antigene approaches relies on the formation of stable duplex and triplex structures.[371,372] In this context, the use of modified nucleobases represents an obvious way to control recognition between nucleic acids. The non-standard nucleobases employed so far with PNA are limited, compared with the repertoire of backbone modifications described. Structures of nucleobase-modified PNA are illustrated in *Figure 69*.

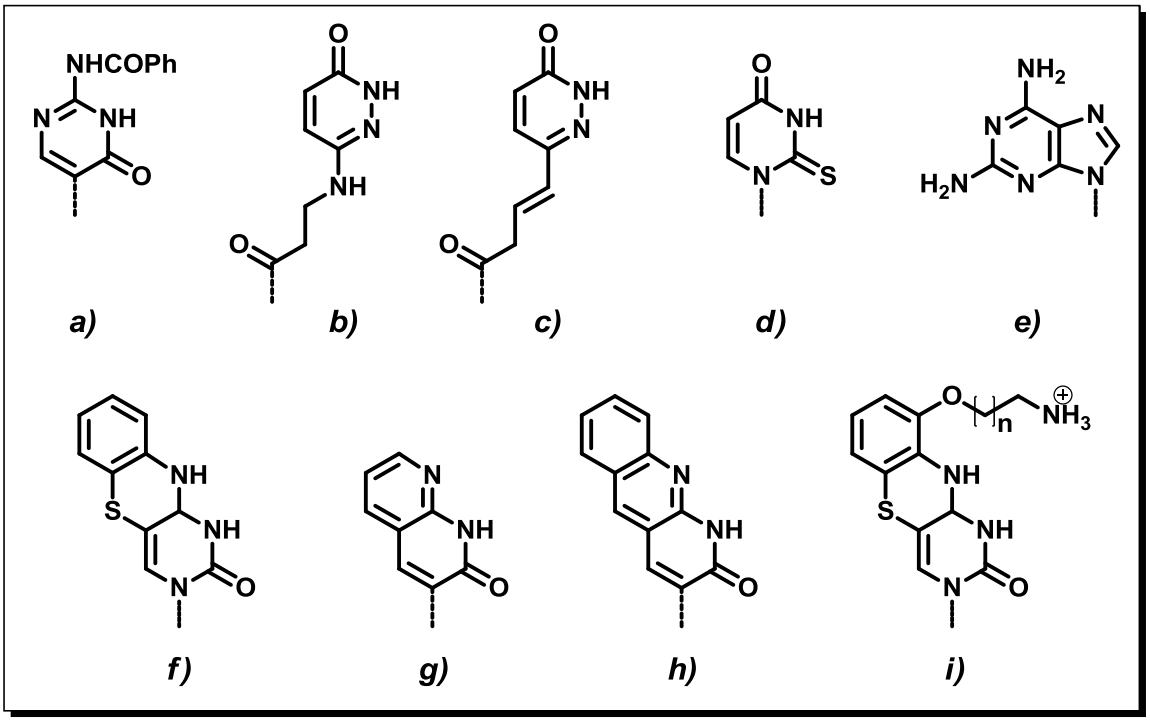

Figure 69 *- Structures of nucleobase-modified PNA.*

Substitution of natural bases for analogues can be used for interfering with the hybridization process; for example, N^4-benzoyl cytosine (*Figure 69a*) has been shown to cause inhibition of triplex formation, whereas E-base (*Figure 69b*), rationally designed to recognise T-A base pair, stabilises a triplex even when the target strand contains one or two pyrimidine residues.[373,374] In fact, triplex formation is generally restricted to oligopurine strands whereas a substantial destabilisation is observed when pyrimidine residues are introduced. However, the binding affinity of E•T-A triplet is far from optimal, which might partially be due to excessive flexibility of the linker between the backbone and the nucleobase. In order to address the issue of flexibility, a conformationally constrained E-base analogue (*Figure 69c*), was synthesised.[375] Surprisingly, no improvement was found, a result that could mean that local flexibility has only little influence on the thermodynamics of oligonucleotide hybridization. As said, 2-Thiouracil (*Figure 69d*) along with 2,6-diaminopurine (*Figure 69e*) was used as a non-natural base pair in PNA-DNA recognition and was shown, for the first time, to lead to a phenomenon termed as "double duplex invasion". Pyrimidines which have extended aromatic moieties as a means of increasing the stacking energy and hence the stability of the hybridized complexes represent another class of modified nucleobases.

Incorporation of tricyclic phenothiazine (*Figure 69f*) as a substitute for cytosine and bicyclic/tricyclic naphthyridinones (*Figure 69g-h*) as substitutes for thymine showed a modest affinity increase, whereas tricyclic cytosine analogues based on the phenoxazine gave the highest increase in affinity and sequence specificity towards targets.[376] This result demonstrates that factors other than mere molecular stacking overlap, such as electronic factors, contribute to base pair stacking stabilities.

Interesting modification on nucleobases have also been carried out to yield fluorescent PNA monomers and oligomers (*Figure 70*).

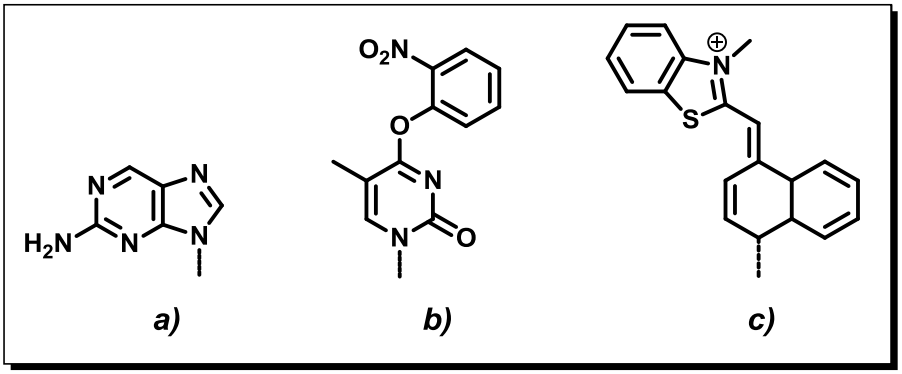

Figure 70 *- Structures of fluorescent nucleobase-modified PNA.*

2-Aminopurine, being intrinsically fluorescent, can be used to study PNA-DNA interaction dynamics.[377] O^4-(*o*-nitrophenyl)thymine (*Figure 70b*) PNA monomer was reported as valuable intermediate for the introduction of fluorescent compounds into PNA oligomers.[378] Thiazole orange (*Figure 70c*) is the first base to fulfill the demands desired for a fluorescent universal base.[379] Thanks to its remarkable base stacking ability, it pairs well against all four canonical DNA bases maintaining duplex stability. In addition to this, the sensitivity of its fluorescence to a neighbouring base mismatch, it is suitable for homogeneous single-nucleotide-polymorphism detection.[380]

5.3.2 PNAs with Modified Backbone

Since the first report of *aeg*PNA, many research groups have started the synthesis of backbone modified peptide nucleic acids in order to improve or modify the chemico-physical properties, in particular the solubility, and the binding affinity of classical PNA.

Improvement of the aqueous solubility of PNAs has been achieved by the introduction of charges in the molecule, or by the introduction of ether linkages in the backbone. PNAs are endowed of positive charges by linking a terminal lysine residue[381] (*Figure 71a*), by the introduction of a positive charge in the backbone, or by replacing the acetamide linker to the nucleobase by a flexible ethylene linker (*Figure 71b*).[382]

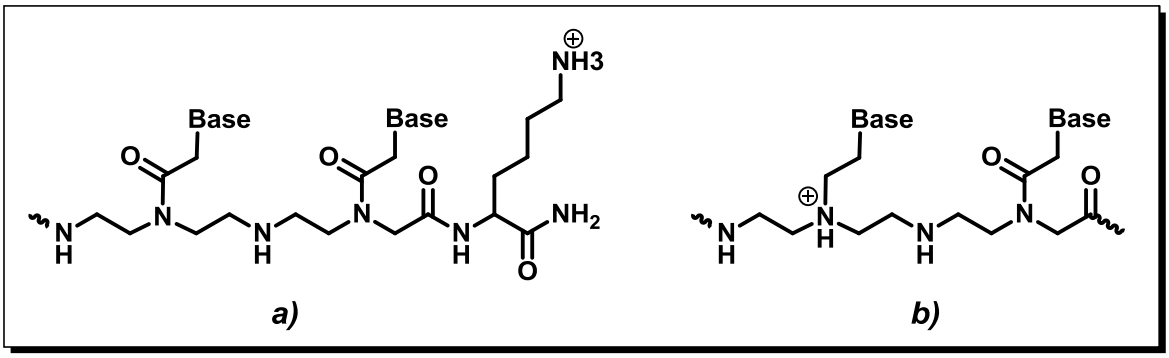

Figure 71 *- Positively charged modified backbone.*

Cationic guanidinium linkages (*Figure 72*) have also recently been introduced into PNA and were found to improve its binding affinity with complementary nucleic acid sequences.[383]

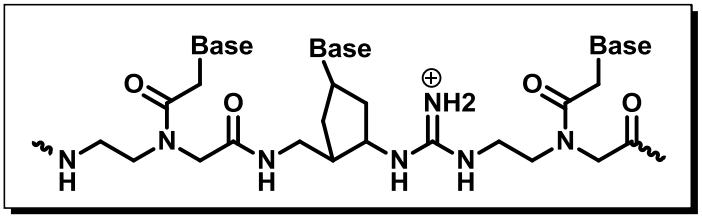

Figure 72 *- Positively charged guanidinium modified backbone.*

Making the PNA anionic also aided in increasing its water-solubility as in the case of the phosphonate analogues (*Figure 73*), but was accompanied by a decrease in the binding affinity to complementary nucleic acid sequences.[384]

Efimov *et al*.[384a] have described the synthesis of homopyrimidine pPNA oligomers containing *N*-(2-hydroxyethyl)phosphonoglycine (pPNA-O), or *N*-(2-aminoethyl)phosphono glycine (pPNA-N). These oligomers did form complexes with complementary DNA/RNA, but with a much lower stability than PNA.

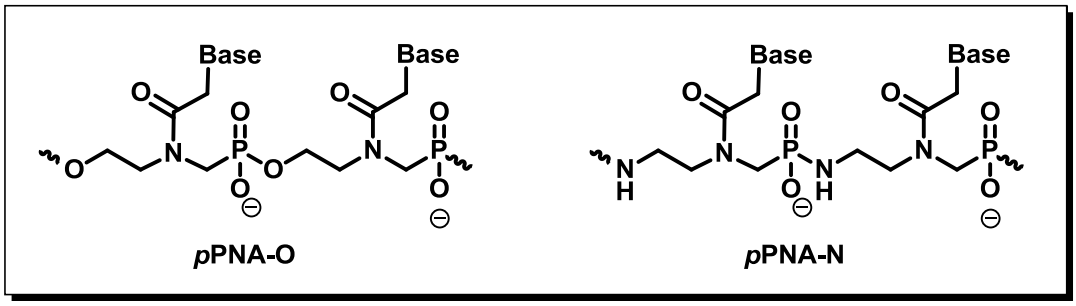

Figure 73 *- Anionic charged modified backbone.*

Increased water solubility was also achieved by putting an ether linkage in the PNA backbone (*Figure 74*).[385]

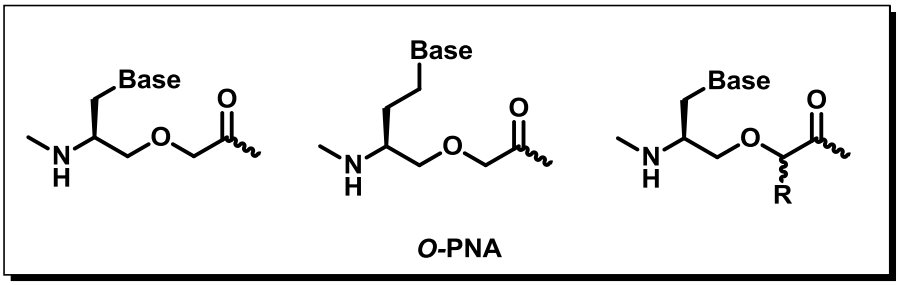

Figure 74 *- O-ether modified backbone.*

In the attempt to make the backbone rigid, alkyl and cyclic substituents have been introduced.[386] 3-, 5- and 6-member rings have been appended in various position of the backbone. The rationale behind the design of such constrained PNA is to obtain a preorganised structure with high selectivity in the binding of DNA/RNA. As the presence of rotamers around the tertiary amide bond in *aeg*PNA interferes with the hybridization process, it was postulated that connecting the nucleobase to the cycle inhibits the rotation, overcoming the problem of the rotamers. Examples of conformationally blocked PNA (*Figure 75*) are represented by the aminoprolyl PNA (ap-PNA), aminoethylprolyl PNA (aep-PNA), aminoethylpyrrolidinone PNA (aepone-PNA), pyrrolidine PNA, cyclopropane (cpr), cyclopentyl (cp) and cyclohexyl (ch) PNA.

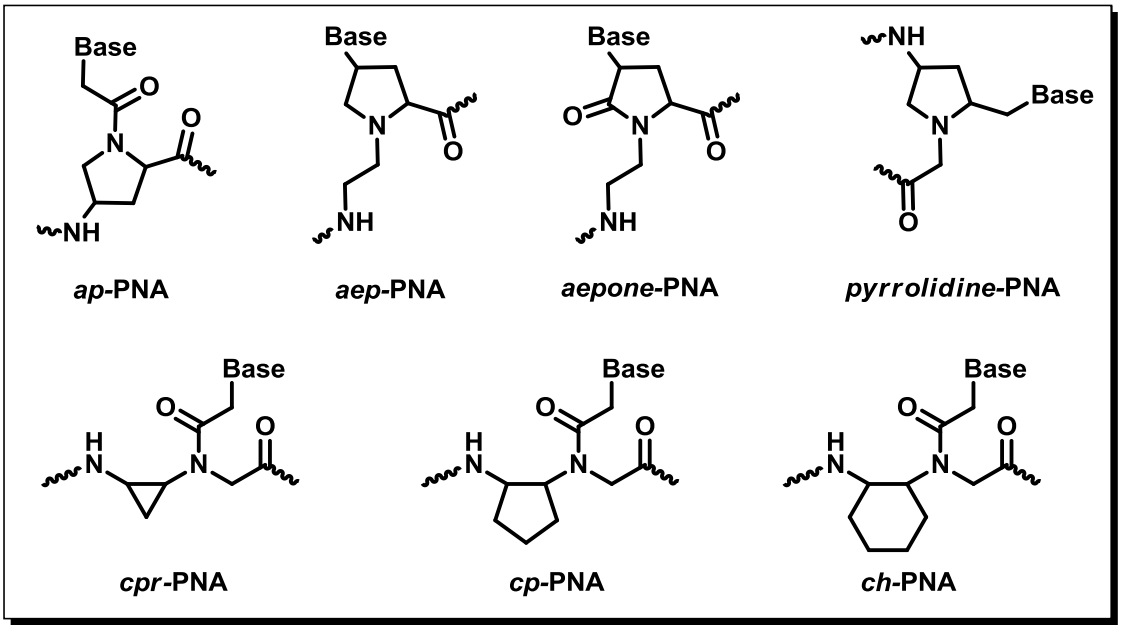

Figure 75 *- Rigid modified backbone.*

Introduction of a single *ap*-PNA in a PNA sequence results in a stabilisation of the PNA/DNA duplex, whereas homothymine *ap*-PNA do not bind to the target sequence; stereochemistry affects the preference for parallel or antiparallel binding.[387] *Aep*-PNAs are obtained protecting the hydroxyproline carboxyl as an ester, derivatising the nitrogen with an ethylamine moiety and then replacing the OH with the nucleobase. These derivatives bear a positive charge; homothymine decamer binds polyadenilic acid to form 2:1 hybrids, with high affinity and specificity. When hybridized to DNA, they show higher affinity for the antiparallel hybridization than for the parallel.[388] *Aepone*-PNAs also stabilise formation of triple helical structures with DNA partners, while destabilise triplexes formed with polyA.[389] (2*R*,4*S*) *Pyrrolidine*-PNA oligomers form very stable hybrids with complementary DNA and RNA; protonation of the nitrogen does not affect the stability of the hybrids. On the contrary, (2*S*,4*S*) isomers do not stabilise the formation of hybrids with DNA and RNA.[390] *Cp*-PNAs show higher affinity towards RNA than DNA; the (*1*R,2*S*) enantiomers form higher affinity complexes with DNA than the (1*S*,2*R*) enantiomers. Both stabilise PNA_2:DNA and PNA_2:RNA triplexes.[391] Cyclohexyl PNAs were synthesized in the forms (1*S*,2*S*), (1*R*,2*R*), (1*S*,2*R*), (1*R*,2*S*); although the presence of *S*,*S* isomers does not affect the thermal stability of DNA and RNA hybrids, introduction of *R*,*R* isomers results in a destabilisation of the

PNA/DNA or RNA complexes. PNA including the (1*R*,2*S*) isomer exhibits higher hybrid stability and ability to discriminate between DNA and RNA.[392]

5.3.3 PNAs with Fluorescent Probes

The introduction of fluorescent probes in biomolecules may constitute a valuable tool to study their structures and biological activity, opening the possibility to design new fluorescent bioactive molecules that can exploit their peculiar properties for diagnostics or therapeutic applications. For more than thirty years, the conjugation of fluorescent markers to DNA or proteins have been successfully applied and more recently also with PNAs.

In literature are now reported different examples of fluorescent PNAs and their cellular up-take, as well as their capability to hybridize specific DNA or RNA sequences, have been widely studied.

The introduction of a fluorescent molecule in the PNA oligomer can be achieved or by classical reaction in solution, or by solid phase reactions while the oligomer is still attached to the resin support.

In 1996 Kremsky *et al.*[393] reported the functionalization of PNA oligomers with biotin and a fluorescein derivative, with the aim to set up a synthetic protocol to support specific markers in solid phase synthesis.

Fluorescein is one of the most used fluorescent probe and finds wide applications in bioanalytical chemistry,[394] molecular biology and pharmacokinetic studies.[395]

As shown in *Figure 76*, fluorescein itself cannot be directly used in solid phase synthesis (SPS), while its derivatives bearing a carboxylic group are suitable for classical peptide bond formation.

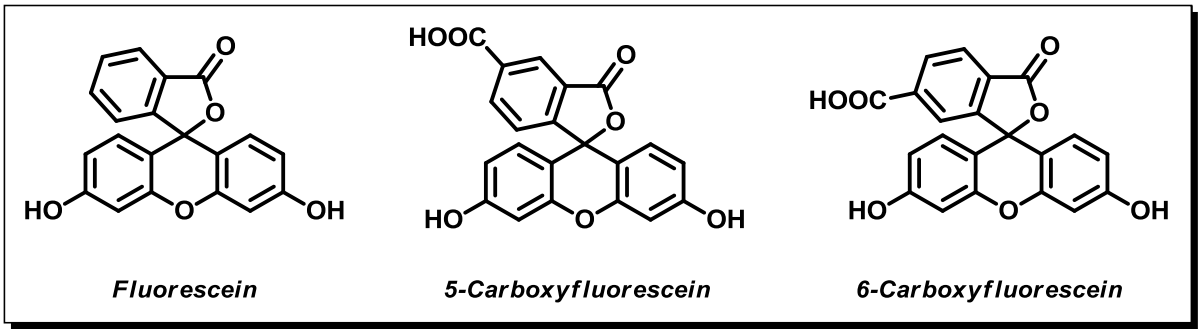

Figure 76 *- Fluorescein and its carboxy-derivatives.*

Carboxyfluorescein derivatives, as pure isomer, are commercially available but are quite expensive; thus a mixture of the two isomers 5- and 6- carboxyfluorescein (61:39) were practically used in SPS.[396]

It's also commercially available the isothiocyanate derivative (FITC, *Figure 77*), that allows the outstanding reaction with free amino groups, by formation of stable thiourea bond.

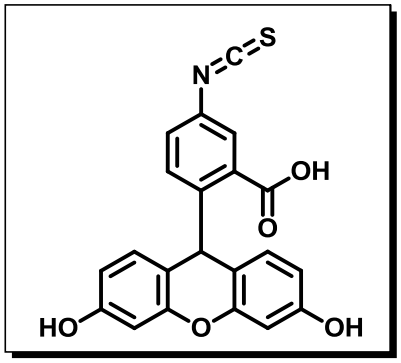

Figure 77 *- Fluorescein isothiocyanate (FITC).*

In molecular biology, also rhodamine and its derivatives were widely used, as an alternative to fluorescein (*Figure 78*).

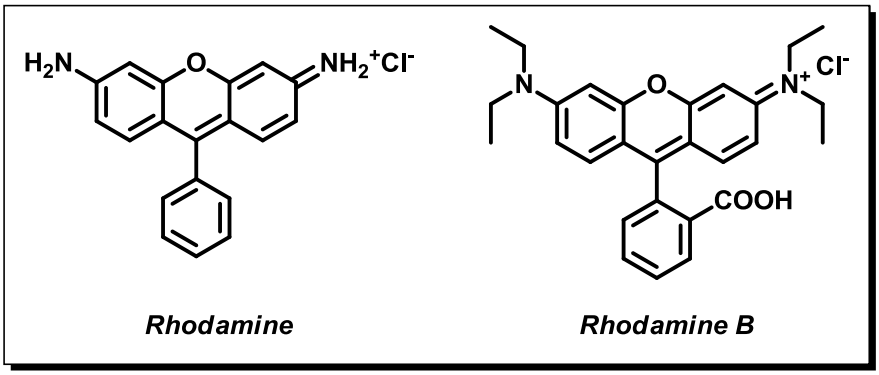

Figure 78 *- Rhodamine and rhodamine B.*

More recently, Englund *et al*[397]. have introduced in the PNA backbone a lysine-based monomer, exploiting the terminal *ε*-amino group to bind the 9-fluorenacetic acid as a fluorescent probe.

5.4 PNA Oligomers Synthesis

Thanks to their pseudopeptide backbone, PNA monomers can be assembled using synthetic methods developed for the peptide synthesis both in solid phase or in solution. Different synthetic strategies have been reported in the literature, but the most used are based on:

- ✓ Boc/Cbz protected monomers (*Figure 79*);
- ✓ Fmoc/Bhoc protected monomers.

In our laboratories the first strategy is routinely used for the synthesis of PNA oligomers, both by manual as automated SPS, starting from commercially available *aeg*A, *aeg*C and *aeg*G monomers, while *aeg*T one is generally synthesized by ourselves.

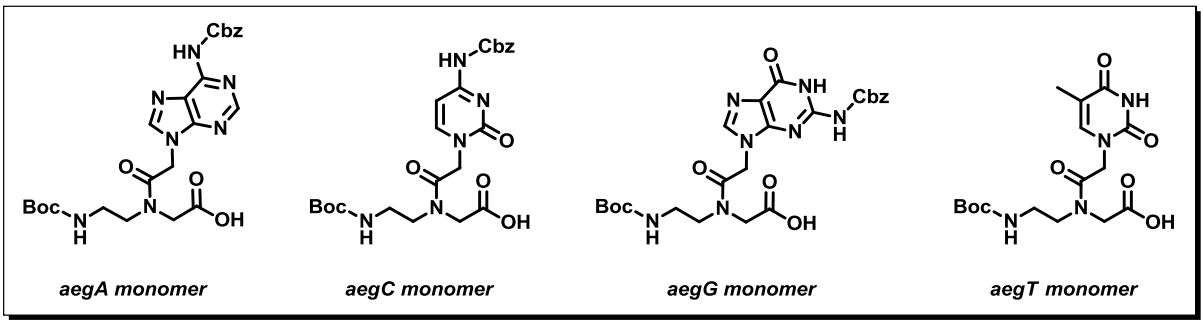

Figure 79 *- Aminoethylglycine A, C, G and T monomers with Boc/Cbz protections.*

The solid support is usually functionalized polystyrene with a cleavable linker. The choice of the linker is very important and depends on the protecting group strategy used. For the Boc/Cbz strategy, the best support is the MBHA resin (*Figure 80a*), in which the acid labile linker can be cleaved with a mixture of trifluoroacetic and trifluoromethanesulfonic acid. In the Fmoc/Bhoc strategy, an acid labile linker can be used, for example the RinkAmide (*Figure 80b*), but best results in the Fmoc chemistry are achieved using a polyethylene glycol derivatized polystyrene resin (PEG-PS) that provides a "solution like" environment for the synthesis. The typical linkers used with this resin are the XAL or PAL linkers (*Figure 80c* and *d*).

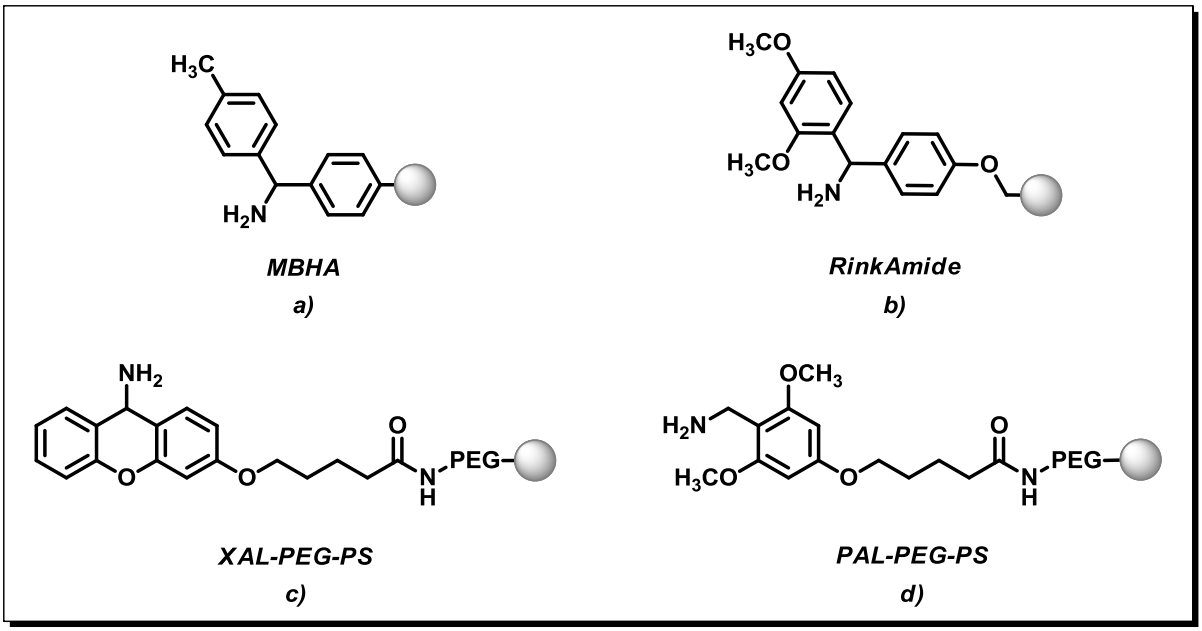

Figure 80 *- Most used solid phase supports for the synthesis of PNAs.*

Independently from the strategy, the solid phase oligomers synthesis (*Scheme 14*) proceeds with the following standard synthetic steps:

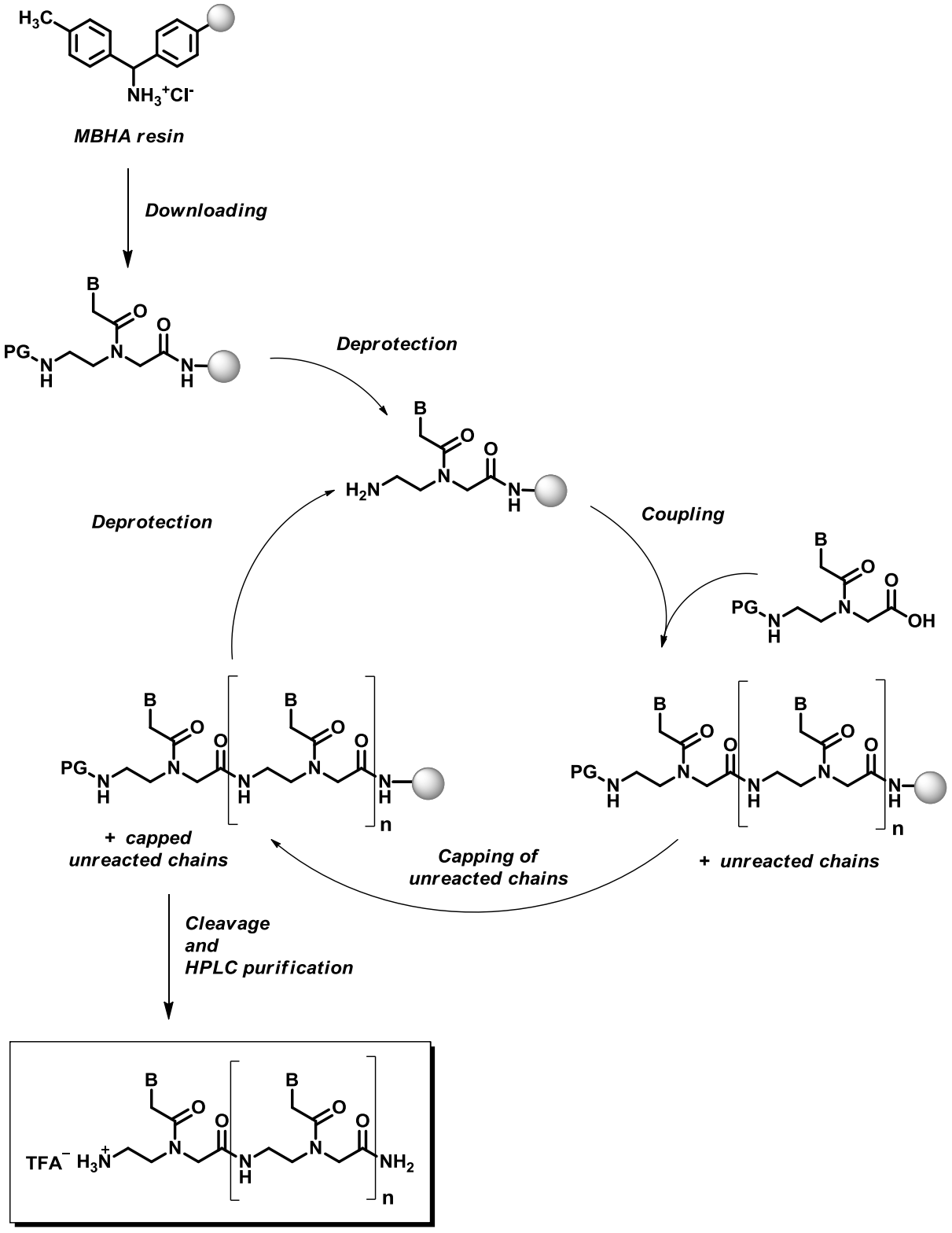

Scheme 14 *- Cyclic synthetic protocol for the SPS of PNA oligomers.*

- ✓ ***Downloading**:* this step consists in the coupling of the first monomer or a properly protected-amino acid (*e.g.* PG_1-Lysine-*Nε*-PG_2, generally used to improve the solubility in water of the final oligomer), to the resin. This reaction is performed using a smaller amount of the monomer with respect to the loading of the resin, in order to avoid the interaction among the oligomer chains on a bead. A typical loading used in the PNA oligomers synthesis is 0,2 mmol/g.

- ✓ ***Deprotection:*** to built the oligomer is necessary to remove the protecting group on the PNA monomer (or amino acid) attached on the resin. For the Boc/Cbz strategy, the Boc group is removed using trifluoroacetic acid (TFA) in presence of *m*-cresol (ratio 95:5). The *m*-cresol was added to function as a scavenger for the *tert*-butyl cations in order to avoid alkylation of the nucleobases.

- ✓ ***Coupling:*** this step is the key step of the chain elongation. Using typical condensing agent (HBTU or HATU gave best results) the carboxylic acid function of a monomer is coupled with the amino group of the monomer attached on the resin and previously deprotected.

- ✓ ***Capping**:* this step is performed in order to avoid that unreacted amino groups can react in the next coupling steps giving mistaken sequence that are more difficult to purify. The preferred capping reagent is acetic anhydride, which reacts very fast with the free amino groups.

Once the oligomer synthesis is completed, the chain is cleaved using the more appropriate reagent (for MBHA resin, TFA and trifluoromethanesulfonic acid -TFMSA- mixture in presence of *m*-cresol and thioanisole). Usually, in the final cleavage also the protecting group of the exocyclic amino moieties of the nucleobases are removed. At last, semipreparative HPLC purification were done to isolate the desired PNA oligomer.

As mentioned above, HBTU and HATU gave the highest coupling yields in PNA synthesis. However, uronium salts react with primary amines to form guanidinium salts, and this

reaction has been shown to cap free α-amines in peptide synthesis efficiently. The capped products are easily identified by mass spectroscopy by the presence of M+100 masses. The higher pKa value of the 2-ethylamine in PNA and the fact that it is less steric hindered makes PNA monomers even more prone to this reaction (*Scheme 15*). Therefore, pre-activation of the monomers and a slight excess or monomer over HATU are employed in the protocol.

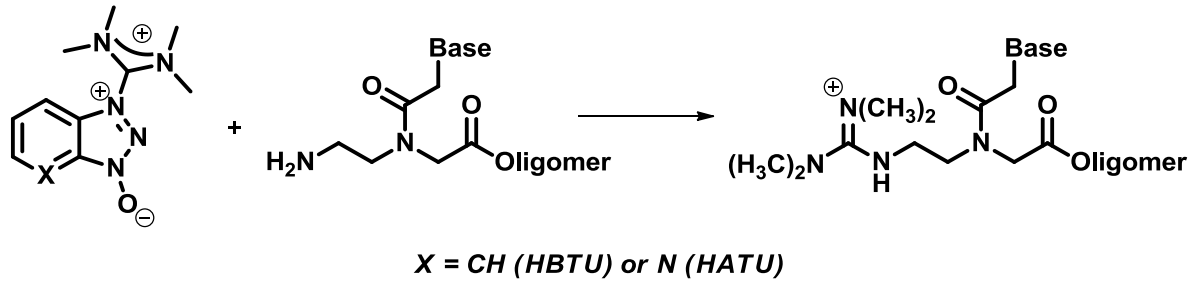

X = CH (HBTU) or N (HATU)

Scheme 15 *- Side reaction between condensing agent and aegPNA monomer.*

5.5 Binding Affinity Evaluation of PNAs

Like other non-covalent structures, the DNA complexes (duplex or triplex) are unstable at high temperatures. When the temperature is increased gradually, this process of heat denaturation, also called melting, begins in areas with a high A-T content. A-T base pairs can be separated more easily than G-C base pairs. The ***Melting Temperature*** (***Tm***) is defined as the temperature at which half of the DNA strands are in the double-helical state and half are in the single strand states (*Figure 81*).

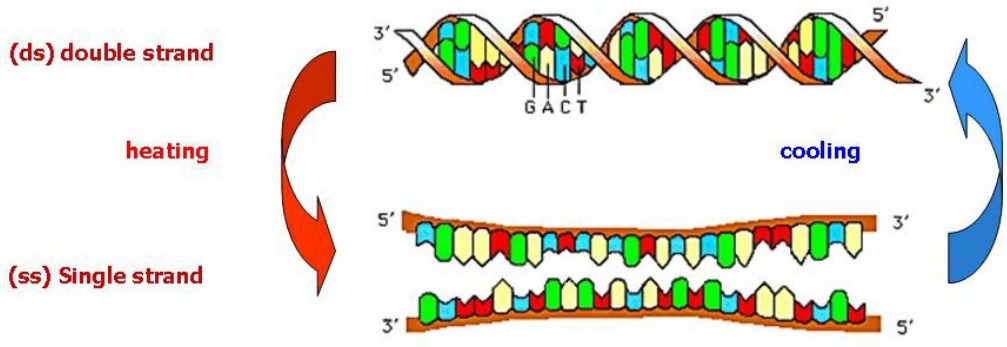

Figure 81 *- Thermal denaturation process of dsDNA.*

The best ways to determine the melting temperature and to evaluate the PNA/DNA interactions are by spectroscopic techniques, as described in the following paragraph, or by Differential Scanning Calorimetry (DSC).

5.5.1 Spectroscopic Techniques for Studying PNA/DNA Interactions

Monitoring the UV absorption at 260 nm as a function of temperature has been extensively used to study the thermal stability of nucleic acid systems and consequently, PNA/DNA hybrids as well. Increasing the temperature perturbs this system, inducing a structural transition by causing disruption of hydrogen bonds between the base-pairs, diminished stacking between adjacent nucleobases, and larger torsional motions in the backbone leading to a loss of secondary and tertiary structure. This is evidenced by an increase in the UV absorption at 260nm, termed as 'hyperchromicity'. The magnitude of hyperchromicity is a measure of the extent of the secondary structure present in nucleic acids. The process is cooperative and the plot of the absorbance at 260 nm *versus* the temperature is sigmoidal and the inflexion point corresponds to the ***Tm*** (F*igure 82*). This also represents a two-state "all or none" model for nucleic acid melting, i.e. the nucleic acids exist in only two states, either as duplexes or as single strands and at varying temperatures, the relative proportions change. A non-sigmoidal (e.g., linear) transition with low hyperchromicity is a consequence of non-duplexation (non-complementation). In many cases, the transitions are broad and the exact ***Tm*** are obtained from the peak in the first derivative plots. This technique has provided valuable information regarding complementary interactions in nucleic acid hybrids involving DNA, RNA and PNA. Generally homothymine PNAs (*aeg*$[T]_{10}$-PNA) binds complementary DNA (with formation of a triplex) with strong affinity, as demonstrate from its ***Tm*** of 72 °C, while standard sequence PNAs (*aeg*[STD]-PNA) form stable duplex with natural nucleic acid with a ***Tm*** of 53 °C.[398]

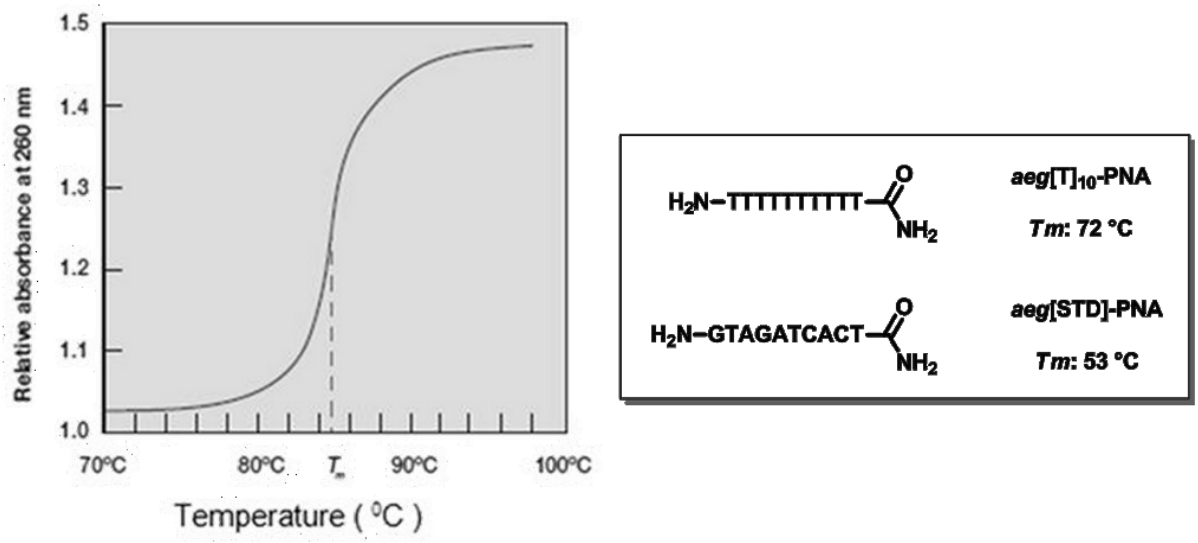

Figure 82 *- Example of thermal denaturation plot and Tm values for reference PNAs reported in literature.*

5.6 Magnetic Peptide Nucleic Acids

Peptide Nucleic Acids (PNAs), as we have already seen, are mimics of natural oligonucleotides, in which each ribose phosphate unit is replaced by an aminoethylglycine unit. PNAs bind complementary DNA and RNA strands with an excellent affinity and sequence specificity due to the absence of electrostatic interference of their neutral chain with polyanionic backbone oligonucleotide. In addition, PNAs exhibit greater mismatch selectivity and chemical and enzymatic stability compared to natural oligonucleotides. All of these features have attracted significant interest, which has arisen in view of their potential in gene diagnosis and therapy. However, the first generation of PNAs suffers from some drawbacks, which hamper the full exploitation of them in gene therapy, including low cell uptake and some low solubility in physiological media. To overcome these problems, and to improve their physical-chemical properties, many modified PNAs have been synthesized in recent years following different strategies as previously reported. Along with the recent advances in DNA technology, the integration with nanostructured systems is expected to improve PNA properties and applicabilities.

In this context, superparamagnetic iron oxide nanoparticles attracted our attention because of their unique magnetic properties, which can be controlled rigorously and activated easily

by applying an external magnetic field. In most cases, specific surface biofunctionalization is required for the successful utilization of SPIONs in biomedicine. In several instances, single-stranded DNA was successfully supported on magnetic nanoparticles and tested in hybridization experiments and single-nucleotide polymorphism analysis.[399] In contrast, PNAs have been seldom considered and, to our knowledge, only two examples have been reported so far. In the first study, PNA was connected to the γ-Fe_2O_3 nanoparticles by exploiting the largely adopted thiol chemistry. Hybridization and mismatch experiments with ssDNA were conducted by surface-enhanced Raman scattering (SERS).[400] More recently, the synthesis of gold coated cobalt ferrite nanoparticles functionalized with thiol-PNAs was reported.[401] However, we are aware that the interest in SPION-PNA nanoconjugate could spread well beyond this preliminary information, eventually conditioning the potential of PNA in biology and medicine. Several PNA applications, which are characteristic of DNA technology, would benefit from such an innovation, including cell uptake and site-directed delivery, control and tunability of the degree of PNA loading on nanoparticle surface, size and morphology of nanoconjugates, and rapid and reliable assessment of DNA hybridization by T_2 relaxation measurements complemented by conventional determination of the melting temperature of hybrids.

In our laboratories, we discovered a versatile, effective synthetic platform for the development of monomer and decamer PNA nanoconjugates, starting from synthetic PNA and nanometer-sized maghemite.[277] Some SPION-PNA nanoconjugates have been already synthesized and their structures are reported in *Figure 83*.[402] The sequence-selective DNA recognition and sequestration ability of the resulting SPION-PNA were assessed according to their capability of enhancing the T_2 relaxation response in aqueous solutions under conventional hybridization conditions with complementary DNA.[277]

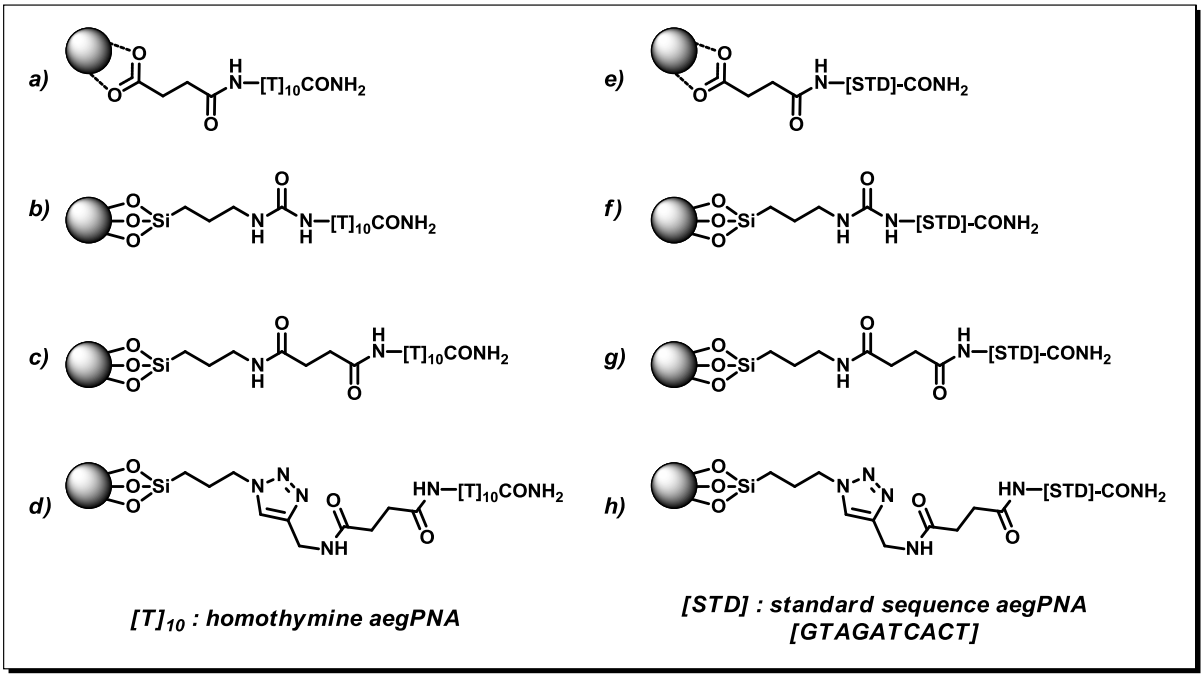

Figure 83 *- Library of SPION-PNA nanoconjugates that have been already synthesized in our laboratories.*

As generally reported in literature, two main decamers were used as reference compounds: a homothymine ***[T]$_{10}$*** and a so called standard sequence ***[STD]*** PNAs. The standard sequence has the characteristic to present all the four nucleobases in the oligomer. The repeating *aeg*PNA monomer units are shown in *Figure 84*.

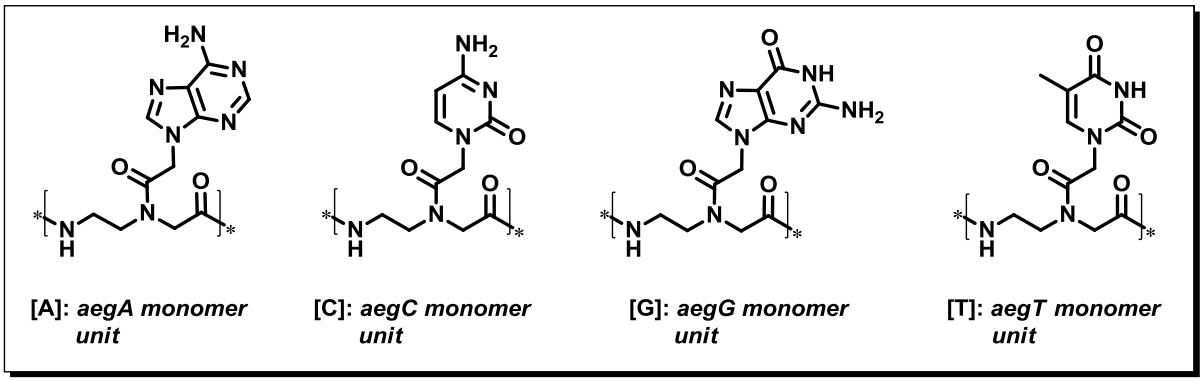

Figure 84 *- Repeating aegPNA monomer units.*

The current strategies to anchor PNAs onto SPIONs can involve passive non-covalent adsorption on the outer particle surface (by a carboxylate group for instance, *Figure 83a* and *e*) or the formation of a more stable covalent bond by using appropriate linkers between the

nanoparticles and the biomolecule (e.g. by sylilation reaction, *Figure 83b-d* and *f-h*). These surface functionalization methodologies have been already widely explained in *Chapter 4*.

All these nanoconjugates demonstrated to be able to bind with strong affinity the complementary DNA, regardless of the presence of the SPIONs. Melting temperature where determined confirming the value reported in literature for the same PNA oligomers non-grafted onto nanoparticle surface.

One of the main drawback of PNAs is their low solubility in physiological media and, as explained before *[see section 5.1.4]*, one solution consists in the introduction of positive charges thanks to the presence of lysine residues in the oligomeric chain.

In previous research works, [403] we were able to synthesize new modified PNAs bearing one or more lysine residues at the *C*-terminus; these oligomers show higher solubility in water than the corresponding non-modified PNAs (*Figure 85a-e*). At the same way, we investigate the solubility of $[T]_{10}$ and *[STD]* PNAs anchored onto SPIONs (*Figure 85f* and *g*). As expected, the solubility of the nanosystems is lower than the corresponding non-supported decamers, but are very promising values, if we consider the presence of the magnetic metallic core. The introduction of lysine residues has so demonstrated to be a simple and very efficient tool to overcome solubility problems.

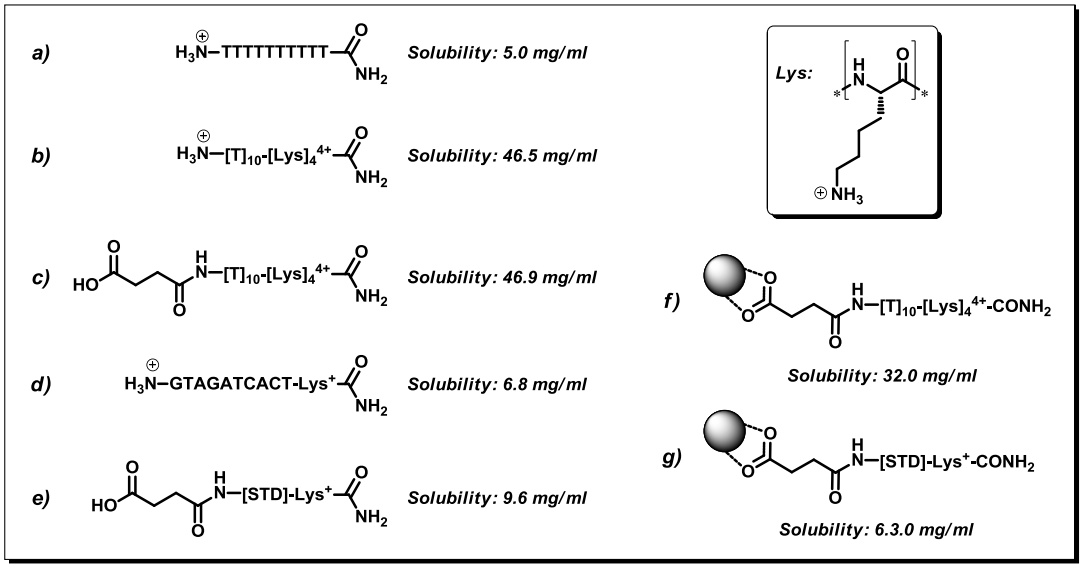

Figure 85 *- Solubility of some homothymine and standard sequence PNAs in water. Positive charges derive from strong acidic cleavage condition (TFA/TFMSA mixture).*

5.7 New Fluorescent Magnetic PNAs

As reported in *section 5.3.3*, the introduction of fluorescent probes in PNAs may be a powerful tool to study their structures and biological activity, as well as to employ them in diagnostics.

In this Ph.D. Thesis we decided to synthesize new fluorescent PNA nanoconjugates that combine the presence of a magnetic metallic core, PNA strands and a fluorescent probe.

For this purpose we synthesized the two new nanoconjugates **36** and **37**, reported in *Figure 86*, in which a homothymine and a standard sequence decamers were modified with a succinic linker at the *N*-terminus and with a lysine at the *C*-terminus. The free carboxylic moiety can be exploited to bind in a non-covalent interaction the SPION surface, while the *ε*-free amino group of the lysine residue can be used to bind the fluorescent probe, in this case the fluorescein isothiocyanate (FITC, *Figure 77*), leading to the formation of the corresponding thiourea (FITU, *Figure 86*).

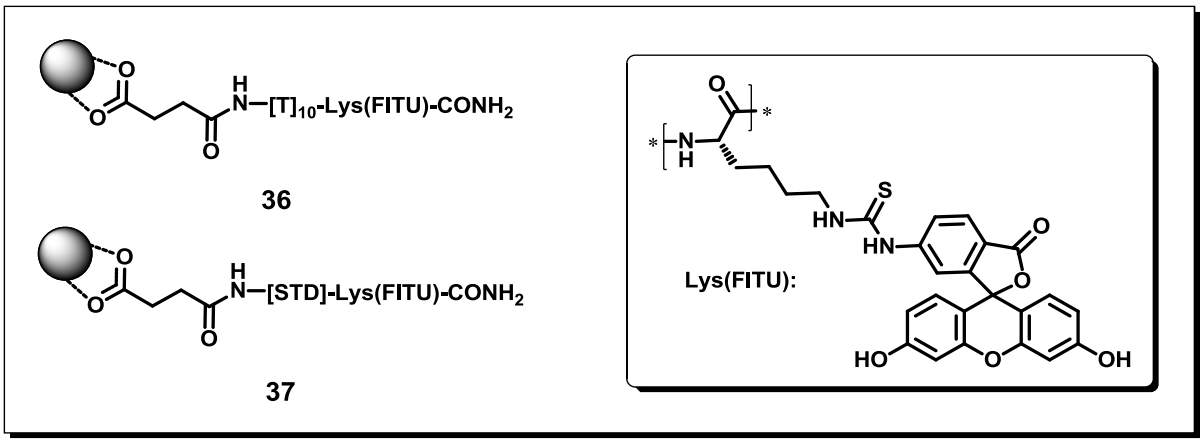

Figure 86 *- New fluorescent PNA nanoconjugates* **36** *and* **37**.

The synthetic protocol for the synthesis of **36** and **37** is reported in *Scheme 16*.

The MBHA resin was manually downloaded with the *N(α)*-Boc-*N(ε)*-Fmoc-*L*-lysine in order to obtain the functionalized resin **38** with a final loading of 0.2 mmol/g. Then, automated solid phase synthesis with Boc strategy was conducted on a peptide synthesizer "ABI 433A", according to Apllied Biosystems ABI 433A peptide synthesis 3 ml reactor vessel user's

manual. Boc-deprotection, coupling and capping reactions were cyclically performed, till the desired PNA oligomers were obtained. Manual Boc-deprotection of the *N*-terminus was achieved, affording the supported PNAs **39** and **40**, that after neutralization with DIPEA were coupled with succinic anhydride. PNAs **41** and **42**, endowed with the succinic linker, undergo Fmoc-deprotection of the *ε*-lysine amino group and then were directly reacted on solid phase with fluorescein isothiocyanate (FITC), leading to the formation of the corresponding fluorescein isothiourea derivatives (FITU). After total cleavage from the resin and HPLC purification, PNAs **43** and **44** were supported onto SPIONs by formation of a non-covalent interaction. Nanoconjugates **36** and **37** were isolated and characterized by E.A., FTIR and UV-Vis spectroscopy to confirm the grafting of the fluorescent PNAs onto the nanoparticles surface. Furthermore, to confirm the ability of **36** and **37** to recognize and bind complementary DNA, the melting temperature ***Tm*** of the hybrids formed were determined.

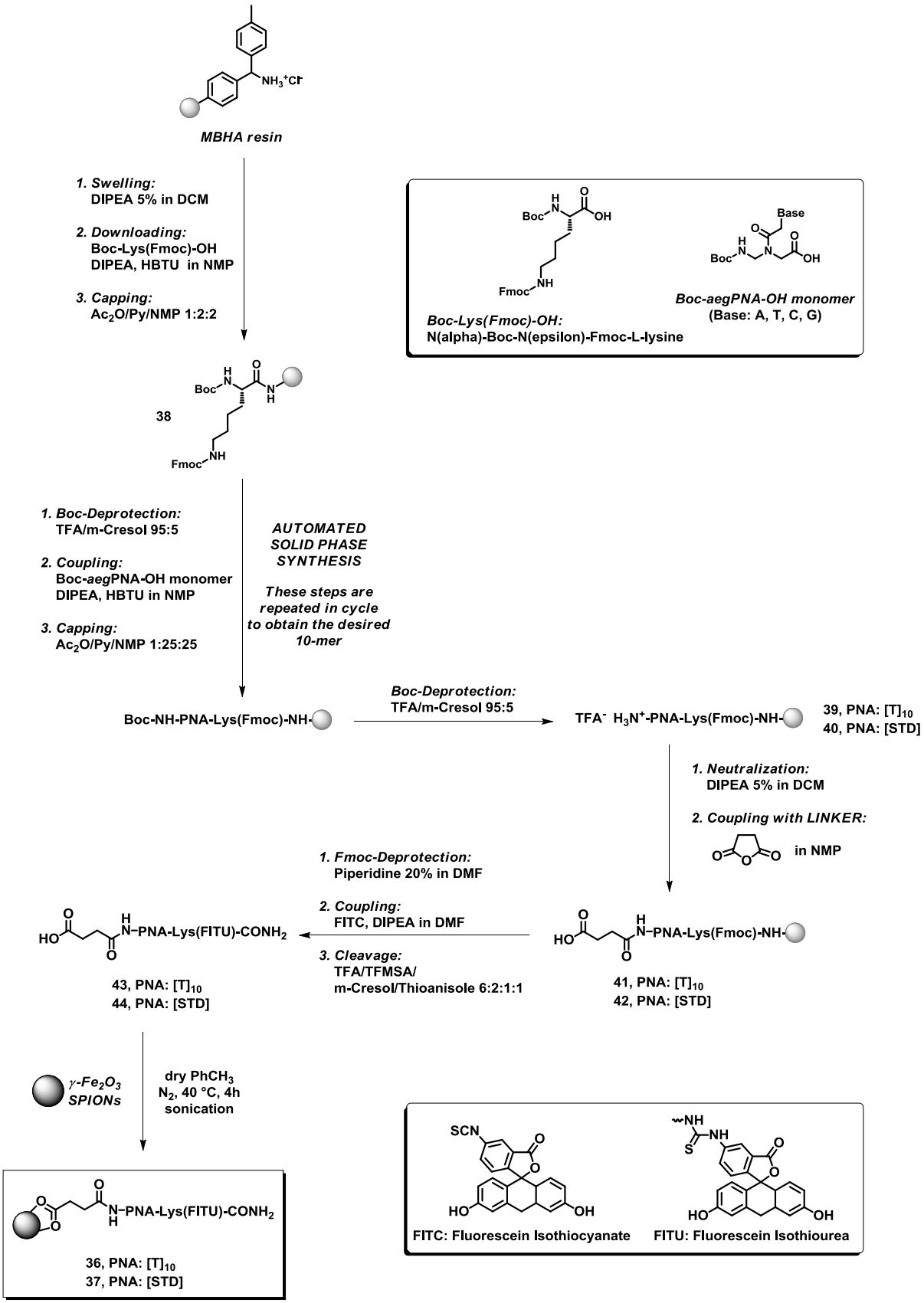

Scheme 16 *- Synthesis of new fluorescent PNA nanoconjugates* **36** *and* **37**.

5.7.1 Determination of the Final Loading of Nanoconjugate **36** *and* **37**

As previously mentioned in *section 4.2.1*, from E.A. is possible to obtain important information about the quantity of organic molecules adsorbed onto the SPIONs surface. In an analogous way, **36** and **37** were analyzed by E.A. and the corresponding loadings were determined (*Table 11*).

Nanoconjugate	***Loading***		
	Tot % org	*mmol/g_{NPs}*	*N°$_{molecules}$/NP*
36	14.08	0.042	≈ 80
37	26.78	0.080	≈ 170

Table 11 *- Loading of nanoconjugates* **36** *and* **37***.*

In the case of bionanoconjugates could be quite interesting to know how many bioactive molecules are grafted onto a single nanoparticle. So, in order to determine the number of organic molecules *per* one nanoparticle, a calculation method was set up starting from two main approximation: i) the nanoparticles must be considered completely composed by iron (III) oxide and ii) the nanoparticles have a uniform spherical shape.

Commercially available SPIONs used in this work have a dimension of 10±2 nm of diameter and given density for Fe_2O_3 is 4.90×10^6 g/m^3. Thus, the volume of a single SPION is 5.24×10^{-25} m^3 and its mass corresponds to 2.57×10^{-18} g.

E.A. gives us the total percentage in weight of the organic part loaded onto SPIONs *[Tot % org]*, from which is possible to determine the mass of a single nanoconjugate using the following equation:

$$Mass_{nanoconjugate}[g] = \frac{Mass_{nanoparticle}[2.57 \cdot 10^{-18} g]}{1 - \frac{Tot\ \%\ org}{100}}$$

Then, knowing the mass of a single nanoconjugate and the mass of a single naked nanoparticle, we can calculate the mass of the organic part loaded onto the SPION:

$$Mass_{organic\ part}[g] = Mass_{nanoconjugate}[g] - Mass_{nanoparticle}[2.57 \cdot 10^{-18} g]$$

At last, the approximate number of organic molecules loaded onto a single SPION can be obtained from the following equation, in which *MW* is the molecular weight of the organic molecule and N_A the Avogadro number (6.023x10^{23} molecules/mol):

$$Loading\left[\frac{N°_{molecules}}{NP}\right] = \frac{Mass_{organic\ part}[g]}{MW\left[{}^{g}/_{mol}\right]} \cdot N_A \left[6.023 \cdot 10^{23} \frac{N°_{molecules}}{mol}\right]$$

In this way was possible to calculate the number of PNA strands on each SPION and the results are reported in *Table 11*.

5.7.2 FTIR Characterization of 36 *and* 37

FTIR spectroscopy has demonstrated to be a powerful tool to verify the effective grafting of organic molecules onto SPIONs. So, nanoconjugates **36** and **37** were analyzed in transmittance mode (blank KBr) and the spectra obtained are here reported in *Figure 87* and *Figure 88*, respectively.

In both spectra are clearly visible the main vibrational modes referred to the presence of PNA strands grafted onto the nanoparticle surface; in particular are shown the strong broad band at high wavenumber related to the FeO-H and N-H stretchings, the peaks in range 2970-2930 cm^{-1} of aliphatic C-H stretchings, the strong band referred to C=O vibrational modes (1678 and 1658 cm^{-1}, respectively) and the characteristic absorption of Fe-O bonds at low frequencies.

Thanks to this technique we were able to confirm the effective grafting of homothymine and standard sequence PNAs onto SPIONs.

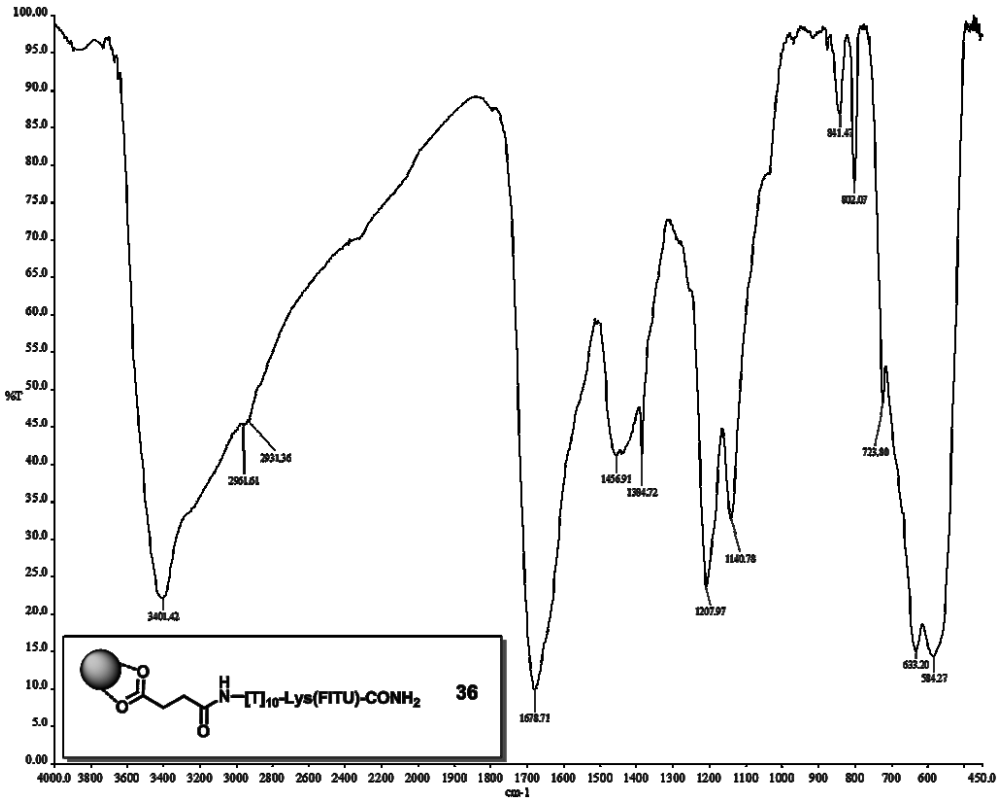

Figure 87 *- FTIR spectrum of nanoconjugate* **36**.

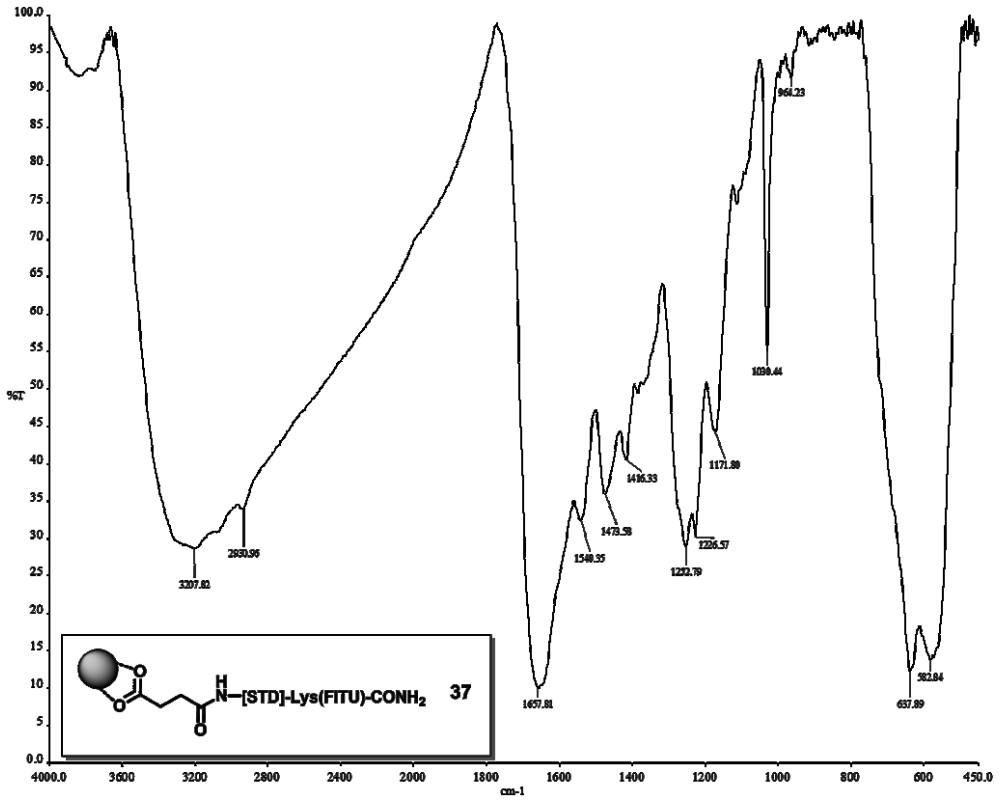

Figure 88 *- FTIR spectrum of nanoconjugate* **37**.

5.7.3 UV-Vis Spectroscopy Characterization

Naked SPIONs in diluted aqueous solution (the dilution serves to prevent the precipitation of nanoparticles), under UV-Vis irradiation in the range of 200-800 nm, are not able to absorb the incident light and, as results, scattering phenomena occur. This is clearly visible from the UV-VIS spectrum of naked SPIONs, reported in *Figure 89a* (*black line*), in which the interference scattering signal is recorded.

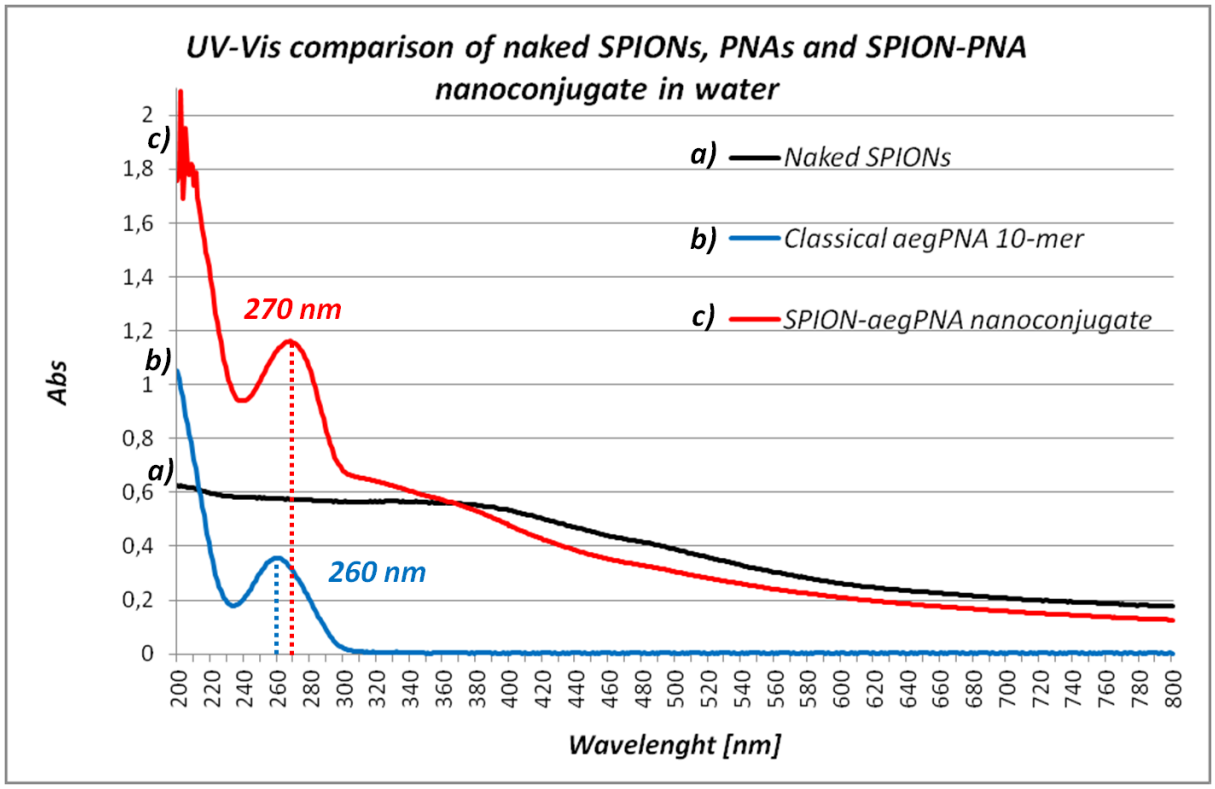

Figure 89 *- UV-Vis spectra of a) naked SPIONs (black line), b) a classical aegPNA decamer (blue line) and c) a SPION-PNA nanoconjugate (red line) in water.*

The classical 4 nucleobases (A, T, C and G) have a characteristic absorption at 260 nm, and their extinction coefficients are the following:

- ✓ $\varepsilon_{[260\ nm]}$ Adenine: 13.7 $mM^{-1}cm^{-1}$;
- ✓ $\varepsilon_{[260\ nm]}$ Cytosine: 6.6 $mM^{-1}cm^{-1}$;
- ✓ $\varepsilon_{[260\ nm]}$ Guanine: 11.7 $mM^{-1}cm^{-1}$;
- ✓ $\varepsilon_{[260\ nm]}$Thymine: 8.6 $mM^{-1}cm^{-1}$.

Thus, PNAs have a strong absorption peak centered at 260 nm (*Figure 89b, blue line*) and their extinction coefficients can be calculated as the arithmetic sum of those of the individual bases that comprise the oligomeric chains:

- ✓ $\varepsilon_{[260\ nm]}$ homothymine PNA (***[T]$_{10}$***): 86 $mM^{-1}cm^{-1}$;
- ✓ $\varepsilon_{[260\ nm]}$ standard sequence PNA (***[STD]***, GTAGATCACT): 101.78 $mM^{-1}cm^{-1}$.

When a strong "UV-Vis active" molecule is loaded onto the nanoparticle surface, its characteristic absorption peaks can be clearly visible despite of the presence of the nanoparticles scattering. In *Figure 89c* (*red line*), the UV-Vis spectrum of a SPION-PNA nanoconjugate is compared with naked SPIONs and free PNAs UV-Vis absorptions in water solution. A slight diagnostic bathochromic effect of 10 nm was detected when PNA oligomers are grafted onto SPIONs (maximum absorption at ca. 270 nm).

PNAs **36** and **37** were so characterized by UV-Vis spectroscopy, considering that in addition they bear a fluorescein moiety with a strong visible absorption at about 500 nm.

To do this, few milligrams of nanoconjugates were diluted in distilled water and the saturated solutions, after different cycles of vortex/sonication, were decanted for at least one hour leaving to precipitate the large aggregates. The upper suspensions were then collected for UV-Vis analysis.

The results obtained for nanoconjugates **36** and **37**, are shown in *Figure 90* and *91*, respectively.

In both cases, beyond the scattering of nanoparticles in suspension, clearly comes out the absorption peak at about 270 nm typical of the PNA oligomers that, once loaded onto SPIONs show the bathochromic shift of ca. 10 nm; while at about 500 nm a peak related to the fluorescein molecule is also present. These data confirm the formation of the fluorescent SPION-PNA nanoconjugates.

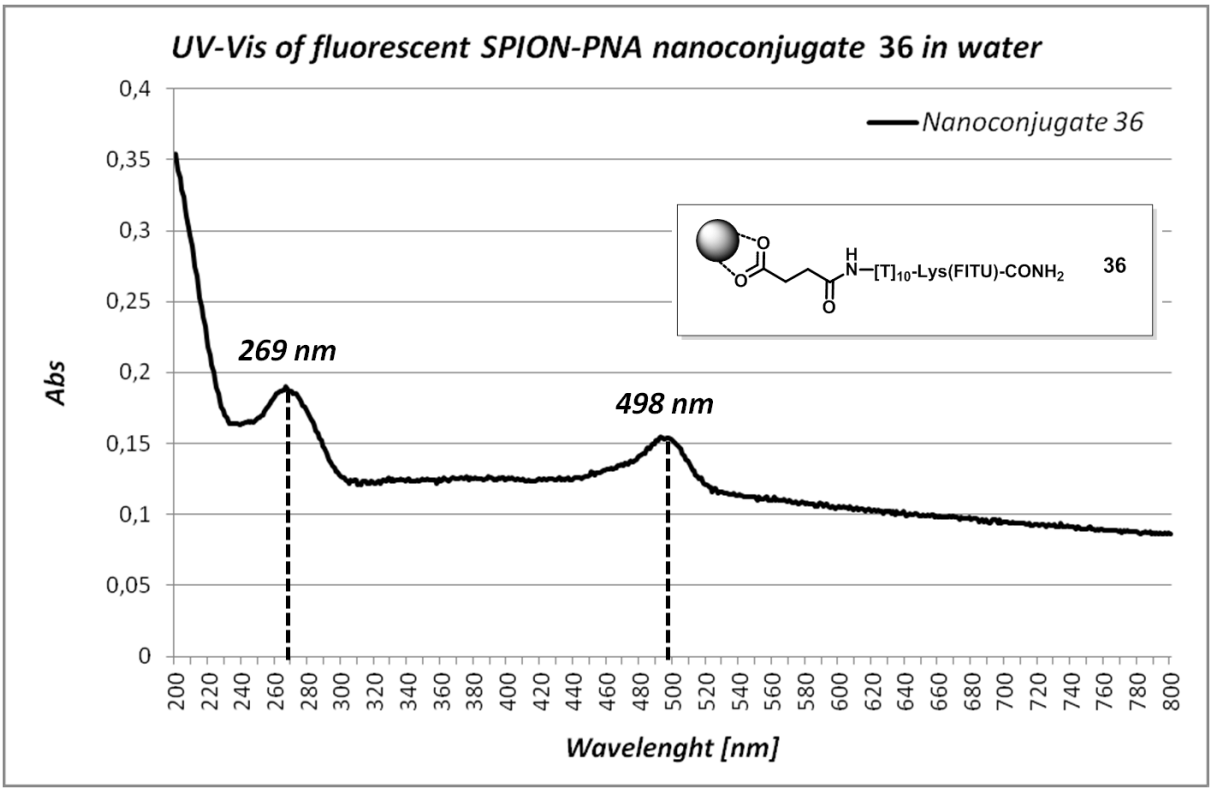

Figure 90 *- UV-Vis spectrum of nanoconjugate* **36** *in water.*

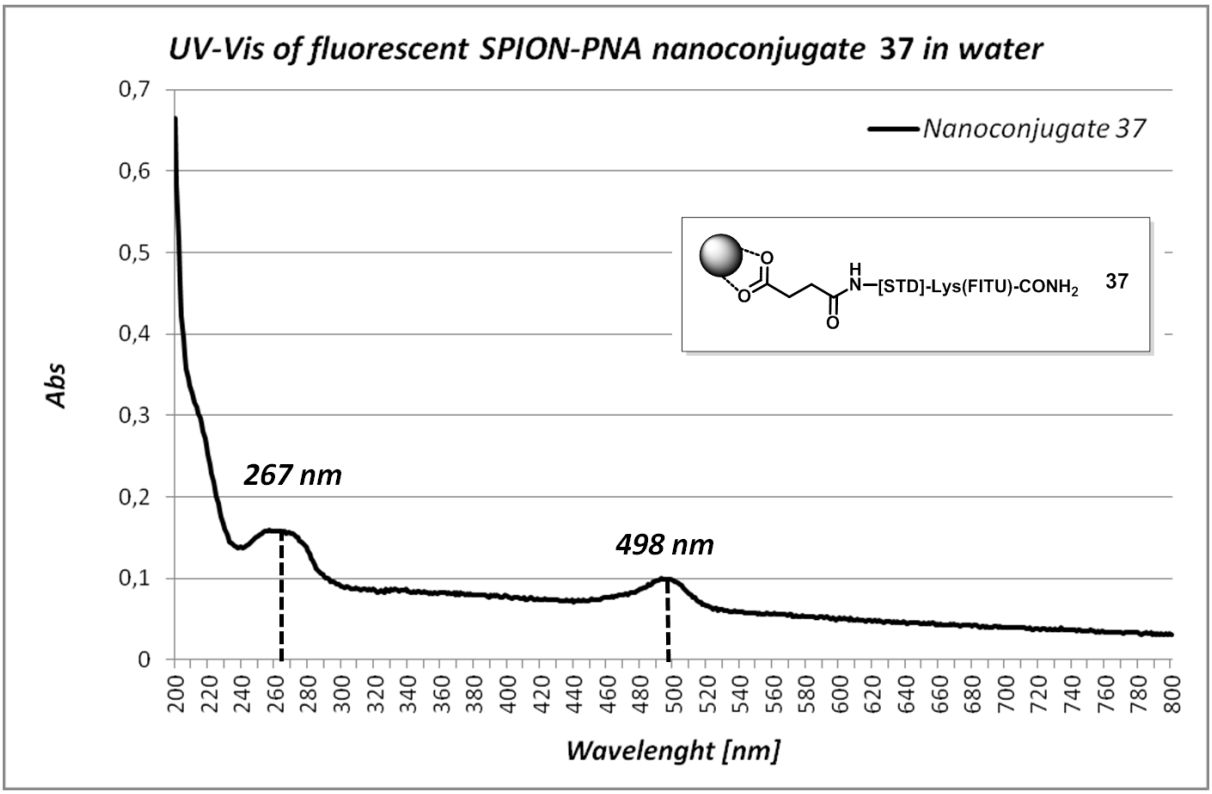

Figure 91 *- UV-Vis spectrum of nanoconjugate* **37** *in water.*

5.7.4 Hybridization of **36** *and* **37** *with Complementary DNAs: Determination of the Melting Temperatures*

In order to evaluate the binding affinity of nanoconjugates **36** and **37** towards the complementary DNAs, denaturation experiments were conducted on the hybrids formed and melting temperature ***Tm*** were determined monitoring the variation of the absorbance at 260 nm against the temperature.

PNA complexes with the corresponding complementary nucleic acid oligomers were constituted by mixing together stoichiometric quantities of the involved oligomers with the DNA strands in a pH 7 buffer of 100 mM NaCl, 10 mM sodium phosphate, 0.1 mM EDTA to achieve a final concentration of 2.5 μM for **37**, homoadenine and standard sequence DNAs, while 5 μM concentration was obtained for **36** (homothymine PNA forms PNA_2:DNA triplex with complementary DNA, so a double concentration of PNA is needed).

The samples were annealed by first heating at 90 °C in a sand bath for 10 minutes followed by slow cooling to room temperature. They were then kept at room temperature for at least half an hour and refrigerated overnight prior to running the melting experiments.

UV-melting experiments were carried out by a spectrophotometer connected to a Peltier temperature controller *[for more details on the method, refereed to section 5.9.1]*. The collected absorbance data were plotted against the temperature values and denaturation curves were obtained.

Nanoconjugate **36** was so hybridized with the complementary homoadenine DNA (5'-AAAAAAAAAA-3') and the heating and cooling curves obtained are reported in *Figure 92*.

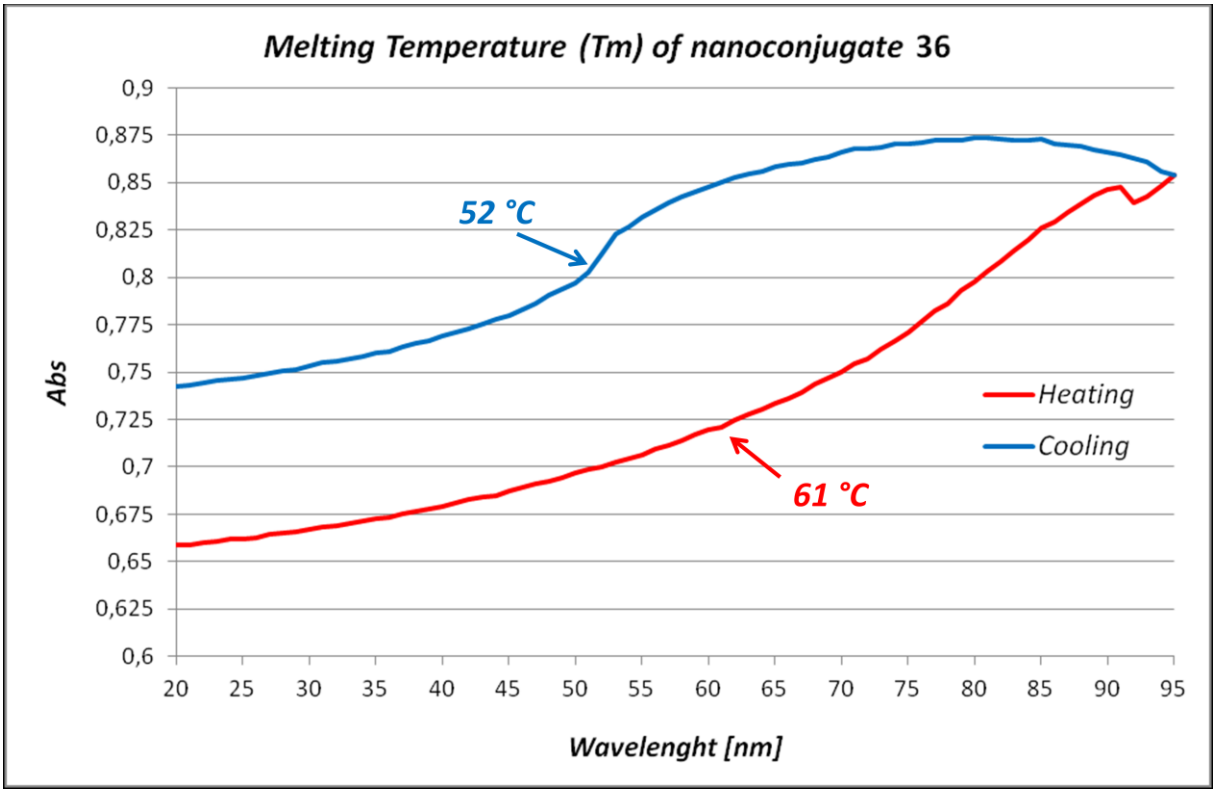

Figure 92 *- Denaturation curves for PNA_2:DNA hybrid formed between nanoconjugate* **36** *and homoadenine DNA.*

The heating curve does not present a net inflection point, maybe due to the low presence of triplex species in solution generated during the annealing process. Despite this, by fist derivative calculation a relative maximum was obtained at 61 °C. This value is lower than the reported one for classical homothymine PNA, equal to 72 °C *[see section 5.5.1]*, but we have to consider that **36** is supported onto a metallic nanoparticle core and also bears a strong hydrophobic group, like fluorescein. As a consequence of this new heating cycle, the following cooling curve (corresponding to the formation of triplex complexes) shows a net inflection point at 52 °C, sign that triplex species were now effectively formed. It's to note that denaturation process are characterized by hysteresis phenomenon, so the cooling curve always present a lower ***Tm*** respect to the heating one.

In the same way, nanoconjugate **37** was hybridized with the complementary antiparallel standard sequence DNA (5'-AGTGATCTAC-3'), with the formation of duplex PNA:DNA. Denaturation curves are here reported in *Figure 93*.

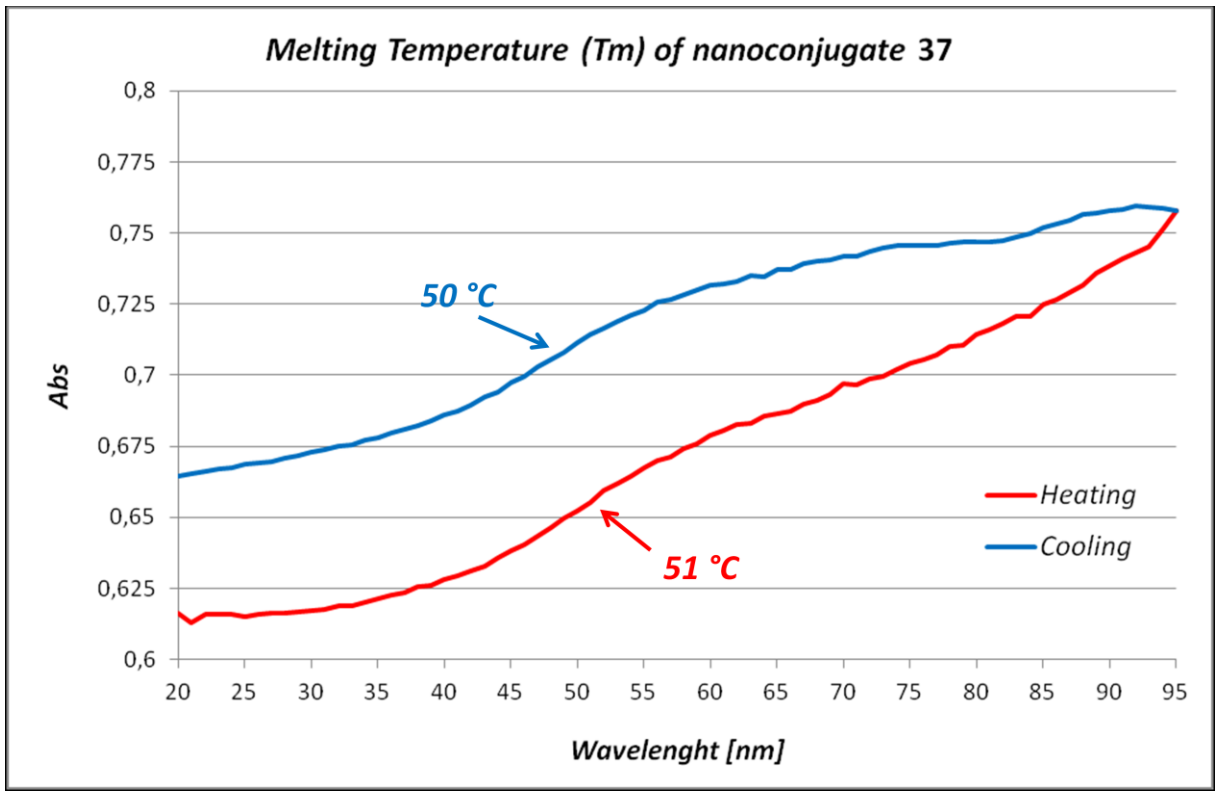

Figure 93 *- Denaturation curves for PNA:DNA hybrid formed between nanoconjugate* **37** *and antiparallel standard sequence DNA.*

Classical standard sequence PNA:DNA hybrid has a ***Tm*** of 53 °C *[see section 5.5.1]*, value that was confirmed by the denaturation of the duplex formed between **37** and its complementary DNA. In fact, from the heating curves was possible to obtain a ***Tm*** of 51 °C, an outstanding results if consider that **37** is grafted onto SPION surface and bear a fluorescein probe. Cooling curve was also recorded obtaining an inflection point at 50 °C, further confirming the formation of duplex species.

5.7.5 Conclusions

Concerning the synthesis of new fluorescent SPION-PNA nanoconjugates, we can conclude that an efficient synthetic protocol for the synthesis of this new class of nanocompounds was set up. Two new supported PNAs, **36** and **37**, were synthesized and characterized confirming the grafting by a non-covalent interaction between a succinic linker and the nanoparticle surface, while a lysine residue can be efficiently used to bind different kind of probes, such as fluorescein, directly with SPS.

Denaturation experiments were performed on **36** and **37**, with formation of the corresponding PNA_2:DNA and PNA:DNA hybrids, respectively. The ***Tm*** values obtained are very encouraging, if we consider that strong binding affinity were obtained regardless of the presence of a strong hydrophobic fluorescent probe and despite the anchoring onto SPIONs.

5.8 Synthesis of New SPION-PNA Nanoconjugates Exploiting NCO-based Heterobifunctional Linkers

In *section 5.7*, we have just seen how PNAs can be easily modified introducing during SPS amino acid residues, linkers or probes, as well as how these oligomers can be grafted by a non-covalent interaction onto a nanoparticle surface.

Having established the easy anchoring of isocyanate onto the SPIONs surface and having demonstrated that simple properly orthogonal functionalized NCO-based molecules can be efficiently used as heterobifunctional linkers *[see section 4.2]*, we decided to use this new anchoring methodology in the synthesis of new SPION-PNA nanoconjugates.

So, in this Ph.D. research project the *N*-terminus cysteine modified homothymine and standard sequence PNA oligomers were supported onto functionalized nanoparticles **20** *[see section 4.4]*, in order to obtained the two new NCO-based SPION-PNA nanoconjugates **45** and **46** (*Figure 94*).

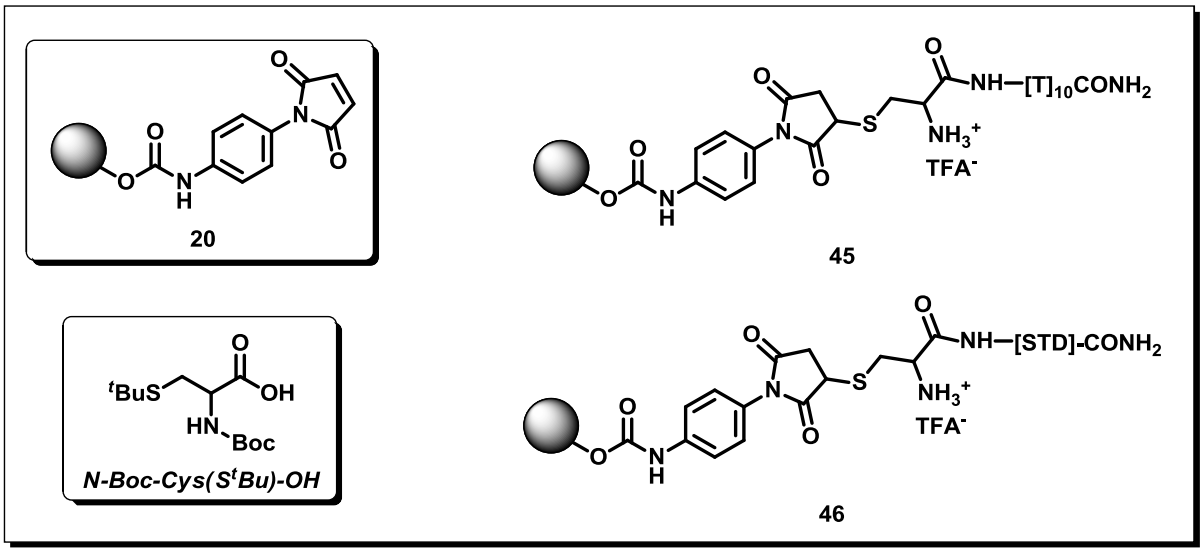

Figure 94 *- New NCO-based SPION-PNA nanoconjugates* **45** *and* **46***. Are also shown the structures of the starting functionalized nanoparticles* **20** *and of the N(α)-Boc-S-*^{t}*butylmercapto cysteine.*

PNA oligomers were so synthesized as reported in *Scheme 17*.

The MBHA resin was manually downloaded with the thymine monomer in order to obtain the functionalized resin **47** with a final loading of 0.2 mmol/g. Always by manual SPS, the other PNA monomers were cyclically coupled following the Boc-deprotection, coupling and capping steps, till the desired oligomers were obtained. Boc-deprotection of the *N*-terminus, coupling with *N(α)*-Boc-S-^{t}butylmercapto cysteine and capping of the unreacted chains, followed by total cleavage from the resin led to the desired modified PNAs **48** and **49**. Thanks to the strong acidic condition of the cleavage step, the removal of cysteine protecting groups was simultaneously achieved, obtaining the free thiol group necessary for Michael addition on the maleimido moiety of nanoconjugate **20**. Finally, PNAs **48** and **49** were supported onto SPIONs **20** by formation of a covalent C-S bond, affording the two new nanoconjugates **45** and **46** that were isolated and characterized by E.A., FTIR and UV-Vis spectroscopy to confirm the grafting of the oligomers onto the nanoparticles surface. Furthermore, to check the ability of **45** and **46** to recognize and bind complementary DNAs, the melting temperature ***Tm*** of the hybrids formed were determined.

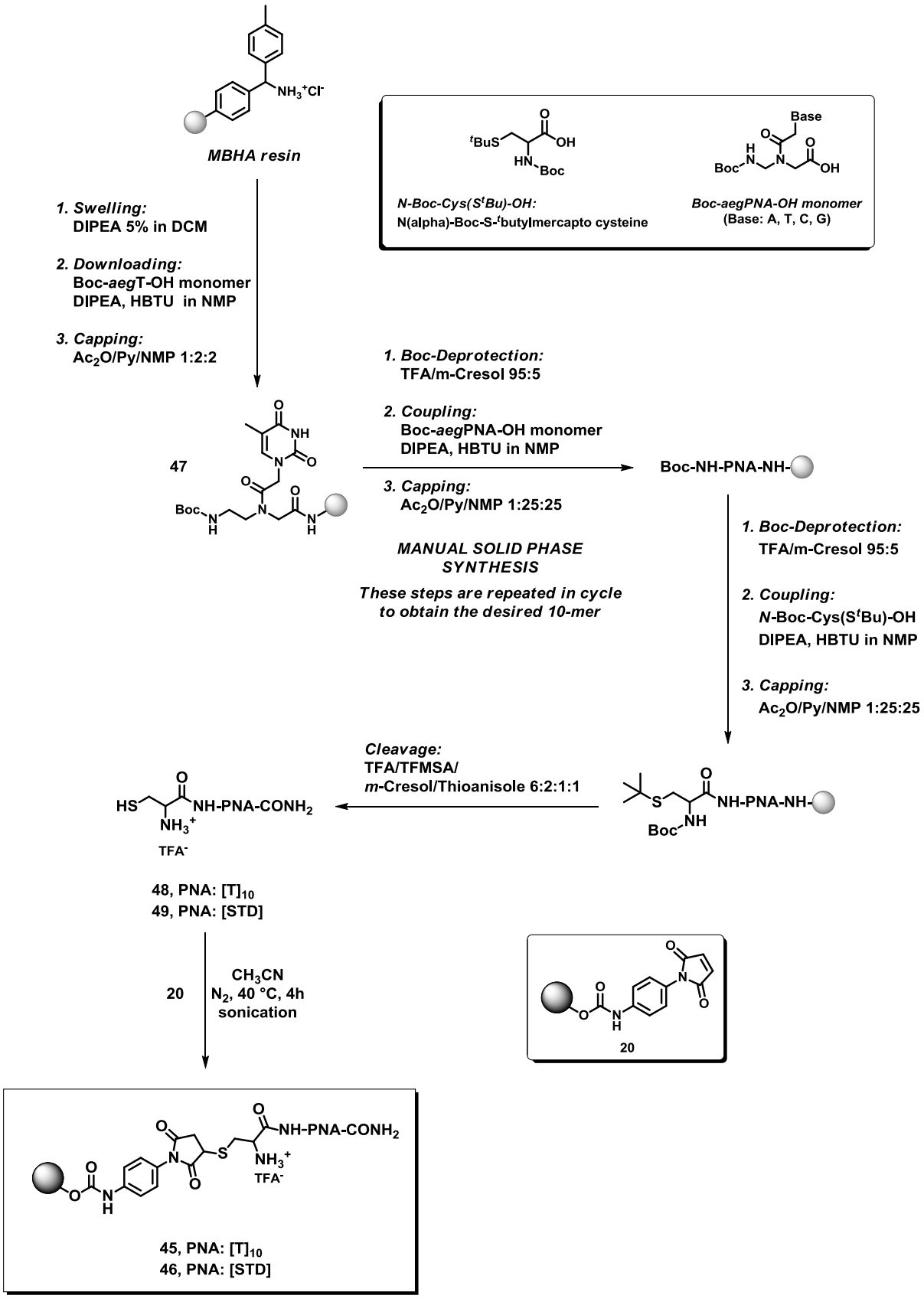

Scheme 17 *- Synthesis of new NCO-based SPION-PNA nanoconjugates* **45** *and* **46**.

5.8.1 Determination of the Final Loading of Nanoconjugate 45 *and* 46

As previously mentioned in *section 5.7.1*, E.A. were conducted on nanoconjugates **45** and **46** and the corresponding loadings were determined (*Table 12*).

Nanoconjugate	***Loading***		
	Tot % org	*mmol/g_{NPs}*	*N°$_{molecules}$/NP*
45	54.33	0.18	≈ 610
46	34.65	0.11	≈ 270

Table 12 *- Loading of nanoconjugates* **45** *and* **46***.*

The high loading value of the starting nanoconjugate **20** (31.07%, equal to 1.44 mmol/g_{NPs}) permits to efficiently graft a higher number of molecules *per* nanoparticle than those obtained for nanoconjugates **36** and **37**, in which a direct non-covalent adsorption onto the nanoparticle surface occurs.

So, having demonstrated the possibility to easily tune the loading of the NCO-based heterobifunctional linker onto the SPIONs surface, we can also easily modulate the amount of bioactive molecules covalently bonded to the linker.

5.8.2 FTIR Characterization of 45 *and* 46

In order to confirm the grafting of PNA oligomers onto SPIONs, nanoconjugates **45** and **46** were analyzed by FTIR in transmittance mode (blank KBr) and the spectra obtained are here reported in *Figure 95* and *Figure 96*, respectively.

In both spectra, at high wavenumbers, are present the broad vibrational band corresponding to FeO-H and N-H stretchings and the aromatic and aliphatic C-H stretching modes. Classical strong bands at low frequency values (in the range 640-550 cm^{-1}, υ Fe-O) confirm the presence of the iron oxide core.

In the case of homothymine PNA (*Figure 95*), the strong broad band at 1674 cm^{-1} corresponds to all the stretching modes of carbonyl groups, as amides, imides and carbamate. Also C-O and C-N stretching peaks are well visible at 1227-1101 cm^{-1}.

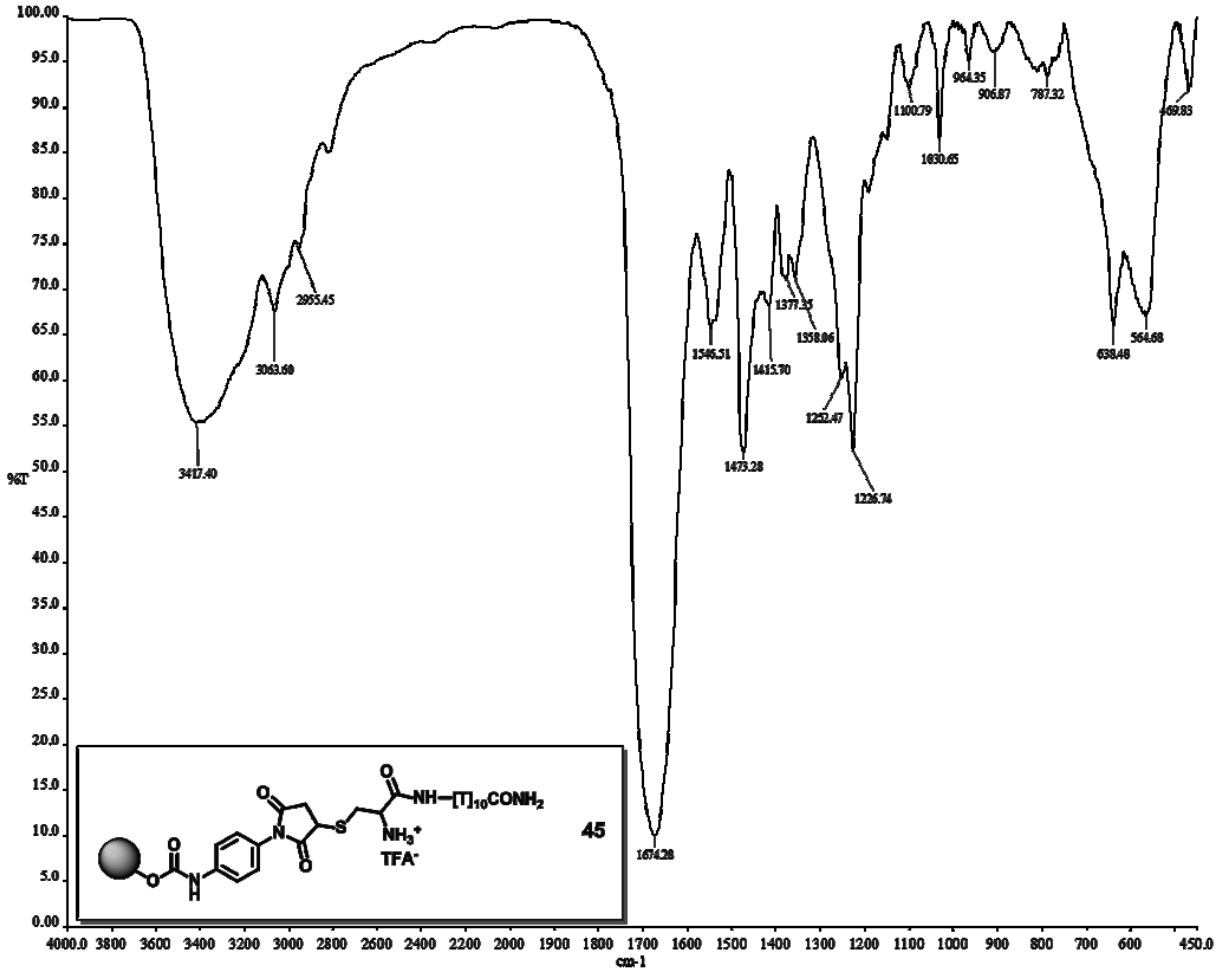

Figure 95 *- FTIR spectrum of nanoconjugate* **45***.*

For supported standard sequence PNA (*Figure 96*), a partially covered peak related to the C=O of the imide moieties (1710 cm^{-1}) comes out from the broad band related to the amides and the carbamate C=O groups (1644 cm^{-1}). Thanks to the presence of all the four nucleobases in the sequence, and consequently thanks to the higher number of C-O, C-N, C=C and aromatic C-H groups, nanoconjugate **46** shows, with higher intensity, the classical vibrational modes referred to these kind of bonds.

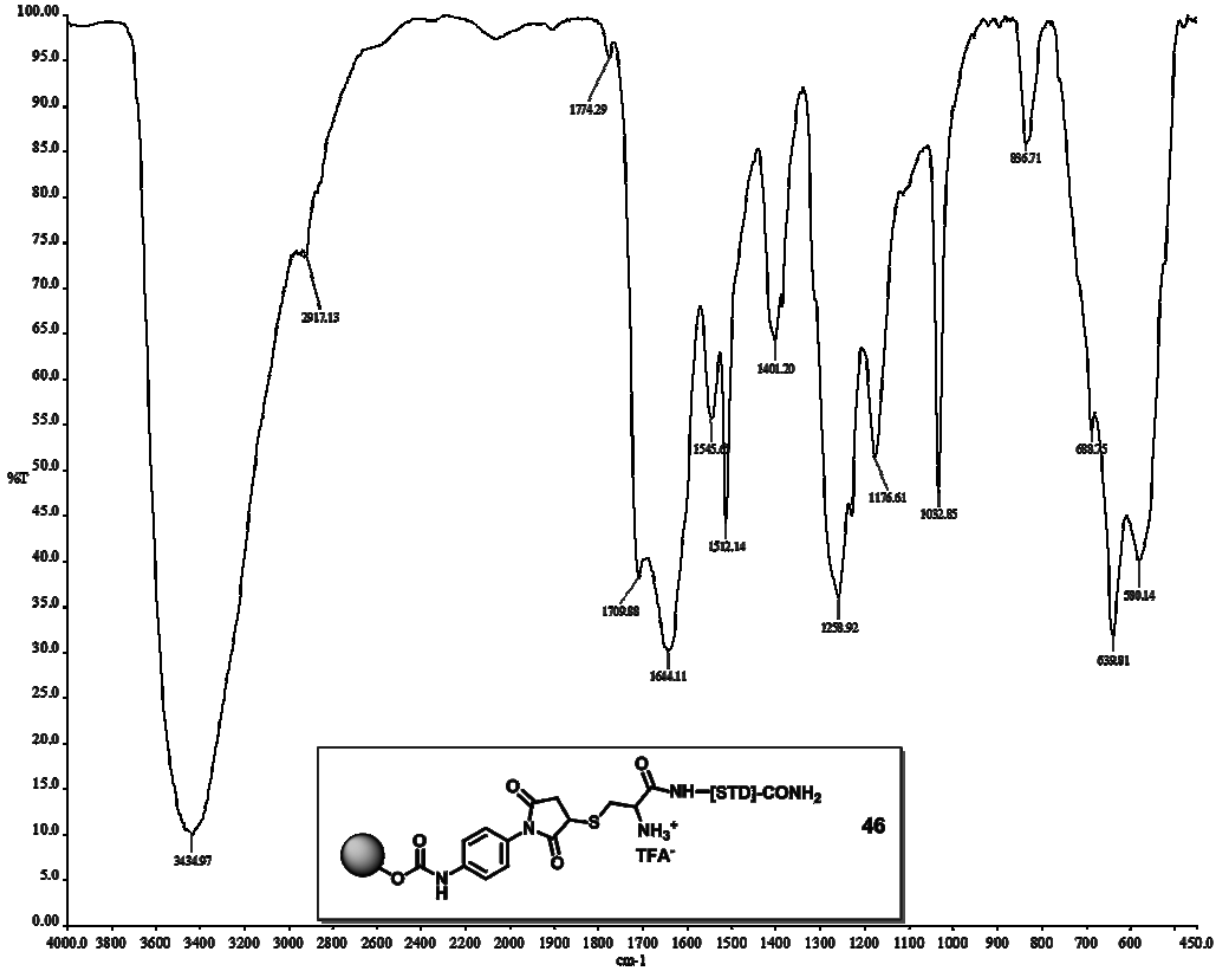

Figure 96 *- FTIR spectrum of nanoconjugate* **46***.*

From these results we can state that the *N*-terminus cysteine PNAs **48** and **49** have effectively reacted with the functionalized nanoparticles **20**, affording the desired nanoconjugates **45** and **46**.

5.8.3 UV-Vis Spectroscopy Characterization

In *section 5.7.3*, we have clearly seen how SPION-PNA nanoconjugates can be easily characterized by UV-Vis spectroscopy thanks to the presence of the strong absorption of the nucleobases.

As done for nanoconjugates **36** and **37**, the UV-Vis absorption spectra in water of the new SPION-PNA nanosystems **45** and **46** were recorded (*Figure 97* and *98*, respectively).

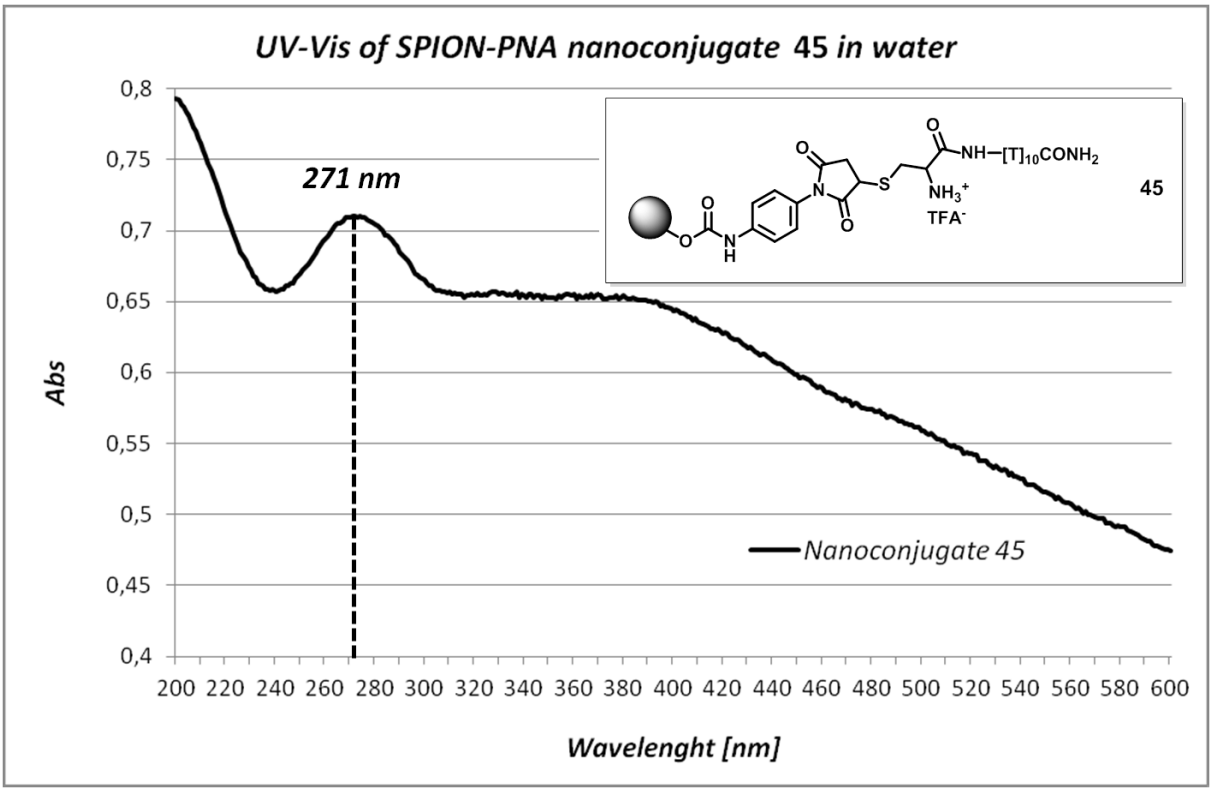

Figure 97 *- UV-Vis spectrum of nanoconjugate* **45** *in water.*

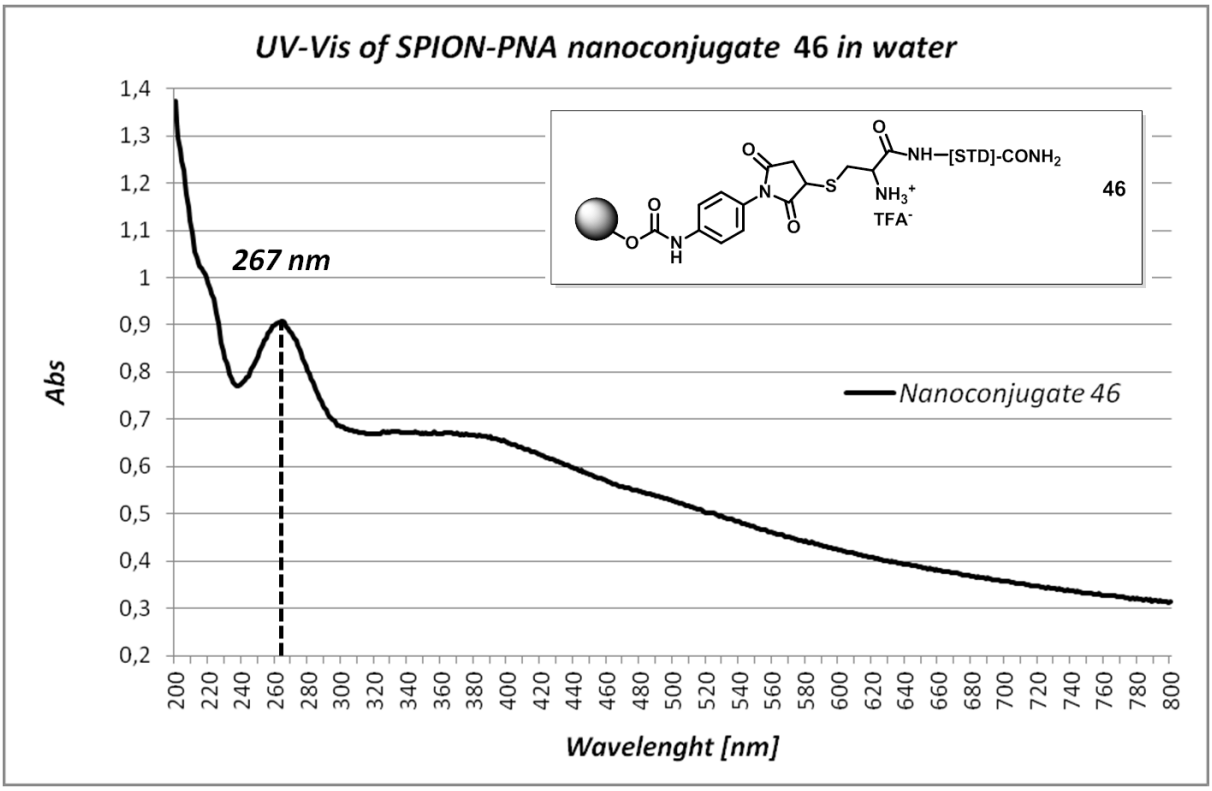

Figure 98 *- UV-Vis spectrum of nanoconjugate* **46** *in water.*

Both spectra clearly show the strong absorption peak of PNA strands grafted onto SPIONs at about 270 nm, while from 320 nm the broad shouldered scattering of the nanoparticles is present. The scattering phenomena, together with the bathochromic shift of the PNA absorption peak, confirmed also in these cases, the presence of the PNA oligomers onto the SPION surface.

5.8.4 Hybridization of **45** *and* **46** *with Complementary DNAs: Determination of the Melting Temperatures*

As previously done for nanoconjugates **36** and **37**, the binding affinity of nanoconjugates **45** and **46** towards the complementary DNAs was evaluated by denaturation experiments and melting temperature ***Tm*** were determined monitoring the variation of the absorbance at 260 nm against the temperature.

PNA_2:DNA (for the homothymine sequence) and PNA:DNA complexes were prepared as previously explained and UV-melting experiments were carried out, collecting absorbance data against the temperature variations.

Nanoconjugate **45** was so hybridized with the complementary homoadenine DNA (5'-AAAAAAAAAA-3') and the heating and cooling curves obtained are reported in *Figure 99*.

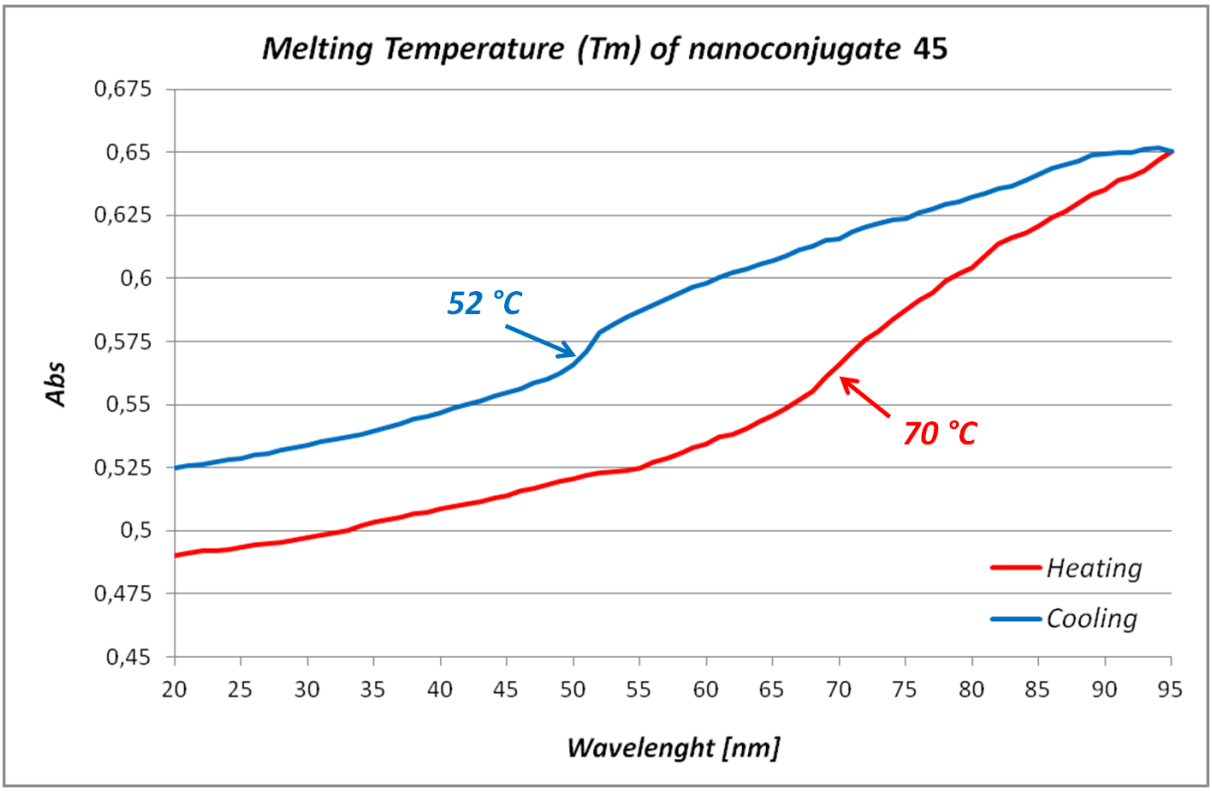

Figure 99 *- Denaturation curves for PNA_2:DNA hybrid formed between nanoconjugate* **45** *and homoadenine DNA.*

The heating curve shows an inflection point at 70 °C, that perfectly matches the reported value for classical homothymine PNA, equal to 72 °C *[see section 5.5.1]*; the following cooling curve also present a net inflection point at 52 °C. As stated, the denaturation process are characterized by hysteresis phenomenon, so the cooling curve always present a lower ***Tm*** respect to the heating one, but the presence of the inflection point during the cooling process is the confirmation that effectively **45** is able to recognize the complementary DNA.

In the same way, nanoconjugate **46** was hybridized with the complementary antiparallel standard sequence DNA (5'-AGTGATCTAC-3'), with the formation of duplex PNA:DNA. Denaturation curves are here reported in *Figure 100*.

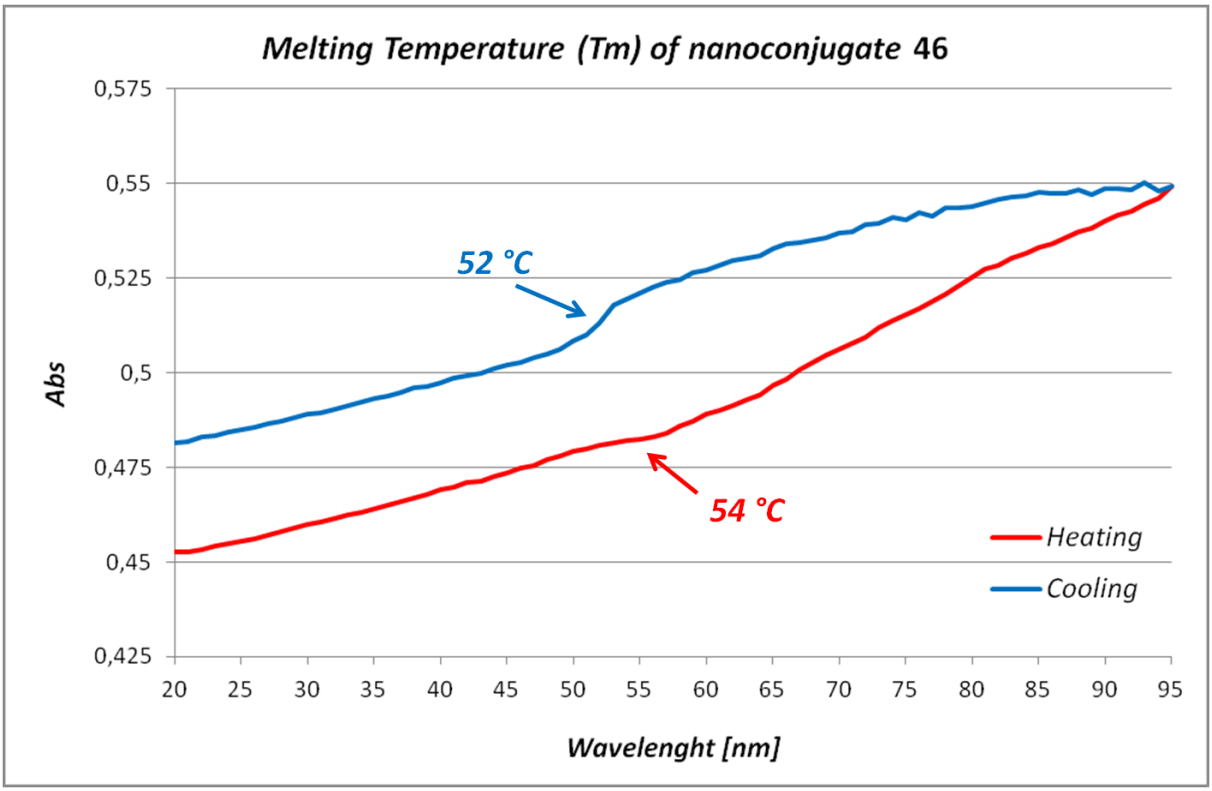

Figure 100 *- Denaturation curves for PNA:DNA hybrid formed between nanoconjugate* **37** *and antiparallel standard sequence DNA.*

Classical standard sequence PNA:DNA hybrid has a ***Tm*** of 53 °C *[see section 5.5.1]*, value that was confirmed by the denaturation of the duplex formed between **46** and its complementary DNA. In fact, from the heating curves was possible to obtain a ***Tm*** of 54 °C, an outstanding results if consider that **46** is covalently anchored onto nanoparticles surface. Cooling curve was also recorded obtaining an inflection point at 52 °C, further confirming the formation of duplex species.

5.8.5 Conclusions

Concerning the use new NCO-based heterobifunctional linkers, we have demonstrated that properly modified PNA can be efficiently loaded onto functionalized SPION. So, two new covalently supported PNAs, **45** and **46**, were synthesized and characterized.

Denaturation experiments were performed on **45** and **46**, with formation of the corresponding PNA_2:DNA and PNA:DNA hybrids, respectively. The ***Tm*** values obtained

confirm the strong affinity binding capacity of these nanoconjugates towards the complementary DNAs, regardless of the presence of nanoparticles.

5.9 Experimental Section

5.9.1 Materials and Methods

All reagents and solvents were purchased in higher grade from commercial suppliers and used without further purification, unless otherwise stated. Dry solvents over molecular sieves, solvents for peptide synthesis and HPLC solvents (P.A., ACS reagent or Chromasolve Grade) were obtained from Sigma Aldrich.

γ-Fe_2O_3 SPIONs were purchased from Alpha Aesar and stored away from moisture.

The Boc-*aeg*PNA-OH monomers were purchased from ASM Research Chemicals; Boc-*aeg*T-OH monomer can be also prepared as reported in literature.

The complementary DNA oligonucleotides were purchased from Primm Srl.

All weightings of reagents were carried out with analytical balance Mettler Toledo AB135-S/FACT.

Vials ALLTECH of 1.5 ml, 4 ml, 8 ml, 25 ml and 50 ml with frits of PTFE were used as reactor for manual solid phase synthesis. Automated solid phase syntheses were performed with peptide synthesizer "ABI 433A" of Applera Italia, according to Applied Biosystems ABI 433A Peptide Synthesis 3 mL Reaction Vessel User's Manual for the MBHA (4-methylbenzhydrylamine hydrochloride salt) resin. The software for peptide synthesis is Syntassist 2.0, installed on the PC unit linked to the synthesizer.

Commercially available MBHA resin (VWR International) with a 0.63 mmol/g loading, was downloaded to 0.2 mmol/g with the proper amino acid (*e.g. N(α)*-Boc-*N(ε)*-Fmoc-*L*-lysine, MBHA resin **38**) or PNA monomer (*e.g.* Boc-*aeg*T-OH, MBHA resin **47**) following the procedure recommended on the ABI 433A instrument manual, as follow:

1. Wash 1.0 g MBHA resin twice in DCM.

2. Wash the resin with 5% DIPEA in DCM for 3 minutes.
3. Wash the resin twice in DCM. The resin is now neutralized.
4. Dissolve 0.20 mmol (amino acid or PNA monomer) in 2.5 ml NMP.
5. Add 0.4 mmol DIPEA to the monomer solution.
6. Dissolve 75 mg (0.19 mmol) HBTU in 2.5 ml NMP, and add this to the monomer solution.
7. Activate the monomer for 2 minutes.
8. Add the activated monomer solution to the neutralized resin.
9. Allow the reaction to proceed for at least 1 hour.
10. Filter the resin.
11. Wash the resin with 1xNMP.
12. Prepare 50 ml of capping solution using a 1:2:2 ratio of acetic anhydride, pyridine and NMP.
13. Add the capping solution to the resin and allow the reaction to proceed for 1 hour. Successful capping will produce a negative Kaiser test.
14. Wash the resin with DMF.
15. Wash the resin with 4xDCM.
16. Wash the resin with 5% DIPEA in DCM.
17. Wash the resin with 4xDCM.
18. Dry the resin in vacuum.

The cleavage procedure to remove PNA oligomers from the MBHA resin is the following:

1. Wash the resin 2xTFA.
2. Make 1 ml of cleavage solution TFA/TFMSA/*m*-cresol/thioanisole 6:2:1:1.
3. Add the cleavage solution to the resin and allow the reaction to proceed for 1 hour on a orbital shaker.
4. Filter the resin and recover the solution in a centrifuge tube.
5. Wash the resin with TFA.
6. Filter the resin and add this solution to the one recovered at point 4.
7. Repeat point 5 and 6 three times.

8. Remove volatiles by nitrogen stream to afford a black/brown oil.
9. Add cold diethyl ether to the tube and mix. A white precipitate forms.
10. Put the tube at -20 °C for 1 hour to complete the precipitation.
11. Centrifuge and remove the supernatant.
12. Wash the solid with fresh ether, mix, centrifuge and remove the solution.
13. Repeat point 12 four/five times.
14. Dry the crude PNA first by nitrogen stream and then in vacuum.

HPLC of PNA oligomers were performed with a HPLC AGILENT 1100 Series, using an analytical column DISCOVERY® BIO WIDE PORE C18 (15 cm x 4.6 mm, 5 µm) and a semi-preparative column DISCOVERY® BIO WIDE PORE C18 (25 cm x 10 mm, 10 µm).

MALDI-TOF spectra were recorded with a Bruker Daltonics Omniflex. A pulsed nitrogen laser (337 nm) were used to generate ions that have been accelerated in a 20 kV field. The instrument was calibrated in the range from 0 to 20 KDa. Generally, sinapinic acid and 2,5-dihydroxybenzoic acid (DHB) matrixes were used.

A lyophilizer Telstar Cryodos were used to isolate pure PNA oligomers from aqueous solutions.

To dry the nanoparticles was used a rotating vacuum dryer from Büchi. Once dried, the nanoparticles are stored in a desiccator filled with anhydrous salts.

A sonicator Elma Elmasonic S 30H was used to perform reactions with nanoparticles.

UV-Visible spectrophotometer Thermo Electron Corporation “Evolution 500” was used to analyze PNA oligomers and SPION-PNA nanoconjugates in water. The concentration of the PNA oligomers was calculated based on their absorption at 260nm.

Elemental Analysis were performed in the division of Inorganic, Metallorganic and Analytical Chemistry, from the Department of Chemistry in the University of Milan with a Perkin Elmer instrument.

Infrared spectra of nanoconjugates were acquired on a Spectrum One FTIR spectrophotometer (Perkin Elmer) in the range 4000-450 cm^{-1} in transmittance mode. 0.5

mg of nanoparticles were diluted in 150 mg FTIR grade KBr and ground in an agate mortar. KBr was previously dried at 125°C under vacuum. Then mixed powder was pressed at 9 tons for 3 min to obtain slim semitransparent tablet. Spectra were recorded selecting 64 scans and 4 cm^{-1} resolution. The background of pure KBr was separately recorded using the same conditions and automatically subtracted from sample spectra. These analysis were performed in collaboration with the Professor Stradi's reaserch group in the Laboratory of Instrumental Analysis of the division of Organic Chemistry "A. Marchesini", Department of Pharmaceutical Science in University of Milan.

UV-melting experiments were carried out by a Peltier Agilent 9090A connected to a spectrophotometer Agilent 8453. The absorbance at 260 nm was recorded following this protocol: from 19.5 °C to 20 °C (2' hold time), from 20 °C to 94 °C (1 °C *per* 0.2' hold time), from 94 °C to 95 °C (4' hold time) and then 95 °C to 20 °C (-1 °C *per* 0.2' hold time). The ***Tm*** of the PNA_2:DNA and PNA:DNA complexes was automatically calculated by the "Denaturation Program" installed in the PC unit connected to the instrument, as the inflection point of the heating and cooling curves in the plot of absorbance *vs* temperature.

5.9.2 Experimental Procedures

5.9.2.1 Synthesis of Amino-aeg[T]$_{10}$-Lys(Fmoc)-MBHA Resin, Trifluoroacetic Salt 39

Starting from the downloaded Lys(Fmoc)-MBHA resin **38**, automated solid phase synthesis with Boc-strategy was performed in order to obtain the supported homothymine PNA decamer **39**. A control cleavage was done on a small amount of the resin, to check the formation of the desired product. ***HPLC (reverse phase):*** retention time 20.90 min, elution gradient from water (+ 0.1% TFA)/AcN 95:5 to pure AcN in 60 min. ***MALDI-TOF:*** 3028.9 [M] (calculated 3028.97).

5.9.2.2 Synthesis of N-succinylamide-aeg[T]$_{10}$-Lys(Fmoc)-MBHA Resin 41

After neutralization of supported PNA **39** with DIPEA 5% in DCM, succinic anhydride (20 eq respect to the theoretical free amino groups) dissolved in 1 ml of NMP was added to the resin and left under vigorous shaking for 4 hours. The resin was then washed with 9xNMP

and 5xDCM, affording the succinic modified homothymine PNA decamer **41**. A control cleavage was done on a small amount of the resin, to check the formation of the desired product. ***HPLC (reverse phase):*** retention time 20.92 min, elution gradient from water (+ 0.1% TFA)/AcN 95:5 to pure AcN in 60 min. ***MALDI-TOF:*** 3130.1 [M] (calculated 3130.05).

5.9.2.3 Synthesis of N-succinylamide-aeg[T]$_{10}$-Lys(FITU)-CONH$_2$ Decamer **43**

Fmoc-deprotection of **41** was achieved washing the resin with 20% piperidine in DMF (3x2 ml, 5' shaking each time). After deprotection, the resin was washed with 5xDMF and then treated with a fluorescein isothiocyanate (FITC) solution in DMF (4 eq respect to the theoretical free lysine amino groups) and DIPEA (8 eq) and left overnight at the orbital shaker. The resin was so washed with 5xDMF and 5xDCM, affording the supported desired PNA oligomer. A control cleavage was done on a small amount of the resin, to check the formation of **43**. Having confirmed the formation of the product, total cleavage and semipreparative HPLC on reverse phase were done, affording **43** as a yellow fluorescent solid. ***HPLC (reverse phase):*** retention time 8.22 min, elution gradient from water (+ 0.1% TFA)/AcN 80:20 to pure AcN in 80 min. ***MALDI-TOF:*** 3298.2 [M] (calculated 3299.20).

5.9.2.4 Synthesis of NP-succinylamide-aeg[T]$_{10}$-Lys(FITU)-CONH$_2$ SPION-PNA Nanoconjugate **36**

The modified fluorescent homothymine PNA **43** (16 mg, 0.005 mmol) was added to a suspension of naked SPIONs (16 mg) in dry $PhCH_3$ (5 ml), previously sonicated at 40 °C for 30'; the mixture was stirred, under sonication, at 40 °C for 4 h. After this time the obtained suspension was centrifugated at 5000 r/min for 10' and the supernatant was removed. The solid residue was first washed with fresh $PhCH_3$ (3x5 ml), then with MeOH (2x5 ml) and at last with Et_2O (3x5 ml) and vortex/sonication/centrifugation were cyclic repeated for each washing. Functionalized NPs were dried on air for a night and then in a rotating vacuum drier for a day, to afford **36** (20 mg) as a light brown powder. ***Loadings from E.A.:*** 14.08% (equal to 0.043 mmol/g_{NPs}, ≈80 molecules/NP). ***FTIR (cm^{-1}) in trasmittance (blank KBr):*** 3401 (υ, FeO-H and N-H), 2962-2931 (υ, aliphatic C-H), 1679 (broad υ, C=O imides, amides and carboxylate), 1457, 1385, 1208-1141 (υ, C-O and C-N), 842-803 (δ, C-H), 633-584 (υ, Fe-O). ***UV-Vis (λ_{max}, nm) in water:*** 269 (PNA), 498 (fluorescein). ***Tm (complementary homoadenine DNA) in water at 260 nm:*** 61 °C (heating), 52° C (cooling).

5.9.2.5 Synthesis of Amino-aeg[STD]-Lys(Fmoc)-MBHA Resin, Trifluoroacetic Salt 40

Starting from the downloaded Lys(Fmoc)-MBHA resin **38**, automated solid phase synthesis with Boc-strategy was performed in order to obtain the supported homothymine PNA decamer **40**. A control cleavage was done on a small amount of the resin, to check the formation of the desired product. ***HPLC (reverse phase):*** retention time 19.07 min, elution gradient from water (+ 0.1% TFA)/AcN 95:5 to pure AcN in 60 min. ***MALDI-TOF:*** 3077.7 [M] (calculated 3077.02).

5.9.2.6 Synthesis of N-succinylamide-aeg[STD]-Lys(Fmoc)-MBHA Resin 42

After neutralization of supported PNA **40** with DIPEA 5% in DCM, succinic anhydride (20 eq respect to the theoretical free amino groups) dissolved in 1 ml of NMP was added to the resin and left under vigorous shaking for 4 hours. The resin was then washed with 9xNMP and 5xDCM, affording the succinic modified standard sequence PNA decamer **42**. A control cleavage was done on a small amount of the resin, to check the formation of the desired product. ***HPLC (reverse phase):*** retention time 19.45 min, elution gradient from water (+ 0.1% TFA)/AcN 95:5 to pure AcN in 60 min. ***MALDI-TOF:*** 3177.3 [M] (calculated 3177.09).

5.9.2.7 Synthesis of N-succinylamide-aeg[STD]-Lys(FITU)-CONH$_2$ Decamer 44

Fmoc-deprotection of **42** was achieved washing the resin with 20% piperidine in DMF (3x2 ml, 5' shaking each time). After deprotection, the resin was washed with 5xDMF and then treated with a fluorescein isothiocyanate (FITC) solution in DMF (4 eq respect to the theoretical free lysine amino groups) and DIPEA (8 eq) and left overnight at the orbital shaker. The resin was so washed with 5xDMF and 5xDCM, affording the supported desired PNA oligomer. A control cleavage was done on a small amount of the resin, to check the formation of **44**. Having confirmed the formation of the product, total cleavage and semipreparative HPLC on reverse phase were done, affording **44** as a yellow fluorescent solid. ***HPLC (reverse phase):*** retention time 15.40 min, elution gradient from water (+ 0.1% TFA)/AcN 80:20 to pure AcN in 80 min. ***MALDI-TOF:*** 3345.1 [M] (calculated 3346.22).

5.9.2.8 Synthesis of NP-succinylamide-aeg[STD]-Lys(FITU)-CONH$_2$ SPION-PNA Nanoconjugate **37**

The modified fluorescent standard sequence PNA **44** (26 mg, 0.008 mmol) was added to a suspension of naked SPIONs (26 mg) in dry $PhCH_3$ (5 ml), previously sonicated at 40 °C for 30'; the mixture was stirred, under sonication, at 40 °C for 4 h. After this time the obtained suspension was centrifugated at 5000 r/min for 10' and the supernatant was removed. The solid residue was first washed with fresh $PhCH_3$ (3x5 ml), then with MeOH (2x5 ml) and at last with Et_2O (3x5 ml) and vortex/sonication/centrifugation were cyclic repeated for each washing. Functionalized NPs were dried on air for a night and then in a rotating vacuum drier for a day, to afford **37** (36 mg) as a light brown powder. ***Loadings from E.A.:*** 26.78% (equal to 0.080 mmol/g_{NPs}, ≈170 molecules/NP). ***FTIR (cm^{-1}) in trasmittance (blank KBr):*** 3208 (υ, FeO-H and N-H), 2930 (υ, aliphatic C-H), 1658 (broad υ, C=O imides, amides and carboxylate), 1504, 1473, 1416, 1253, 1227-1172 (υ, C-O and C-N), 1030, 633-584 (υ, Fe-O). ***UV-Vis (λ_{max}, nm) in water:*** 267 (PNA), 498 (fluorescein). ***Tm (complementary STD sequance DNA) in water at 260 nm:*** 51 °C (heating), 50° C (cooling).

5.9.2.9 Synthesis of N-cysteine-aeg[T]$_{10}$-CONH$_2$, Trifluoroacetic Salt **48**

Starting from the downloaded Boc-*aeg*T-MBHA resin **47**, manual solid phase synthesis with Boc-strategy was performed in order to obtain the corresponding supported homothymine PNA decamer. Control cleavages were done during the synthesis on a small amount of the resin, to check the formation of the desired 4-mer, 7-mer and finally 10-mer products. After Boc-deprotection of the *N*-terminus, *N(α)*-Boc-*S*-^{t}butylmercapto cysteine (5 eq respect to the theoretical free amino groups), was coupled whit the supported decamer in presence of HBTU and DIPEA in NMP solution, following the same protocol used for automated SPS of PNA. After capping of all the unreacted chains (negative Kaiser test), a cleavage control was done to check the formation of the desired product. Having confirmed the formation of **48**, total cleavage from the resin led to the desired cysteine modified homothymine PNA decamer. Semipreparative HPLC on reverse phase led to pure **48** (15 mg) as a white solid. ***HPLC (reverse phase):*** retention time 8.78 min, elution gradient from water (+ 0.1% TFA)/AcN 95:5 to pure AcN in 60 min. ***MALDI-TOF:*** 2782.0 [M] (calculated 2782.71).

5.9.2.10 Synthesis of NP-[N-(p-phenylcarbamate)-2,5-dioxopyrrolidin-3-yl]-cysteine-aeg[T]$_{10}$-CONH$_2$, Trifluoroacetic salt, SPION-PNA Nanoconjugate 45

The modified cysteine homothymine PNA **48** (15 mg, 0.005 mmol, 1 eq) was added to a suspension of functionalized SPIONs **20** (15 mg, loading 31.07%, equal to 1.44 mmol/g_{NPs}, 0.022 mmol of organic, 4.3 eq) in dry AcN (5 ml), previously sonicated at 40 °C for 30'; the mixture was stirred, under sonication, at 40 °C for 4 h. After this time the obtained suspension was centrifugated at 5000 r/min for 10' and the supernatant was removed. The solid residue was first washed with fresh AcN (3x5 ml), then with water (2x5 ml), acetone (2x5 ml), at last with Et_2O (3x5 ml) and vortex/sonication/centrifugation were cyclic repeated for each washing. Functionalized NPs were dried on air for a night and then in a rotating vacuum drier for a day, to afford **45** (18 mg) as a light brown powder. ***Loadings from E.A.:*** 54.33% (equal to 0.18 mmol/g_{NPs}, ≈610 molecules/NP). ***FTIR (cm^{-1}) in trasmittance (blank KBr):*** 3417 (broad υ, FeO-H and N-H), 3063 (partially covered υ, ArC-H), 2955 (partially covered υ, aliphatic C-H), 1674 (broad υ, C=O imides, amides, carbamate), 1547 (δ, N-H), 1473, 1416, 1377 (υ, Ar-N), 1358, 1253, 1227-1101 (υ, C-O and C-N), 1032 (δ, ArC-H), 638-565 (υ, Fe-O). ***UV-Vis (λ_{max}, nm) in water:*** 271 (PNA), from 320 broad shouldered scattering of NPs. ***Tm (complementary standard DNA) in water at 260 nm:*** 70 °C (heating), 52° C (cooling).

5.9.2.11 Synthesis of N-cysteine-aeg[STD]-CONH$_2$, Trifluoroacetic Salt 49

Starting from the downloaded Boc-*aeg*T-MBHA resin **47**, manual solid phase synthesis with Boc-strategy was performed in order to obtain the corresponding supported standard sequence PNA decamer. Control cleavages were done during the synthesis on a small amount of the resin, to check the formation of the desired 4-mer, 7-mer and finally 10-mer products. After Boc-deprotection of the *N*-terminus, *N(α)*-Boc-*S*-^{t}butylmercapto cysteine (5 eq respect to the theoretical free amino groups), was coupled whit the supported decamer in presence of HBTU and DIPEA in NMP solution, following the same protocol used for automated SPS of PNA. After capping of all the unreacted chains (negative Kaiser test), a cleavage control was done to check the formation of the desired product. Having confirmed the formation of **49**, total cleavage from the resin led to the desired cysteine modified standard sequence PNA decamer. Semipreparative HPLC on reverse phase led to pure **49** (20 mg) as a white solid. ***HPLC (reverse phase):*** retention time 7.23 min, elution gradient from water (+ 0.1% TFA)/AcN 95:5 to pure AcN in 60 min. ***MALDI-TOF:*** 2831.0 [M] (calculated 2830.76).

5.9.2.12 Synthesis of NP-[N-(p-phenylcarbamate)-2,5-dioxopyrrolidin-3-yl]-cysteine-aeg[STD]-$CONH_2$, Trifluoroacetic salt, SPION-PNA Nanoconjugate 46

The modified cysteine standard sequence PNA **49** (15 mg, 0.005 mmol, 1 eq) was added to a suspension of functionalized SPIONs **20** (15 mg, loading 31.07%, equal to 1.44 mmol/g_{NPs}, 0.022 mmol of organic, 4.3 eq) in dry AcN (5 ml), previously sonicated at 40 °C for 30'; the mixture was stirred, under sonication, at 40 °C for 4 h. After this time the obtained suspension was centrifugated at 5000 r/min for 10' and the supernatant was removed. The solid residue was first washed with fresh AcN (3x5 ml), then with water (2x5 ml), acetone (2x5 ml), at last with Et_2O (3x5 ml) and vortex/sonication/centrifugation were cyclic repeated for each washing. Functionalized NPs were dried on air for a night and then in a rotating vacuum drier for a day, to afford **46** (17 mg) as a light brown powder. ***Loadings from E.A.:*** 34.65% (equal to 0.11 mmol/g_{NPs}, ≈270 molecules/NP). ***FTIR (cm^{-1}) in trasmittance (blank KBr):*** 3435 (broad υ, FeO-H and N-H, partially covered ArC-H), 2917 (partially covered υ, aliphatic C-H), 1710 (partially covered υ, C=O imides), 1644 (broad υ, C=O amides and carbamate), 1545 (δ, N-H), 1512 (υ, C=C), 1401 (υ, Ar-N), 1259-1033 (υ, C-O and C-N), 837 (δ, ArC-H), 640-580 (υ, Fe-O). ***UV-Vis (λ_{max}, nm) in water:*** 267 (PNA), from 320 broad shouldered scattering of NPs. ***Tm (complementary standard DNA) in water at 260 nm:*** 54 °C (heating), 52° C (cooling).

References

[282] P. Nielsen, M. Egholm, R. Berg, O. Buchardt, *Science*. **1991**, *254*, 1497-1500.

[283] M. Egholm, O. Buchardt, L. Christensen, C. Behrens, S.M. Freier, D.A. Driver, R.H. Berg, S.K. Kim, B. Norden, P. Nielsen, *Nature*. **1993**, *365*, 566-8.

[284] V.V. Demidov, V.N. Potaman, M.D. Frank-Kamenetskii, M. Egholm, O. Buchard, S.H. Sönnichsen, P. Nielsen, *Biochem Pharmacol.* **1994**, *48*, 1310.

[285] S.V. Smulevitch, C.G. Simmons, J.C. Norton, T.W. Wise, D.R. Corey, *Nat Biotech.* **1996**, *14*, 1700-1704.

[286] M. Eriksson, P.E. Nielsen, *Nat Struct Biol.* **1996**, *3*, 410-413.

[287] M. Egholm, P.E. Nielsen, O. Buchardt, R.H. Berg, *J. Am. Chem. Soc.* **1992**, *114*, 9677-9678.

[288] S. Brown, S. Thomson, J. Veal, D. Davis, *Science*. **1994**, *265*, 777-780.

[289] L. Betts, J.A. Josey, J.M. Veal, S.R. Jordan, *Science*. **1995**, *270*, 1838-1841.

[290] M. Gellert, M.N. Lipsett, D.R. Davies, *Proc. Natl. Acad. Sci. USA*. **1962**, *48*, 2013–2018.

[291] L.H. Hurley, *Nat. Rev. Cancer.* **2002**, *2*, 188-200.

[292] S. Neidle, G. Parkinson, *Nat. Rev. Drug. Discov.* **2002**, *1*, 383-393.

[293] A. Siddiqui-Jain, C.L. Grand, D.J. Bearss, L.H. Hurley, *Proc. Natl. Acad. Sci. USA.* **2002**, *99*, 11593-11598.

[294] B. Datta, C. Schmitt, B. Armitage, *J. Am. Chem. Soc.* **2003**, *125*, 4111-4118.

[295] Y. Krishnan-Ghosh, D. Liu, S. Balasubramanian, *J Am Chem Soc.* **2004**, *126*, 11009-16.

[296] B. Datta, M.E. Bier, S. Roy, B.A. Armitage, *J Am Chem Soc.* **2005**, *127*, 4199-207.

[297] Y. Krishnan-Ghosh, E. Stephens, S. Balasubramanian, *J Am Chem Soc.* **2004**, *126*, 5944-5.

[298] L. Petraccone, B. Pagano, V. Esposito, A. Randazzo, G. Piccialli, G. Barone, C. Mattia, C. Giancola, *J. Am. Chem. Soc.* **2005**, *127*, 16215-16223.

[299] V. Marin, B. Armitage, *Biochemistry.* **2006**, *45*, 1745-1754.

[300] M. Egholm, L. Christensen, K.L. Dueholm, O. Buchardt, J. Coull, P.E. Nielsen, *Nucleic Acids Res*. **1995**, *23*, 217-222.

[301] H.Kuhn, V.V. Demidov, P.E. Nielsen, M.D. Frank-Kamenetskii, *J Mol Biol.* **1999**, *286*, 1337-1345.

[302] H. Kuhn, V.V. Demidov, M.D. Frank-Kamenetskii, P.E. Nielsen, *Nucleic Acids Res.* **1998**, *26*, 582-587.

[303] J. Lohse, O. Dahl, P.E. Nielsen, *Proc Natl Acad Sci U S A.* **1999**, *96*, 11804-11808.

[304] B. Hyrup, P.E. Nielsen, *Bioorg. Med. Chem.* **1996**, *4*, 5-23.

[305] P. Nielsen, *Pure Appl. Chem.* **1998**, *70*, 105-110.

[306] M. Chakrabarti, F. Schwarz, *Nucl. Acids Res.* **1999**, *27*, 4801-4806.

[307] S. Shakeel, S. Karim, A. Ali, *Journal of Chemical Technology & Biotechnology.* **2006**, *81*, 892-899.

[308] B.D. Gildea, S. Casey, J. MacNeill, H. Perry-O'Keefe, D. Sorensen, J.M. Coull, *Tetrahedron Letters.* **1998**, *39*, 7255-7258.

[309] A. Ray, B. Nordén, *The FASEB journal* **2000**, *14*, 1041-1060.

[310] P.E. Nielsen *et al*., *Proc. Natl. Acad. Sci. USA* **1991**, 3892-3895.

[311] P.E. Nielsen *et al*., *Nucleic Acid Res.* **1993**, *21*, 5332-5336.

[312] C. Carlsson, M. Jonsson, B. Nordén, M.T. Dulay, R.N. Zare, J. Noolandi, P.E. Nielsen, L.C. Tsui, J. Zielenski, *Nature (London)* **1996**, *380*, 207.

[313] D. Rose, *J. Anal. Chem.* **1993**, *65*, 3545-3549.

[314] G.L. Igloi, *Proc. Natl. Acad. Sci. USA* **1998**, *95*, 8562-8567.

[315] BIAcore X Instrument Handbook (1996) Preliminary Ed., Pharmacia Biosensor AB, Uppsala, Sweden.

[316] K.K. Jensen, H. Örum, P.E. Nielsen, B. Nordén, *Biochemistry* **1997**, *36*, 5072-5077.

[317] C. Lu, A.W. Czanderna, Eds (1984) *Applications of Piezoelectric Quartz Crystal Microbalances*, Elsevier, Amsterdam.

[318] Y. Okahata, Y. Matsunobo, K. Ijiro, M. Mukae, A. Murakami, K. Makino, *J. Am. Chem. Soc.* **1992**, *114*, 8299-8300.

[319] Y. Okahata, K. Niikura, Y. Sugiura, M. Sawada, T. Morii, *Biochemistry* **1998**, *37*, 5666-5672.

[320] K. Niikura, H. Matsuno, Y. Okahata, *J. Am. Chem. Soc.* **1998**, *120*, 8537-8538.

[321] J. Wang, P.E. Nielsen, M. Jiang, X. Cai, J.R. Fernandes, D.H. Grant, M. Ozsoz, A. Beglieter, M. Mowat, *Anal. Chem.* **1997**, *69*, 5200-5202.

[322] P.L. Ross, K. Lee, P. Belgrader, *Anal. Chem.* **1997**, *69*, 4197-4202.

[323] M. Egholm, *Nature Biotechnol.* **1997**, *15*, 1346.

[324] T.J. Griffin, W. Tang, L.M. Smith, *Nature Biotechnol.* **1997**, *15*, 1368-1372.

[325] J. Wang, E. Palecek, P.E. Nielsen, G. Rivas, X. Cai, H. Shirashi, N. Dontha, D. Luo, P.A.M. Farias, *J. Am. Chem. Soc.* **1996**, *118*, 267-278.

[326] J.L. Harris, N. Winssinger, *Chem. Eur. J.* **2005**, *11*, 6792-6801.

[327] S. Dall'Angelo, *MSc Thesis in Industrial Chemistry* **2005**, Università degli Studi di Milano.

[328] O. Brandt, J Hoheisel, *TRENDS in Biotechnology* **2004**, *22(12)*, 617-622.

[329] P.S. Walsh, H.A. Erlich, R. Higuchi, *PCR Methods Appl.* **1992**, *1*, 241.250.

[330] D.B. Demers, E.T. Curry, M. Egholm, A.C. Sozer, *Nucleic Acids Res.* **1995**, *23*, 3050-3055.

[331] H.S. Misra, P.K. Pandey, M.J. Modak, R. Vinayak, V.N. Pandey, *Biochemistry* **1998**, *37*, 1917-1925.

[332] M. Koppitz, P.E. Nielsen, L.E. Orgel, *J. Am. Chem. Soc.* **1998**, *120*, 4563-4569.

[333] H. Perry-O'Keefe, X.W. Yao, J.M. Coull, M. Fuchs, M. Egholm, *Proc. Natl. Acad. Sci. USA* **1996**, *93*, 472-480.

[334] A.G. Veselkov, V. Demidov, P.E. Nielsen, M.D. Frank-Kamenetskii, *Nucleic Acids Res.* **1996**, *24*, 2483-2487.

[335] V. Demidov, M.D. Frank-Kamenetskii, M. Egholm, O. Buchardt, P.E. Nielsen, *Nucleic Acids Res.* **1993**, *21*, 2103-2107.

[336] P.M. Lansdorp, N.P. Verwoerd, F.M. van de Rijke, V. Dragowska, M.T. Little, R.W. Dirks, A.K. Raap, H. Tanke, *J. Hum. Mol. Genet.* **1996**, *5*, 685-691.

[337] H. Örum, P.E. Nielsen, M. Jorgensen, C. Larsson, C. Stanley, T. Koch, *BioTechniques* **1995**, *19*, 472-480.

[338] N.E. Møllegaard, O. Buchardt, M. Egholm, P.E. Nielsen, *Proc. Natl. Acad. Sci. USA* **1994**, *91*, 3892-3895.

[339] D.A. Dean, *Advanced Drug Delivery Reviews* **2000**, *44*, 81-95.

[340] G. Wang, X. Xu, D.A. Pace, D.A. Dean, P.M. Glazer, P. Chan, S.R. Goodman, C.F. Hassman, I. Shokolenko, *Nucl. Acids Res.* **1999**, *27*, 2806-2813.

[341] L. Bastide, P.E. Boehmer, G. Villani, B. Lebleu, *Nucl. Acids Res.* **1999**, *27*, 551-554.

[342] M. Pooga, T. Land, T. Bartfai, Ü Langel, *Biomolecular Engineering* **2001**, *17*, 183-192.

[343] T. Bentin, P.E. Nielsen, *Biochemistry* **1996**, *35*, 8863-8869.

[344] P.E. Nielsen, M. Egholm, O. Buchardt, *Gene* **1994**, *149*, 139-145.

[345] J.C. Hanvey, N.C. Peffer, J.E. Bisi, S.A. Thomson, R. Cadilla, J.A. Josey, D.J. Ricca, C.F. Hassman, M.A. Bonham, K.G. Au, S.G. Carter, D.A Bruckenstein, A.L. Boyd, S.A Noble, L.E. Babiss, *Science* **1992**, *258*, 1481-1485.

[346] D. Praseuth, M. Grigoriev, A.L. Guieysse, L.L. Pritchard, A. Harel-Bellan, P.E. Nielsen, C. Helene, *Biochim. Biophys. Acta* **1996**, *1309*, 226-238.

[347] S. Tomac, M. Sarkar, T. Ratilainen, P. Wittung, P.E. Nielsen, B. Nordén, A. Gräslund, *J. Am. Chem. Soc.* **1996**, *118*, 5544-5552.

[348] M. Egholm, L. Christensen, K.L. Dueholm, O. Buchardt, J. Coull, P.E. Nielsen, *Nucleic Acids Res.* **1995**, *23*, 217-222.

[349] B. Armitage, T. Koch, H. Frydenlund, H. Örum, G.B. Schuster, *Nucleic Acids Res.* **1998**, *26*, 715-720.

[350] H. Kuhn, V.V. Demidov, M.D. Frank-Kamenetskii, P.E. Nielsen, *Nucleic Acids Res.* **1998**, *26*, 582-587.

[351] R. Lee, N. Kaushik, M.J. Modak, R. Vinayak, V.N. Pandey, *Biochemistry* **1998**, *37*, 900-910.

[352] H.J. Larsen, P.E. Nielsen, *Nucleic Acids Res.* **1996**, *24*, 458-463.

[353] G. Cutrona, E.M. Carpaneto, M. Ulivi, S. Rondella, O. Landt, M. Ferrarini, L.C. Boffa, *Nature Biotechnol.* **2000**, *18*, 300-303.

[354] L.C. Boffa, S. Scarfi, M.R. Mariani, G. Damonte, V.G. Allfrey, V. Benatti, P.L Morris, *Cancer Research* **2000**, *60*, 2258-2262.

[355] H. Knudsen, P.E. Nielsen, *Nucleic Acids Res.* **1996**, *24*, 494-500.

[356] J.W. Nyce, W.J. Metzger, *Nature* **1997**, *385*, 721-725.

[357] L. Mologni, P. leCoutre, P.E. Nielsen, C. Gambacorti-Passerini, *Nucleic Acids Res.* **1998**, *26*, 1934-1938.

[358] L. Good, P.E. Nielsen, *Proc. Natl. Acad. Sci. USA* **1998**, *95*, 2073-2076.

[359] L. Good, P.E. Nielsen, *Nature Biotechnol.* **1998**, *16*, 355-358.

[360] R.W. Taylor, P.F. Chinnery, D.M. Tumbull, R.N. Lightowlers, *Nature Genet.* **1997**, *15*, 212-215.

[361] E. Uhlmann, A. Peyman, G. Breiphol, D.W. Will, *Angew. Chem. Int. Ed.* **1998**, *37*, 2796-2823.

[362] P.E. Nielsen, M. Egholm, R.H. Berg, O. Buchardt, *Anti-Cancer Drug Design* **1993**, *8*, 53-63.

[363] M.J. Lutz, S.A. Benner, S. Hein, G. Breipohl, E. Uhlmann, *J. Am. Chem. Soc.* **1997**, *119*, 3177-3178.

[364] U. Koppelhus, V. Zachar, P.E. Nielsen, X. Liu, J. Eugen-Olsen, P. Ebbesen, *Nucleic Acids Res.* **1997**, *25*, 2167-2173.

[365] J.C. Norton, M.A. Piatyszek, W.E. Wright, J. Shay, D.R. Corey, *Nat. Biotech.* **1996**, *14*, 615-620.

[366] S.E. Hamilton, C.G. Simmons, I.S. Kathiriya, D.R. Corey, *Chem. Biol.* **1999**, *6*, 343-351.

[367] D.A. Dean, *Adv. Drug. Del. Rev.* **2000**, *44*, 81-95.

[368] A.F. Faruqi, M. Egholm, P.M. Glazer, *Proc. Natl. Acad. Sci. USA* **1998**, *95*, 1398-1403.

[369] G. Wang, M.M. Seidman, P.M. Glazer, *Science* **1996**, *271*, 802-805.

[370] S. Pensato,M. Saviano, A. Romanelli, *Expert Opin Biol Ther.* **2007**, *7*, 1219-32.

[371] E. Uhlmann, A. Peyman, *Chem. Rev.* **1990**, *90*, 543-584.

[372] S.O. Doronina, J. Behr, *Chem. Soc. Rev.* **1997**, *26*, 63-71.

[373] L. Christensen, H.F. Hansen, T. Koch, P.E. Nielsen, *Nucleic. Acids. Res.* **1998**, *26*, 2735-2739.

[374] A. Eldrup, O. Dahl, P.E. Nielsen, *J. Am. Chem. Soc.* **1997**, *119*, 11116-11117.

[375] A.G. Olsen, O. Dahl, P.E. Nielsen, *Bioorg Med Chem Lett.* **2004**, *14*, 1551-1554.

[376] a) A. Eldrup, B. Nielsen, G. Haaima, H. Rasmussen, J. Kastrup, C. Christensen, P.E. Nielsen, *Eur. J. Org. Chem.* **2001**, 1781-1790; b) A. Eldrup, A., C. Christensen, G. Haaima, P.E. Nielsen, *J Am Chem Soc.* **2002**, *124*, 3254-3262; c) K. Rajeev, M. Maier, E. Lesnik, M. Manoharan, *Org. Lett.* **2002**, *4*, 4395-4398.

[377] B.P. Gangamani, V.A. Kumar, *Chem. Commun.* **1997**, 1913-1914.

[378] B.G. de la Torre, R. Eritja, *Bioorg. Med. Chem. Lett.* **2003**, *13*, 391-393.

[379] O. Köhler, O. Seitz, *Chem. Comm.* **2003**, 2938-2939.

[380] a) O. Köhler, D.V. Jarikote, O. Seitz, *ChemBioChem.* **2005**, *6*, 69-77; b) D.V. Jarikote, O. Köhler, E. Socher, O. Seitz, *Eur. J. Org. Chem.* **2005**, 3187-3195.

[381] a) P.E. Nielsen, G. Haaima, A. Lohse, O. Buchardt, *Angew. Chem. Int. Ed.* **1996**, *35*, 1939-1942; b) S. Sforza, G. Haaima, R. Marchelli, P.E. Nielsen, *Eur. J. Org. Chem.* **1999**, 197-204.

[382] B. Hyrup, M. Egholm, O. Buchardt, P.E. Nielsen, *Bioorg. Med. Chem. Lett.* **1996**, *6*, 1083-1088.

[383] D.A. Barawkar, T.C. Bruice, *J. Am. Chem. Soc.* **1999**, *121*, 10418-10419.

[384] a) V.A. Efimov, M.V. Choob, A.A. Buryakova, O.G. Chakhmakhcheva, *Nucleosides, Nucleotides & Nucleic Acids.* **1998**, *17*, 1671-1679; b) V.A. Efimov, A.A. Buryakova, M.V. Choob, O.G. Chakhmakhcheva, *Nucleosides, Nucleotides & Nucleic Acids.* **1999**, *18*, 1393-1396; c) A.C. van der Laan, R. Strömberg, J.H. van Boom, E. Kuyl-Yeheskiely, V.A. Efimov, O.G. Chakhmakhcheva, *Tetrahedron Lett.* **1996**, *37*, 7857-7860; d) A. Peyman, E. Uhlmann, K. Wagner, S. Augustin, G. Breipohl, D.W. Will, A. Schäfer, H. Wallmeier, *Angew. Chem. Int. Ed.* **1996**, *35*, 2636-2638; e) J. Kehler, U. Henriksen, H. Vejbjerg, O. Dahl, *Bioorg. Med. Chem.* **1998**, *6*, 315-322.

[385] a) C. García-Echeverría, D. Hüsken, C.S. Chiesi, K. Altmann, *Bioorg. Med. Chem. Lett.* **1997**, *7*, 1123-1126; b) M. Kuwahara, M. Arimitsu, M. Sisido, *J. Am. Chem. Soc.* **1999**, *121*, 256-257.

[386] a) V. Kumar, K. Ganesh, *Acc. Chem. Res.* **2005**, *38*, 404-412; b) V. Kumar, *Eur. J. Org. Chem.* **2002**, *2002*, 2021-2032.

[387] B.P. Gangamani, M. Decosta, V.A. Kumar, K.N. Ganesh, *Nucleosides, Nucleotides & Nucleic Acids.* **1999**, *18*, 1409-1411.

[388] a) M. D'Costa, V. Kumar, K. Ganesh, *Org. Lett.* **1999**, *1*, 1513-1516; b) M. D'Costa, V. Kumar, K. Ganesh, *Org. Lett.* **2001**, *3*, 1281-1284.

[389] N.K. Sharma, K.N. Ganesh, *Chem Commun (Camb).* **2003**, 2484-2485.

[390] A. Puschl, T. Tedeschi, P.E. Nielsen, *Org. Lett.* **2000**, *2*, 4161-4163.

[391] a) T. Govindaraju, V. Kumar, K. Ganesh, *J. Org. Chem.* **2004**, *69*, 5725-5734; b) T. Govindaraju, V.A. Kumar, K.N. Ganesh, *Chem. Commun.* **2004**, 860-861; c) M.C. Myers, M.A. Witschi, N.V. Larionova, J.M. Franck, R.D. Haynes, T. Hara, A. Grajkowski, D.H. Appella, *Org Lett.* **2003**, *5*, 2695-2698; d) E.A. Englund, Q. Xu, M.A. Witschi, D.H. Appella, *J Am Chem Soc.* **2006**, *128*, 16456-16457; e) P. Lagriffoule, M. Eriksson, K.K. Jensen, P.E. Nielsen, P. Wittung, B. Nordén, O. Buchardt, *Chem. Eur. J.* **1997**, *3*, 912-919.

[392] R. Corradini, S. Sforza, T. Tedeschi, R. Marchelli, *Chirality.* **2007**, *19*, 269-294.

[393] J.N. Kremsky, M. Pluskal, S. Casey, H. Perry-O'Keefe, S.A. Kates, N.D. Sinha, *Tetrahedron Lett.* **1996**, *37(25)*, 4313-4316.

[394] a) F.V. Bright, *Anal. Chem.* **1988**, *60*, 1031A-1039A; b) R.P. Haughland, *Handbook of Fluorescent Probes and Research Chemicals* **1992**, Molecular Probes, Eugene, OR; c) M. Miki, *Eur. J. Biochem.* **1987**, *164*, 229-235.

[395] M. Lu-Steffes *et al*,. *Clin. Chem.* **1982**, *28*, 2278-2282.

[396] M. Adamczyk, J.R. Fishpaugh, K. Heuser, *J. Bioconjugate Chem.* **1997**, *8*, 253-255.

[397] E.A. Englund, D.A. Appella, *Organic Letters* **2005**, *7(16)*, 3465-3467.

[398] R.K. Boeckman, P. Shao, J.J. Mullins, *Organic Synthesis* **2000**, 141.

[399] L. Josephson, J.M. Perez, R. Weissleder, *Angewandte Chemie-International Edition* **2001**, *40(17)*, 3204.

[400] F. Wang, H.B. Shen, J. Feng, H.F. Yang, *Microchimica Acta* **2006**, *153(1-2)*, 15-20.

[401] M. Pita, J.M. Abad, C. Vaz-Dominguez, C. Briones, E. Mateo-Marti, J.A. Martin-Gago, M.D.P. Morales, V.M. Fernandez, *Journal of Colloid and Interface Science* **2008**, *321(2)*, 484-492.

[402] a) G. Prencipe, *PhD Thesis* **2010**, Università degli Studi di Milano; b) P. Verderio, *MSc Thesis* **2009**, Università degli Studi di Milano.

[403] S. Sonzini, *MSc Thesis* **2010**, Università degli Studi di Milano.

Chapter 6: Final Conclusions

6 Conclusions

In this Ph.D. thesis a systematic study concerning the surface modification of superparamagnetic iron oxide nanoparticles, is reported.

In particular, after a brief introduction on the classical techniques currently employed, the discovery of a new covalent grafting methodology based on the reactivity of isocyanate group towards the surface hydroxyl groups of the nanoparticles, is shown.

In order to demonstrate this innovative anchoring system, a small library of isocyanate-base nanoconjugates has been synthesized (**15**-**20**). Analytical and spectroscopical characterizations helped us to point out the effective formation of a covalent carbamate-like bond between a generic isocyanate molecule and the SPIONs surface.

From E.A., the loadings of the obtained nanoconjugates can be determined. Comparing these values with those obtained in classical non-covalent and siloxane-based covalent

interaction, we can state that the presented methodologies led to higher and easily tunable loading respect to the classical methodologies.

FTIR spectroscopy has demonstrated to be the choice technique for the characterization of these kind of nanosystems, giving many information about the nature of the surface grafting.

A first approach in the characterization of these nanoconjugates with HR-MAS NMR spectroscopy was also accomplished, confirming the validity and versatility of this analytical tool in the determination of the structure of organic molecules loaded onto magnetic metallic core. Preliminary DOSY experiments were also performed.

Some of the nanoconjugates bear different additional functional groups (**18**-**20**), those have been demonstrated to be stable in the grafting reaction conditions, while remains still reactive for the binding of other organic molecules (**27**, **28**, **34**, **35**).

Thus, properly functionalized isocyanates could be used as heterobifunctional linkers for the supporting of biomolecules onto SPIONs, opening new strategies for the synthesis of a new class of bionanoconjugates.

From several years, our research group has gained a lot of expertise in the synthesis and characterization of Peptide Nucleic Acids (PNAs) and a small library of SPION-PNA nanoconjugates has been obtained.

In this research work, four new SPION-PNA nanoconjugates have been designed and synthesized (**36**, **37**, **45**, **46**).

36 and **37** are characterized by the presence of a fluorescent probe and have been loaded onto the nanoparticle surface by a carboxylate-base non-covalent interaction, while **45** and **46** were obtained by a covalent C-S bond formation between the properly modified PNAs and the NCO-based functionalize SPIONs **20**.

All these SPIONS-PNA nanoconjugates have shown a strong affinity binding towards the complementary DNA strands, regardless of the presence of the magnetic nanoparticles., opening the possibility to use these systems in theranostic fields.

6.1 Future Perspectives

In this Ph.D. research work, lots of work have been done concerning the surface functionalization of SPIONs, but much more work remains to be done.

In particular, we want to expand the library of NCO-based heterobifunctional linkers introducing different additional functional groups, as well as, introducing properly spacers able to modify the chemo-physical behavior of the functionalized nanoparticles, *e.g.* increasing the water solubility or, otherwise, the hydrophobicity of the systems or tuning the steric hindrance on the surface.

For biological applications, the toxicity and the possible interactions with proteins, enzymes or oligonucleotides have to be studied, as well as, their cellular up take and biodistribution.

In this sense, we have recently started a profitable collaboration with Prof. Seneci's research group of the Dept. of Chemistry, University of Milan, with the aim to support apoptosis inhibitors mimics onto SPIONs and to study their bioactivity. Biological studies will be performed in collaboration with the National Institute of Tumors (INT) in Milan. Only preliminary results were obtained and for this reason are not here reported.

List of Acronyms and Abbreviations

A:	Adenine
Ac:	Acetyl
Ac_2O:	Acetic anhydride
AcN:	Acetonitrile
AcOEt:	Ethyl acetate
aeg:	Aminoethylglycine
aeg[STD]-PNA:	Aminoethylglycine standard sequence PNA
aeg$[T]_{10}$-PNA:	Aminoethylglycine homothymine PNA
AOT:	Aerosol OT or dioctyl sodium sulfosuccinate
APDES:	3-Aminopropyl-ethyl-diethoxysilane
APES:	3-Aminopropyl-diethyl-ethoxysilane
APTES:	3-Aminopropyl-triethoxysilane
BIA:	Biomolecular Interaction Analysis
Boc:	*tert*-Butyloxycarbonyl
Boc-aegPNA-OH:	*N*(Boc)-aminoethylglycine PNA monomer, carboxylic acid
Boc-Lys(Fmoc)-OH:	*N(α)*Boc-N*(ε)*Fmoc-lysine, carboxylic acid
C:	Cytosine
Cbz:	Benzyloxycarbonyl
$CDCl_3$:	Deuterated chloroform
COSY:	Correlation spectroscopy
CTAB:	Cetyltrimethylammonium bromide
Cys:	Cysteine
D:	Diffusion coefficient
DCM:	Dichloromethane
DMF:	Dimethylformamide
DMSO:	Dimethylsulfoxide
DMSO-d_6:	Deuterated dimethylsulfoxide
DNA:	Deoxyribonucleic acid
DOSY:	Diffusion ordered NMR spectroscopy
DPPA:	Diphenylphosphoryl azide

DSC:	Differential scanning calorimetry
E.A.:	Elemental analysis
EDTA:	Ethylenediaminotetraacetic acid
Et_2O:	Diethyl ether
FAB:	Fast atom bombardment
FG:	Functional group
FITC:	Fluorescein isothiocyanate
FITU:	Fluorescein isothiourea
Fmoc:	9-Fluorenylmethoxycarbonyl
FTIR:	Fourier transform infrared spectroscopy
G:	Guanine
HATU:	*O*-(7-Azabenzotriazol-1-yl)-*N,N,N',N'*-tetramethyluronium hexafluorophosphate
HBTU:	*O*-(Benzotriazol-1-yl)-*N,N,N',N'*-tetramethyluronium hexafluorophosphate
HPLC:	High performance liquid chromatography
HR-MAS:	High resolution magic angle spinning
HSQC:	Heteronuclear single quantum correlation
IE.P.:	Isoelectric point
IMS:	Immune magnetic separation
LED:	Longitudinal eddy current delay or Longitudinal encode-decode
Lys:	Lysine
MALDI-TOF:	Matrix assisted laser desorption ionization – Time of flight
MBHA:	4-Methylbenzhydrylamine hydrochloride salt
MDT:	Magnetic drug targeting
MFH:	Magnetic fluid hyperthermia
MNP:	Magnetic nanoparticle
Mp:	Melting point
MPS:	Mononuclear phagocytosis system
MRI:	Magnetic resonance imaging
mRNA:	Messenger ribonucleic acid
MS:	Mass spectroscopy
N-Ac-Cys-OH:	*N*-Acetylcysteine, carboxylic acid
N-Boc-Cys(S^tBu)-OH:	*N(α)*-Boc-*S*-^{t}butylmercapto cysteine
NCO:	Isocyanate
NMP:	*N*-Methylpirrolidone
NMR:	Nuclear magnetic resonance
NP:	Nanoparticle

PABA:	*p*-Aminobenzoic acid
PCR:	Polymerase chain reaction
PFG:	Pulse field gradient
$PhCH_3$:	Toluene
PMBA:	*p*-Maleimidobenzoic acid
PMB-Cl:	*p*-Maleimidobenzoyl chloride
PMP-AZIDE:	*p*-Maleimidobenzoyl azide
PMPI:	*p*-Maleimidophenyl isocyanate
PNA:	Peptide nucleic acid
PVP:	Polyvinylpyrrolidone
Py:	Pyridine
QCM:	Quartz Crystal Microbalance
REE:	Rare earth element
RES:	Reticulendothelial system
RNA:	Ribonucleic acid
SNP:	Single nucleotide polymorphism
SPION:	Superparamagnetic iron oxide nanoparticle
SPR:	Surface Plasmon resonance
SPS:	Solid phase synthesis
T:	Thymine
T_B:	Blocking temperature
TEA:	Triethylamine
TEOS:	Tetraethoxysilane
TESPI:	3-(triethoxysylil)propyl isocyanate
TFA:	Trifluoroacetic acid
TFMSA:	Trifluoromethanesulfonic acid
THF:	Tetrahydrofuran
Tm:	Melting temperature
T_N:	Néel temperature
TOPO:	Trioctylphosphine oxide
USPIO:	Ultrasmall superparamagnetic iron oxide nanoparticle
UV-Vis:	Ultraviolet-visible spectroscopy

Acknowledgments

… ovvero Ringraziamenti!

Spero che nessuno si offenda se almeno questi li scrivo in italiano. Dopo tutta la fatica fatta per scrivere una tesi intera in inglese, almeno questo concedetemelo.

Il mio più sentito ringraziamento va alla Prof.ssa Emanuela Licandro e al Prof. Stefano Maiorana, che fin dal tirocinio, poi la tesi e ora il dottorato mi hanno permesso di imparare, sperimentare, scoprire e a volte anche "giocare" con la chimica organica. Li ringrazio ancor più per il calore umano che mi hanno sempre dimostrato nei momenti di difficoltà sia scientifica che personale.

Un grazie grandissimo va alla Dr. Clara Baldoli, che con i suoi consigli (anche in questo caso scientifici e personali) mi ha aiutato in questo lungo cammino.

Recentemente ho avuto la possibilità di conoscere e collaborare con il Prof. Pierfausto Seneci a cui devo un ringraziamento speciale perché, oltre ad aver contribuito al mio accrescimento culturale, condivide con me le tragedie del pendolarismo lombardo!

Un altro importante ringraziamento va a chi ha collaborato all'ottenimento dei risultati riportati in questa tesi: la Dr. Maria Chiara Sala per tutte le analisi FTIR (finalmente ho imparato ad interpretare uno spettro infrarosso fin nel più piccolo dettaglio!), il Dr. Enrico Caneva per tutti gli esperimenti HR-MAS NMR (è stato un lavoro duro e impegnativo, ma i risultati piano piano stanno arrivando!!!), nonché la Dr. Anna Daghetti per le analisi MALDI-TOF.

Un grazie enorme lo devo a chi, in tutti questi anni, è stato mio responsabile, compagno, studente o collega di laboratorio. Ognuno di voi (non vi cito tutti altrimenti non finirei più!)

merita un encomio particolare, perché diciamocelo… sono veramente insopportabile quando voglio!

Grazie anche a chi ha condiviso con me questi anni di dottorato, in particolare Martina e Vichi… ma quanto ci siamo sbattuti in questi anni!!!

Grazie a tutti gli amici che ho conosciuto in università e a quelli che conosco da una vita, ognuno di voi ha in qualche modo contribuito a questo risultato!

Il mio GRAZIE più sincero va però alla mia famiglia e al mio compagno. Senza di voi e senza di te non ce l'avrei davvero mai fatta!

GRAZIE